SPECTROSCOPIC STUDIES OF THE CONFORMATIONAL STABILITY AND LIGAND BINDING PROPERTIES OF CALMODULIN

Laura Masino

A thesis submitted in partial fulfilment of the requirements
of the University of London for the degree of Doctor of Philosophy

June 2000

Division of Physical Biochemistry
National Institute for Medical Research
Mill Hill
London NW7 1AA

Department of Biochemistry
University College London
Gower Street
London WC1E 6BT

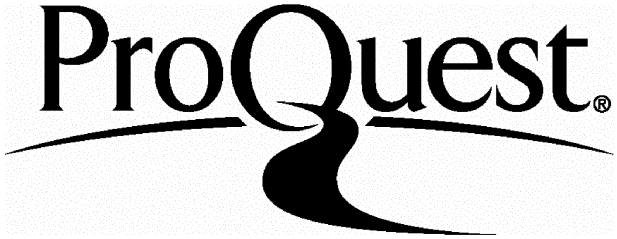

To my parents

ABSTRACT

In this work the conformational stability of calmodulin (CaM) and its tryptic fragments has been investigated using optical spectroscopic techniques such as far-UV circular dichroism, fluorescence, and absorption spectroscopy. CaM is a ubiquitous eukaryotic calcium binding protein that consists of two structurally similar globular domains connected by a flexible linker, and each containing a pair of helix-loop-helix calcium binding motifs.

The results of chemical and thermal denaturation experiments show that the stability of CaM and its isolated domains in the absence of calcium is relatively low and is strongly dependent on ionic strength and temperature. This raises the question of how apo-CaM is stabilised *in vivo* at resting calcium concentrations. In the presence of ligands such as calcium, magnesium, and target peptides, the stability of CaM is greatly enhanced, as predicted by the ligand binding theory. The extent of the stabilising effect depends on the free ligand concentration and on the affinity of the native and denatured states of CaM for the ligand. The interactions of CaM with magnesium have been investigated and the results show that magnesium competes with calcium for the EF-hand sites and reduces the affinity of Ca^{2+}-CaM for targets. As a consequence, magnesium amplifies the intrinsic differences in affinity of the N- and C-domains for calcium and for target sequences. Thus, CaM is extremely sensitive to general environmental conditions as well as to specific ligand interactions. Chemical denaturation studies also show that the behaviour of GuHCl is very complex, owing to its ionic strength contribution and to competition with Ca^{2+}-binding. Therefore urea may be more appropriate in the study of the stability of calmodulin and of proteins that bind metal ions or that are sensitive to changes in the ionic strength of the solution.

Finally, there is experimental evidence that the stability of the isolated domains of CaM is significantly different from that of the domains in the intact protein. This suggests the presence of inter-domain interactions during the process of unfolding. This observation is confirmed by the analysis of the stability of the β-sheet mutants of CaM, which shows that the structural and Ca^{2+}-binding properties of the non-mutated domain can be affected by the mutation on the other domain.

ACKNOWLEDGEMENTS

I would like to thank my supervisor Dr. Peter Bayley for giving me the opportunity to work on this project and for helping me to fulfil my wish to undertake scientific research. I express my gratitude to him for his guidance, for the enthusiasm he instilled in me for biophysical studies, for constructive discussions about my data, and for advice about future work.

I am also extremely grateful to Dr. Stephen Martin, who introduced me step by step to the experimental methods of this laboratory and passed on to me some of his experience with incredible patience and constant attention. I thank him for his support and for being there at any time to answer my questions and to give me help and suggestions about my project. I also thank him for kindly allowing me to use his data analysis programs.

I thank Peter Browne for his help in protein preparation and for the purification of fragment Tr1C, and Dr. Jens Kleinjung for his help with the HPLC technique. Special thanks go to Daniela Romano and Muriel Erent for their friendship, their encouragement, and for sharing with me all the good times as well as the difficult moments of the years spent here.

Finally, I would like to thank my parents for their constant help and support, and for their confidence in my capabilities.

TABLE OF CONTENTS

LIST OF FIGURES

LIST OF TABLES

CHAPTER 5 - Stability and Ca^{2+}-binding properties of the β-sheet mutants of calmodulin

CHAPTER 6 - Interactions of magnesium with calmodulin

ABBREVIATIONS

5,5'-Br_2BAPTA	5,5'-dibromo-1,2-bis(2-aminophenoxy)ethane-*N,N,N',N'*-tetraacetic acid
5-nitro BAPTA	5-nitro-1,2-bis(2-aminophenoxy)ethane-*N,N,N',N'*-tetraacetic acid
Apo-CaM	calcium free calmodulin
CaM	*Drosophila melanogaster* calmodulin
CD	circular dichroism
EDTA	ethylenediaminetetraacetic acid
EGTA	ethylene glycol-bis(β-aminoethyl ether)N,N,N',N'-tetraacetic acid
Hepes	*N*-(2-hydroxyethyl)piperazine-*N*'-(2-ethane sulphonic acid)
Holo-CaM	calcium saturated calmodulin
MES	2-(*N*-morpholino)ethanesulphonic acid
Quin2	2-[[2-bis(carboxymethyl)amino-5-methylphenoxy]methyl]-6-methoxy-8-bis-(carboxymethyl)aminoquinoline
sk-MLCK	skeletal muscle myosin light chain kinase
sm-MLCK	smooth muscle myosin light chain kinase
TNS	2-(p-toluidino)naphthalene-6-sulfonic acid
Tr1C	N-terminal tryptic fragment of calmodulin (residues 1-75)
Tr2C	C-terminal tryptic fragment of calmodulin (residues 78-148)
Tris	tris(hydroxymethyl)methylamine

CHAPTER 1

INTRODUCTION

1.1 Calmodulin

Calmodulin (CaM) is a highly conserved calcium-binding protein which mediates a variety of calcium-dependent physiological processes in all eukaryotic cells. The cellular events regulated by CaM include muscle contraction, neuronal signal transduction, cell growth and division, and cell motility (Davis, 1992). Calcium binding to CaM induces a conformational change in the protein that enables Ca^{2+}-CaM to bind with high affinity (K_d 10^{-7} to 10^{-11} M) and activate a wide range of target proteins. Many Ca^{2+}-CaM-dependent proteins are involved in cell signalling through phosphorylation or dephosphorylation of intracellular proteins, or participate in signal transduction by modulating levels of intracellular second messengers such as Ca^{2+}, cAMP, cGMP, and nitric oxide, or, finally, are involved in the regulation of cytoskeletal elements (Crivici and Ikura, 1995). The activation of targets by CaM occurs predominantly through Ca^{2+}-dependent pathways, but some Ca^{2+}-independent mechanisms have also been found.

1.1.1 The structure of calmodulin

CaM is a small (M_r = 16,700 D) acidic protein which comprises 148 amino acids. At neutral pH, the total number of negatively charged residues is 38, whereas that of positively charged residues is 14. Although the distribution of charges on the surface of the protein is different for Ca^{2+}-free and Ca^{2+}-saturated CaM, the overall charge of the protein is clearly negative for both forms. The isoelectric point (pI) is approximately 4.1 (Coyne et al., 1985; Wandosell et al., 1986).

The crystal structure of Ca^{2+}-CaM was first solved by Babu et al. (1985) at 3.0 Å, subsequently solved by Kretsinger et al. (1986) at 1.9 Å, and further refined by other groups (Babu et al., 1988; Chattopadhyaya et al., 1992). The crystal form of Ca^{2+}-CaM is a dumbbell-shaped molecule, approximately 65 Å long, composed of two structurally similar globular domains (N-terminal and C-terminal), each containing a pair of helix-loop-helix calcium binding motifs (EF-hands). The two domains are separated by an interconnecting α-helix of approximately eight turns. The two calcium binding loops within each domain are connected by a short antiparallel β-sheet which involves hydrogen bonding between the hydrophobic residues at position 8 in each loop (Ile-27 and Ile-63 in the N-terminal domain, and Ile-100 and Val-136 in the C-terminal domain). Both domains of Ca^{2+}-CaM have a large, solvent-exposed hydrophobic surface which is composed of a number of residues clustered around a central core formed by the short β-sheet structure. Each surface has a deep hydrophobic cavity in the centre and is surrounded by a polar rim which is rich in negatively charged residues. Among the hydrophobic amino acids which become exposed upon calcium binding, the occurrence of Met residues is particularly high. Of the nine Met residues present in CaM, four are in each of the solvent exposed hydrophobic surfaces, contributing 46% of the total accessible surface area of the hydrophobic patches (O'Neil and DeGrado, 1990).

The NMR structures of Ca^{2+}-CaM are closely similar to the crystal structures; however, they showed that residues 78-81, corresponding to the middle section of the central helix, adopt a non-helical conformation in solution and have a high degree of mobility (Ikura et al., 1990; Ikura et al., 1991; Barbato et al., 1992). Thus, the central region acts as a flexible linker between the two domains, allowing them to adopt a variety of positions with respect to each other and to bind CaM targets. The average

conformation of the molecule in solution is also more compact than the elongated crystal form.

Upon calcium binding, CaM undergoes a conformational transition that increases its affinity for various target proteins. The mechanism of activation of CaM by calcium has been intensively investigated but the details remained unclear until the solution structure of Ca^{2+}-free CaM (apo-CaM) was solved. Before then, most of the speculations about the Ca^{2+}-induced conformational changes of CaM were based on the model proposed by Strynadka and James (1988), which predicted the structure of apo-CaM based on the crystal structure of the highly homologous (51% sequence identity) protein troponin C. In 1995, the NMR solution structures of apo-CaM and of its C-terminal domain (Figure 1.1) allowed a direct comparison of the apo- and Ca^{2+}-forms of the protein (Finn et al., 1995; Kuboniwa et al., 1995; Zhang et al., 1995a). They showed that the secondary structure of apo-CaM (in its folded form) is closely similar to that of Ca^{2+}-CaM and the main differences between the two forms are in helix packing. Upon Ca^{2+} binding, the two helices in each EF-hand, which are nearly antiparallel in the absence of calcium, shift to a more perpendicular orientation. This results in a more extended conformation and in the exposure of the hydrophobic patch observed on the surface of each domain of Ca^{2+}-CaM, which drives the binding of target molecules. Circular dichroism (CD) measurements also indicate that Ca^{2+} binding induces an increase in the helical content of the protein (Martin and Bayley, 1986). The deep hydrophobic cavities observed in the centre of the Ca^{2+}-CaM domains are completely absent in apo-CaM. However, even in the absence of calcium, both the C- and the N-terminal domains contain a cluster of hydrophobic residues, which in the N-domain is partially surrounded by acidic residues. The resulting surface in each apo-domain is thus negatively charged but partially hydrophobic. Owing to the tight helix packing of apo-CaM and to the exposure of the hydrophobic pockets in Ca^{2+}-CaM, their structures are often referred to as the "closed" and "open" conformations, respectively.

CaM can be cleaved proteolytically with trypsin into two closely homologous domains (48 % sequence identity, 69 % similarity), which retain the secondary and tertiary structure that they have in the intact protein, as assessed by NMR spectroscopy (Thulin et al., 1984; Finn et al., 1995). Several studies have shown that the optical spectroscopic (Martin and Bayley, 1986), kinetic (Martin et al., 1985; Suko et al.,

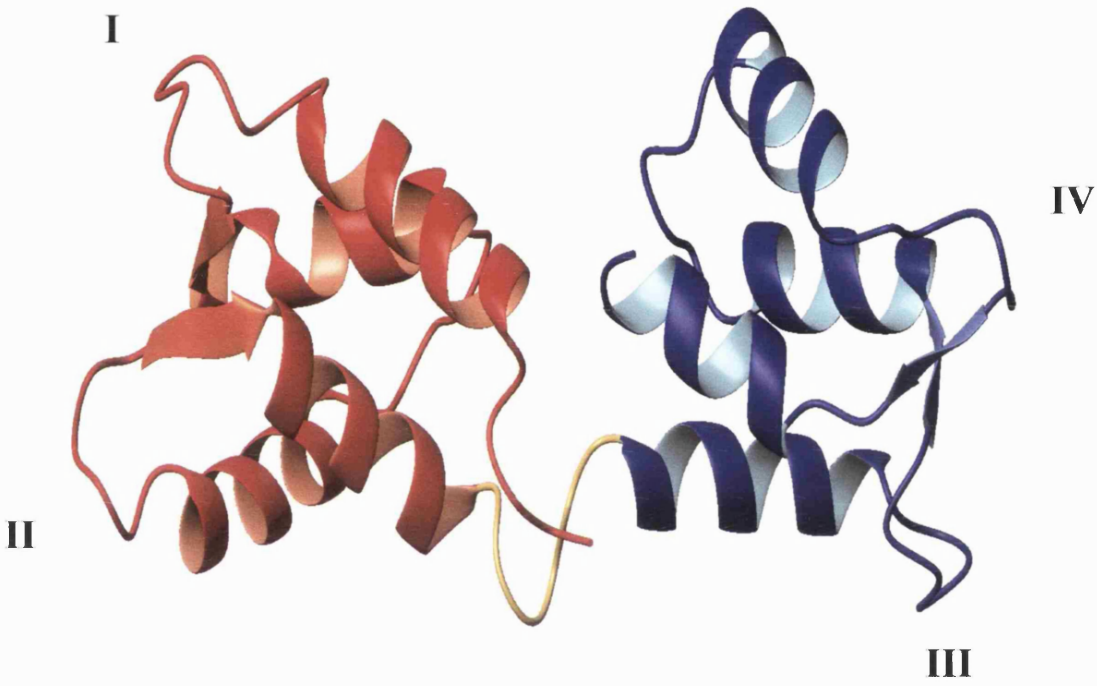

Figure 1.1 Solution structure of calcium-free calmodulin. The N-domain is shown in red, the C-domain in blue, and the flexible central linker which connects the two domains is shown in yellow. Numbers I to IV indicate the four calcium binding loops. The figure was prepared using the coordinates deposited by Kuboniwa et al. (1995) (PDB entry code 1CFC).

1986), and calcium binding (Linse et al., 1991a; Martin et al., 1996) properties of intact CaM are well represented by a summation of those of its tryptic fragments. Therefore it has been concluded that the two domains of CaM behave as two independent units. This observation has also been confirmed by the NMR solution structures of holo-CaM (Ikura et al., 1991) and apo-CaM (Zhang et al., 1995a), in which no contacts between the two domains were detected. However, optical spectroscopy and scanning microcalorimetry studies on the stability and the calcium binding properties of CaM mutants have suggested that the two domains may interact (Martin et al., 1992; Mukherjea et al., 1996; Protasevich et al., 1997). Evidence that the presence of one domain does affect the calcium-binding properties of the other has also been reported for WT CaM in proteolytic footprinting studies (Sorensen and Shea, 1998) and for mutants of the related protein, troponin C (Moncrieffe et al., 1999).

1.1.2 Calcium binding

The EF-hand is a strongly conserved structural element widely distributed in the family of calcium binding proteins, which includes CaM, troponin C, parvalbumin, oncomodulin, calbindin, S100 proteins, and myosin light chains. The name EF-hand was introduced by R. H. Kretsinger to describe the structure of a calcium binding site involving helices E and F of parvalbumin (Kretsinger and Nockolds, 1973). This motif comprises a helix-loop-helix sequence of 29 residues and two EF-hand sites are usually associated in the same protein to yield a highly cooperative calcium binding system. The calcium binding functions are contained largely in the loop sequence, which consists of twelve consecutive residues (Falke et al., 1994). The calcium ion is coordinated by seven oxygen ligands, five of which are provided by carboxylate side-chains, one by a backbone carbonyl, and one by a water molecule. The six amino acids in the loop which are involved in calcium coordination are in positions 1, 3, 5, 7, 9 and 12. The residue in position 12 is strongly conserved and in nearly all known EF-hands is a glutamate, which contributes both its carboxyl oxygens to Ca^{2+} coordination. Two non-coordinating positions within the loop are also conserved: Gly at position 6 and the hydrophobic residue at position 8, which is predominantly Ile or Val.

In spite of the high sequence homology and structural similarity of the EF-hand motifs in calcium binding proteins, the calcium affinities of EF-hands range over four

orders of magnitude, from ~ 10^9 M^{-1} in parvalbumin to ~ 10^5 M^{-1} in the low affinity sites of CaM (Davis, 1992). One of the future challenges is to identify the features of the EF-hand motif that determine the affinity for calcium; at present, it is not possible to predict the affinity of a particular site even when the three-dimensional structure is known.

CaM contains a pair of EF-hands in each globular domain. Ca^{2+} binding sites III and IV in the C-terminal domain have higher affinity than sites I and II in the N-terminal domain (Thulin et al., 1984; Martin et al., 1985) and positive cooperativity is observed between the two sites in each domain (Linse et al., 1991a). Studies on the Ca^{2+} binding properties of CaM and its tryptic fragments Tr1C and Tr2C (corresponding to the N- and C-terminal domains of CaM, respectively) have also shown that the isolated domains of CaM retain the Ca^{2+} binding properties that they have in the intact molecule and that there is no cooperativity between the two globular domains in intact CaM (Linse et al., 1991a). The phenomenon of positive cooperativity in Ca^{2+} binding is widespread in EF-hand domains containing a pair of interacting sites. Positive cooperativity is particularly important for Ca^{2+}-sensor proteins such as CaM, because it allows the protein to exert its regulatory effect over a narrow range of calcium concentration. The intracellular [Ca^{2+}] is ~ 0.1 μM under resting conditions and increases to 1-10 μM upon stimulation (Berridge et al., 1998). At present, the mechanism which underlies positive cooperativity within EF-hand sites is not understood. It has been suggested that the short β-sheet structure which links two neighbouring calcium binding loops back to back may play an important role in cooperativity (Falke et al., 1994).

The stoichiometric (or macroscopic) Ca^{2+} binding constants for CaM can be accurately determined using the chromophoric Ca^{2+} chelator method (Linse et al., 1991a) or flow dialysis (Porumb, 1994). The values obtained using these methods are in reasonable agreement and are in the range 10^4 to 10^6 M^{-1}. The stoichiometric Ca^{2+} binding constants determined for CaM and its tryptic fragments using the chromophoric chelator 5,5'-Br_2BAPTA are listed in Table 1.1 (the chromophoric Ca^{2+} chelator method is described in Section 2.3.3 , Chapter 2).

Table 1.1 Macroscopic Ca^{2+}-binding constants for CaM and its tryptic fragments [a]

Protein	$\log(K_1)$	$\log(K_2)$	$\log(K_3)$	$\log(K_4)$	$\log(K_1K_2)$	$\log(K_3K_4)$
WT CaM	5.33	6.32	4.33	5.33	11.65	9.67
Tr1C	4.62	5.17			9.78	
Tr2C	5.32	6.21			11.53	

[a] From Bayley et al. (1996). Tr1C and Tr2C correspond to the isolated N- and C-terminal domains, respectively. Measurements were made at 20 °C in 25 mM Tris, pH 8.0, 100 mM KCl.

1.1.3 Specificity of calmodulin for calcium

In spite of the important role that Ca^{2+}-CaM plays in the regulation of a wide variety of cellular events, CaM shows a surprisingly broad specificity for binding metal ions. Many divalent as well as trivalent cations have been shown to interact with CaM (Klee, 1988; Ouyang and Vogel, 1998). They can be divided into two classes: those which, like Ca^{2+}, induce the conformational change that allows CaM to bind and activate targets and those which interact with CaM but do not induce the same conformational change and thus do not result in activation of target proteins. Among the divalent cations, many, including Cd^{2+}, Zn^{2+}, Pb^{2+}, Hg^{2+}, and Mn^{2+}, bind to CaM with relatively high affinity and are able to promote activation of target enzymes, but, when present at high concentrations inhibit CaM activity (Klee, 1988; Ozawa et al., 1999). The inhibition could be a result of binding at non-specific sites on CaM. However, it is unlikely that the binding of these metals to CaM is significant under physiological conditions, since their intracellular concentration is well below that needed for their interaction with CaM.

Among the trivalent lanthanides, Tb^{3+} has been used to study the mechanism of activation of CaM by Ca^{2+} (Martin et al., 1986). The affinity of CaM for Tb^{3+} (10^8-10^9

M^{-1}) is much higher than that for Ca^{2+}; it has been proposed that the ability of lanthanides to replace Ca^{2+} in a number of proteins arises from the similar ionic size and coordinating properties of these ions (Martin and Richardson, 1979). Unlike Ca^{2+}, Tb^{3+} binds sites I and II (N-terminal domain) with higher affinity than sites III and IV (C-terminal domain).

The specificity of EF-hands for Ca^{2+} and, when appropriate, Mg^{2+} can arise from charge or size selectivity (Falke et al., 1994). Charge selectivity is controlled by the net negative charge surrounding the ion binding site. If the cation bound to the site does not have sufficient positive charge density, electrostatic repulsion between the negatively charged residues in the loop prevents close packing of the coordinating array, thus destabilising the binding site. This is why monovalent ions such as K^+ and Na^+, which are the highest in concentration among the various metal ions inside the cell, are excluded from binding to EF-hand sites (Linse et al., 1991a; Linse et al., 1991b). Size selectivity is based on constraints imposed by the coordination number (Ca^{2+} is the only divalent ion which prefers seven-fold coordination) and by the size of the binding cavity (Falke et al., 1994).

1.1.4 Magnesium binding

Mg^{2+} is the most abundant divalent ion in mammalian cells and its intracellular and extracellular concentrations are kept nearly constant at 0.5-2 mM in most multicellular organisms (Ebel and Gunther, 1980). Mg^{2+} concentration is thus 100 to 10,000-fold in excess over cytosolic calcium concentration (~ 0.1 to 1-10 μM, see above). Several studies have shown that CaM binds Mg^{2+}, although the reported binding constants vary considerably, ranging from 10^2 to 10^4 M^{-1} (Haiech et al., 1981; Tsai et al., 1987; for reviews see Cox et al., 1984, and Klee, 1988). The affinity of CaM for Mg^{2+} is much lower than that for Ca^{2+} and spectroscopic and structural studies have shown that the binding of Mg^{2+} does not induce the major conformational changes caused by Ca^{2+} binding (Seamon, 1980; Drabikowski et al., 1982; Klee, 1988; Ohki et al., 1997). Recent NMR studies on the N-terminal domain of CaM have also indicated that the overall conformation of Mg^{2+}-bound Tr1C is similar to the "closed" apo-form, as opposed to the "open" Ca^{2+}-bound conformation (Malmendal et al., 1998; Malmendal et al., 1999b).

The mechanism of binding of Mg^{2+} to CaM is still a matter of debate and controversies concerning the number of sites and the existence (or not) of direct competition between Ca^{2+} and Mg^{2+} still exist. The generally accepted model is that Ca^{2+} and Mg^{2+} share the same binding sites on both domains, thus competing directly with each other (Haiech et al., 1981; Tsai et al., 1987; Ohki et al., 1997). Crystal and NMR structures of Mg^{2+} bound to the EF-hand proteins parvalbumin and calbindin have confirmed this model, showing that Mg^{2+} and Ca^{2+} can compete for the same sites (Declercq et al., 1991; Andersson et al., 1997). There is also strong evidence that Mg^{2+} binds more strongly to the N-terminal domain of CaM than to the C-terminal domain, showing opposite domain preference to Ca^{2+}. However, flow dialysis and microcalorimetry studies have suggested that Mg^{2+} binds to four sites which are distinct from the EF-hand Ca^{2+} binding sites (Milos et al., 1986; Gilli et al., 1998). According to this interpretation, Mg^{2+} does not act as a direct competitor for Ca^{2+} binding, but rather as an allosteric effector.

Mg^{2+} has a strong preference for 6-fold coordination in an octahedral symmetry, as opposed to Ca^{2+}, which has less stringent demands on the number of coordinating oxygen ligands (often 6-8) (Falke et al., 1994). This property of Mg^{2+} binding, together with its smaller ionic radius, probably forms the structural basis of the discrimination of Ca^{2+} binding proteins against Mg^{2+}. The crystal structures of Mg^{2+} bound to EF-hand proteins have shown that the 6-fold coordination of Mg^{2+} is achieved in a similar way to the 7-fold coordination of Ca^{2+} (Declercq et al., 1991; Andersson et al., 1997). In parvalbumin, this switch in the coordination number is enabled by the glutamate side chain at position 12 of the EF-hand loop, which provides bidentate coordination of Ca^{2+}, but rotates to yield monodentate coordination when the site is occupied by Mg^{2+}. In the calbindin D_{9k} EF-hand, the Glu at position 12 is not used for direct ligation of Mg^{2+}. An NMR study of the N-terminal domain of CaM suggests a similar coordination for CaM also, without ligation to the residue in the twelfth loop position (Malmendal et al., 1998). Mutational studies of CaM have shown that the Glu at position 12 plays an important role in the conformational change induced by Ca^{2+} binding (Martin et al., 1992; Maune et al., 1992a; Evenäs et al., 1997). This binding mode could thus explain why Mg^{2+} does not induce the major structural rearrangements that occur upon Ca^{2+} binding.

A consequence of the small effects of Mg^{2+} on the structure of CaM is that the exposure of the hydrophobic surfaces which drive the interaction of Ca^{2+}-CaM with

target molecules does not occur upon binding of Mg^{2+}. This is probably why the Mg^{2+}-CaM complex, unlike those formed with other divalent cations such as Zn^{2+}, Cd^{2+}, Pb^{2+}, Sr^{2+}, and Ba^{2+}, binds with low affinity to the target peptide corresponding to the CaM binding domain of skeletal muscle myosin light chain kinase (sk-MLCK) (Ouyang and Vogel, 1998; Ozawa et al., 1999). The possible role of Mg^{2+} in target recognition by Ca^{2+}-CaM has been investigated by NMR (Ohki et al., 1993; Ohki et al., 1997). The results have been taken to indicate that the presence of Mg^{2+} decreases the affinity of Ca^{2+}-CaM for different target peptides, and these authors suggest that Mg^{2+} could act as an inhibitor of the formation of active Ca^{2+}-CaM-target complexes.

1.2 Interaction of calmodulin with targets

An increase in intracellular Ca^{2+} concentration promotes interaction of CaM with a number of different enzymes, including protein kinases and phosphatases, NAD kinase, adenylate cyclase, nitric oxide synthase, phosphodiesterase, ion channels, calcium pumps, and cytoskeletal proteins. The mechanism by which CaM recognises and binds such a wide range of target proteins is particularly interesting, because, although no single consensus sequence for binding CaM exists, the complexes formed are highly specific and of high affinity (Crivici and Ikura, 1995). Many of the known target enzymes are regulated by a form of intrasteric inhibition, in which substrate binding is prevented by a pseudo-substrate inhibitory domain of the enzyme. Upon an increase of intracellular calcium concentration, the interaction of Ca^{2+}-CaM with the enzyme induces a conformational change that relieves the auto-inhibition, enabling the target protein to become functionally active (Crivici and Ikura, 1995). The interaction of CaM with its targets has been difficult to study at the molecular level because of the large size and the structural complexity of the target enzymes. Therefore, the information available about the structure of these complexes and the different modes of recognition has been obtained from studies of CaM interacting with model peptides and peptide fragments of the calmodulin-binding domains of several target proteins.

1.2.1 Sequence motifs for calmodulin recognition

The calmodulin-binding domains have little sequence homology, but in various targets they have been shown to be a short region of 14-26 residues with the propensity to form a basic amphiphilic α-helix (BAA motif) (O'Neil and DeGrado, 1990). The characteristic feature of a BAA motif is the presence of clusters of basic and hydrophobic residues on opposing faces of a helical region. Many of the target peptides studied are unstructured in solution and adopt a helical conformation when the complex is formed. This was first observed in CD studies, which have shown that the helicity of the complex is greater than that of the sum of the individual components (Klevit et al., 1985).

Both the hydrophobic and the charged nature of the target peptides seem to contribute to binding to CaM. In particular, the hydrophobic residues of the peptide can interact with the hydrophobic surfaces exposed in Ca^{2+}-CaM, and the positively charged residues of the peptide can make specific salt bridges with the acidic residues surrounding the hydrophobic patches on each domain of CaM. The high abundance of Met residues on the hydrophobic surfaces of Ca^{2+}-CaM may also be a key feature of target recognition and CaM's functional versatility, since the conformational flexibility of Met side chains may allow CaM to adjust to the specific structural characteristics of different peptides (O'Neil and DeGrado, 1990; Siivari et al., 1995; Yuan et al., 1998).

In a recent review, the common elements in the many reported CaM binding regions from different proteins were examined (Rhoads and Friedberg, 1997). A primary requirement for Ca^{2+}-dependent CaM binding seems to be the presence in the peptide of two hydrophobic residues that are separated by 12 intervening residues and anchor the peptide to the two domains of CaM. Based on the positions of these conserved hydrophobic residues, the Ca^{2+}-dependent CaM binding motifs can be grouped into two major classes, designated as motifs 1-8-14 and 1-5-10. Most of the high affinity Ca^{2+}-CaM binding proteins conform to the first motif, with a net charge of 3+ to 6+. The second motif is characteristic of the CaM binding region of CaM kinase II.

1.2.2 Structures of calmodulin-target peptide complexes

The solution structure of Ca^{2+}-CaM complexed with a 26-residue peptide (M13) corresponding to the CaM binding region of sk-MLCK was solved in 1992 using multidimensional NMR (Ikura et al., 1992). The structure shows that the two domains of CaM retain essentially the same conformation as that of Ca^{2+}-CaM. However, the central flexible region (residues 78-81) expands to include residues 74-82. The central linker thus allows the two domains to surround the peptide, which adopts an α-helical conformation. Therefore, the overall shape of the complex Ca^{2+}-CaM-peptide is compact. The peptide lies in a hydrophobic channel formed by the two domains of CaM and its N-terminal portion interacts predominantly with the C-domain of CaM whereas its C-terminal portion interacts with the N-domain of CaM. Two hydrophobic residues of the peptide, Trp-4 and Phe-17, separated by 12 residues, seem to fit into the hydrophobic pockets of Ca^{2+}-CaM, anchoring the peptide to the two domains of the protein. As a result of the formation of the complex, both the hydrophobic surfaces of Ca^{2+}-CaM and the sk-MLCK peptide are largely buried and most of the interactions between them involve van der Waals contacts between side chains.

Crystal structures of complexes of calmodulin with target peptides from smooth muscle MLCK (sm-MLCK) and CaM kinase II indicate similar modes of interaction (Meador et al., 1992; Meador et al., 1993). In the case of CaM kinase II, the two hydrophobic residues which anchor the peptide to the protein (Leu-10 and Leu-19) are only separated by 8 residues. To accommodate this change, the central linker region of Ca^{2+}-CaM is further unwound (residues 73-83) to enable these interactions to form. Thus, the flexible linker acts as a hinge, allowing the two domains to fold around target peptides of different length. Binding patterns similar to that of the Ca^{2+}-CaM-MLCK complexes have also been observed for peptides derived from various other target proteins, such as nitric oxide synthase and CaM kinase I (Zhang and Yuan, 1998). The peptides from these enzymes form amphiphilic α-helices and bind to Ca^{2+}-CaM in an antiparallel orientation, with the N-terminal region of the peptide interacting with the C-terminal domain of CaM (Zhang et al., 1995b).

The structure of CaM complexed with the MLCK peptides has been used as a model for the interaction of CaM with its targets and to explain much of the experimental data obtained for CaM-target complexes. However, other modes of interaction have also been observed, which are substantially different. Some target

peptides, for example, may bind CaM in a reverse orientation or without adopting a helical conformation (Crivici and Ikura, 1995). Optical spectroscopic studies of the interaction between the isolated CaM domains and peptides derived from sk-MLCK have shown that, although binding of Trp-4 of the peptide to the C-domain of CaM promotes the antiparallel orientation of the peptide in the complex, binding with opposite peptide polarity is also possible (Barth et al., 1998).

The model of a single α-helical target also fails to represent the interaction of CaM with proteins which contain two non-contiguous CaM binding domains. In the case of phosphorylase kinase, two distinct regions in the regulatory domain of the catalytic subunit (γ) have been shown to bind Ca^{2+}-CaM simultaneously (Dasgupta et al., 1989). Upon formation of the complex, CaM remains in an extended conformation, and one peptide (Phk5) adopts a helical structure, whilst the other (Phk13) is in a non-helical, elongated conformation (Trewhella et al., 1990). Thus, the overall shape of the complex is different from the collapsed structure of CaM bound to the MLCK peptide. Ca^{2+}-CaM has also been shown to interact in a similar way with caldesmon (CaD), a protein involved in the regulation of smooth muscle contraction. Ca^{2+}-CaM binds simultaneously to two non-contiguous segments of CaD and adopts an extended conformation (Krueger et al., 2000).

Novel interactions of CaM with target proteins are continuously being discovered. Very recently, the solution structure of the complex formed by Ca^{2+}-CaM and CaM-dependent kinase kinase (CaMKK) has been determined (Osawa et al., 1999). In this structure, the CaMKK peptide uses a unique CaM binding mechanism, that differs from those observed before. The fold of the peptide in the complex comprises an α-helix and a hairpin-like loop, whose C-terminus folds back onto the helix. In addition, the peptide orientation with respect to the two CaM domains is opposite to that detected in all other complexes of CaM with target peptides. The N- and C-terminal domains of Ca^{2+}-CaM interact with two hydrophobic side chains of the peptide (Trp-444 and Phe-459) separated by 14 residues. Therefore this mode of interaction represents a new and distinct class of Ca^{2+}-CaM target recognition. A novel interaction mechanism has also been found recently between CaM and the C-terminal domain of the voltage-dependent sodium channel (VDSC) α-subunit (Mori et al., 2000). The CaM binding region in this protein contains both IQ and BAA motifs. The peptide comprising the IQ motif binds both to apo-CaM and Ca^{2+}-CaM, whereas the

peptide containing the BAA sequence binds only to Ca^{2+}-CaM. It is proposed that changes in the intracellular Ca^{2+} concentration may regulate the transition between two different conformations of the complex.

1.2.3 Models for the mechanism of target activation

Calcium binding studies have shown that, in the presence of target proteins and peptides, the apparent affinity of CaM for calcium is greatly increased (Olwin and Storm, 1985; Yazawa et al., 1987; Yazawa et al., 1992; Peersen et al., 1997). This also means that the presence of calcium enhances the affinity of CaM for the target by the same factor. The extent of this effect varies depending on the specific target studied and on environmental conditions. For example, in the case of the WFF peptide from the CaM binding domain of sk-MLCK, the affinity of CaM for the peptide is increased by calcium by a factor of $\sim 10^7$ (Martin et al., 1996). Thus, the target activation properties of CaM are finely tuned by the coupled equilibria and kinetics of calcium and target binding, allowing CaM to satisfy the diverse requirements of different signalling pathways.

An important characteristic of the mechanism of target binding is the differential affinity of the interactions of the N- and C-terminal domains with calcium and with target sequences. The role of individual CaM domains in the activation of target enzymes has been extensively investigated (for a review, see Klee, 1988). When isolated, the two domains can bind target peptides and proteins with reduced affinity, but apparently both domains have to interact with the target sequence in order to have efficient activation of the enzyme. It has also been shown that, although the domains contain some common determinants for interactions with target molecules, they can make distinct contributions to target binding and activation (Newton et al., 1984; Persechini et al., 1994; Bayley et al., 1996; Barth et al., 1998). Spectroscopic studies of CaM in the presence of the peptide WFF have shown that in this complex the preferential interaction is between the C-domain of CaM and the N-terminal portion of WFF (Martin et al., 1996). Thus, the C-domain has higher affinity for calcium (see Table 1.1) and for this target sequence. Evidence for a similar binding mode has also been provided in the case of several other target sequences, with the C-domain binding to the target with higher affinity than the N-domain.

On the basis of these observations, a general mechanism for Ca^{2+}-CaM-target interaction has been proposed, in which an intermediate CaM-enzyme complex is formed at resting calcium concentrations (Bayley et al., 1996). In this complex, only the C-domain of CaM is Ca^{2+}-loaded and bound to the enzyme, whereas the N-domain of CaM is Ca^{2+}-free and not bound to the target. Under these conditions, the pseudo-substrate sequence of the enzyme is still bound to the catalytic domain and the enzyme is inactive. An increase in calcium concentration causes saturation of the N-domain and the subsequent binding of this domain to the enzyme, inducing its activation by displacing the inhibitory domain from the catalytic site. The mechanism proposed in this model allows a rapid response to transient increases of calcium concentration and suggests a possible differential role for the two domains of CaM in recognition and activation of target proteins.

1.2.4 Calcium-independent interactions with targets

CaM can also interact with proteins in a Ca^{2+}-independent manner. Neuromodulin, for example, binds to apo-CaM more tightly than to Ca^{2+}-CaM under low ionic strength conditions (Alexander et al., 1987). NMR studies have shown that the neuromodulin peptide interacts predominantly with the C-domain of CaM and adopts an α-helical conformation (Urbauer et al., 1995). A possible role for neuromodulin could be that of a plasma membrane-associated CaM trap that releases CaM into the cytosol in response to increases in Ca^{2+} concentration. Other proteins which bind to CaM in a Ca^{2+}-independent manner are neurogranin and unconventional myosins (e.g. intestinal brush border myosin I). The CaM binding sites in neuromodulin, neurogranin, and unconventional myosins contain the consensus sequence IQxxxRGxxxR, known as the IQ motif (Rhoads and Friedberg, 1997). This sequence is comprised of hydrophobic and basic residues, and both hydrophobic and electrostatic interactions are known to be crucial for binding of CaM to these target proteins. In conventional myosins, the IQ motifs are responsible for binding the regulatory and essential light chains. This motif therefore serves as a binding site for different EF-hand proteins. However, not all the proteins which bind CaM in a Ca^{2+}-independent manner contain an IQ motif and additional consensus sequences for Ca^{2+}-independent interaction are likely to exist.

Structural analysis of apo-CaM has shown that the C-terminal domain of the protein adopts a "semi-open" conformation, as opposed to the "closed" conformation of the apo-N-terminal domain (Swindells and Ikura, 1996). A similar "semi-open" conformation was previously observed in the crystal structure of the essential light chain of scallop myosin (Houdusse and Cohen, 1995). Therefore, Swindells and Ikura proposed that apo-CaM may interact with the IQ motif of its target proteins primarily through the C-terminal domain. This hypothesis agrees with the observations of Urbauer et al. (1995) on the complex of apo-CaM with the neuromodulin peptide (see above).

A different group of proteins which interact with CaM in a Ca^{2+}-independent manner is that of proteins containing CaM as a subunit that does not dissociate even at low Ca^{2+} concentration (Crivici and Ikura, 1995). An example is phosphorylase kinase (PhK), a multimeric enzyme complex with an $(\alpha\beta\gamma\delta)_4$ subunit composition (Dasgupta et al., 1989). CaM is the δ subunit of the complex and remains tightly associated with the complex at low Ca^{2+} concentration, but the activation of the catalytic subunit is Ca^{2+}-dependent.

1.3 Mutational studies of calmodulin

Site-directed mutagenesis has been widely employed in order to study structural and functional properties of proteins and to examine the role of individual residues in the conformational stability and function of the protein. The mechanisms of calcium binding and target recognition and activation by CaM have been extensively investigated in several mutational studies of CaM and CaM-target complexes.

Many of the mutagenesis studies aimed at understanding the factors contributing to CaM's calcium affinity and specificity have focused on the highly conserved bidentate Glu at position 12 of the loop. In a series of studies, this residue has been mutated to either Gln or Lys in all of the four calcium binding loops of CaM, thus generating single, double and quadruple mutants (Beckingham, 1991; Mukherjea et al., 1996). The proteins in which the Glu is replaced with a Gln are called the BQ series, and the proteins in which the Glu is replaced with a Lys are called the BK series. Calcium binding and calcium dissociation from these mutant proteins have been

studied by flow dialysis (Maune et al., 1992b), CD (Maune et al., 1992a), NMR (Starovasnik et al., 1992; Evenäs et al., 1997), and stopped flow (Martin et al., 1992). The results indicated that the mutations greatly decrease the calcium affinity of the mutated site, effectively eliminating calcium binding at this site. The mutations also decrease the calcium affinity of the other site in the same domain, with the greatest effects observed for mutations in the C-terminal domain. In addition, there is evidence that mutations in one domain affect calcium binding at the non-mutated domain, suggesting the existence of interactions between the N- and C-domains of these mutant proteins. These studies showed that the bidentate Glu plays an important structural role in the Ca^{2+}-induced conformational changes of CaM. This explains the observation that the mutations in the BQ and BK series decrease the ability of CaM to bind and activate target enzymes (Gao et al., 1993; Mukherjea and Beckingham, 1993). However, spectroscopic studies have shown that the binding of these mutant calmodulins to target peptides, although occurring with reduced affinity, restores the native structure of the proteins, compensating for the structural deficiencies introduced by the mutations (Findlay et al., 1995b).

Similar results were also obtained by Haiech et al. (1991), who mutated the Glu at position 12 in sites II and IV to Ala. These proteins bind two calcium ions only, but the binding of calcium to the mutated domain is fully recovered upon binding to a target sequence. Interestingly, it was shown that even a very conservative mutation, such as that of Asp to Glu at position 5 in loop IV, can cause a dramatic decrease of calcium affinity in the mutated site and in the paired, non-mutated site in the same domain (Wu and Reid, 1997). This mutation also induces a significant decrease in the affinity for the enzyme phosphodiesterase and a reduction in the regulatory activity. Other mutational studies (Tan et al., 1996) have addressed the coupling between calcium binding and the subsequent conformational transition by inserting disulfide bridges that lock the globular domains of CaM in its Ca^{2+}-free conformation. Tan and coworkers showed that the inhibition of the calcium-induced conformational changes results in a decrease of the calcium affinity and in the loss of ability to activate target enzymes.

The modes of interaction of CaM with target sequences and the role of specific residues in determining the affinity of CaM for targets have been investigated in several mutational studies (for a review, see Zhang & Yuan, 1998). These works showed that the Met residues which contribute significantly to the exposed hydrophobic surfaces of

Ca^{2+}-CaM are critical for the interaction with targets. The flexibility and high polarisability of the Met side chains allow the protein to accommodate targets of different sizes and to interact favourably with the solvent in the absence of targets. In addition to the Met-rich hydrophobic surfaces, the flexible linker region also plays an important role in CaM's functional versatility (Zhang & Yuan, 1998, and references therein). Studies of mutations in the central region of CaM have shown that it affects the relative orientation of the two globular domains and that its length can be adjusted to interact with one CaM binding region or with two non-contiguous sequences in a target enzyme.

Other mutagenesis studies have addressed the question of CaM's conformational stability and the relationship between stability and function. The effects of single residue mutations in the hydrophobic core of both domains of CaM were studied by replacing the hydrophobic residue at position 8 in each calcium binding loop with a Gly (Browne et al., 1997). The residue at this position contributes to the short β-sheet region which links the two loops in the same domain and forms the hydrophobic core of the domain. The results indicated that the thermal stability of the mutated domain is strongly reduced, but the binding of Ca^{2+} and of a target sequence compensates for the conformational deficiency induced by the mutation. Thus, it was shown that the stability of CaM is very sensitive to individual mutations and that the β-structure between adjacent Ca^{2+}-binding sites plays an important role in the protein's stability.

Finally, the role of electrostatic residues in the stability of apo-SynCaM was investigated by mutating residues ^{82}EEE^{84} to ^{82}KKK^{84} and ^{118}DEE^{120} to ^{118}KKK^{120} (Protasevich et al., 1997). The results showed that mutations of these charged residues in the central helix and in the C-terminal domain of apo-SynCaM alter the thermodynamic stability of the protein and also affect the conformation of the N-terminal domain, thus suggesting the existence of interdomain interactions.

1.4 Protein folding and stability

1.4.1 Protein folding

Protein folding is the process in which an extended polypeptide chain acquires compact packing through the formation of specific secondary and tertiary interactions, to give a functional three-dimensional structure. In recent years, a renewed interest in protein folding has emerged owing to the progress in molecular biology, which has provided access to thousands of new sequences. The number of possible conformations that an unfolded polypeptide chain could adopt is astronomically large and the time required for a random search of all possible conformers is much longer than is feasible on a biological time scale. This is referred to as the Levinthal paradox, and its conclusion is that proteins do not fold by sampling the entire conformational space randomly, but through some directed process (Levinthal, 1968). The "protein folding problem", then, refers to the questions how and why a protein folds in a specific native conformation and which stabilising interactions occur that prevent the protein from fluctuating between different conformations (Creighton, 1992). This problem has been addressed using two distinct approaches: one is the study of the physical chemical principles that underlie protein stability and folding pathways, and the other is the prediction of the three-dimensional structure of a protein from its amino acid sequence (Honig, 1999).

After Levinthal's argument led to a search of defined pathways, the problem of protein folding has been addressed by trying to identify and analyse metastable structures thought to be intermediate states along the folding pathway. Owing to the fast kinetics of protein folding and to the transient nature of the intermediate states, such pathways are difficult to study kinetically. However, advances in experimental kinetic techniques have made it possible to demonstrate the occurrence of intermediates and to characterise their structural properties (for a review, see Clarke and Waltho, 1997). At the beginning of the 80's, the term "molten globule" was introduced to describe intermediate states observable under equilibrium conditions (Ohgushi and Wada, 1983). A molten globule is characterised by a conformation which is slightly less compact than the native one, with a high content of native secondary structure, but a fluctuating tertiary structure (Creighton, 1992). This state has been proposed to be a general kinetic intermediate in protein folding.

On the basis of these observations, many different models have been proposed for the mechanism of folding (for reviews, see Fersht, 1997, and Yon, 1997). Among them, the "framework model" and the "diffusion-collision model" propose that local elements of secondary structure could form as early folding steps and diffuse until they collide and associate to give the tertiary structure. In contrast, the "hydrophobic-collapse model" postulates that a protein would rapidly collapse around its hydrophobic side chains, to form an intermediate state from which secondary structure can then form. The classical "nucleation model", together with the recent "nucleation-condensation model" proposed by Fersht (1997), suggests that some neighbouring residues form native secondary structure elements that act as a nucleus from which the native structure can rapidly propagate.

Although originating from different experimental and theoretical approaches, these models have similar features and, in general, three common stages in the process of protein folding can be identified, based on data available from a variety of proteins (Matthews, 1993). Initially the unfolded protein collapses to a more compact form containing hydrophobic surfaces and secondary structure elements stabilised mainly by hydrogen bonds. This species consists of an ensemble of conformations that are in dynamic equilibrium and may contain non-native structural elements. *In vitro* experiments have shown that this initial reaction normally occurs in less than 5 ms. The following phase involves further development of secondary structure and the beginning of specific tertiary interactions, with the formation of subdomains and domains not yet properly docked. This stage may consist of more than one kinetic step and occurs in the 5-1000 ms time range. The final stage corresponds to the formation of non-covalent interactions throughout the protein, which result in a compact packing of the interior of the protein and in the active three dimensional structure.

The "classical view" of protein folding is based on phenomenological kinetic models and on experimental techniques which probe the average behaviour of proteins. According to this view, protein folding is a set of mechanistically defined steps which proceed via a limited number of intermediates and a well defined pathway (Shakhnovich, 1997). Recently, new statistical mechanics models and advances in the experimental methods have led to a "new view" of the kinetics of protein folding (Dill and Chan, 1997). This new view regards the macroscopic states (such as the native, unfolded or intermediate states) as statistical distributions of individual chain conformations and replaces the pathway concept of sequential events with the funnel

concept of parallel events. According to this theory, proteins reach their native conformation by a progressive organisation of an ensemble of partly folded structures down a folding funnel. Folding is thus considered as a multi-pathway diffusion-like process in which a single stable macroscopic state (the native state) can be reached by multiple routes in conformational space.

However, the term "neo-classical view" has been recently coined (Pande et al., 1998), to emphasise the point that the use of statistical mechanics ensembles and the results of lattice models are not necessarily inconsistent with the classical pathway concept. Indeed, the picture emerging from recent experimental progress is remarkably consistent with older ideas, such as the formation of secondary structure elements or the hydrophobic collapse of the denatured state as early events in the folding process (Honig, 1999).

The study of protein refolding *in vitro* has always been accompanied by the question of whether biosynthetic folding *in vivo* occurs with the same mechanism. According to Anfinsen's postulate, all the information necessary to achieve the native three-dimensional structure of a protein in a given environment is contained in its amino acid sequence, and neither external factors nor the input of energy are required to attain this conformation (Anfinsen, 1973). However, protein factors are, in fact, involved in polypeptide folding inside the cell. The molecular chaperones, for example, bind partially unfolded proteins in order to prevent improper folding and subsequent aggregation (Yon, 1997, and references therein). The effect of molecular chaperones on folding intermediates is best understood in the case of the Hsp60/Hsp10 proteins in bacteria (GroEL/GroES in *E. coli*), mitochondria, and chloroplasts (Seckler and Jaenicke, 1992, and references therein). Other enzymes and polypeptide binding proteins also contribute to the protein folding process *in vivo*, thus allowing the newly synthesised polypeptide chains to reach their destination inside the cell and to acquire their functional three-dimensional structure. Nevertheless, experimental results have shown that only a small fraction of proteins requires the presence of a chaperone to fold correctly and recent studies have indicated that spontaneous folding *in vivo* is governed by the same principles as protein refolding *in vitro* (Hartl, 1996).

1.4.2 Kinetic studies of protein folding

The kinetics of the unfolding and refolding reactions of a variety of proteins have been intensively studied with the aim of characterising folding pathways, populated intermediates and transition states. Refolding or unfolding *in vitro* are initiated by rapidly transferring a protein from denaturing conditions to an environment in which the native conformation is favoured, or vice versa. This is usually achieved using a stopped-flow mixing device and these processes are often studied as functions of denaturant concentration. For a simple, one-step reaction (U $\leftrightarrow$ N) with no intermediates, the reciprocal relaxation time (τ^{-1}) is the sum of the forward and reverse rate constants. These rate constants are thus measured at different denaturant concentrations and then extrapolated to non-denaturing conditions in order to have the rates of folding and unfolding in the absence of denaturant. As the concentration of denaturant is increased, unfolding becomes more rapid whilst refolding becomes slower (Clarke and Waltho, 1997).

The stopped-flow technique limits the experimental observations to timescales of milliseconds and longer. However, many steps in the process of protein folding occur on much faster timescales and are complete within the dead time of rapid mixing devices (~ 1 ms). The study of fast events in protein folding has only recently become possible with the development of new time-resolved experimental methods, such as laser photolysis, optical electron transfer, and laser-induced temperature jump (for reviews see Plaxco and Dobson, 1996; Eaton et al., 1997; Callender et al., 1998). These techniques are capable of initiating and monitoring the fast events in protein folding with temporal resolution down to picoseconds. These new approaches have shown that sub-millisecond processes in protein folding include the collapse of the polypeptide chain and the formation of structural elements such as helices, β structure, turns, and loops. They have also provided evidence that the formation of secondary and tertiary structures can take place on nanosecond and microsecond timescales, respectively. An upper limit on the rate of protein folding has recently been proposed based on new experiments on the rate of intrachain diffusion (Hagen et al., 1996; McCammon, 1996). Hagen and coworkers have suggested that the time required for a random-coil protein to collapse to a compact structure cannot be shorter than ~ 1 μs. As new fast kinetic methods are refined and become more generally available, the knowledge of the folding

process improves and a detailed description of the complex dynamics of protein folding becomes possible.

1.4.3 Methods of denaturation and data analysis

The native structures of proteins are stabilised by a combination of hydrogen bonds, van der Waals interactions, electrostatic interactions and the hydrophobic interaction. However, under physiological conditions the folded structures are only marginally stable and can often be disrupted by changes in the environment, such as a rise in temperature, variation of pH, increase in pressure or the addition of denaturing agents. This process is called denaturation, it is usually reversible and does not involve changes in the covalent structure of the protein (Creighton, 1993).

Although the denatured state of a protein has no definite structure, but only an averaged, fluctuating conformation that is very labile, in most cases it is far from being a random coil, defined as a state in which no interactions occur between side chains. In fact, there is evidence that even under extreme denaturing conditions the unfolded state can retain significant amounts of secondary structure, some of which involve non-native interactions (Shortle, 1996). Moreover, denatured states obtained under various unfolding conditions can have different physical properties, although they are indistinguishable thermodynamically, having the same enthalpy and heat capacity (Creighton, 1993). In particular, it has been shown that the thermally unfolded forms of several proteins have residual non-random structure, whereas proteins unfolded using chemical denaturants, such as urea or guanidine hydrochloride (GuHCl), seem to approach more closely the random coil behaviour (Matthews, 1993, and references therein). Thus, GuHCl and urea seem to be more effective in disrupting the non-covalent interactions that define the native structure.

Despite intensive investigation, the mechanism by which chemical denaturants destabilise the folded conformations of proteins is not yet fully understood. It is not clear whether the effect of these agents on proteins is indirect and involves a change in the properties of the solvent, or is direct and can be regarded as ligand binding. At high concentrations, denaturants can cause substantial changes in the behaviour of aqueous solvents, by disrupting the dynamic network of hydrogen bonds of water (Creighton, 1993). Moreover, it has been shown that urea and GuHCl interact with both polar and

non polar surfaces more favourably than water does. As a consequence, urea and GuHCl increase the solubility of polar and non polar molecules in proportion to their accessible surface areas. Thus, unfolding may occur because all of the constituent parts of a protein are more soluble in urea and GuHCl solutions than in water. These effects would indirectly perturb the folded conformation of proteins through changes in the properties of the solvent.

However, evidence has also been provided that denaturants can interact directly with proteins. Crystallographic studies have shown that GuHCl and urea bind to ribonuclease A and dihydrofolate reductase, respectively, and that the two denaturants have similar effects on the native structures of the proteins (Dunbar et al., 1997). The results indicated that both GuHCl and urea form hydrogen bonds to the protein, but van der Waals interactions are also observed. In addition, the denaturants interact with both the protein side chains and the backbone and it does not appear that any particular type of amino acid is a preferential target for denaturant binding. NMR studies have also shown that urea interacts directly with proteins (Dotsch et al., 1995). Finally, a recent calorimetry study has also suggested a model in which urea denatures proteins by decreasing the hydrophobic effect and by directly binding to the protein via hydrogen bonds (Zou et al., 1998).

For most small globular proteins, denaturation has been shown to approach closely a two state unfolding mechanism, $N \leftrightarrow U$, in which only the native (N) and the unfolded (U) states are significantly populated at equilibrium (Pace, 1986). The transition from N to U (or vice versa) is usually highly cooperative. The conformational stability of a protein is defined as the difference in free energy between these two states under physiological conditions: $\Delta G = G_U - G_N$. For most globular proteins ΔG is between 5 and 15 kcal/mol (Pace, 1990). It has been suggested that the relatively low stability of the folded conformation of these proteins could be an important factor contributing to their turnover in the cell, or could provide the basis of flexibility in their function.

In chemical unfolding experiments, ΔG is measured over a range of denaturant concentration and the free energy of unfolding in water ($\Delta G°$) is then obtained by extrapolation. Four methods have been proposed for the analysis and interpretation of chemical denaturation data:

1) The simplest model is the **Linear Extrapolation Method (LEM)**, which assumes a linear dependence of the ΔG of unfolding on the denaturant concentration and is empirical in nature. The equation used to fit the data is:

$$\Delta G = \Delta G° + m\,[D]$$

where m is a negative number which indicates the dependence of the free energy on the denaturant concentration [D]. The m values collected for a large number of proteins have been shown to correlate strongly with the change in the accessible surface area upon unfolding and with the change in heat capacity at constant pressure, ΔC_p (Myers et al., 1995). Hence, the m values may be affected by the extent of solvent accessibility of the denatured state (Shortle and Meeker, 1986; Wrabl and Shortle, 1999).

2) The **Tanford model** is based on studies of the transfer of amino acids and peptides from water to aqueous urea or GuHCl solutions (Tanford, 1970). As noted above, the solubility of these model compounds is observed to increase with increasing urea or GuHCl concentration and this could explain the ability of these chemicals to unfold proteins. The equation used in this model is:

$$\Delta G = \Delta G^{o} + \overline{\alpha} \sum_{i} n_i \, \delta g_{tr,i}$$

where $\delta g_{tr,i}$ is the free energy for transfer of a group of type i from water to denaturant, n_i is the total number of groups of type i present in the protein, and $\overline{\alpha}$ is an average value of the fractional change in the degree of exposure of the different groups when the protein unfolds. The estimates of $\Delta G°$ obtained with this model from GuHCl-induced denaturation curves are usually greater than those from urea-induced denaturation experiments.

3) The **Denaturant binding model** assumes that the denaturant molecules bind to a discrete number of sites on the protein (Aune and Tanford, 1969). Unfolding is thought to occur because more binding sites are exposed to the solvent in the unfolded form than in the native form. If the sites are identical and non-interacting, it follows that:

$$\Delta G = \Delta G° - \Delta n\, RT \ln (1 + ka)$$

where Δn is the difference in the number of denaturant binding sites on U and N, k is the equilibrium constant for binding at each site, and a is the activity of the denaturant.

The values of $\Delta G°$ calculated with this method are in good agreement with the ones obtained with the Tanford model. Thus, also in this case different estimates for $\Delta G°$ are obtained using GuHCl and urea. Both models 2) and 3) predict an upward curvature in the dependence of ΔG on denaturant concentration and therefore give a larger estimate of $\Delta G°$ than determined by the LEM.

4) The **Solvent-exchange model** is similar to the denaturant binding model, since it also assumes that proteins have a definite number of independent denaturant binding sites (Schellman, 1994; Schellman and Gassner, 1995). However, this model considers the action of denaturants as more similar to solvation than binding. Thus, a distinguishing feature of model 4) is the formal inclusion of solvent in the reaction between protein and denaturant.

At present it is not clear which of these methods gives the best estimate for $\Delta G°$. The LEM always gives the lowest estimate for $\Delta G°$ and, in the case of GuHCl, the difference between the models seems to be more pronounced (Pace, 1986). The results obtained from calorimetric studies of thermal denaturation agree either with the LEM or with the other two models, depending on the protein under study. However, the LEM presents the advantage of being very simple and of giving similar values for $\Delta G°$ from GuHCl and urea denaturation curves. Therefore this method is the most frequently used in studies of protein unfolding (Myers et al., 1995).

In the case of thermal unfolding, the stability of a protein is measured as a function of temperature. The model which describes the changes in free energy (ΔG), enthalpy (ΔH) and entropy (ΔS) with temperature for a two-state unfolding transition is based on the thermodynamic relation $\Delta G = \Delta H - T\Delta S$, and on the assumption that the change in heat capacity at constant pressure, ΔC_p, is constant within experimental error (Privalov and Khechinashvilli, 1974). This is called the "model of constant ΔC_p" and the free energy of unfolding is related to temperature through the Gibbs-Helmholtz equation (Schellman, 1987):

$$\Delta G = \Delta H_o - T\Delta S_o + \Delta C_p(T - T_o - T \ln (T/T_o))$$

where ΔH_o and ΔS_o are the values of ΔH and ΔS at any reference temperature T_o.

1.4.4 Stability of calmodulin

The conformational stability of a protein is obviously related to its structural and functional properties. Knowledge of the effect of environmental factors and the binding of ligands on the native conformation of a protein such as CaM may be essential for understanding its conformational adaptability and the regulatory mechanism mediated by this protein. However, the conformational stability of CaM has not yet been characterised thoroughly.

Previous investigations on the stability of CaM and its fragments, performed with optical spectroscopy and/or microcalorimetry, showed that Ca^{2+}-CaM has a very high thermal stability, with a transition midpoint higher than 90 °C for both domains (Brzeska et al., 1983; Tsalkova and Privalov, 1985; Martin and Bayley, 1986). These studies also showed that in the absence of Ca^{2+}, CaM is much less stable and the melting temperature is more than 40 °C lower than in the presence of Ca^{2+}, thus indicating that the binding of Ca^{2+} has a dramatic stabilising effect. Brzeska and coworkers (1983) also reported the melting temperatures for CaM and its isolated domains in the presence of Mg^{2+}, which was shown to have an effect similar to but smaller than that of Ca^{2+}. Tsalkova and Privalov (1985) reported similar conclusions about the effects of Ca^{2+} and Mg^{2+}; according to their results, the thermal unfolding profiles for CaM correspond to three distinct transitions, which they assigned to the unfolding of the N-terminal domain and of sites III and IV in the C-terminal domain of CaM.

Chemical unfolding experiments have also been performed in previous studies on CaM's stability. Urea denaturation curves showed that apo-CaM was completely unfolded at 6 M urea, whereas Ca^{2+}-CaM retained 60% of its structure at this urea concentration (Martin and Bayley, 1986). A similar increase in CaM's stability was also obtained in the presence of Cd^{2+}, which behaves as a close analogue of Ca^{2+}.

Several studies have also concluded that the apo N-domain is more stable than the apo C-domain both when isolated (Brzeska et al., 1983; Sorensen and Shea, 1998) and in the intact protein (Browne et al., 1997; Protasevich et al., 1997). NMR studies on the structure of apo-CaM confirmed these observations, showing that the core of the C-domain is more solvent-exposed and dynamic than that of the N-domain (Urbauer et al., 1995) and that the backbone amide hydrogen exchange rates are much faster in the

C-domain (Kuboniwa et al., 1995). Kuboniwa and coworkers also observed a minor conformer for the C-domain, in which helix F in site III is not formed.

All the studies mentioned above have approached the problem of the thermodynamic stability of CaM with different methods and have reached similar conclusions about the stability properties of CaM and its globular domains. However, these observations have been made under different experimental conditions and have failed to characterise fully the effects of environmental factors and ligand binding on CaM's stability. Moreover, none of the previous reports have investigated the mechanism and the kinetic properties of CaM's unfolding and refolding processes. A systematic study of these aspects is therefore needed. The characterisation of the conformational stability of CaM as a function of solvent conditions will provide significant insights on the ligand binding and target activation properties of this protein. Finally, the study of the folding mechanism of a two-domain protein such as CaM addresses general questions related to protein folding, such as the stability of an isolated domain relative to that of the whole protein, and the relationship between ligand binding and stability.

1.5 Aims of this work

The aim of this work is to characterise quantitatively the conformational stability of CaM and its constituent domains as a function of binding of ligands, such as Ca^{2+}, Mg^{2+}, and target sequences. In particular, the objectives of this work are:

- to measure the thermodynamic stability of CaM under different solvent conditions and characterise the effect of environmental factors such as temperature, ionic strength and pH on the stability of the protein;
- to investigate the relative stability of the N- and C-terminal domains of CaM when isolated and when in the intact protein;
- to rationalise the effects of ligand binding (Ca^{2+}, Mg^{2+}, and target peptides) on CaM's stability;

- to study the interactions of CaM with Mg^{2+}, in order to understand the possible physiological role that it exerts in the stability and target activating properties of CaM;
- to measure the effects of single mutations on the stability of CaM and to characterise the folding and Ca^{2+} binding properties of a series of CaM mutants (β-sheet mutants).

The experimental approach involves equilibrium studies on the stability of CaM and its isolated domains using thermal and chemical denaturation, monitored spectroscopically using far-UV CD and tyrosine fluorescence and absorption. The kinetic properties of the processes of unfolding/refolding and of Ca^{2+} dissociation are measured using the stopped-flow technique. Finally, the interactions of CaM with Ca^{2+}, Mg^{2+}, and target sequences are investigated using direct titration methods, the chromophoric chelator method, and competition assays.

CHAPTER 2

MATERIALS AND METHODS

2.1 Materials

2.1.1 Chemicals

All standard chemicals used in this work, including the denaturants guanidine hydrochloride (GuHCl) and urea, were obtained from local suppliers and were of the highest purity commercially available. Calcium and magnesium solutions were prepared by dilution from standard volumetric solutions (BDH). The sources of all other materials are indicated at the appropriate point in the following sections. The standard calcium-containing buffer used in this work consisted of 25 mM Tris, 100 mM KCl, and 1 mM $CaCl_2$ (pH 8.0). The standard calcium-free buffer consisted of 25 mM Tris, 100 mM KCl (pH 8.0), treated with Chelex-100 (Sigma) to remove residual calcium (see Section 2.1.2).

2.1.2 Preparation of Ca^{2+}-free buffer

All buffers for experiments with the apo-proteins were treated with Chelex-100 (Sigma) to reduce contaminating calcium to acceptable levels. The residual calcium concentration was then estimated using the chromophoric calcium chelator 5,5'-Br_2BAPTA (Calbiochem), with the following procedure:

- A solution of 5,5'-Br_2BAPTA (~ 30 μM) in Ca^{2+}-free buffer was prepared and its absorbance was measured at 263 nm (A_1);
- EDTA was then added to a final concentration of ~ 80 μM to produce calcium-free chelator, and the absorbance of this solution was measured at 263 nm (A_2);
- $CaCl_2$ was then added to give a final concentration of ~ 800 μM (i.e., in excess over both 5,5'-Br_2BAPTA and EDTA) to produce calcium-saturated chelator, and the absorbance of this solution was measured at 263 nm (A_3) and at 239 nm.

The absorbance at 239 nm was used to calculate an accurate value for the 5,5'-Br_2BAPTA concentration, using $\varepsilon_{239} = 1.6 \times 10^4\ M^{-1}cm^{-1}$. After appropriate correction for dilution, an approximate value for the residual calcium concentration was then calculated as:

$$[Ca^{2+}] = [BAPTA](A_2 - A_1)/(A_2 - A_3)$$

Residual calcium contamination was always less than 2 μM.

2.1.3 Purification of WT calmodulin

Drosophila melanogaster CaM was cloned by Dr. Dai-Rong Su and the clone was a gift from Prof. Kathy Beckingham (Rice University, Houston, Texas, USA). The protein was over-expressed in *Escherichia coli* using the method described in Browne et al. (1997) and was purified using the following affinity chromatography procedure. 100 g of cells from a 40 litre bacterial culture were resuspended in 400 ml of a buffer consisting of 25 mM Tris, 50 mM KCl, 1 mM $CaCl_2$, and 1 mM PMSF (pH 7.5). The cells were then broken by sonication and centrifuged at 4° C for 30 minutes in a Beckman 45 Ti rotor (40,000 rpm). The supernatant was made to 500 mM KCl and 2 mM $CaCl_2$ and loaded onto a 200 ml phenyl sepharose affinity column (Pharmacia), pre-equilibrated in a buffer consisting of 25 mM Tris, 500 mM KCl, and 2 mM $CaCl_2$ (pH 7.5). After washing the column extensively with the equilibration buffer, CaM was

eluted using a buffer consisting of 25 mM Tris, 500 mM KCl, and 5 mM EDTA (pH 7.5). CaM-containing fractions were identified using Bradford reagent, UV absorption spectroscopy, and SDS gel electrophoresis, and were concentrated using Amicon Diaflow equipment. Additional purification was achieved by using a second phenyl sepharose column. Finally, the sample was loaded onto a Sephadex G-75 gel filtration column (Pharmacia; 100 × 2.6 cm column, 0.25 ml/min flow rate) that had been pre-equilibrated with a buffer consisting of 25 mM Tris, 100 mM KCl, and 1 mM $CaCl_2$ (pH 7.5), and was eluted with the same buffer. This final purification step was used to remove the small amount of contaminating high molecular weight proteins still present, thereby producing CaM of very high purity (>99%). The purity of the samples was routinely assessed using absorption spectrophotometry, SDS gel electrophoresis, and mass spectrometry.

2.1.4 Preparation of Ca^{2+}-free calmodulin

Ca^{2+}-free calmodulin (apo-CaM) was prepared by treating samples of 1 - 1.5 mM CaM (in 1 mM Ca^{2+}) with ~ 8 mM EDTA. The sample was then desalted using a Pharmacia G-25 PD-10 column previously equilibrated with Ca^{2+}-free standard buffer. Apo-CaM concentrations were determined using extinction coefficients of 1874 M^{-1} cm^{-1} at 279 nm and 2179 $M^{-1}cm^{-1}$ at 259 nm (Maune et al., 1992b).

2.1.5 Preparation of calmodulin fragments

The fragments corresponding to the N-domain (Tr1C) and to the C-domain (Tr2C) of calmodulin were prepared by trypsin digestion using a modification of the method described by Persechini et al. (1994). CaM at a concentration of 0.5 mg/ml was cleaved in a buffer containing 40 mM NH_4HCO_3 and 1 mM $CaCl_2$ by adding bovine pancreas trypsin (Sigma) to a final concentration of 2 μg/ml and incubating for 45 min at 30 °C. The trypsinolysis reaction was terminated by adding soy-bean trypsin inhibitor (Sigma) to a concentration of 10 μg/ml. The digest was loaded onto a Pharmacia Mono Q ion exchange column pre-equilibrated in 25 mM Tris and 1 mM $CaCl_2$ (pH 8.0) at room temperature. Bound proteins were eluted at a flow rate of 1 ml/min by linearly increasing the NaCl concentration from 0 to 500 mM at a rate of

2%/min. The column fractions containing the fragments Tr1C or Tr2C were identified using absorption spectroscopy and then pooled and further purified by repeating the ion exchange chromatography step. In this second purification step, the conditions described above were used for Tr1C, except that the NaCl concentration was increased linearly from 0 to 250 mM at a rate of 1%/min. For Tr2C, the column was equilibrated with 25 mM Tris and 0.1 mM EDTA rather than 1 mM $CaCl_2$. In the absence of calcium, Tr2C elutes at an NaCl concentration 60 mM higher than in the presence of calcium, allowing good separation of Tr2C and soy-bean trypsin inhibitor. The fractions containing Tr1C or Tr2C were pooled and concentrated using an Amicon Centriprep device with a M_r 3000 cut-off membrane. The purity of the samples was assessed by HPLC chromatography and mass spectrometry, which both showed the absence of contaminants. Mass spectrometry indicated that the predominant fragment for the Tr1C preparation was residues 1-75 of calmodulin and, for the Tr2C preparation, residues 78-148. The concentration of Tr2C was determined by absorption spectroscopy, using the same extinction coefficient as for intact CaM (i.e., 1578 M^{-1} cm^{-1} at 279 nm for the Ca^{2+}-loaded form). For Tr1C, which lacks tyrosine and tryptophan, the extinction coefficient for four phenylalanines was calculated to be 690 $M^{-1}cm^{-1}$ at 259 nm (Gill and von Hippel, 1989).

2.1.6 Preparation of calmodulin mutants

Cloning, expression and purification of the mutant proteins CaM(I27G), CaM(I63G), CaM(I100G), CaM(V136G), CaM(V136A), and CaM(V136P) were performed by J.P. Browne and M.C. Frise as described in Browne et al. (1997). The proteins were purified using the procedure described for WT CaM (Section 2.1.3). For I63G and V136G an additional ion exchange chromatography step was used in order to separate small amounts of proteolytic fragments of CaM from the intact protein. This ion exchange chromatography was performed on a 5/5 Mono Q column (Pharmacia) with a 40 min 50-500 mM KCl gradient in 25 mM Tris, 1 mM $CaCl_2$ (pH 7.5). The purity of the samples was routinely assessed by SDS gel electrophoresis and mass spectrometry. The concentration of the N-domain mutant calmodulins was determined by absorption spectroscopy, using the same extinction coefficients as for WT CaM (i.e. ε_{259} = 2120 M^{-1} cm^{-1} and ε_{279} = 1578 M^{-1} cm^{-1} for Ca^{2+}-saturated protein), assuming

that the mutations in the N-domain would not affect the optical properties of the Phe's and of Tyr-138 in the C-domain. The concentration of the C-domain mutants was determined either using the extinction coefficient of WT CaM at 259 nm, or the extinction coefficients calculated for a 9:1 mixture of Phe and Tyr (see Section 3.3.1, Chapter 3).

2.1.7 Peptides

The peptides WFF_u (KRRWKKNFIAVSAANRFK), FFF_u (KRRFKKNFIA VSAANRFK), and NM2 (Ac-ATKWQASFRGHITRKKLKG-NH_2) were synthesised on an Applied Biosystems 430A peptide synthesizer and purified by HPLC on a C18 column. Purity was assessed by HPLC and mass spectrometry. Concentrations were determined spectrophotometrically using calculated extinction coefficients of 5560 $M^{-1}cm^{-1}$ at 280 nm for NM2 and WFF_u (1 tryptophan) and 517.5 $M^{-1}cm^{-1}$ at 259 nm (3 phenylalanines) for FFF_u (Gill and von Hippel, 1989). WFF_u is an 18 residue peptide corresponding to part of the CaM binding sequence of skeletal muscle myosin light chain kinase and FFF_u is WFF_u with a W4F substitution (Findlay et al., 1995a). NM2 is a 19 residue peptide corresponding to the CaM binding sequence of neuromodulin but with an I4W substitution (Chapman et al., 1991).

2.2 Experimental techniques

2.2.1 Absorption spectroscopy

Absorption spectra were recorded using a Cary 3E UV/Visible spectrophotometer. The measurements were made in 10 mm fused silica cuvettes at 20 °C. All spectra were corrected for Rayleigh light scattering contributions using a non-linear least squares fitting procedure which assumed that the contribution from scattering was proportional to λ^{-4}. The concentration of CaM samples was determined from the corrected absorption spectra using the following extinction coefficients: ε_{259} = 2179 M^{-1} cm^{-1} and ε_{279} = 1874 M^{-1} cm^{-1} for Ca^{2+}-free CaM and ε_{259} = 2120 M^{-1} cm^{-1} and ε_{279} = 1578 M^{-1} cm^{-1} for Ca^{2+}-saturated CaM (Maune et al., 1992b).

2.2.2 Fluorescence spectroscopy

The intrinsic fluorescence of proteins derives principally from the aromatic residues Tyr and Trp. Both the quantum yield (fluorescence intensity) and the wavelength of maximum emission can be affected by changes in the environment of the side chain. In the case of Trp, for example, the position of the emission maximum is often taken as a measure of the extent to which the Trp is buried in the protein interior. The emission maximum of Trp can vary from ~ 355 nm, when Trp is exposed to water, to ~ 322 nm, when it is totally buried. In the case of Tyr, changes in the environment can affect the quantum yield but the emission maximum generally remains at approximately 306 nm. Thus, fluorescence spectroscopy can be a sensitive probe of perturbations of the folded state of a protein.

The fluorescence signal of *Drosophila* calmodulin derives entirely from Tyr-138, which is situated in the C-terminal domain. Therefore fluorescence measurements monitor changes in the environment of Tyr-138 and give specific information about the C-domain. Fluorescence emission spectra were recorded using a SPEX FluoroMax fluorimeter, with excitation at 280 nm (bandwidth 1.7 nm) and emission scanned from 290 to 400 nm (bandwidth 5 nm). UV-transmitting plastic cuvettes were employed, with a pathlength of 1 cm. CaM concentrations used were in the range 10-20 μM. In order to improve signal to noise ratio, denaturant titrations were performed by recording time scans with excitation at 280 nm and emission at 320 nm for a total time of 1 minute for each scan. GuHCl and urea gave a background signal which was measured in control titrations and then subtracted from the signal of the sample.

2.2.3 Circular dichroism spectroscopy

The circular dichroism (CD) spectra of proteins in the far-UV region of the spectrum (190-250 nm) derive almost entirely from the amide chromophore, with (usually) small contributions from aromatic residues (Yang et al., 1986). These spectra reflect protein secondary structure and the far-UV CD spectrum of a protein can be used to estimate its secondary structure content (Greenfield, 1996). The near-UV CD bands of proteins (250-340 nm) arise from Phe, Tyr, Trp, and cystinyl groups, and they reflect the tertiary and quaternary structure of the protein. CD intensities in this region depend on the extent to which the residue is mobile (protein rigidity) and the extent to

which the aromatic ring interacts with its surroundings (Strickland, 1974). The far- and near-UV CD signals are therefore sensitive probes of protein secondary and tertiary structure respectively.

CD measurements were performed using a Jasco J-715 spectropolarimeter. Far-UV CD spectra were recorded at 20 °C using 1 or 10 mm fused silica cuvettes with CaM concentrations in the range 5-10 μM. Near-UV CD spectra were measured using 1 cm cuvettes with CaM concentrations in the range 400-600 μM. For each spectrum, four scans were averaged and the baseline subtracted. CD intensities are presented as the CD absorption coefficient calculated using the molar concentration of protein (= $\Delta\varepsilon_M$) rather than on a mean residue weight (MRW) basis. Values of $\Delta\varepsilon_{MRW}$ may be calculated as $\Delta\varepsilon_{MRW} = \Delta\varepsilon_M/N$, where N is the appropriate number of peptide bonds (= 74, 70, and 147 for Tr1C, Tr2C, and CaM, respectively).

2.2.4 Stopped flow

The stopped flow technique is a rapid mixing method in which reactions can be monitored on the millisecond to second time scale. In this technique two solutions are rapidly mixed and then the flow of the mixed reactants is abruptly stopped by the use of a back syringe. After the flow stops, the reaction is followed in real time with a suitable fluorescence or absorbance detection system. The dead-time of the instrument is defined as the age of the solution at the instant of stopping and it is the shortest time from which reactions can be monitored. It is typically in the range 1-6 ms.

In this work kinetic measurements were performed using a Hi-Tech SF-61MX Multi-Mixing stopped flow spectrofluorimeter. The dead-time of the instrument is ~ 2 ms. The excitation monochromator was set to 280 nm and the emission of Tyr-138 was monitored using a cut-on filter at 310 nm. The measurements were performed at 20 °C and all concentrations quoted in the results sections of Chapters 3, 4 and 5 are those after the 1:1 stopped-flow mixing.

2.3 Theory and experimental procedures

2.3.1 Calcium binding to calmodulin

The binding of four calcium ions to CaM may be described using either stoichiometric (macroscopic) or intrinsic (microscopic or site) association constants. The mathematical relationship between these constants, and other important features of the calcium binding process, are described in this section.

2.3.1.1 Stoichiometric and intrinsic binding constants

The four stoichiometric (macroscopic) association constants for calcium binding are defined in the following scheme:

$$CaM \xleftrightarrow{K_1} Ca\text{-}CaM \xleftrightarrow{K_2} Ca_2\text{-}CaM \xleftrightarrow{K_3} Ca_3\text{-}CaM \xleftrightarrow{K_4} Ca_4\text{-}CaM$$

with

$$K_1 = [Ca\text{-}CaM] / ([CaM][Ca])$$
$$K_2 = [Ca_2\text{-}CaM] / ([Ca\text{-}CaM][Ca])$$
$$K_3 = [Ca_3\text{-}CaM] / ([Ca_2\text{-}CaM][Ca])$$
$$K_4 = [Ca_4\text{-}CaM] / ([Ca_3\text{-}CaM][Ca])$$

The intrinsic (microscopic or site) association constants are defined in the scheme shown in Figure 2.1. k_I, k_{II}, k_{III}, and k_{IV} are the intrinsic association constants for a calcium ion binding to sites I, II, III, IV, respectively, when all the other sites are empty. $k_{II(I)}$ is the intrinsic association constant for Ca^{2+} binding to site II when site I is occupied, $k_{III(I,II)}$ is the intrinsic association constant for Ca^{2+} binding to site III when sites I and II are occupied, and so on. The large number of constants required can be reduced dramatically by introducing interaction (or cooperativity) factors that define the effect of occupancy of one site on the affinity at another. Thus, the factor $\alpha_{I,II}$ defines the effect of occupancy of site II on the affinity at site I, and so on. Then, for binding at site I for example:

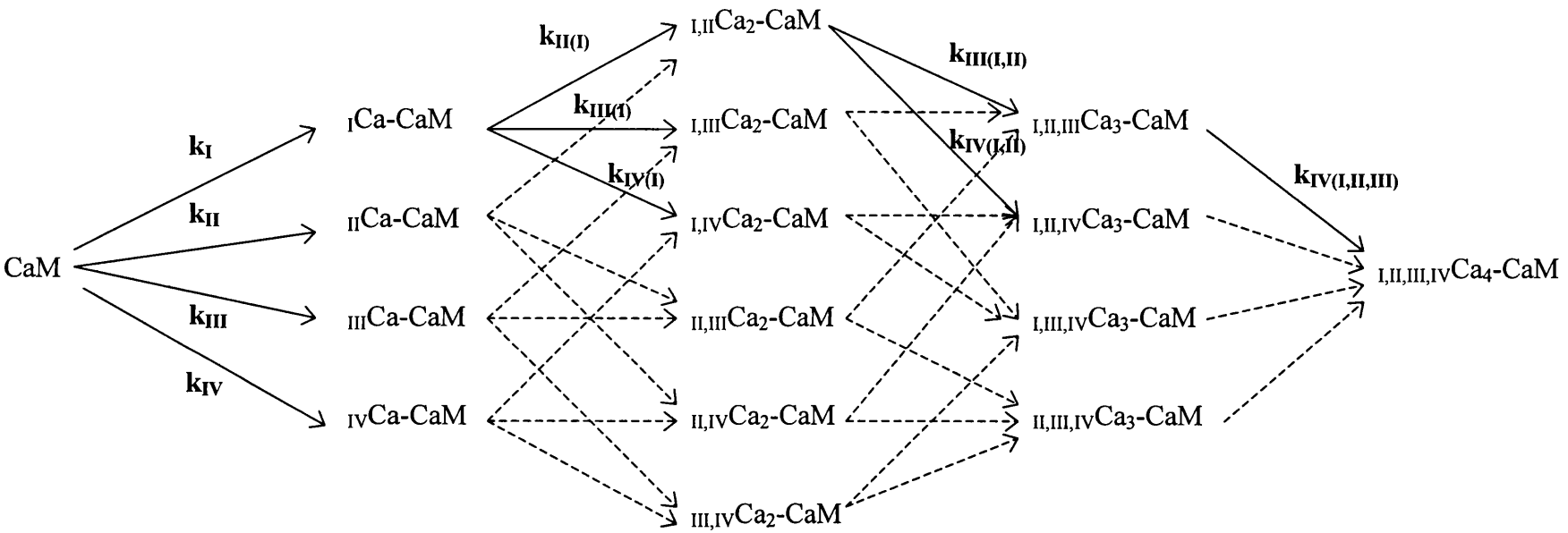

Figure 2.1 Schematic representation of Ca^{2+} binding to CaM. The subscript after Ca indicates the total number of Ca^{2+} ions bound. The subscript before Ca indicates the sites which are occupied by calcium. k_I, k_{II}, k_{III}, and k_{IV} are the intrinsic association constants for a Ca^{2+} ion binding to site I, II, III, and IV, respectively, when all the other sites are empty. $k_{II(I)}$ is the intrinsic association constant for Ca^{2+} binding to site II when site I is occupied, $k_{III(I,II)}$ is the intrinsic association constant for Ca^{2+} binding to site III when sites I and II are occupied, and so on. For simplicity, only a few intrinsic association constants are indicated.

$k_{I(II)} = k_I\alpha_{I,II}$ $k_{I(III)} = k_I\alpha_{I,III}$ $k_{I(IV)} = k_I\alpha_{I,IV}$

$k_{I(II,III)} = k_I\alpha_{I,II}\alpha_{I,III}$ $k_{I(II,IV)} = k_I\alpha_{I,II}\alpha_{I,IV}$ $k_{I(III,IV)} = k_I\alpha_{I,III}\alpha_{I,IV}$

$k_{I(II,III,IV)} = k_I\alpha_{I,II}\alpha_{I,III}\alpha_{I,IV}$

Only six interaction factors are necessary in all because, for example, $k_Ik_{II}\alpha_{II,I}$ must be equal to $k_{II}k_I\alpha_{I,II}$ (see Fig. 2.1) and so $\alpha_{II,I}$ must be equal to $\alpha_{I,II}$. For simplicity, the interaction factors are assumed to be additive. The four stoichiometric association constants are then related to the four intrinsic association constants (k_I to k_{IV}) and the six possible interaction factors $\alpha_{I,II}$, $\alpha_{I,III}$, $\alpha_{I,IV}$, $\alpha_{II,III}$, $\alpha_{II,IV}$, and $\alpha_{III,IV}$ as follows:

$$K_1 = k_I + k_{II} + k_{III} + k_{IV}$$

$$K_2 = \frac{k_Ik_{II}\alpha_{I,II} + k_Ik_{III}\alpha_{I,III} + k_Ik_{IV}\alpha_{I,IV} + k_{II}k_{III}\alpha_{II,III} + k_{II}k_{IV}\alpha_{II,IV} + k_{III}k_{IV}\alpha_{III,IV}}{K_1}$$

$$K_3 = \frac{k_Ik_{II}k_{III}\alpha_{I,II}\alpha_{I,III}\alpha_{II,III} + k_Ik_{II}k_{IV}\alpha_{I,II}\alpha_{I,IV}\alpha_{II,IV} + k_Ik_{III}k_{IV}\alpha_{I,III}\alpha_{I,IV}\alpha_{III,IV}}{K_1K_2} + \frac{k_{II}k_{III}k_{IV}\alpha_{II,III}\alpha_{II,IV}\alpha_{III,IV}}{K_1K_2}$$

$$K_4 = \frac{k_Ik_{II}k_{III}k_{IV}\alpha_{I,II}\alpha_{I,III}\alpha_{I,IV}\alpha_{II,III}\alpha_{II,IV}\alpha_{III,IV}}{K_1K_2K_3}$$

If there are no inter-domain interactions then $\alpha_{I,III} = \alpha_{I,IV} = \alpha_{II,III} = \alpha_{II,IV} = 1$ and these expressions reduce to:

$$K_1 = k_I + k_{II} + k_{III} + k_{IV}$$

$$K_2 = \frac{k_I k_{II}\alpha_{I,II} + k_I k_{III} + k_I k_{IV} + k_{II} k_{III} + k_{II} k_{IV} + k_{III} k_{IV}\alpha_{III,IV}}{K_1}$$

$$K_3 = \frac{k_I k_{II} k_{III}\alpha_{I,II} + k_I k_{II} k_{IV}\alpha_{I,II} + k_I k_{III} k_{IV}\alpha_{III,IV} + k_{II} k_{III} k_{IV}\alpha_{III,IV}}{K_1 K_2}$$

$$K_4 = \frac{k_I k_{II} k_{III} k_{IV}\alpha_{I,II}\alpha_{III,IV}}{K_1 K_2 K_3}$$

The corresponding expressions for the two stoichiometric association constants for Tr1C and Tr2C are, of course, much simpler.

For Tr1C (N-domain, sites I and II):

$K_1 = k_I + k_{II}$ $\quad$ $K_2 = k_I k_{II}\alpha_{I,II} / K_1$ $\quad$ $K_1 K_2 = k_I k_{II}\alpha_{I,II}$

For Tr2C (C-domain, sites III and IV):

$K_1 = k_{III} + k_{IV}$ $\quad$ $K_2 = k_{III} k_{IV}\alpha_{III,IV} / K_1$ $\quad$ $K_1 K_2 = k_{III} k_{IV}\alpha_{III,IV}$

Sites III and IV in the C-terminal domain of intact CaM bind calcium significantly more strongly than sites I and II in the N-terminal domain, i.e. k_{III} and $k_{IV} > k_I$ and k_{II}.

Thus $\quad$ $K_1 K_2 \sim k_{III} k_{IV}\alpha_{III,IV}$, (i.e. reflecting C-domain binding),

and $\quad$ $K_3 K_4 \sim k_I k_{II}\alpha_{I,II}$ (i.e. reflecting N-domain binding).

Therefore, for WT-CaM, the product of the constants K_1 and K_2 is often used to describe Ca^{2+} binding to the C-domain and the product of the constants K_3 and K_4 is used to describe Ca^{2+} binding to the N-domain. The constants $K_{av(N)}$ and $K_{av(C)}$ are frequently used to represent the average calcium affinity for the N- and C-domains of intact CaM. These constants are defined as:

$$K_{av(N)} = \sqrt{K_3 K_4} \qquad K_{av(C)} = \sqrt{K_1 K_2}$$

Figure 2.2A shows calculated calcium binding profiles for CaM and its isolated fragments. The saturation curves were calculated using the method described in the following section with the stoichiometric binding constants reported in Table 1.1 in Chapter 1. The sum of the curves for Tr1C and Tr2C reproduces almost exactly the profile for intact CaM. This indicates that the calcium binding properties (affinity and cooperativity) of Tr1C are very similar to those of the N-domain whilst the properties of Tr2C are very similar to those of the C-domain. Thus, as far as Ca^{2+} binding is concerned, the two domains in intact CaM can be considered to behave as two independent units.

2.3.1.2 Calculating concentrations

Knowing the stoichiometric association constants K_1, K_2, K_3, and K_4 and the total concentrations of CaM and calcium, it is possible to calculate the concentrations [CaM], [Ca-CaM], [Ca_2-CaM], [Ca_3-CaM], [Ca_4-CaM], and [Ca], where [CaM] indicates the concentration of Ca^{2+}-free CaM and [Ca] the concentration of free calcium. Total concentrations of protein and calcium (CaM_{TOT} and Ca_{TOT}) are given by:

$$Ca_{TOT} = [Ca] + [Ca\text{-}CaM] + 2[Ca_2\text{-}CaM] + 3[Ca_3\text{-}CaM] + 4[Ca_4\text{-}CaM] \quad (2.1)$$

$$CaM_{TOT} = [CaM] + [Ca\text{-}CaM] + [Ca_2\text{-}CaM] + [Ca_3\text{-}CaM] + [Ca_4\text{-}CaM] \quad (2.2)$$

From Eq. (2.2):

$$CaM_{TOT} = \frac{[Ca\text{-}CaM]}{K_1[Ca]} + [Ca\text{-}CaM] + K_2[Ca\text{-}CaM][Ca] +$$
$$+ K_2K_3[Ca\text{-}CaM][Ca]^2 + K_2K_3K_4[Ca\text{-}CaM][Ca]^3$$

and

$$[Ca\text{-}CaM] = \frac{CaM_{TOT}}{\frac{1}{K_1[Ca]} + 1 + K_2[Ca] + K_2K_3[Ca]^2 + K_2K_3K_4[Ca]^3}$$

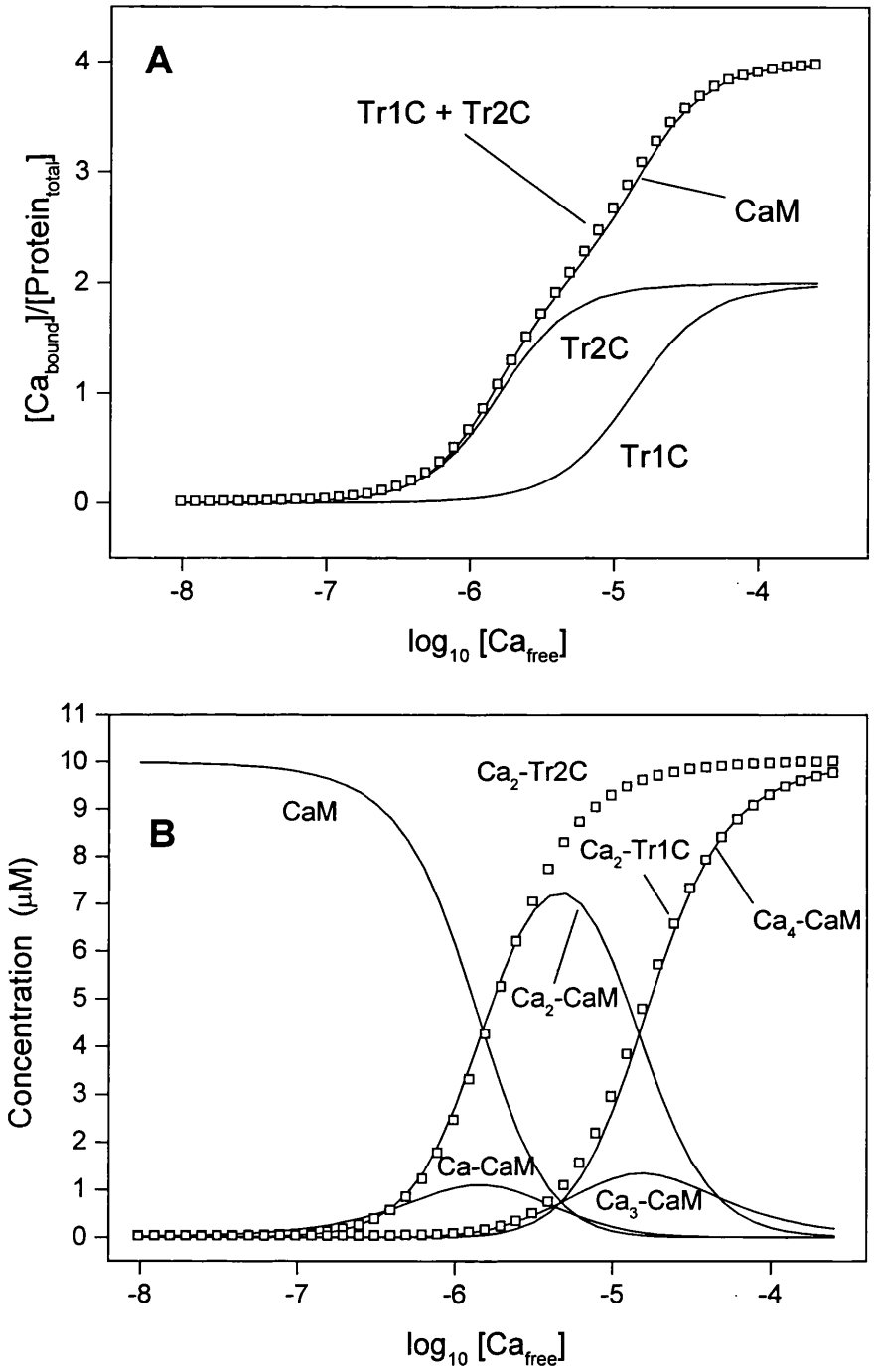

Figure 2.2 **(A)** Ca^{2+}-binding profiles for CaM and its isolated fragments. **(B)** Concentrations of the species CaM, Ca-CaM, Ca_2-CaM, Ca_3-CaM, Ca_4-CaM, Ca_2-Tr1C, and Ca_2-Tr2C as a function of free calcium concentration. The stoichiometric binding constants used for the calculations of the curves in (A) and (B) are reported in Table 1.1 (Chapter 1).

From Eq. (2.1):

$$Ca_{TOT} = [Ca] + [Ca\text{-}CaM] + 2K_2[Ca\text{-}CaM][Ca] + 3K_2K_3[Ca\text{-}CaM][Ca]^2 +$$

$$+ 4K_2K_3K_4[Ca\text{-}CaM][Ca]^3$$

and

$$[Ca\text{-}CaM] = \frac{Ca_{TOT} - [Ca]}{1 + 2K_2[Ca] + 3K_2K_3[Ca]^2 + 4K_2K_3K_4[Ca]^3}$$

Equating the two expressions for [Ca-CaM] and cross-multiplying gives:

$$CaM_{TOT}(1 + 2K_2[Ca] + 3K_2K_3[Ca]^2 + 4K_2K_3K_4[Ca]^3) =$$

$$= (Ca_{TOT} - [Ca])(\frac{1}{K_1[Ca]} + 1 + K_2[Ca] + K_2K_3[Ca]^2 + K_2K_3K_4[Ca]^3)$$

Multiply both sides by [Ca]:

$$CaM_{TOT}[Ca](1 + 2K_2[Ca] + 3K_2K_3[Ca]^2 + 4K_2K_3K_4[Ca]^3) =$$

$$= (Ca_{TOT} - [Ca]) / K_1 + (Ca_{TOT}[Ca] - [Ca]^2)(1 + K_2[Ca] + K_2K_3[Ca]^2 +$$

$$+ K_2K_3K_4[Ca]^3)$$

Then

$$CaM_{TOT}[Ca] + 2K_2CaM_{TOT}[Ca]^2 + 3K_2K_3CaM_{TOT}[Ca]^3 +$$

$$+ 4K_2K_3K_4CaM_{TOT}[Ca]^4 =$$

$$= Ca_{TOT} / K_1 - [Ca] / K_1 + Ca_{TOT}[Ca] + K_2Ca_{TOT}[Ca]^2 + K_2K_3Ca_{TOT}[Ca]^3 +$$

$$+ K_2K_3K_4Ca_{TOT}[Ca]^4 - [Ca]^2 - K_2[Ca]^3 - K_2K_3[Ca]^4 - K_2K_3K_4[Ca]^5 .$$

Then

$$[Ca]^5 (K_2K_3K_4) + [Ca]^4 (K_2K_3 - K_2K_3K_4\, Ca_{TOT} + 4K_2K_3K_4\, CaM_{TOT}) +$$

$$+ [Ca]^3(K_2 - K_2K_3\, Ca_{TOT} + 3K_2K_3\, CaM_{TOT}) +$$

$$+ [Ca]^2(1 - K_2Ca_{TOT} + 2K_2\, CaM_{TOT}) + [Ca](1 / K_1 - Ca_{TOT} + CaM_{TOT}) -$$

$$- Ca_{TOT}/K_1 = 0$$

[Ca] is then given as the solution of the equation:

$$C_5[Ca]^5 + C_4[Ca]^4 + C_3[Ca]^3 + C_2[Ca]^2 + C_1[Ca] + C_0 = 0$$

where

$$C_5 = K_2K_3K_4$$
$$C_4 = K_2K_3 - K_2K_3K_4Ca_{TOT} + 4K_2K_3K_4CaM_{TOT}$$
$$C_3 = K_2 - K_2K_3Ca_{TOT} + 3K_2K_3CaM_{TOT}$$
$$C_2 = 1 - K_2Ca_{TOT} + 2K_2CaM_{TOT}$$
$$C_1 = 1 / K_1 - Ca_{TOT} + CaM_{TOT}$$
$$C_0 = - Ca_{TOT} / K_1$$

[Ca-CaM] is then derived from the expression given above, i.e.:

$$[Ca - CaM] = \frac{Ca_{TOT} - [Ca]}{1 + 2K_2[Ca] + 3K_2K_3[Ca]^2 + 4K_2K_3K_4[Ca]^3}$$

and the remaining concentrations are calculated from the expressions for the stoichiometric association constants.

Figure 2.2B shows an example of calculation of the concentrations of the species CaM, Ca-CaM, Ca_2-CaM, Ca_3-CaM, and Ca_4-CaM as a function of the free calcium concentration. The constants used in this calculation are given in Chapter 1 (Table 1.1). Because of cooperativity between sites within a domain the species Ca-CaM and Ca_3-CaM are only formed at low concentration. Similar calculations for the isolated fragments show that the appearance of Ca_2-Tr2C and Ca_2-Tr1C parallel the appearance of Ca_2-CaM and Ca_4-CaM, respectively. This shows that the species Ca_2-CaM is formed predominantly (but not entirely) of CaM molecules with a Ca^{2+}-saturated C-domain and a Ca^{2+}-free N-domain, consistent with the C-domain having higher calcium affinity than the N-domain.

2.3.1.3 Magnesium/calcium competition

The scheme in Figure 2.3 shows a formal representation of the interaction of a calmodulin domain (D) with Ca^{2+} and Mg^{2+}, which assumes that Ca^{2+} and Mg^{2+} compete for the same sites. k_A and k_B are the intrinsic constants for the binding of Ca^{2+} to the two sites of the domain (i.e., sites I and II in the N-domain or sites III and IV in the C-domain); k^*_A and k^*_B are the intrinsic constants for the binding of Mg^{2+} to the two sites; α_{Ca}, α_{Mg}, and $\alpha_{Mg\&Ca}$ are Ca^{2+}-Ca^{2+}, Mg^{2+}-Mg^{2+}, and Mg^{2+}-Ca^{2+} interaction (or cooperativity) factors. The first and second subscripts denote the occupancy of sites A and B. The intrinsic constants are defined as follows:

$$k_A = \frac{[D_{Ca,0}]}{[D_{0,0}][Ca]} \qquad k_B = \frac{[D_{0,Ca}]}{[D_{0,0}][Ca]}$$

$$k^*_A = \frac{[D_{Mg,0}]}{[D_{0,0}][Mg]} \qquad k^*_B = \frac{[D_{0,Mg}]}{[D_{0,0}][Mg]}$$

The apparent stoichiometric association constants for Ca^{2+} in the presence of Mg^{2+} are given by:

$$K_{1,app} = \frac{[Ca_1 \cdot D]}{[D][Ca]} \qquad K_{2,app} = \frac{[Ca_2 \cdot D]}{[Ca_1 \cdot D][Ca]}$$

where D indicates a CaM domain and Ca_1·D and Ca_2·D indicate all the species with one and two Ca^{2+} ions bound, respectively. Then the stoichiometric constants $K_{1,app}$ and $K_{2,app}$ can be expressed in terms of the intrinsic constants as:

$$K_{1,app} = \frac{[D_{Ca,0}] + [D_{0,Ca}] + [D_{Ca,Mg}] + [D_{Mg,Ca}]}{([D_{0,0}] + [D_{Mg,0}] + [D_{0,Mg}] + ([D_{Mg,Mg}])[Ca]} =$$

$$= \frac{k_A[D_{0,0}][Ca] + k_B[D_{0,0}][Ca] + k_A k^*_B \alpha_{Mg\&Ca}[D_{0,0}][Ca][Mg]}{([D_{0,0}] + k^*_A[D_{0,0}][Mg] + k^*_B[D_{0,0}][Mg] + k^*_A k^*_B \alpha_{Mg}[D_{0,0}][Mg]^2)[Ca]} +$$

$$+ \frac{k^*_A k_B \alpha_{Mg\&Ca}[D_{0,0}][Ca][Mg]}{([D_{0,0}] + k^*_A[D_{0,0}][Mg] + k^*_B[D_{0,0}][Mg] + k^*_A k^*_B \alpha_{Mg}[D_{0,0}][Mg]^2)[Ca]} =$$

$$= \frac{k_A + k_B + k_A k^*_B \alpha_{Mg\&Ca}[Mg] + k^*_A k_B \alpha_{Mg\&Ca}[Mg]}{1 + k^*_A[Mg] + k^*_B[Mg] + k^*_A k^*_B \alpha_{Mg}[Mg]^2}$$

and

$$K_{2,app} = \frac{[D_{Ca,Ca}]}{([D_{Ca,0}] + [D_{0,Ca}] + [D_{Ca,Mg}] + [D_{Mg,Ca}])[Ca]} =$$

$$= \frac{k_A k_B \alpha_{Ca}}{k_A + k_B + k_A k^*_B \alpha_{Mg\&Ca}[Mg] + k^*_A k_B \alpha_{Mg\&Ca}[Mg]}$$

Then the product of $K_{1,app}$ and $K_{2,app}$ is:

$$K_{1,app}K_{2,app} = \frac{k_A k_B \alpha_{Ca}}{1 + k^*_A[Mg] + k^*_B[Mg] + k^*_A k^*_B \alpha_{Mg}[Mg]^2}$$

As shown in Section 2.3.1.1, for a single domain the intrinsic Ca^{2+} association constants are related to the stoichiometric association constants as follows:

$K_1 = k_A + k_B$ $\qquad$ $K_2 = (k_A k_B \alpha_{Ca})/ K_1$

$K_1K_2 = k_A k_B \alpha_{Ca}$

Similarly, for Mg^{2+}:

$K^*_1 = k^*_A + k^*_B$ $\qquad$ $K^*_2 = (k^*_A k^*_B \alpha_{Mg})/ K^*_1$

$K^*_1K^*_2 = k^*_A k^*_B \alpha_{Mg}$

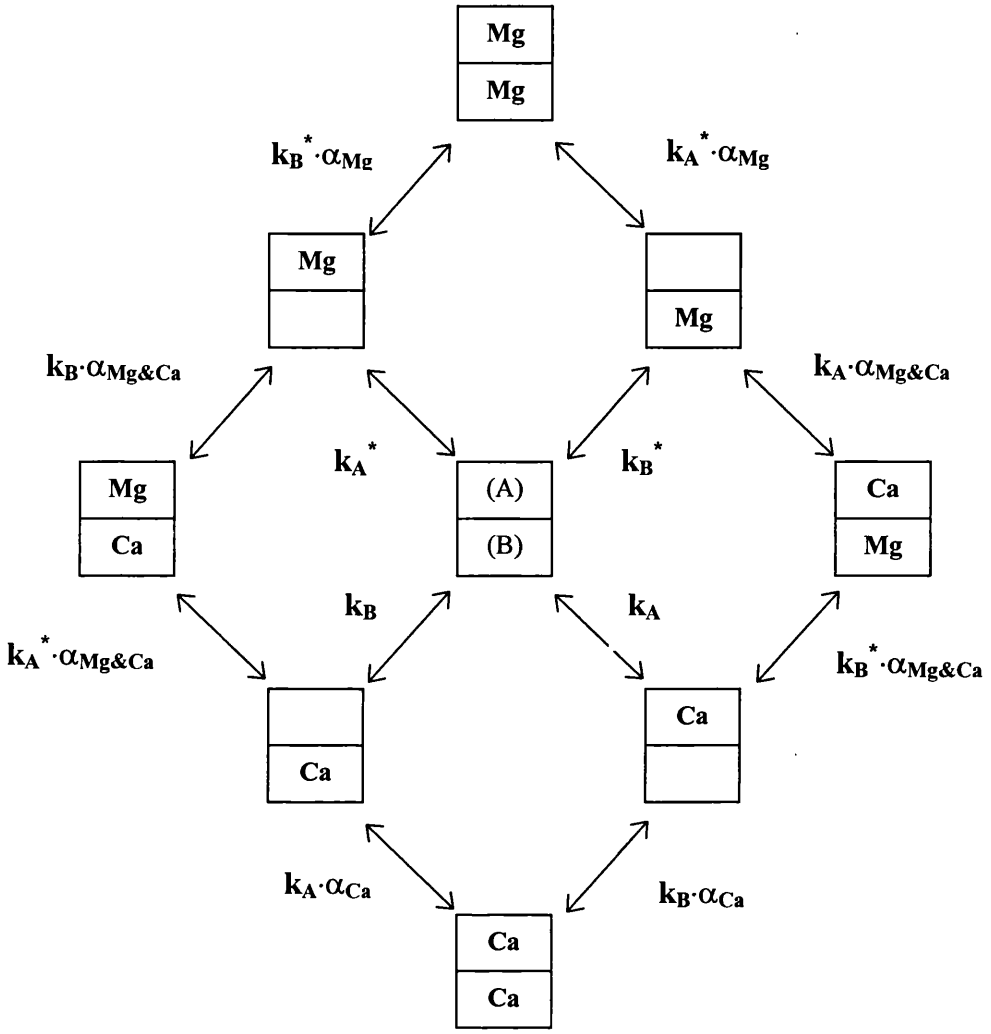

Figure 2.3 Schematic representation of Ca^{2+} and Mg^{2+} binding to a calmodulin domain. k_A and k_B are the intrinsic constants for the binding of Ca^{2+} to the two sites of the domain; k^*_A and k^*_B are the intrinsic constants for the binding of Mg^{2+} to the two sites; α_{Ca}, α_{Mg}, and $\alpha_{Mg\&Ca}$ are Ca^{2+}- Ca^{2+}, Mg^{2+}- Mg^{2+}, and Mg^{2+}- Ca^{2+} interaction (or cooperativity) factors.

Then the product $K_{1,app}K_{2,app}$ can also be expressed as:

$$K_{1,app}K_{2,app} = \frac{K_1K_2}{1 + K^*_1[Mg] + K^*_1K^*_2[Mg]^2}$$

The average Ca^{2+} affinity of a domain in the presence of Mg^{2+} is then approximately equal to:

$$K^{Ca}_{av(D),app} = \sqrt{K_{1,app}K_{2,app}} \approx \frac{K^{Ca}_{av(D)}}{1 + K^{Mg}_{av(D)}[Mg]}$$

2.3.2 Determination of chelator affinities

Description of experiment

The two Ca^{2+}-chelators used in this work were 5,5'-Br_2BAPTA (Calbiochem) and 5-nitro-BAPTA (Molecular Probes). A Ca^{2+}-free solution of chelator (30-50 μM) was prepared using the chosen buffer. This solution was then titrated with a stock solution of calcium and the absorption at 263 nm (5,5'-Br_2BAPTA) or 430 nm (5-nitro-BAPTA) was recorded. The titration was continued until the absorption reached a constant value. The total chelator concentration was calculated from the absorption spectrum using the following extinction coefficients: ε_{239} = 1.6 x 10^4 $M^{-1}cm^{-1}$ for 5,5'-Br_2BAPTA in the presence of excess calcium, and ε_{430} = 1.2 x 10^4 $M^{-1}cm^{-1}$ or ε_{340} = 6 x 10^3 $M^{-1}cm^{-1}$ for 5-nitro BAPTA in the absence of calcium and in the presence of excess calcium, respectively. The total calcium concentration at each point was corrected for the presence of any contaminating calcium (see Section 2.1.2.).

Theory and data analysis

The chelator (Q) is assumed to bind calcium with simple 1:1 stoichiometry according to the following scheme:

$$Ca + Q \xleftrightarrow{K_d} Ca\text{-}Q \qquad \text{with} \qquad K_d = \frac{[Ca][Q]}{[Ca\text{-}Q]}$$

Total concentrations of Ca and chelator (Ca_{TOT} and Q_{TOT}) are given by:

$$Ca_{TOT} = [Ca] + [Ca\text{-}Q]$$
$$Q_{TOT} = [Ca\text{-}Q] + [Q]$$

Therefore

$$K_d = \frac{(Ca_{TOT} - [Ca - Q])(Q_{TOT} - [Ca - Q])}{[Ca - Q]}$$

[Ca-Q] is then the root of the quadratic:

$$[Ca\text{-}Q]^2 - [Ca\text{-}Q](K_d + Ca_{TOT} + Q_{TOT}) + Ca_{TOT}\, Q_{TOT} = 0$$

and the remaining concentrations are calculated using:

$$[Q] = Q_{TOT} - [Ca\text{-}Q]$$
$$[Ca] = Ca_{TOT} - [Ca\text{-}Q]$$

The measured optical signal at a single wavelength is given by:

$$\text{Signal} = \varepsilon(Q)[Q] + \varepsilon(Ca\text{-}Q)[Ca\text{-}Q] \qquad (2.3)$$

where $\varepsilon(Q)$ and $\varepsilon(Ca\text{-}Q)$ are the specific optical properties (extinction coefficients in this case) of Q and Ca-Q, respectively.

The experimental data were fitted to Eq. (2.3) with $\varepsilon(Q)$, $\varepsilon(Ca\text{-}Q)$, and the K_d as the variables, using a standard non-linear least squares fitting procedure written by Dr. Stephen Martin (N.I.M.R.). The calcium association constants ($K_{Ca} = 1/K_d$) determined for 5,5'-Br_2BAPTA and 5-nitro-BAPTA at 20°C and an ionic strength of 0.1M are $5.7 \cdot 10^5$ and $3.3 \cdot 10^4$ M^{-1}, respectively.

2.3.3 Determination of stoichiometric association constants for calcium binding using chromophoric calcium chelators

Description of experiment

The experimental approach used here was originally described by Linse et al. (1991a) and has been developed further by this laboratory (Bayley et al., 1996; Martin et al., 1996). A mixture of chelator (30-50 μM) plus apo-protein (20-60 μM) was prepared in a Ca^{2+}-free solution of the chosen buffer. This solution was then titrated with a stock solution of calcium (which contained protein at the same concentration as in the starting solution) and the absorption at 263 nm (5,5'-Br_2BAPTA) or 430 nm (5-nitro BAPTA) was recorded. The titration was continued until the absorption reached a constant value. The total calcium concentration at each point was corrected for the presence of any contaminating calcium (see Section 2.1.2.).

Theory and data analysis

The experimental system is described by the following equilibria and association constants, in which CaM, Ca, and Q represent calmodulin, calcium and chelator, respectively.

$$CaM + Ca \xleftrightarrow{K_1} Ca\text{-}CaM \qquad K_1 = \frac{[Ca\text{-}CaM]}{[CaM][Ca]}$$

$$Ca\text{-}CaM + Ca \xleftrightarrow{K_2} Ca_2\text{-}CaM \qquad K_2 = \frac{[Ca_2\text{-}CaM]}{[Ca\text{-}CaM][Ca]}$$

$$Ca_2\text{-}CaM + Ca \xleftrightarrow{K_3} Ca_3\text{-}CaM \qquad K_3 = \frac{[Ca_3\text{-}CaM]}{[Ca_2\text{-}CaM][Ca]}$$

$$Ca_3\text{-}CaM + Ca \xleftrightarrow{K_4} Ca_4\text{-}CaM \qquad K_4 = \frac{[Ca_4\text{-}CaM]}{[Ca_3\text{-}CaM][Ca]}$$

$$Ca + Q \xleftrightarrow{K_{CaQ}} Ca\text{-}Q \qquad K_{CaQ} = \frac{[Ca\text{-}Q]}{[Ca][Q]}$$

The absorbance at any wavelength for a mixture of calcium, chelator, and calmodulin (at constant concentration) is given by:

$$A = \varepsilon_{CaQ}[Ca\text{-}Q] + \varepsilon_{Q}[Q] + A_{CaM}$$

where ε_{CaQ} and ε_{Q} are the appropriate extinction coefficients, and A_{CaM} is the absorbance from the calmodulin, which is assumed not to change as the protein binds the calcium.

Substituting $[Q] = Q_{TOT} - [Ca\text{-}Q]$ in the expression for K_{CaQ} gives:

$$K_{CaQ} = \frac{[Ca\text{-}Q]}{[Ca][Q]} = \frac{[Ca\text{-}Q]}{[Ca](Q_{TOT} - [Ca\text{-}Q])}$$

Then

$$[Ca\text{-}Q] = K_{CaQ}([Ca]Q_{TOT} - [Ca][Ca\text{-}Q]) = K_{CaQ}[Ca]Q_{TOT} - K_{CaQ}[Ca][Ca\text{-}Q]$$

Therefore

$$[Ca\text{-}Q](1 + K_{CaQ}[Ca]) = K_{CaQ}[Ca]Q_{TOT}$$

and

$$[Ca\text{-}Q] = \frac{K_{CaQ}[Ca][Q_{TOT}]}{1 + K_{CaQ}[Ca]} \qquad (2.4)$$

Substituting $[Q] = Q_{TOT} - [Ca\text{-}Q]$ in the expression for A gives:

$$A = \varepsilon_{CaQ}[Ca\text{-}Q] + \varepsilon_{Q}(Q_{TOT} - [Ca\text{-}Q]) + A_{CaM}$$

Then

$$A = \varepsilon_{CaQ}\left(\frac{K_{CaQ}[Ca][Q_{TOT}]}{1 + K_{CaQ}[Ca]}\right) + \varepsilon_{Q}[Q_{TOT}] - \varepsilon_{Q}\frac{K_{CaQ}[Ca][Q_{TOT}]}{1 + K_{CaQ}[Ca]} + A_{CaM} =$$

$$= \varepsilon_{Q}[Q_{TOT}] + (\varepsilon_{CaQ}[Q_{TOT}] - \varepsilon_{Q}[Q_{TOT}])\frac{K_{CaQ}[Ca]}{1 + K_{CaQ}[Ca]} + A_{CaM}$$

As [Ca] $\rightarrow \infty$ then A $\rightarrow$ $\varepsilon_{CaQ}[Q_{TOT}] + A_{CaM}$ (= A_{MIN}, the absorbance in the presence of saturating calcium).

As [Ca] $\rightarrow$ 0 then A $\rightarrow$ $\varepsilon_{Q}[Q_{TOT}] + A_{CaM}$ (= A_{MAX}, the absorbance in the complete absence of calcium). Note: For most of the chelators used the absorbance decreases on adding calcium, hence the definition of A_{MAX} and A_{MIN}.

Then

$$\varepsilon_{CaQ}[Q_{TOT}] - \varepsilon_{Q}[Q_{TOT}] = A_{MIN} - A_{MAX}$$

and

$$A = A_{MAX} - (A_{MAX} - A_{MIN})\frac{K_{CaQ}[Ca]}{1 + K_{CaQ}[Ca]}$$

Note: A_{MAX} and A_{MIN} apply to the starting solution (and include a contribution from the calmodulin, see above). Therefore one needs to correct each absorbance reading for dilution (if necessary) by using the following equation:

$$A = \left(A_{MAX} - (A_{MAX} - A_{MIN})\frac{K_{CaQ}[Ca]}{1 + K_{CaQ}[Ca]} \right) \frac{[Q_{TOT(S)}]}{[Q_{TOT}]} \qquad (2.5)$$

where $[Q_{TOT(S)}]$ is the total concentration of Q in the starting solution, and Q_{TOT} is the actual concentration at any point.

In order to fit the data to Eq.(2.5) one needs to calculate the concentration of free calcium. The total concentration of calcium present is given by:

$$[Ca_{TOT}] = [Ca] + [Ca\text{-}Q] + [Ca\text{-}CaM] + 2[Ca_2\text{-}CaM] + 3[Ca_3\text{-}CaM] + 4[Ca_4\text{-}CaM] \qquad (2.6)$$

The Adair equation relates the ratio [Protein Bound Calcium]/[Total Protein] to the free calcium concentration in the following way:

$$\frac{[\text{Protein Bound Calcium}]}{[\text{Total Protein}]} = \frac{K_1[Ca] + 2K_1K_2[Ca]^2 + 3K_1K_2K_3[Ca]^3 + 4K_1K_2K_3K_4[Ca]^4}{1 + K_1[Ca] + K_1K_2[Ca]^2 + K_1K_2K_3[Ca]^3 + K_1K_2K_3K_4[Ca]^4}$$

But

[Protein Bound Calcium] = [Ca-CaM] + 2[Ca_2-CaM] + 3[Ca_3-CaM] + 4[Ca_4-CaM]

Therefore

$$\frac{[Ca\text{-}CaM]+2[Ca_2\text{-}CaM]+3[Ca_3\text{-}CaM]+4[Ca_4\text{-}CaM]}{[CaM_{TOT}]}= \tag{2.7}$$

$$=\frac{K_1[Ca]+2K_1K_2[Ca]^2+3K_1K_2K_3[Ca]^3+4K_1K_2K_3K_4[Ca]^4}{1+K_1[Ca]+K_1K_2[Ca]^2+K_1K_2K_3[Ca]^3+K_1K_2K_3K_4[Ca]^4}$$

Substituting (2.4) and (2.7) in (2.6) and rearranging:

$$[Ca_{TOT}]-[Ca]-\frac{K_{CaQ}[Ca][Q_{TOT}]}{1+K_{CaQ}[Ca]}-$$

$$-[CaM_{TOT}]\frac{K_1[Ca]+2K_1K_2[Ca]^2+3K_1K_2K_3[Ca]^3+4K_1K_2K_3K_4[Ca]^4}{1+K_1[Ca]+K_1K_2[Ca]^2+K_1K_2K_3[Ca]^3+K_1K_2K_3K_4[Ca]^4}=0$$

This equation can be solved for [Ca] using the Newton-Raphson method.

The experimental data were fitted to Eq. (2.5) with K_1 to K_4 as the variables, using a standard non-linear least squares fitting procedure written by Dr. Stephen Martin (N.I.M.R.). In experiments with the tryptic fragments of calmodulin (Tr1C and Tr2C), the stoichiometric constants K_3 and K_4 were set to zero. The association constant for the chelator was held constant at the value determined in a separate experiment (see Section 2.3.2).

2.3.4 Determination of peptide affinities by direct fluorometric titration

The affinity of CaM for a tryptophan-containing peptide with a K_d in the range 1 nM to 20 μM can be accurately determined using direct fluorometric titration methods. This experimental approach is based on the fact that the fluorescence emission of the peptide tryptophan changes when the peptide is bound to CaM (see, for example, Findlay et al., 1995b).

Description of experiment

A solution of the peptide (generally 0.5 - 2.0 μM) was prepared using the chosen buffer. This solution was then titrated with a stock solution of CaM and the fluorescence intensity at 322 nm was recorded. Whenever possible, the titration was continued until the fluorescence reached a constant value. A control titration in the absence of the peptide was generally performed in order to obtain an accurate value for the specific (tyrosine) fluorescence of CaM, which makes a small contribution to the fluorescence intensity measured at 322 nm.

Theory and data analysis

The target peptide (Pep) is assumed to bind to calmodulin (CaM) with simple 1:1 stoichiometry according to the following scheme:

$$CaM + Pep \xleftrightarrow{K_d} CaM - Pep \qquad \text{with} \qquad K_d = \frac{[CaM][Pep]}{[CaM - Pep]}$$

Total concentrations of CaM and peptide (CaM_{TOT} and Pep_{TOT}) are given by:

$$CaM_{TOT} = [CaM] + [CaM\text{-}Pep]$$
$$Pep_{TOT} = [CaM\text{-}Pep] + [Pep]$$

Therefore

$$K_d = \frac{(CaM_{TOT} - [CaM - Pep])(Pep_{TOT} - [CaM - Pep])}{[CaM - Pep]}$$

[CaM-Pep] is then the root of the quadratic:

$$[CaM\text{-}Pep]^2 - [CaM\text{-}Pep](K_d + CaM_{TOT} + Pep_{TOT}) + CaM_{TOT}Pep_{TOT} = 0$$

and the remaining concentrations are calculated using:

$$[Pep] = Pep_{TOT} - [CaM\text{-}Pep]$$
$$[CaM] = CaM_{TOT} - [CaM\text{-}Pep]$$

The measured optical signal is then given by:

$$\text{Signal} = \varepsilon(\text{CaM})[\text{CaM}] + \varepsilon(\text{Pep})[\text{Pep}] + \varepsilon(\text{CaM-Pep})[\text{CaM-Pep}] \quad (2.8)$$

where ε(CaM), ε(Pep), and ε(CaM-Pep) are the specific optical properties (fluorescence intensity in this case) of CaM, Pep and CaM-Pep, respectively.

The experimental data were fitted to Eq. (2.8) with the specific optical properties and the K_d as the variables, using a standard non-linear least squares fitting procedure written by Dr. Stephen Martin (N.I.M.R.). For improved accuracy in the analysis, ε(CaM) was generally determined in a separate control titration performed without peptide (see above).

2.3.5 Determination of peptide affinities using a competition assay

The affinity of CaM for a peptide which is spectroscopically silent (i.e., does not contain tryptophan) cannot generally be determined by direct fluorometric titration. In this case, the affinity is measured using a competition assay, in which the silent peptide is used to displace a tryptophan-containing peptide from its complex with CaM. This method is based on the assumption that the two peptides compete for a single binding site on CaM and allows one to determine the affinity of CaM for the silent peptide when the affinity for the tryptophan-containing peptide is known. Alternatively, this method can be also used to measure the affinity of a tryptophan-containing peptide, if the affinity of CaM for a silent peptide is known. This latter approach is particularly useful if the K_d for the tryptophan-containing peptide is too low to be measured using conventional methods.

Description of experiment

A solution of the Trp-containing peptide was prepared in the chosen buffer and the fluorescence emission intensity at 330 nm was recorded. CaM was then added to the sample and the intensity at 330 nm was recorded again. The concentrations of peptide and CaM (generally ~ 2 μM) were chosen to have [peptide] > [CaM], in order to ensure that there was little free CaM present during the titration. The sample solution was then titrated with small aliquots of concentrated silent peptide and the fluorescence intensity at 330 nm was recorded. Whenever possible, the titration was continued until all the Trp-containing peptide has been displaced. A control titration without Trp-

containing peptide was performed in order to determine the specific (tyrosine) fluorescence properties of CaM and of the complex of CaM with the silent peptide.

Theory and data analysis

CaM interacts with the Trp-containing peptide (W) and the spectroscopically silent peptide (S) according to the following scheme:

$$CaM + W \xleftrightarrow{K_W} CaM\text{-}W \qquad \text{with } K_W = \frac{[CaM\text{-}W]}{[CaM][W]}$$

$$CaM + S \xleftrightarrow{K_S} CaM\text{-}S \qquad \text{with } K_S = \frac{[CaM\text{-}S]}{[CaM][S]}$$

Total concentrations of CaM, Trp-containing peptide, and silent peptide (CaM_{TOT}, W_{TOT}, and S_{TOT}) are given by:

$$CaM_{TOT} = [CaM] + [CaM\text{-}W] + [CaM\text{-}S]$$
$$W_{TOT} = [W] + [CaM\text{-}W]$$
$$S_{TOT} = [S] + [CaM\text{-}S]$$

Then

$$[W] = \frac{[CaM\text{-}W]}{K_W[CaM]} \qquad W_{TOT} = \frac{[CaM\text{-}W]}{K_W[CaM]} + [CaM\text{-}W]$$

Then

$$W_{TOT} = [CaM\text{-}W]\left(1 + \frac{1}{K_W[CaM]}\right) = [CaM\text{-}W]\left(\frac{K_W[CaM]+1}{K_W[CaM]}\right)$$

and

$$[CaM\text{-}W] = \frac{W_{TOT}K_W[CaM]}{K_W[CaM]+1}$$

In the same way one can show that

$$[CaM\text{-}S] = \frac{S_{TOT}K_S[CaM]}{K_S[CaM]+1}$$

Substituting these expressions for [CaM-W] and [CaM-S] in the equation for CaM_{TOT} gives:

$$CaM_{TOT} = [CaM] + \frac{W_{TOT}K_W[CaM]}{K_W[CaM]+1} + \frac{S_{TOT}K_S[CaM]}{K_S[CaM]+1}$$

Expanding this equation gives:

$$-CaM_{TOT}K_SK_W[CaM]^2 - CaM_{TOT}K_W[CaM] - CaM_{TOT}K_S[CaM] - CaM_{TOT} +$$
$$+ K_SK_W[CaM]^3 + K_W[CaM]^2 + K_S[CaM]^2 + [CaM] + W_{TOT}K_SK_W[CaM]^2 +$$
$$+ W_{TOT}K_W[CaM] + S_{TOT}K_SK_W[CaM]^2 + S_{TOT}K_S[CaM] = 0$$

[CaM] is then the root of the cubic equation:

$$[CaM]^3(K_SK_W) + [CaM]^2(-CaM_{TOT}K_SK_W + K_W + K_S + W_{TOT}K_SK_W +$$
$$S_{TOT}K_SK_W) + [CaM](-CaM_{TOT}K_W - CaM_{TOT}K_S + 1 + W_{TOT}K_W + S_{TOT}K_S) -$$
$$- CaM_{TOT} = 0$$

and the remaining concentrations are calculated using:

$$[CaM\text{-}W] = \frac{W_{TOT}K_W[CaM]}{K_W[CaM]+1} \qquad [CaM\text{-}S] = \frac{S_{TOT}K_S[CaM]}{K_S[CaM]+1}$$

$$[W] = \frac{[CaM\text{-}W]}{K_W[CaM]} \qquad [S] = \frac{[CaM\text{-}S]}{K_S[CaM]}$$

The measured optical signal is then given by:

$$Signal = \varepsilon(CaM)[CaM] + \varepsilon(W)[W] + \varepsilon(CaM\text{-}S)[CaM\text{-}S] + \varepsilon(CaM\text{-}W)[CaM\text{-}W] \quad (2.9)$$

where ε(CaM), ε(W), ε(CaM-S), and ε(CaM-W) are the specific optical properties (fluorescence in this case) of CaM, W, CaM-S and CaM-W respectively.

The experimental data were fitted to Eq. (2.9) with the specific optical properties and the unknown association constant (either K_S or K_W) as the variables, using a standard non-linear least squares fitting procedure written by Dr. Stephen Martin (N.I.M.R.). For improved accuracy in the analysis, ε(CaM) and ε(CaM-S) were generally determined in a separate control titration performed without peptide (see above).

2.3.6 Chemical and thermal denaturation

Description of the experiments

In the **chemical unfolding** experiments a protein sample (either CaM or one of its isolated fragments) was prepared in the chosen buffer (generally 25 mM Tris, 100 mM KCl, pH 8.0) and the appropriate spectrum was recorded at 20 °C. In the experiments performed with the apo-proteins the sample contained 20 – 200 μM EDTA in order to chelate the residual calcium present in the buffer. In the experiments performed in the presence of Mg^{2+}, the solvent used contained 50 μM EGTA in order to chelate selectively the residual calcium (and not the magnesium) present in solution. Protein concentrations were typically 10 μM (far-UV CD), 20 μM (fluorescence), and 400 μM (absorbance). The sample was then titrated with aliquots of a stock solution of concentrated GuHCl or urea containing protein at the same concentration as in the starting sample. This avoids complications which would otherwise arise from the large dilution of the protein during the titration. This particular approach is possible with these proteins because chemical denaturation is reversible (see below) and refolding is fast (see Section 3.3.6, Chapter 3). A new spectrum was recorded after each denaturant addition and the signal at a fixed wavelength was monitored as a function of changing denaturant concentration. The wavelengths used in the far-UV CD and absorption measurements were 220 and 288 nm respectively; tyrosine fluorescence was measured at 320 nm, with excitation at 280 nm. Chemical denaturation is more than 95% reversible for all the protein studied here, since spectroscopic signals characteristic of

the native protein are recovered upon dilution of the denaturant to non-denaturing concentrations.

Thermal denaturation experiments were performed by measuring fluorescence at 320 nm in 10 mM HEPES, pH 7.5, 100 mM KCl and by measuring far-UV CD (220 nm) and absorption (288 nm) in 25 mM Tris, pH 8.0, 100 mM KCl. Apo protein solutions were heated from 10 to 80°C at ~ 1°C/min and the sample temperature was measured using an immersed thermocouple (Comark). In some of the thermal unfolding experiments performed with absorption spectroscopy 20% methanol was added to the standard buffer, in order to allow measurements to be made to low temperatures. The temperature range used in these experiments was from -8 °C to 80 °C. Far-UV CD studies have shown that the secondary structure of CaM is barely affected by 20% methanol (Bayley and Martin, 1992). Reversibility of thermal denaturation for all the proteins studied was assessed to be more than 95% following cooling to 10°C at a rate of 1 °C/min.

Theory and data analysis

Chemical and thermal denaturation data for the isolated domains (and for intact CaM with absorption and fluorescence measurements of Tyr-138) were fitted to a two-state model describing the unfolding as a single transition between native (N) and unfolded (U) states. For denaturation of the intact protein monitored by far-UV CD the situation is more complex as the signal derives from two domains. The theoretical approaches and the data analysis procedures used in these two cases are described in the following sections.

2.3.6.1 Chemical and thermal denaturation - simple two-state unfolding

The protein is unfolded according to the following simple scheme:

$$\text{Native} \xleftrightarrow{K} \text{Unfolded} \qquad \text{where} \quad K = \frac{[\text{Unfolded}]}{[\text{Native}]}$$

The free energy of unfolding is defined as:

$$\Delta G = G_U - G_N = - RT \ln K$$

where G_U and G_N are the free energies of the unfolded and native state, respectively.

In the case of **chemical denaturation** the free energy of unfolding of the protein is assumed to depend on denaturant concentration according to the following equation:

$$\Delta G = \Delta G° + m[D]$$

where $\Delta G°$ is the free energy for unfolding in the absence of denaturant, m is a constant that describes the linear dependence of ΔG on denaturant concentration, and [D] is the denaturant concentration. This is referred to as the Linear Extrapolation Method (LEM), which is the model most frequently used in the analysis of protein denaturation data (Pace, 1986; Myers et al., 1995). K may be calculated from:

$$K = \exp(-\Delta G/RT)$$

and the fractions of native (F_N) and unfolded (F_U) protein present are given as:

$$F_U = K / (1+K) \qquad \text{and} \qquad F_N = 1 - F_U$$

The optical signals of the native (Opt_N) and unfolded (Opt_U) forms of proteins (including those studied here) frequently vary with denaturant concentration. For simplicity, this dependence is assumed to be linear and therefore described by the following equations:

$$Opt_N = I_N + S_N[D]$$
$$Opt_U = I_U + S_U[D]$$

The change in the optical signal as a function of denaturant concentration is then given by:

$$\text{Signal} = \{I_N + S_N[D]\}F_N + \{I_U + S_U[D]\}F_U \qquad (2.10)$$

The experimental data were fitted to Eq. (2.10), with $\Delta G°$, m, and the I and S values as variables, using a standard non-linear least squares fitting procedure written by Dr. Stephen Martin (N.I.M.R.). The denaturant concentration at the midpoint of the transition, $[D]_{1/2}$, is calculated as $-\Delta G^o/m$.

In spite of the apparent simplicity of the LEM analysis procedure, fitting chemical denaturation data is seldom straightforward. This is mainly because the signals of the native and unfolded states (Opt_N and Opt_U, see above) vary with denaturant concentration and the parameters defining this dependence (I and S) are not always well defined by the experimental data. This is particularly true when the protein unfolds at very low (or very high) denaturant concentration, when the pre- (or post-) transition region is limited, or even absent altogether (see for example Figures 3.3, 3.5, and 3.8 in Chapter 3). In these cases, the analysis was performed by making assumptions based on the information obtained from other experimental curves measured for the same protein.

An additional problem is that the parameters $\Delta G°$ and m are highly correlated in the analysis; as a consequence, the midpoint of the transition ($[D]_{1/2} = -\Delta G°/m$) is determined much more reproducibly than individual $\Delta G°$ and m values. In order to overcome this problem, average m values (m_{av}) were calculated from 23 (urea) and 8 (GuHCl) determinations with Tr1C and Tr2C. The values of m_{av} determined in this way were -0.92 ± 0.05 kcal/(mol·M) for urea and -1.65 ± 0.23 kcal/(mol·M) for GuHCl. These values are similar to those found for other globular proteins of this size (Myers et al., 1995). The individual $\Delta G°_{20}$ values reported in the Results sections of Chapters 3, 4, and 5 for Tr1C and Tr2C were therefore calculated as $[D]_{1/2} \cdot m_{av}$. Values for the N- and C-domains of intact CaM were determined using the m_{av} values determined for Tr1C and Tr2C, respectively. This allows a more reasonable comparison of $\Delta G°_{20}$ values obtained from different sets of experimental data.

In spite of the problems described above, it was generally possible to obtain consistent parameters from the analyses of experiments repeated up to four times and the errors in individual $\Delta G°_{20}$ values reported in this work are estimated to be of the order of 5-10%.

In the case of **thermal denaturation**, the temperature dependence of free energy (ΔG), enthalpy (ΔH), and entropy (ΔS) of unfolding is described by the following equations:

$$\Delta H = \Delta H_o + \Delta C_p (T - T_o)$$
$$\Delta S = \Delta S_o + \Delta C_p \ln (T/T_o)$$
$$\Delta G = \Delta H_o - T\Delta S_o + \Delta C_p (T - T_o - T \ln (T/T_o))$$

where T is the temperature (°K), ΔH_o and ΔS_o are the values of ΔH and ΔS at any reference temperature T_o, and ΔC_p is the change in heat capacity at constant pressure (Schellman, 1987). In this model, ΔC_p is assumed to be independent of temperature (Privalov and Khechinashvilli, 1974). The last equation is referred to as the Gibbs-Helmholtz equation and can also be written as:

$$\Delta G = \Delta H_m (1 - T/T_m) + \Delta C_p (T - T_m - T \ln (T/T_m))$$

where T_m is the transition midpoint temperature (°K) and ΔH_m is the enthalpy at the midpoint temperature.

F_U and F_N are calculated from K as described above. The optical signals of the native and denatured forms of the protein are assumed to be linearly-dependent on the temperature as follows:

$$Opt_N = I_N + S_N T$$
$$Opt_U = I_U + S_U T$$

The change in the optical signal as a function of temperature is then given by:

$$Signal = \{I_N + S_N T\}F_N + \{I_U + S_U T\}F_U \qquad (2.11)$$

The experimental data were fitted to Eq. (2.11), with ΔH_m, ΔC_p, T_m, and the I and S values as variables, using a standard non-linear least squares fitting procedure written by Dr. Stephen Martin (N.I.M.R.). In practice, ΔC_p is very poorly defined by the data and was kept constant in the fit.

2.3.6.2 Chemical and thermal denaturation – biphasic unfolding curves

Unfolding of a protein such as CaM with two domains (N and C) must be represented, at least formally, by a scheme such as the following:

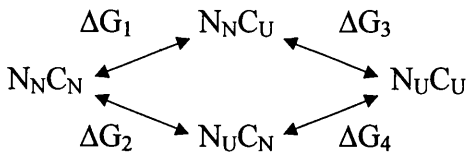

where the subscripts represent the state (either native (N) or unfolded (U) of the two domains). In principle, all four ΔG values may be different. However, experimental data are never going to be sufficiently precise to allow determination of all four values. Therefore, one of two simplified approaches may be used to analyse the data: to treat the system as two separate two-state transitions (one for each domain, Protasevich et al., 1997) or to treat it as a three-state transition with an intermediate state (Sorensen and Shea, 1998). The former treatment assumes that $\Delta G_1 = \Delta G_4$ and $\Delta G_2 = \Delta G_3$; the latter assumes that unfolding occurs exclusively via one pathway (i.e., the upper or the lower). Therefore, both treatments are approximations. In practice, computer simulation of such a system (with four different ΔG values) shows that the two analysis methods return essentially indistinguishable values for the two ΔG values used in the analysis (Martin, S. R.; unpublished observations).

(A) Two two-state transitions

The protein is treated as though it were a mixture of two separate proteins (numbered 1 and 2). The proteins are unfolded according to the following simple scheme:

$$\text{Native}_1 \xleftrightarrow{K_1} \text{Unfolded}_1 \qquad \text{where} \quad K_1 = \frac{[\text{Unfolded}_1]}{[\text{Native}_1]}$$

$$\text{Native}_2 \xleftrightarrow{K_2} \text{Unfolded}_2 \qquad \text{where} \quad K_2 = \frac{[\text{Unfolded}_2]}{[\text{Native}_2]}$$

In the case of **chemical denaturation**, the free energies of unfolding of the proteins are assumed to depend on denaturant concentration according to the LEM:

$$\Delta G_1 = \Delta G°_1 + m_1[D]$$
$$\Delta G_2 = \Delta G°_2 + m_2[D]$$

where $\Delta G°_1$ and $\Delta G°_2$ are the free energies for unfolding of the proteins in the absence of denaturant and m_1 and m_2 are the constants that describe the linear dependence of the ΔG's on denaturant concentration. K_1 and K_2 may be calculated as:

$$K_1 = \exp(-\Delta G_1/RT) \quad \text{and} \quad K_2 = \exp(-\Delta G_2/RT)$$

and the fractions of native ($F_{N,1}$ and $F_{N,2}$) and unfolded ($F_{U,1}$ and $F_{U,2}$) proteins present are given as:

$$F_{U,1} = K_1 / (1+K_1) \text{ and } F_{N,1} = 1 - F_{U,1}$$
$$F_{U,2} = K_2 / (1+K_2) \text{ and } F_{N,2} = 1 - F_{U,2}$$

The optical signals of the native and denatured forms of the proteins are assumed to be linearly-dependent on the denaturant concentration as follows:

$$Opt_{N,1} = I_{N,1} + S_{N,1}[D]$$
$$Opt_{U,1} = I_{U,1} + S_{U,1}[D]$$
$$Opt_{N,2} = I_{N,2} + S_{N,2}[D]$$
$$Opt_{U,2} = I_{U,2} + S_{U,2}[D]$$

The change in optical signal as a function of denaturant concentration is then given by:

$$\text{Signal} = [\{I_{N,1} + S_{N,1}[D]\}F_{N,1} + \{I_{U,1} + S_{U,1}[D]\}F_{U,1}] + [\{I_{N,2} + S_{N,2}[D]\}F_{N,2} +$$
$$+ \{I_{U,2} + S_{U,2}[D]\}F_{U,2}] \qquad (2.12)$$

The experimental data were fitted to Eq. (2.12), with the $\Delta G°$'s, m's and the I and S values as variables, using a standard non-linear least squares fitting procedure written by Dr. Stephen Martin (N.I.M.R.).

In the case of **thermal denaturation** the treatment is the same, except that the ΔG values are given by the Gibbs-Helmholtz equation as:

$$\Delta G_1 = \Delta H_{m,1}\,(1\text{-}T/T_{m,1}) + \Delta C_{p,1}(T - T_{m,1} - T \ln (T/T_{m,1})$$

$$\Delta G_2 = \Delta H_{m,2}\,(1\text{-}T/T_{m,2}) + \Delta C_{p,2}(T - T_{m,2} - T \ln (T/T_{m,2})$$

where T is the temperature (°K), the T_m's are the transition midpoint temperatures, ΔH_m's are the enthalpies at the midpoints, and ΔC_p's are the heat capacity changes. The optical signals of the native and denatured forms of the protein are assumed to be linearly-dependent on the temperature as follows:

$$Opt_{N,1} = I_{N,1} + S_{N,1}T$$
$$Opt_{U,1} = I_{U,1} + S_{U,1}T$$
$$Opt_{N,2} = I_{N,2} + S_{N,2}T$$
$$Opt_{U,2} = I_{U,2} + S_{U,2}T$$

The change in the optical signal as a function of temperature is then given by:

$$\text{Signal} = [\{I_{N,1} + S_{N,1}T\}F_{N,1} + \{I_{U,1} + S_{U,1}T\}F_{U,1}] + [\{I_{N,2} + S_{N,2}T\}F_{N,2} + \\ + \{I_{U,2} + S_{U,2}T\}F_{U,2}] \qquad (2.13)$$

The experimental were fitted to Eq. (2.13), with the ΔH_m's, ΔC_p's, T_m's, and the I and S values as variables, using a standard non-linear least squares fitting procedure written by Dr. Stephen Martin (N.I.M.R.). In practice, the ΔC_p's are very poorly defined by the data and were therefore held constant in the fits.

(B) Three-state transition

The protein unfolds via an intermediate according to the following scheme:

$$\text{Native} \xleftrightarrow{K_{NI}} \text{Intermediate} \qquad \text{where} \quad K_{NI} = \frac{[\text{Intermediate}]}{[\text{Native}]}$$

$$\text{Intermediate} \xleftrightarrow{K_{IU}} \text{Unfolded} \qquad \text{where} \quad K_{IU} = \frac{[\text{Unfolded}]}{[\text{Intermediate}]}$$

In the case of **chemical unfolding**, the free energies of unfolding for the two steps are assumed to depend on denaturant concentration according to the following equations (LEM):

$$\Delta G_{NI} = \Delta G°_{NI} + m_{NI}[D]$$

$$\Delta G_{IU} = \Delta G°_{IU} + m_{IU}[D]$$

where ΔG_{NI} and ΔG_{IU} are the free energies of unfolding for the two steps in the absence of denaturant and m_1 and m_2 are constants that describe the linear dependence of the ΔG's on denaturant concentration.
K_{NI} and K_{IU} may be calculated as:

$$K_{NI} = \exp(-\Delta G_{NI}/RT) \qquad \text{and} \qquad K_{IU} = \exp(-\Delta G_{IU}/RT)$$

and the fractions of native (F_N), intermediate (F_I) and unfolded (F_U) proteins present are given as:

$$F_N = 1 / (1+ K_{NI} + K_{NI}K_{IU})$$
$$F_I = K_{NI} / (1+ K_{NI} + K_{NI}K_{IU})$$
$$F_U = K_{NI}K_{IU} / (1+ K_{NI} + K_{NI}K_{IU})$$

The optical signals of the native, intermediate, and unfolded forms of the protein are assumed to be linearly-dependent on the denaturant concentration as follows:

$$Opt_N = I_N + S_N[D]$$
$$Opt_I = I_I + S_I[D]$$
$$Opt_U = I_U + S_U[D]$$

The change in the optical signal as a function of denaturant concentration is then given by:

$$\text{Signal} = \{I_N + S_N[D]\}F_N + \{I_I + S_I[D]\}F_I + \{I_U + S_U[D]\}F_U \qquad (2.14)$$

The experimental data were then fitted to Eq. (2.14), with the $\Delta G°$'s, m's and the I and S values as variables, using a standard non-linear least squares fitting procedure written by Dr. Stephen Martin (N.I.M.R.).

In the case of **thermal denaturation** the treatment is the same except that the ΔG values are given by the Gibbs-Helmholtz equation as:

$$\Delta G_{NI} = \Delta H_{m,NI} (1\text{-}T/T_{m,\,NI}) + \Delta C_{p,NI} (T - T_{m,NI} - T \ln (T/T_{m,NI})$$

$$\Delta G_{IU} = \Delta H_{m,IU} (1\text{-}T/T_{m,IU}) + \Delta C_{p,IU} (T - T_{m,\,IU} - T \ln (T/T_{m,\,IU})$$

where T is the temperature (°K), the T_m's are the transition midpoint temperatures, ΔH_m's are the enthalpies at the midpoint temperatures, and ΔC_p's are the heat capacity changes.

The optical signals of the native, intermediate, and unfolded forms of the protein are assumed to be linearly-dependent on the temperature as follows:

$$Opt_N = I_N + S_N T$$
$$Opt_I = I_I + S_I T$$
$$Opt_U = I_U + S_U T$$

The change in the optical signal as a function of denaturant concentration is then given by:

$$\text{Signal} = \{I_N + S_N T]\}F_N + \{I_I + S_I T\}F_I + \{I_U + S_U T\}F_U \qquad (2.15)$$

The experimental data were fitted to Eq. (2.15), with the $\Delta H°_m$'s, ΔC_p's, T_m's, and the I and S values as variables, using a standard non-linear least squares fitting procedure written by Dr. Stephen Martin (N.I.M.R.). In practice, the ΔC_p's are very poorly defined by the data and were therefore held constant in the fits.

In the case of biphasic unfolding, the problems connected with the data analysis are similar to those discussed for simple two-state unfolding, deriving from the poor definition of the pre- and post-transition baselines, and the strong correlation between the $\Delta G°$ and *m* values. In addition, it is virtually impossible to determine the optical properties of the intermediate state in the three-state model (or of state U for the first transition and of state N for the second transition, in the two two-state transitions model), since the separation between the two transitions (i.e. the difference in the midpoints) is almost always small. In some cases it was necessary to fix these values in the fits. Nevertheless, the parameters obtained from the analyses of the same

experiment repeated more than once are generally found to be in good agreement with each other and the errors in individual ΔG values are estimated to be of the order of 5-10%.

2.3.7 Effects of ligand binding on stability

Ligand binding to the native and/or denatured states of a protein must affect the stability of the protein. The change in stability resulting from binding is the ligand interaction free energy, $\Delta G_{b(X)}$, given by Schellman (1975) as:

$$\Delta G_{b(X)} = -RT \ln \Sigma_X$$

where Σ_X is the binding polynomial for the ligand to state X (either native (N) or unfolded (U)).

For two-state unfolding, the net interaction free energy is the difference in interaction free energies for the native and unfolded states:

$$\Delta\Delta G_b = \Delta G_{b(U)} - \Delta G_{b(N)} = -RT \ln(\Sigma_U/\Sigma_N)$$

In the case of a ligand binding to a single site on both the native and unfolded states of a protein with different affinities this is given by:

$$\Delta\Delta G_b = -RT \ln\left(\frac{1+K'_L[L]}{1+K_L[L]}\right)$$

where K_L and K'_L are the association constants for the ligand binding to the native and the unfolded states, respectively and [L] is the free ligand concentration. In the simpler case of ligand binding only to the native state of the protein (e.g. the interaction of CaM with a target peptide), the above expression becomes:

$$\Delta\Delta G_b = -RT \ln\left(\frac{1}{1+K_L[L]}\right) = +RT \ln\left(1+K_L[L]\right)$$

In the case of calcium binding to an isolated CaM domain $\Delta\Delta G_b$ is given by:

$$\Delta\Delta G_b = -RT \ln\left(\frac{1+K'_1[Ca]+K'_1K'_2[Ca]^2}{1+K_1[Ca]+K_1K_2[Ca]^2}\right) \quad (2.16)$$

where [Ca] is the free calcium concentration and the K_i and K'_i are the stoichiometric calcium association constants for binding to the native and unfolded states of that domain, respectively. Since calcium binds preferentially to the native state, the ligand interaction free energy is stabilising. The maximum possible stabilising free energy at any particular calcium concentration is obtained when there is no binding to the unfolded state, i.e.:

$$\Delta\Delta G_b = -RT \ln\left(\frac{1}{1+K_1[Ca]+K_1K_2[Ca]^2}\right) \quad (2.17)$$

Since the isolated domains show positive cooperativity in calcium binding (Linse et al., 1991a; Bayley et al., 1996), K_2 is greater than K_1 and at high calcium concentrations (e.g., >200 μM) Eq. (2.16) reduces to:

$$\Delta\Delta G_b = -RT \ln\left(\frac{1}{K_1K_2[Ca]^2}\right)$$

If calcium also binds to the unfolded state then the stabilising free energy due to calcium binding attains a limiting value at sufficiently high [Ca] (i.e., at $[Ca]^2 > 1/(K'_1K'_2)$), given by:

$$\Delta\Delta G_b(\text{limit}) = -RT \ln\left(\frac{K'_1K'_2}{K_1K_2}\right)$$

2.3.8 Kinetics of Ca^{2+}-dissociation and unfolding/refolding

Description of the experiments

Kinetic measurements were performed by monitoring tyrosine fluorescence changes using a Hi-Tech SF-61MX Multi-Mixing stopped flow spectrofluorimeter (see Section 2.2.4). The kinetics of Ca^{2+}-dissociation from the C-domain of CaM and the CaM mutants were studied by mixing 12 μM CaM (in 5 mM Ca^{2+}) with 20 mM EDTA. The kinetics of refolding and unfolding were studied at fixed denaturant concentrations (2.5 – 5.5 M) by adding calcium (refolding) or by removing calcium (unfolding). The kinetics of refolding of Tr2C and the C-domain of CaM were studied by stopped-flow mixing a solution of unfolded apo-Tr2C or apo-CaM (12 μM) in urea with a solution containing urea and calcium (0.3 – 5 mM). Similarly, the kinetics of unfolding were studied by stopped-flow mixing a solution of folded holo-CaM (12 μM plus 5 mM Ca^{2+}) in urea with a solution containing urea and EDTA (20 mM). These processes were studied as a function of calcium and urea concentration.

Theory and data analysis

In the case of the calcium dissociation, the kinetics are simple. The dissociation of the two Ca^{2+} ions from a CaM domain occurs according to the following scheme:

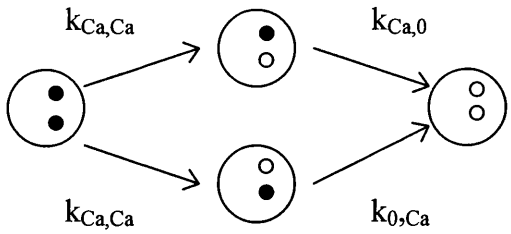

where $k_{Ca,Ca}$ is the rate constant for the dissociation of Ca^{2+} from one site when the other site is still occupied (assumed to be the same whichever calcium dissociates first – see Martin et al., 1985), and $k_{Ca,0}$ and $k_{0,Ca}$ are the two rate constants for the dissociation of Ca^{2+} from one site when the other site is empty. Previous studies have shown that the dissociation of the second Ca^{2+} ion is much faster than that of the first because when one site is empty the cooperativity between the two sites has been lost

(Malmendal et al., 1999a). Then, since $k_{Ca,0}$ and $k_{0,Ca} >> k_{Ca,Ca}$, the rate limiting step is the dissociation of the first calcium and the dissociation of the two Ca^{2+} ions from a CaM domain occurs with single exponential kinetics, with an observed rate equal to $k_{Ca,Ca}$. Several kinetic models had to be considered to describe the folding and unfolding reactions. The kinetic equations that relate the observed rates to intrinsic rate constants are more complex than for calcium dissociation and are discussed in Chapter 3.

Stopped-flow traces were fitted using the Hi-Tech software to either one or two exponential functions. For a single exponential the equation is:

$$\text{Signal} = \Delta V \exp(-kt) + V(\text{inf})$$

where ΔV is the total amplitude of the signal, k is the observed rate and V(inf) is the signal at infinite time ($t = \infty$). For a double exponential the equation is:

$$\text{Signal} = \Delta V_1 \exp(-k_1 t) + \Delta V_2 \exp(-k_2 t) + V(\text{inf})$$

where k_1 and k_2 are the two observed rates and the other parameters are defined as above.

CHAPTER 3

CHEMICAL AND THERMAL DENATURATION

3.1 Introduction

The thermodynamic stability of CaM and its constituent domains has been studied as a function of binding of Ca^{2+} using thermal and chemical denaturation, monitored spectroscopically using steady-state and kinetic techniques.

Previous studies on the stability of CaM and its fragments have shown that apo-CaM is much less stable than Ca^{2+}-CaM (holo-CaM) and that the apo-N-domain is more stable than the apo-C-domain both when isolated and when part of the intact protein (see Section 1.4.4, Chapter 1). However, these studies have been performed under different experimental conditions and a systematic study was needed in order to understand the mechanism of unfolding of CaM and the thermodynamic coupling of ligand binding and stability. The physical properties of CaM studied here relate to the specific questions of the stability of the protein *in vivo* and the independence of the CaM domains.

3.2 Materials and methods

The experimental approaches employed in the studies described in this chapter (optical spectroscopy, urea- and GuHCl-induced denaturation, thermal denaturation, and stopped-flow kinetics) are fully described in Chapter 2. Far-UV CD has been employed to monitor the unfolding of the intact protein and of the isolated domains; Tyr-138 fluorescence and absorption have been used to monitor selectively the unfolding of the C-domain in intact CaM and of Tr2C. Chemical denaturation is more than 95% reversible for all the proteins studied here, since spectroscopic signals characteristic of the native protein are recovered upon dilution of the denaturant to non-denaturing concentrations. Reversibility of thermal denaturation was assessed to be more than 95% following cooling to 10°C at a rate of 1 °C/min.

Some of the important mathematical relationships are now summarised here for convenience. The theory and data analysis procedures for two-state unfolding transitions are discussed in Sections 2.3.6.1 in Chapter 2. According to the Linear Extrapolation model (LEM), the free energy of unfolding (ΔG) for a simple two-state transition is given by:

$$\Delta G = \Delta G^\circ + m\,[D]$$

where ΔG° is the free energy for unfolding in the absence of denaturant and m is a constant that describes the dependence of ΔG on denaturant concentration ([D]). Owing to the high correlation between the parameters ΔG° and m in the analyses of chemical unfolding data, the ΔG°_{20} values (i.e. the free energies of unfolding at 20 °C) reported in the Tables were calculated using average m values, m_{av}. For urea m_{av} = -0.92 ± 0.05 kcal/(mol·M); for GuHCl m_{av} = -1.65 ± 0.23 kcal/(mol·M) (see Section 2.3.6.1).

In the case of thermal denaturation, the free energy of unfolding is given by the Gibbs-Helmholtz equation as:

$$\Delta G = \Delta H_m (1-T/T_m) + \Delta C_p (T - T_m - T \ln (T/T_m))$$

where T is the temperature (°K), T_m is the transition midpoint temperature, ΔH_m is the enthalpy at the midpoint temperature, and ΔC_p is the heat capacity change. Biphasic unfolding transitions have been analysed by treating the system as two separate two-state transitions (see Section 2.3.6.2).

In the case of calcium binding to a CaM domain the full expression for the ligand interaction free energy is:

$$\Delta\Delta G_b = -RT\ln\left(\frac{1+K'_1[Ca]+K'_1K'_2[Ca]^2}{1+K_1[Ca]+K_1K_2[Ca]^2}\right)$$

where [Ca] is the free calcium concentration and the K_i and K'_i are the stoichiometric calcium association constants for binding to the native and unfolded states of that domain, respectively. Simpler forms of this equation apply under particular conditions (see Section 2.3.7, Chapter 2).

3.3 Results

3.3.1 The optical properties of calmodulin

All of the experiments described here depend upon the fact that the optical properties of *Drosophila* CaM (far- and near-UV CD, Tyr-138 absorption and fluorescence) are markedly altered when the protein is denatured and are also strongly influenced by calcium binding. Figures 3.1 and 3.2 show the absorption, Tyr-138 fluorescence, far-UV CD and near-UV CD spectra of CaM under different solvent conditions. The spectra of apo-CaM (recorded in 25 mM Tris, 0.2 M KCl and labelled apo) are substantially different from those of Ca^{2+}-saturated CaM (recorded in 25 mM Tris, 0.1 M KCl, 1 mM $CaCl_2$ and labelled Ca), as described in detail elsewhere (Martin and Bayley, 1986; Bayley and Martin, 1992).

The absorption, Tyr-138 fluorescence, and near-UV CD spectra of unfolded CaM are labelled U and were recorded in 25 mM Tris, 0.1 M KCl, and 6 M GuHCl. The absorption spectrum is, as expected, closely similar to the spectrum of a 9:1 mole ratio mixture of Phe and Tyr (Maune et al., 1992b); the fluorescence spectrum has an intensity that is intermediate between that of apo-CaM and holo-CaM, owing to the unusually low intensity of the Tyr-138 emission of fully folded apo-CaM; the near-UV CD spectrum is almost eliminated, because of the increased mobility of the aromatic residues in the unfolded state. The far-UV CD spectrum of unfolded CaM (U) was

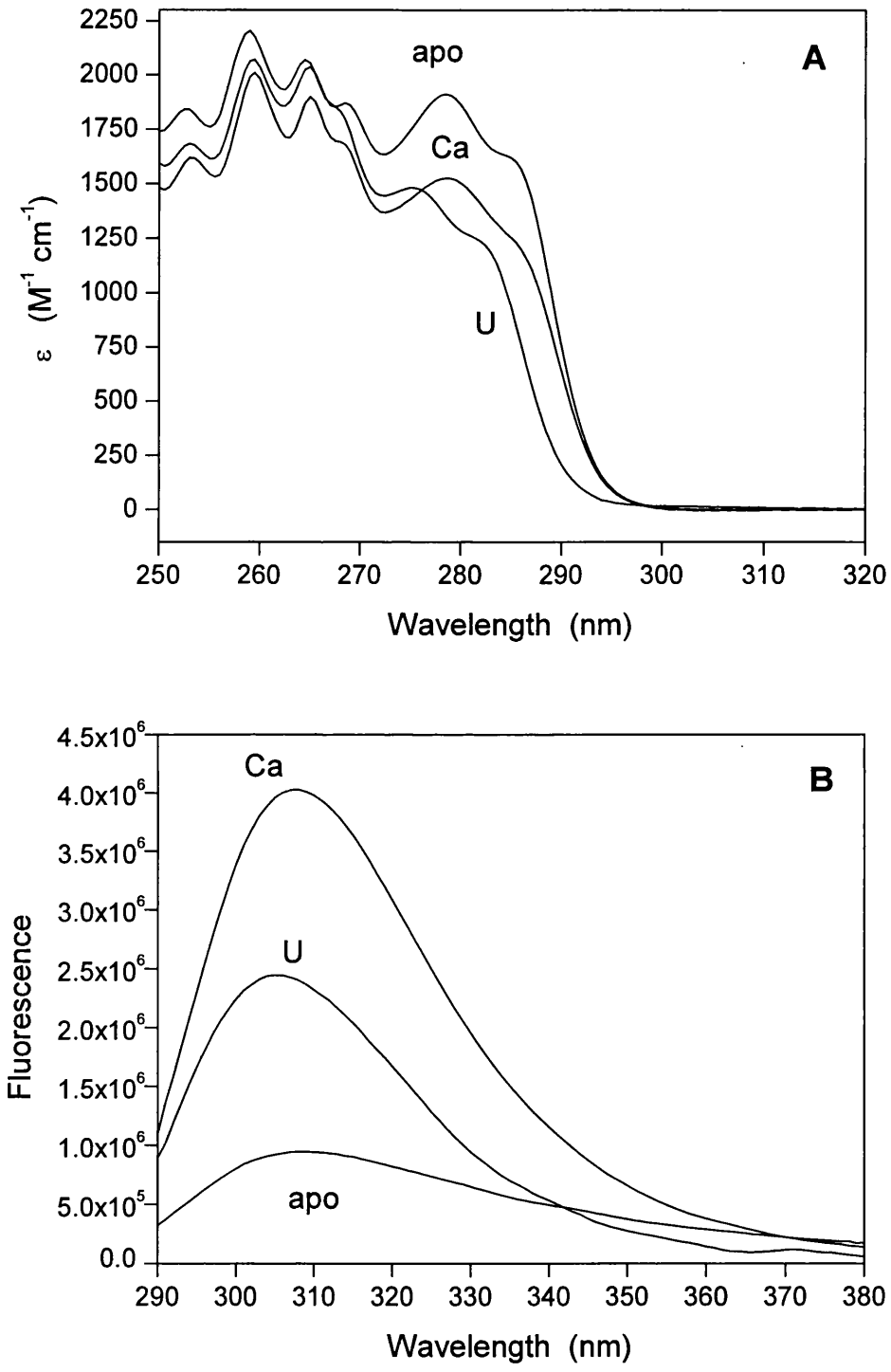

Figure 3.1 Absorption **(A)** and Tyr-138 fluorescence **(B)** spectra of CaM recorded at 20 °C under different solvent conditions. (apo), apo-CaM in 0.2 M KCl; (Ca), Ca^{2+}-CaM in 0.1 M KCl, 1 mM $CaCl_2$; (U) unfolded CaM in 0.1 M KCl, 6 M GuHCl.

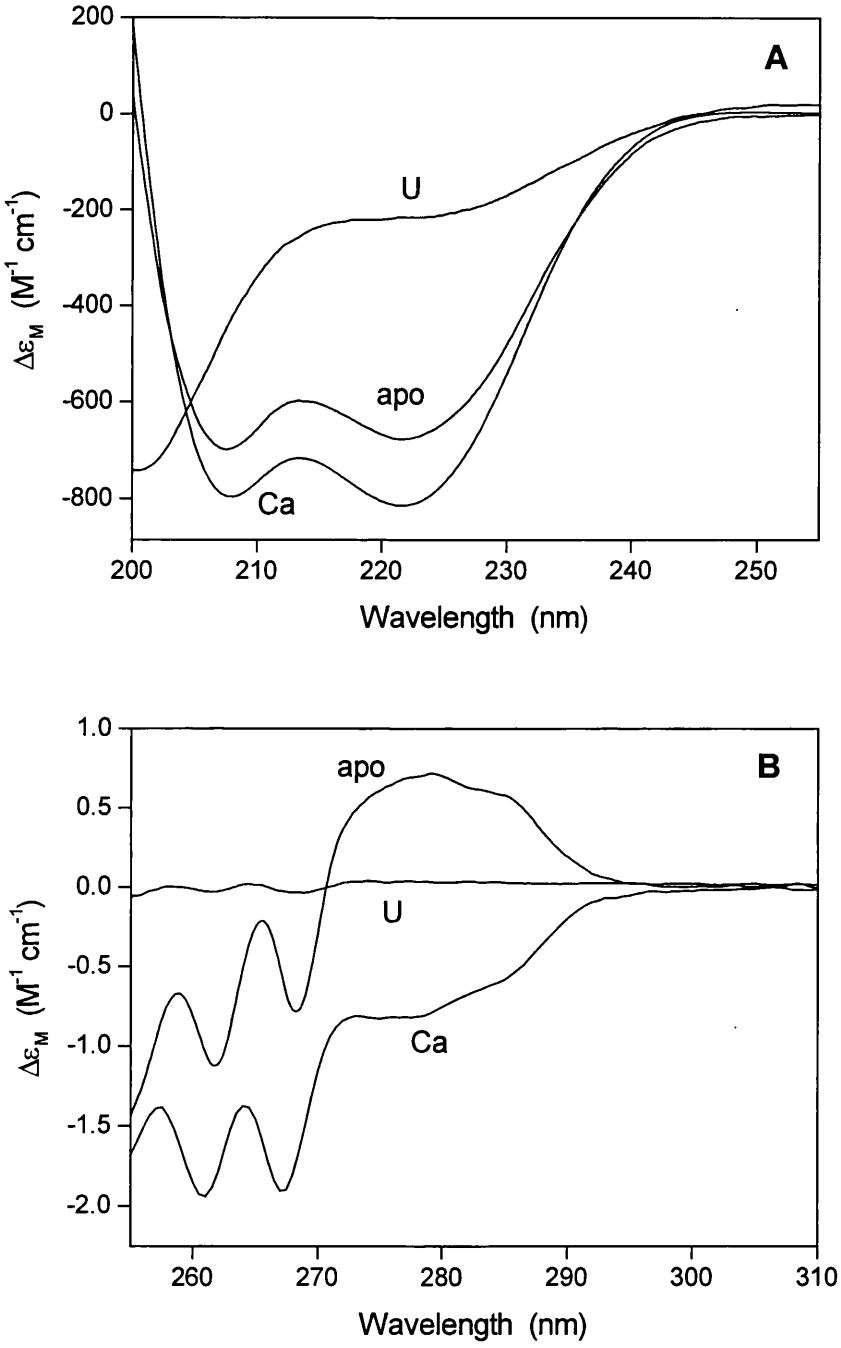

Figure 3.2 Far- **(A)** and near- **(B)** UV CD spectra of CaM under different solvent conditions. (apo), apo-CaM in 0.2 M KCl at 20 °C; (Ca), Ca^{2+}-CaM in 0.1 M KCl and 1 mM $CaCl_2$, at 20 °C. The spectrum for unfolded CaM (U) was recorded in 25 mM Hepes at 75 °C in the case of far-UV CD and in 25 mM Tris, 0.1 M KCl, 6 M GuHCl, at 20 °C in the case of near-UV CD.

recorded in 25 mM Hepes at 75 °C and shows the characteristics of a random coil (Yang et al., 1986; Venyaminov et al., 1993).

3.3.2 Chemical denaturation of apo-proteins

Chemical denaturation of apo-CaM and its isolated fragments has been studied with the denaturants urea and GuHCl using far-UV CD, absorption and fluorescence spectroscopy.

Figure 3.3 shows typical far-UV CD and Tyr-138 fluorescence data for urea-induced denaturation of apo-Tr1C and apo-Tr2C. The unfolding curves conform to simple two-state transitions in all cases. Table 3.1 summarises the results of the LEM analyses for these proteins. The free energies of unfolding ($\Delta G°_{20}$) for apo-Tr1C and apo-Tr2C are 2.84 and ~ 1.97 kcal/mol respectively; thus, apo-Tr1C is more stable than apo-Tr2C by ~ 0.9 kcal/mol. The agreement between the far-UV CD and Tyr-138 fluorescence data for Tr2C is well within the experimental error of ~ 5-10%.

The far-UV CD curve for urea-unfolding of intact apo-CaM (Fig. 3.3A) clearly shows two resolvable transitions, which are denoted as CaM-1 and CaM-2 in Table 3.1. The $\Delta G°_{20}$ values are 1.52 kcal/mol for the transition CaM-1 and 3.73 kcal/mol for the transition CaM-2. The simplest interpretation is that the two transitions correspond to unfolding of individual calmodulin domains. This hypothesis is supported by the fact that denaturant *m* values determined for the two transitions are very similar to those obtained for the isolated fragments. Based on the observation that apo-Tr1C is more stable than apo-Tr2C, the CaM-1 and CaM-2 transitions have been assigned to the unfolding of the C-domain and the N-domain of apo-CaM, respectively. The data for intact apo-CaM obtained using fluorescence and absorption measurements (Tyr-138, C-domain) are shown in Figure 3.3B and Table 3.1. The unfolding parameters ($\Delta G°_{20}$ = 1.58 and 1.56 kcal/mol for fluorescence and absorption, respectively) are closely similar to those obtained for the CaM-1 transition using far-UV CD ($\Delta G°_{20}$ = 1.52 kcal/mol). This observation confirms the assignment of the CaM-1 transition to the unfolding of the C-domain of apo-CaM.

Figure 3.3A shows that the urea unfolding curve for intact apo-CaM is not reproduced by the sum of the unfolding curves for the isolated fragments. Consistent with this observation, the analyses (Table 3.1) show that the stabilities of the isolated

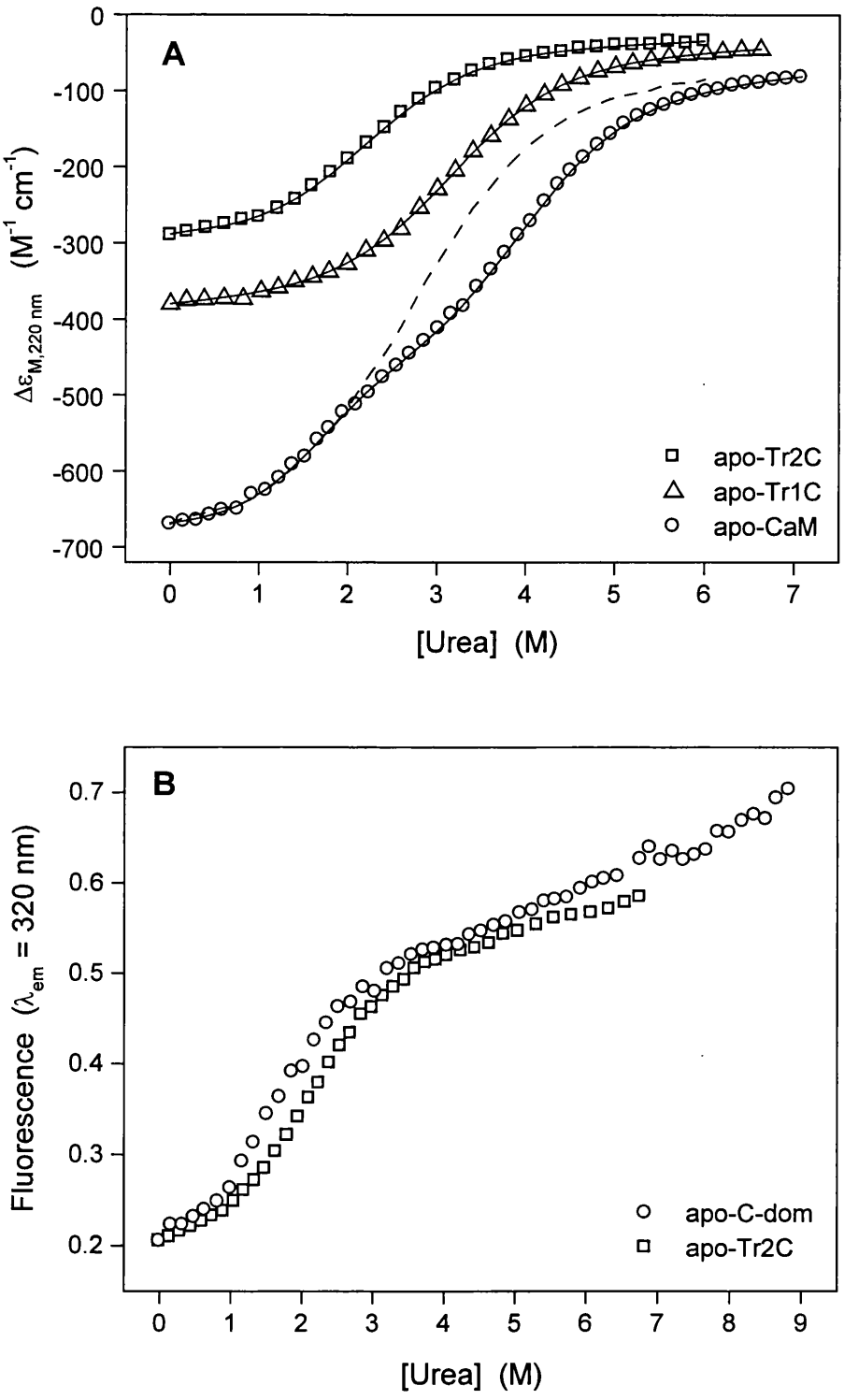

Figure 3.3 Urea-induced denaturation of apo-CaM (○), apo-Tr1C (△), and apo-Tr2C (□), measured at 20 °C in 25 mM Tris, 100 mM KCl, pH 8, using far-UV CD **(A)** and Tyr-138 fluorescence **(B)**. The solid lines are the computed best fits. The dotted line represents the sum of the curves for Tr1C and Tr2C.

Table 3.1 Urea-unfolding of apo-Tr1C, apo-Tr2C, and apo-CaM

Transition	Method[a]	m (kcal/(mol·M))	$[U]_{1/2}$ (M)	$\Delta G°_{20}$[b] (kcal/mol)
apo-Tr1C	CD	-0.91	3.09	2.84
apo-Tr2C	CD	-0.98	2.17	2.0
apo-Tr2C	Flu	-1.10	2.11	1.94
apo-CaM-1[c]	CD	-1.12	1.65	1.52
apo-CaM-2[c]	CD	-0.92	4.05	3.73
apo-CaM-C[c]	Flu	-1.22	1.72	1.58
apo-CaM-C	Abs	-0.97	1.70	1.56

[a] CD, Flu, and Abs identify unfolding monitored using far-UV CD, Tyr-138 fluorescence, and Tyr-138 absorption.

[b] $\Delta G°_{20}$ values were calculated as $-[U]_{1/2} \cdot m_{av}$, with m_{av} = -0.92 kcal/mol·M (see Section 2.3.6.1, Chapter 2).

[c] CaM-1 and CaM-2 indicate the first and second transitions resolved for intact CaM (far-UV CD), assigned to the C- and N-domains respectively. CaM-C represents unfolding of the C-domain in intact CaM (absorption and fluorescence of Tyr-138).

domains are significantly different from those of the corresponding domains in intact CaM. In particular, the C-domain in apo-CaM (CaM-1 transition) is destabilised by ~ 0.4 kcal/mol compared to free apo-Tr2C whilst the N-domain in apo-CaM (CaM-2 transition) is stabilised by ~ 0.9 kcal/mol compared to free apo-Tr1C.

For GuHCl-induced denaturation, the pattern of behaviour is essentially the same as that observed with urea. Typical far-UV CD data for apo-CaM, apo-Tr1C and apo-Tr2C are shown in Figure 3.4A and the results of the LEM analyses are given in Table 3.2. The $\Delta G°_{20}$ values for apo-Tr1C and apo-Tr2C are 3.37 and 2.39 kcal/mol respectively, and therefore apo-Tr1C is more stable than apo-Tr2C by ~ 1 kcal/mol. The two resolvable transitions in apo-CaM have again been assigned to the unfolding of the two CaM domains. The relative stability of the fragments suggests that the transition CaM-1 may be assigned to the C-domain and the transition CaM-2 to the N-domain, as for urea. The GuHCl-induced unfolding of the C-domain in intact apo-CaM has also been monitored using Tyr-138 fluorescence and absorption. Typical curves are shown in Figure 3.4B and the results of the analyses are in Table 3.2. The $\Delta G°_{20}$ values of 2.08 kcal/mol (fluorescence) and 2.13 kcal/mol (absorption) are in good agreement with the value of 2.19 kcal/mol obtained with far-UV CD for the transition CaM-1 and therefore these data confirm the assignment of this transition to the C-domain.

As observed for urea, the unfolding curve for intact apo-CaM cannot be represented by the sum of the unfolding curves for the isolated fragments (Fig. 3.4A). The results of the analyses (Table 3.2) again show that the N-domain of apo-CaM is more stable than apo-Tr1C (by ~ 0.6 kcal/mol), whilst the C-domain of apo-CaM is less stable than apo-Tr2C (by ~ 0.25 kcal/mol).

Depending on the spectroscopic technique employed to monitor unfolding of CaM and its domains, the protein concentrations used varied in the range 10 – 400 μM. The results obtained using different methods generally agree within experimental error. This observation shows that the unfolding process is not dependent on protein concentration and thus the proteins do not aggregate under the experimental conditions used.

It is evident from a comparison of Tables 3.1 and 3.2 that the $\Delta G°_{20}$ values determined with GuHCl are consistently larger than those obtained with urea. The possible reasons for this observation will be explored in Chapter 4.

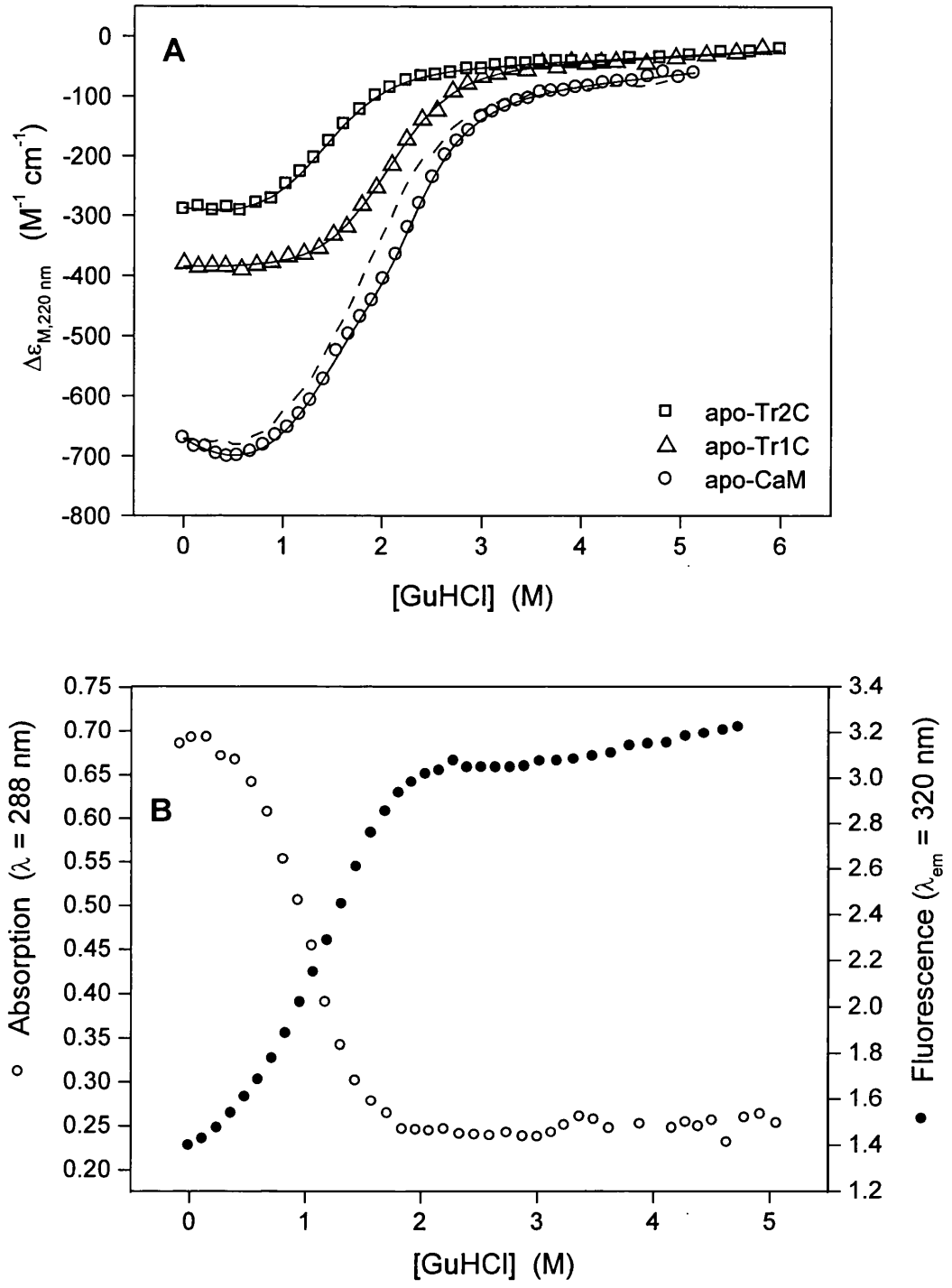

Figure 3.4 **(A)** GuHCl-induced denaturation of apo-CaM (○), apo-Tr1C (△), and apo-Tr2C (□), measured at 20 °C in 25 mM Tris, 100 mM KCl, pH 8, using far-UV CD. The solid lines are the computed best fits. The dotted line represents the sum of the curves for Tr1C and Tr2C. **(B)** GuHCl-induced denaturation of apo-CaM (C-domain) measured at 20 °C in 25 mM Tris, 100 mM KCl, pH 8, using Tyr-138 absorption (○) and fluorescence (●).

Table 3.2 GuHCl-unfolding of apo-Tr1C, apo-Tr2C, and apo-CaM

Transition	Method[a]	m (kcal/(mol·M))	$[G]_{1/2}$ (M)	$\Delta G°_{20}$[b] (kcal/mol)
apo-Tr1C	CD	-1.79	2.04	3.37
apo-Tr2C	CD	-1.97	1.45	2.39
apo-CaM-1[c]	CD	-1.99	1.33	2.19
apo-CaM-2[c]	CD	-1.92	2.38	3.93
apo-CaM-C[c]	Fluo	-1.97	1.26	2.08
apo-CaM-C	Abs	-2.06	1.29	2.13

[a] CD, Flu, and Abs identify unfolding monitored using far-UV CD, Tyr-138 fluorescence, and Tyr-138 absorption.

[b] $\Delta G°_{20}$ values were calculated as $-[G]_{1/2} \cdot m_{av}$, with m_{av} = -1.65 kcal/mol·M (see Section 2.3.6.1, Chapter 2).

[c] CaM-1 and CaM-2 indicate the first and second transitions resolved for intact CaM (far-UV CD), assigned to the C- and N-domains respectively. CaM-C represents unfolding of the C-domain in intact CaM (absorption and fluorescence of Tyr-138).

3.3.3 Chemical denaturation of calcium-saturated proteins

3.3.3.1 Isolated domains

The chemical unfolding of the calcium-saturated (holo) forms of the isolated domains has been monitored using far-UV CD and Tyr-138 fluorescence spectroscopy. Figure 3.5 shows typical far-UV CD data for the urea-induced denaturation of the holo-forms of Tr1C and Tr2C in the presence of 0.3 mM calcium; the unfolding profiles for

the apo-forms are included for comparison. It is evident that the holo-proteins are, as expected, substantially more stable than the apo-proteins. Table 3.3 summarises the results of the LEM analyses and shows that the measured stabilities ($\Delta G°_{20}$) of holo-Tr1C and holo-Tr2C in 0.3 mM calcium are 6.04 and 6.27 kcal/mol, respectively. This stabilising effect of calcium is predicted by the theory of ligand binding (see Section 2.3.7, Chapter 2), which shows that when a ligand binds to the native state of a protein more strongly that it binds to the denatured state, the binding of the ligand stabilises the native form of the protein against unfolding.

The $\Delta G°_{20}$ values in Table 3.3 also show that the binding of calcium causes a reversal of the relative stability of the isolated holo-domains compared to their apo-forms, so that at $[Ca^{2+}] \geq 0.3$ mM, holo-Tr2C becomes more stable than holo-Tr1C, even though apo-Tr2C is less stable than apo-Tr1C. This observation is consistent with the fact that Tr2C (containing sites III and IV) binds calcium more strongly than Tr1C (containing sites I and II). The product of the two measured stoichiometric calcium association constants K_1K_2 is $6.1 \cdot 10^9$ M^{-2} for Tr1C and $3.35 \cdot 10^{11}$ M^{-2} for Tr2C (Bayley et al., 1996). As a consequence, the ligand interaction free energy for Tr2C is expected to be higher than that for Tr1C (see Eq. (2.17) in Section 2.3.7, Chapter 2).

In the case of GuHCl, the denaturation profiles for the isolated domains were obtained at 1, 10 and 100 mM calcium and are shown in Figure 3.6. As observed for urea-unfolding, the relative stability of the two domains is reversed and holo-Tr2C is more stable than holo-Tr1C at all calcium concentrations studied here. The experimental curves and the results of the analyses (Table 3.3) indicate that as the calcium concentration is increased, the proteins become increasingly more stable. This is predicted by Equation (2.16) (Section 2.3.7, Chapter 2), which shows that the stabilising effect of calcium binding depends on the calcium affinities of both the native and denatured states, as well as on the free calcium concentration. The GuHCl-induced unfolding of holo-Tr2C in the presence of 1 mM Ca^{2+} has also been monitored by Tyr-138 fluorescence spectroscopy. The results (Table 3.3) are in fair agreement with the far-UV CD data.

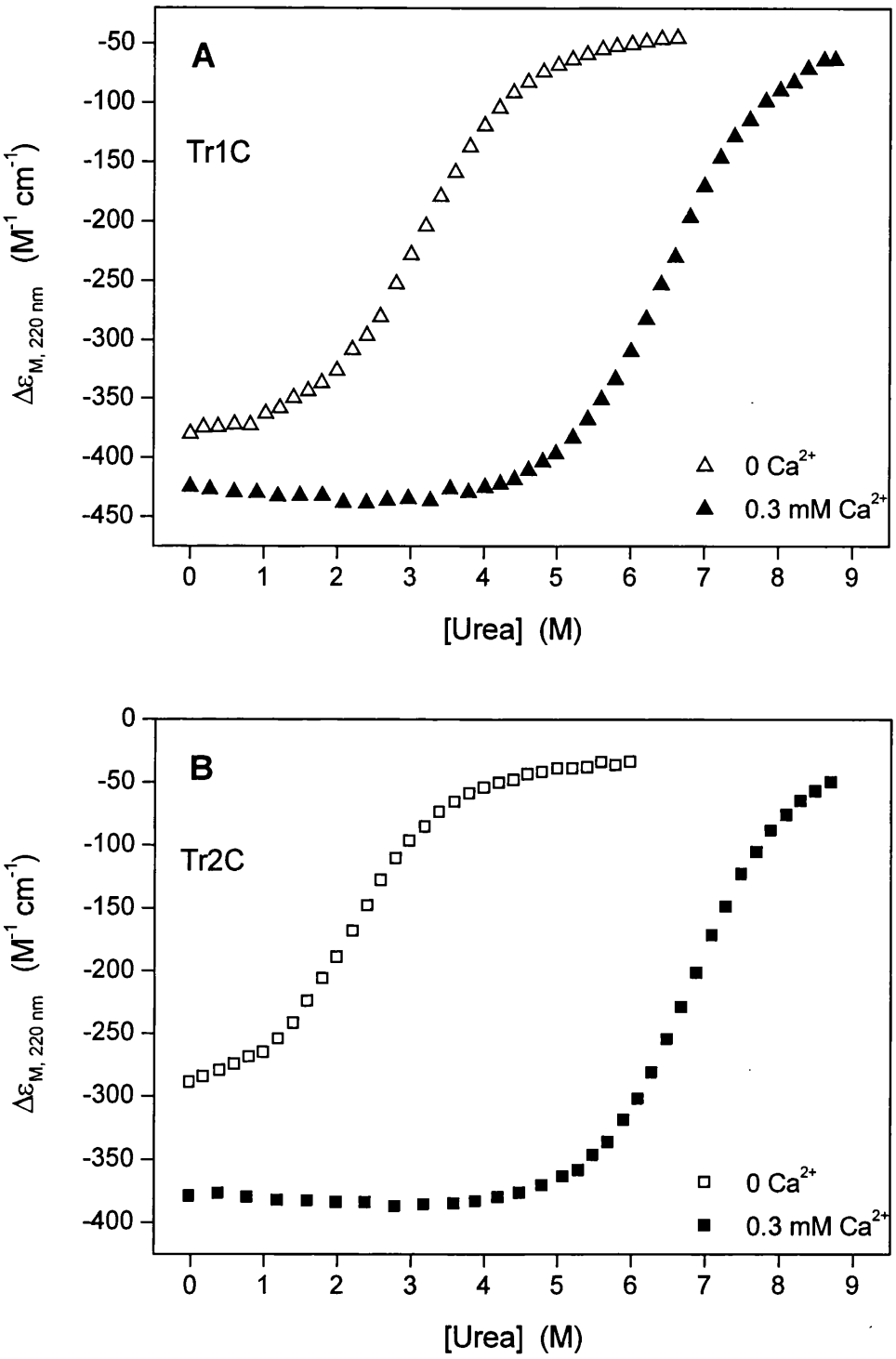

Figure 3.5 (A) Urea-induced denaturation of Tr1C at 0 (△) and 0.3 (▲) mM Ca^{2+}. **(B)** Urea-induced denaturation of Tr2C at 0 (□) and 0.3 (■) mM Ca^{2+}. The curves were measured at 20 °C in 25 mM Tris, 100 mM KCl, pH 8, using far-UV CD.

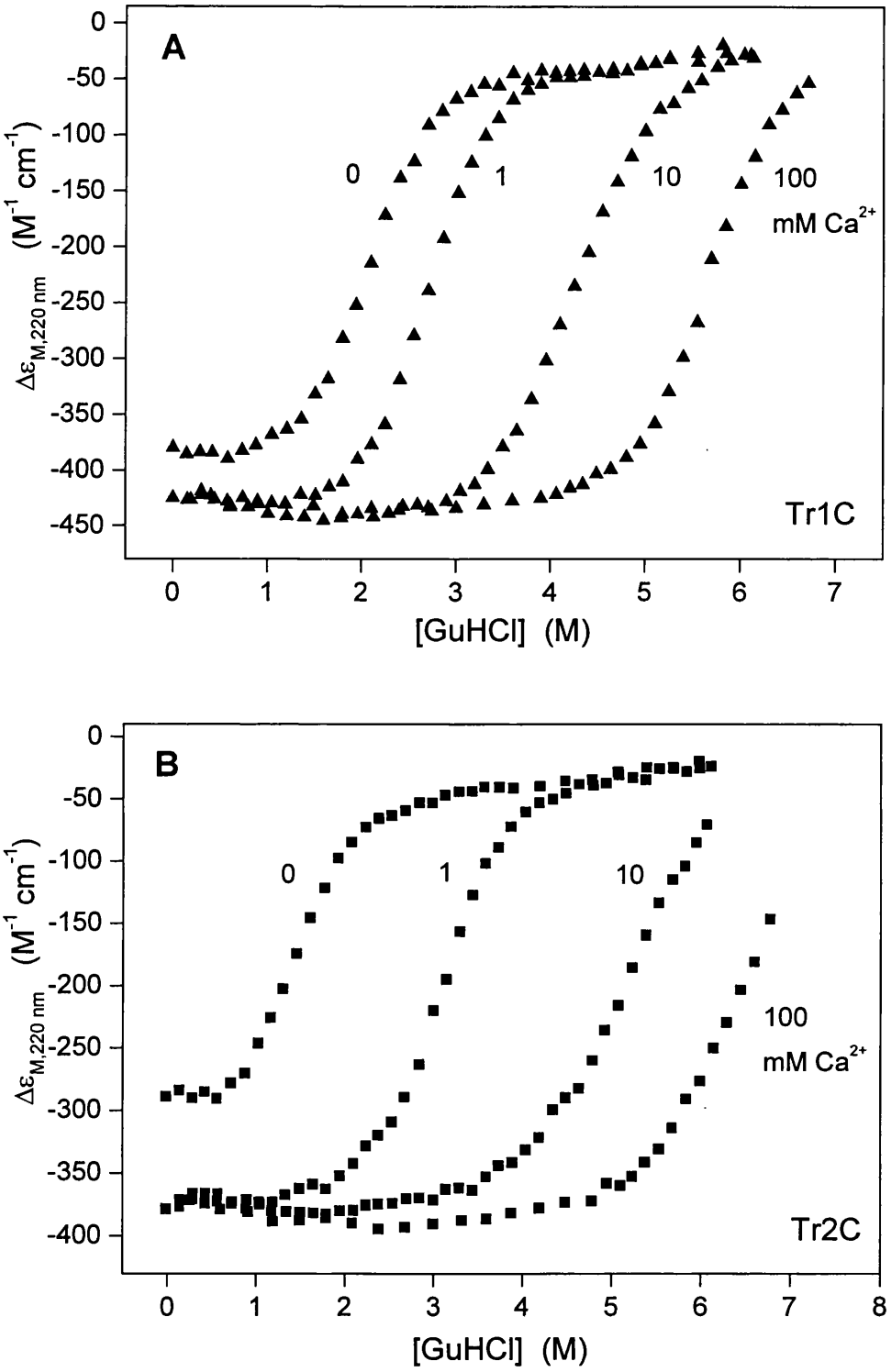

Figure 3.6 GuHCl-induced denaturation of Tr1C (▲) **(A)** and Tr2C (■) **(B)** at $[Ca^{2+}]$ = 0, 1, 10 and 100 mM. The curves were measured at 20 °C in 25 mM Tris, 100 mM KCl, pH 8, using far-UV CD.

Table 3.3 Urea- and GuHCl-unfolding of holo-Tr1C and holo-Tr2C

Protein	Denaturant	Method[a]	$[Ca^{2+}]$ (mM)	m (kcal/mol·M)	$[D]_{1/2}$ (M)	ΔG°_{20}[b] (kcal/mol)	$\Delta\Delta G_b$(obs)[c] (kcal/mol)	$\Delta\Delta G_b$(calc)[d] (kcal/mol)
Tr1C	Urea	CD	0.3	-0.85	6.56	6.04	3.23	3.67
Tr2C	Urea	CD	0.3	-0.91	6.81	6.27	4.3	6.01
Tr1C	GuHCl	CD	1.0	-1.77	2.67	4.41	1.04	5.07
		CD	10.0	-1.26	4.16	6.86	3.49	7.76
		CD	100.0	-1.51	5.66	9.34	5.97	10.44
Tr2C	GuHCl	CD	1.0	-1.64	3.09	5.10	2.71	7.41
		Flu	1.0	-1.64	3.23	5.33	-	-
		CD	10.0	-1.08	5.12	8.45	6.06	10.09
		CD	100.0	-0.99	6.40	10.56	8.17	12.77

[a] CD, Flu, and Abs identify unfolding monitored using far-UV CD, Tyr-138 fluorescence, and Tyr-138 absorption.

[b] ΔG°_{20} values were calculated as $-[D]_{1/2} \cdot m_{av}$, with m_{av} = -0.92 kcal/mol·M (urea) and -1.65 kcal/mol·M (GuHCl) (see Section 2.3.6.1, Chapter 2).

[c] $\Delta\Delta G_b$(obs) values were calculated as ΔG°_{20}(plus calcium) - ΔG°_{20}(apo) using ΔG°_{20}(apo) values from Tables 3.1 and 3.2.

[d] $\Delta\Delta G_b$(calc) values were calculated as $-RT \ln\{1/(K_1K_2[Ca^{2+}]^2)\}$ (see Section 3.2) with $K_1K_2 = 6.1 \cdot 10^9$ M^{-2} for Tr1C and $K_1K_2 = 3.35 \cdot 10^{11}$ M^{-2} for Tr2C (Bayley et al., 1996).

3.3.3.2 Intact CaM

The chemical unfolding of intact holo-CaM has been monitored by far-UV CD, fluorescence and absorption spectroscopy at several different calcium concentrations. Typical far-UV CD curves obtained using urea (at 0, 0.3, 0.6, and 1 mM calcium) and GuHCl (at 0, 1, 10, and 100 mM calcium) are shown in Figure 3.7. As in the case of apo-CaM, the curves have been analysed as pairs of two-state transitions (CaM-1 and CaM-2), and each transition has been assigned to the unfolding of a single CaM domain. Table 3.4 summarises the results of the LEM analyses for the far-UV CD experiments. Figures 3.8 and 3.9 show the unfolding profiles of the C-domain in intact CaM measured using Tyr-138 fluorescence and absorption at different calcium concentrations. The results of the analyses are listed in Table 3.5.

In the case of GuHCl, the assignment of the CaM-1 and CaM-2 transitions is unambiguous. The relative stabilities of the isolated fragments and the comparison of the far-UV CD and fluorescence/absorption data identifies the CaM-2 transition with the C-domain, even though the midpoint and ΔG^{o}_{20} values determined from fluorescence and absorption data are somewhat higher than those determined from the CD data. It is therefore clear that, as observed with the isolated domains, the order of domain stabilities in intact holo-CaM is reversed compared to that in apo-CaM, with the C-domain now more stable than the N-domain. This is again consistent with the fact that sites III and IV (C-domain) have greater affinity for calcium than sites I and II (N-domain).

In the case of urea-induced denaturation, the assignment of the CaM-1 and CaM-2 transitions is not unambiguous because the isolated holo-domains show very similar stability. Comparison with the Tyr-138 fluorescence results does, however, suggest that the CaM-2 transition probably corresponds to unfolding of the C-domain and thus that, as with GuHCl, the holo-C-domain is more stable than the holo-N-domain.

Figure 3.10 shows the urea- and GuHCl-unfolding curves for intact holo-CaM monitored by far-UV CD. Calcium concentrations were 0.3 mM for urea and 1.0 mM for GuHCl. It is evident that the curves for intact holo-CaM cannot be represented as the sum of the unfolding curves for the isolated fragments. The N-domain in holo-CaM is destabilised compared to holo-Tr1C whilst the C-domain in holo-CaM is stabilised

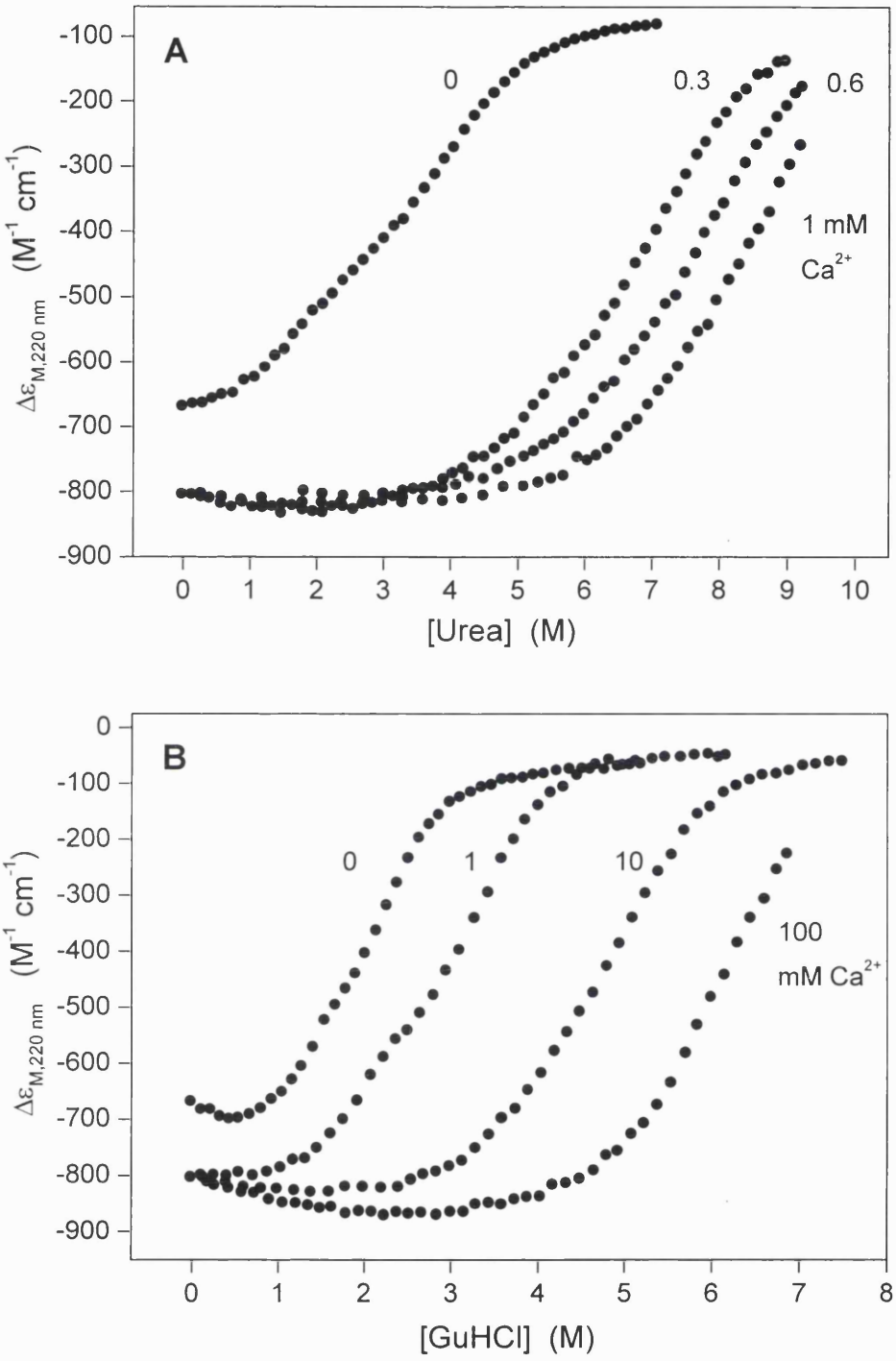

Figure 3.7 **(A)** Urea-induced denaturation of CaM at $[Ca^{2+}]$ = 0 (a), 0.3 (b), 0.6 (c) and 1 (d) mM. **(B)** GuHCl-induced denaturation of CaM at $[Ca^{2+}]$ = 0 (a), 1 (b), 10 (c) and 100 (d) mM. Unfolding was monitored in 25 mM Tris, 100 mM KCl, pH 8, at 20 ^{o}C, using far-UV CD.

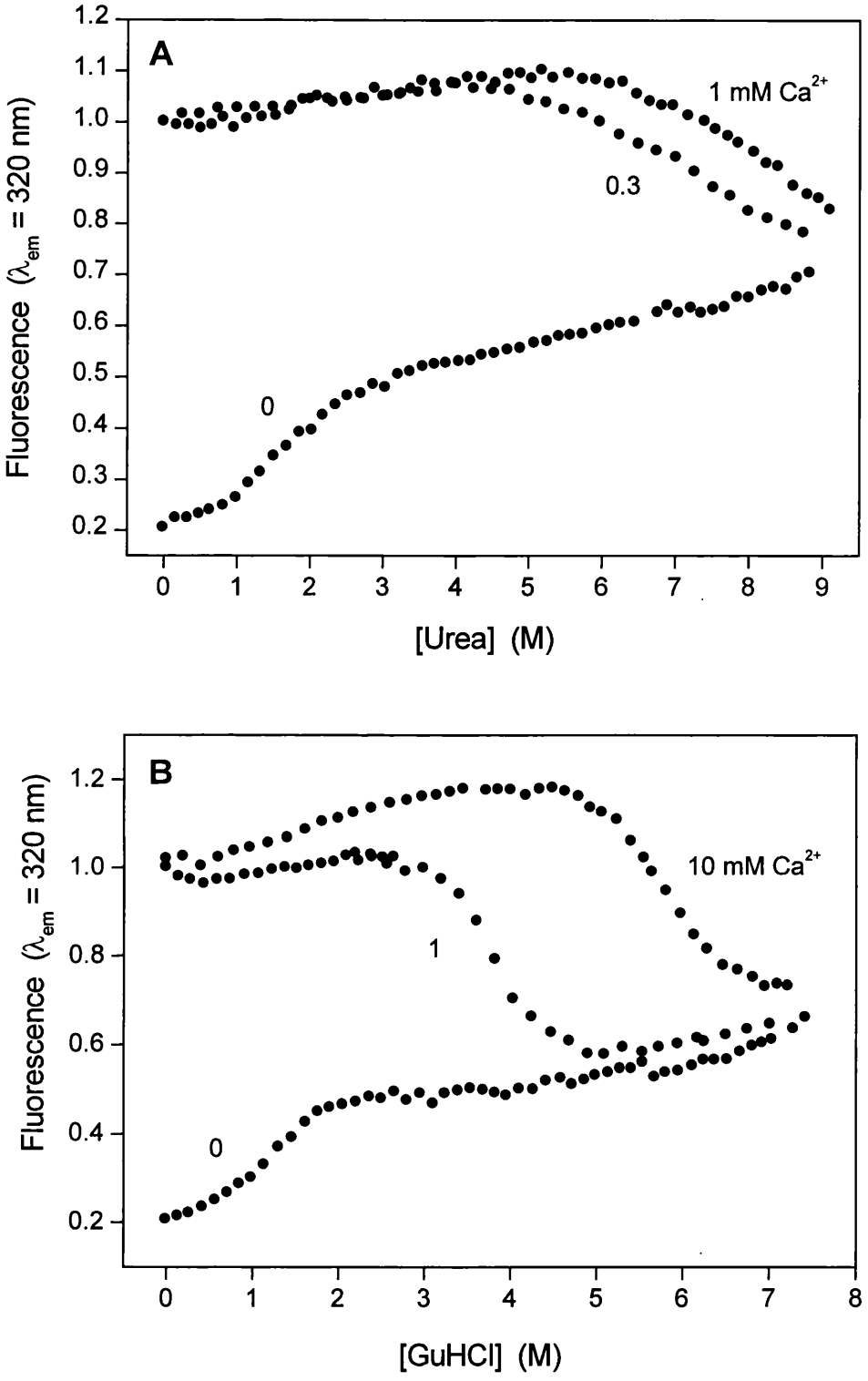

Figure 3.8 **(A)** Urea-induced denaturation of CaM (C-domain) at $[Ca^{2+}] = 0$ (a), 0.3 (b), and 1 (c) mM. **(B)** GuHCl-induced denaturation of CaM (C-domain) at $[Ca^{2+}] = 0$ (a), 1 (b), and 10 (c) mM. Unfolding was monitored in 25 mM Tris, 100 mM KCl, pH 8, at 20 °C, using Tyr-138 fluorescence.

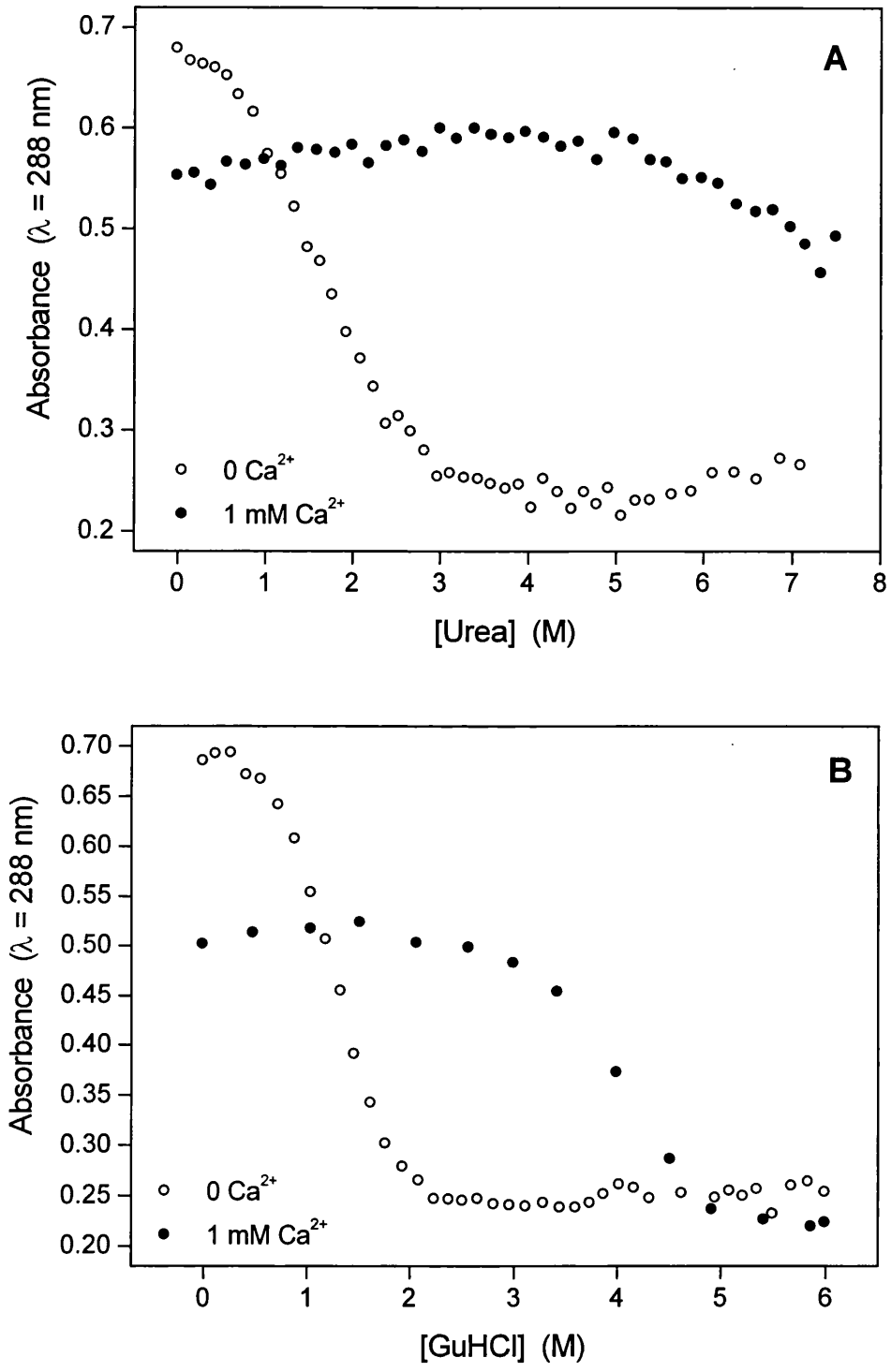

Figure 3.9 Urea- **(A)** and GuHCl- **(B)** induced denaturation of CaM (C-domain) at 0 (○) and 1 (•) mM Ca^{2+}. Unfolding was monitored in 25 mM Tris, 100 mM KCl, pH 8, at 20 °C, using Tyr-138 absorption.

compared to holo-Tr2C (Tables 3.3 and 3.4). This is the opposite of the situation observed with apo-CaM, where the N-domain is stabilised compared to apo-Tr1C whilst the C-domain is destabilised compared to apo-Tr2C. Thus, in both cases (for apo- and for holo-CaM) the less stable domain in the intact protein is destabilised relative to the corresponding isolated domain, whilst the more stable domain is stabilised compared to the corresponding isolated domain.

As noted above (Section 3.2), average *m* values have been used in the analysis of urea- and GuHCl-unfolding curves to calculate $\Delta G°_{20}$ as $-[D]_{1/2} \cdot m_{av}$. However, there are clearly significant variations in the individual *m* values. In the case of GuHCl-unfolding of the Ca^{2+}-saturated fragments, for example, the *m* values seem to decrease as calcium concentration is increased (Table 3.3). A similar trend is obtained with

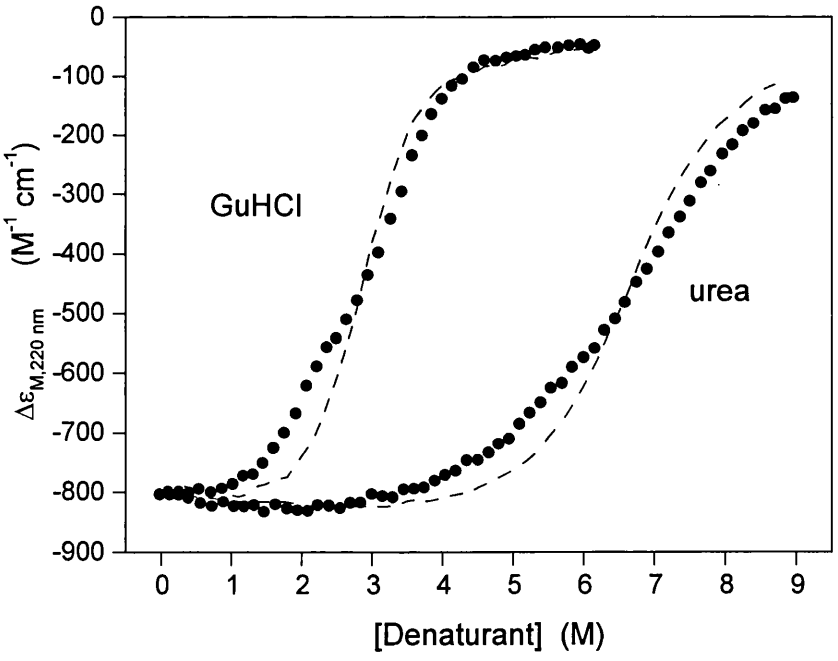

Figure 3.10 GuHCl- and urea-induced denaturation of CaM (•) at 1 and 0.3 mM Ca^{2+}, respectively. The dotted line represents the sum of the curves for Tr1C and Tr2C measured under the same conditions. Unfolding was monitored in 25 mM Tris, 100 mM KCl, pH 8, at 20 °C, using far-UV CD.

Table 3.4 Urea- and GuHCl-unfolding of holo-CaM monitored by far-UV CD

Transition	Denaturant	$[Ca^{2+}]$ (mM)	m (kcal/mol·M)	$[D]_{1/2}$ (M)	ΔG°_{20} [a] (kcal/mol)
CaM-1[b]	Urea	0.3	-0.63	5.38	4.95
CaM-2[b]			-0.92	7.40	6.81
CaM-1	Urea	0.6	-0.64	6.44	5.92
CaM-2			-0.86	8.05	7.41
CaM-1	GuHCl	1.0	-2.05	1.99	3.28
CaM-2			-1.58	3.37	5.56
CaM-1	GuHCl	10.0	-0.91	3.93	6.48
CaM-2			-1.24	5.21	8.60
CaM-1	GuHCl	100.0	-0.67	5.28	8.71
CaM-2			-1.61	6.30	10.40

[a] ΔG°_{20} values were calculated as $-[D]_{1/2} \cdot m_{av}$, with m_{av} = -0.92 kcal/mol·M (urea) and -1.65 kcal/mol·M (GuHCl) (see Section 2.3.6.1, Chapter 2).

[b] CaM-1 and CaM-2 indicate the first and second transitions resolved for intact CaM, assigned to the N- and C- domains respectively.

intact holo-CaM (Tables 3.4 and 3.5). In addition, in the biphasic curves obtained with either denaturant for intact holo-CaM using far-UV CD, the *m* values measured for the transition CaM-1 are consistently lower (except for one case) than the ones measured for the transition CaM-2. In contrast, in the case of the apo-proteins the *m* values show little variation either for the isolated fragments or for the domains in intact CaM; they are all in the range -0.9 to -1.1 kcal/(mol·M) for urea and -1.8 to -2.0 kcal/(mol·M) for

Table 3.5 Urea- and GuHCl-unfolding of the holo-CaM C-domain monitored by Tyr-138 fluorescence and Tyr-138 absorption

Denaturant	Method [a]	$[Ca^{2+}]$ (mM)	m (kcal/mol·M)	$[D]_{1/2}$ (M)	ΔG°_{20} [b] (kcal/mol)
Urea	Flu	0.3	-0.58	6.91	6.36
Urea	Flu	1.0	-0.57	8.16	7.51
Urea	Abs	1.0	-0.48	7.75	7.13
GuHCl	Flu	1.0	-1.71	3.84	6.34
GuHCl	Abs	1.0	-1.63	3.88	6.40
GuHCl	Flu	10.0	-1.15	5.82	9.60

[a] Flu and Abs identify unfolding monitored using Tyr-138 fluorescence and Tyr-138 absorption.

[b] ΔG°_{20} values were calculated as $-[D]_{1/2} \cdot m_{av}$, with m_{av} = -0.92 kcal/mol·M (urea) and -1.65 kcal/mol·M (GuHCl) (see Section 2.3.6.1, Chapter 2).

GuHCl (Tables 3.1 and 3.2). Because the individual ΔG° and m values are highly correlated it is difficult to assess whether the apparent variation in m values observed with the holo proteins has real significance or merely reflects experimental error. However, since the variation in individual m values in repeated measurements is of the order of 10-15%, even in experimentally ideal cases, it can be concluded that the variation most probably derives from difficulties in the analysis procedures and that the use of m_{av} is appropriate.

3.3.3.3 Stabilisation by calcium

As predicted by the theory of ligand binding (Schellman, 1975), the binding of calcium increases the stability of CaM and its isolated fragments. However, this stabilising effect is significantly smaller than expected in most cases. In Table 3.3, the experimentally observed and theoretically calculated ligand interaction free energies for Tr1C and Tr2C are compared. The experimentally observed ligand interaction free energies ($\Delta\Delta G_b$(obs)) have been calculated at each calcium concentration as $\Delta G°_{20}$(holo) - $\Delta G°_{20}$(apo), whilst the theoretically calculated values have been obtained using the equation $\Delta\Delta G_b(calc) = -RT \ln \{1/(K_1K_2[Ca^{2+}]^2)\}$ (see Section 2.3.7, Chapter 2), with the assumption that the binding of calcium to the denatured state is not significant. The $\Delta\Delta G_b$(calc) values therefore represent the maximum possible stabilising free energy for a given calcium concentration. The agreement between $\Delta\Delta G_b$(obs) and $\Delta\Delta G_b$(calc) is generally rather poor for both denaturants ($\Delta\Delta G_b$(obs) is always less than $\Delta\Delta G_b$(calc)) but the difference is particularly marked in the case of GuHCl. There is a large difference between the $\Delta G°_{20}$ values obtained for the holo-domains with the two denaturants. Thus, for example, the $\Delta G°_{20}$(holo) values determined for the isolated domains using urea in the presence of 0.3 mM calcium (6.04 kcal/mol for Tr1C and 6.27 kcal/mol for Tr2C) are higher than those determined using GuHCl in the presence of 1 mM calcium (4.41 kcal/mol for Tr1C and 5.10 kcal/mol for Tr2C), whilst they should clearly be lower.

The observation that the stabilisation conferred by calcium binding is less than predicted may have two possible explanations:

1) The assumption that binding of calcium to the unfolded state is insignificant could be incorrect. As Eq. (2.16) shows (Section 2.3.7, Chapter 2), such binding would reduce the total ligand interaction free energy.
2) The denaturant could interfere directly with the binding of calcium to the native state of the proteins. This would reduce K_1K_2 and thereby reduce the ligand interaction free energy (see Eq. (2.17), Section 2.3.7, Chapter 2)

In order to investigate the first possibility, calcium titrations to high [Ca^{2+}] have been performed with intact CaM in the presence of high concentrations of GuHCl using far-UV CD spectroscopy. The experimental data are shown in Figure 3.11A. In 1 mM Ca^{2+} and 5.5 M GuHCl, the protein is totally unfolded, as the far-UV CD intensity

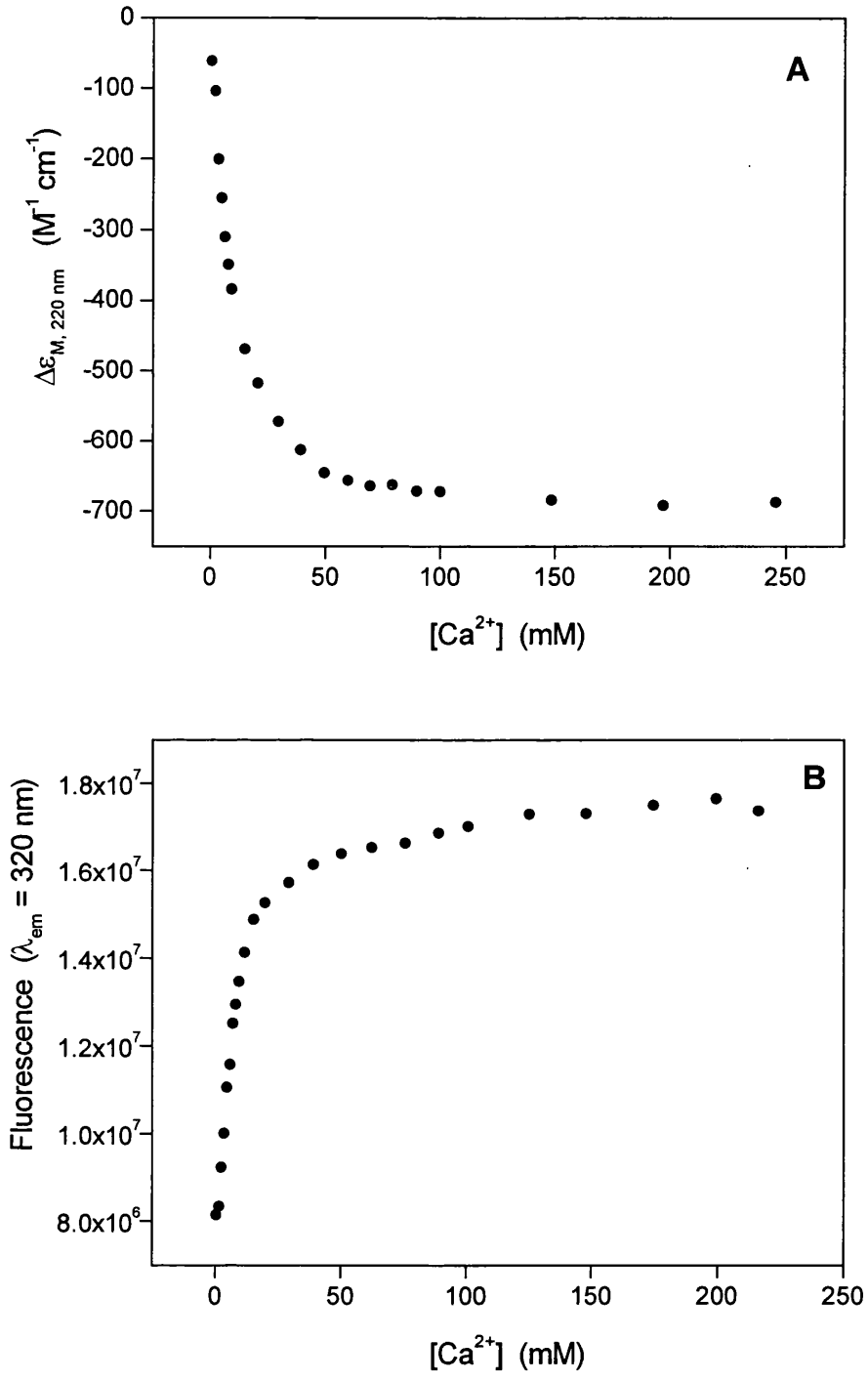

Figure 3.11 Calcium titrations of CaM in the presence of 5.5 M GuHCl, monitored using far-UV CD **(A)** and Tyr-138 fluorescence **(B)**. The experiments were performed in 25 mM Tris, 100 mM KCl, pH 8, at 20 °C.

shows (see also the GuHCl-denaturation profile of intact CaM in 1 mM Ca^{2+} in Figure 3.7B). As the calcium concentration is increased above 1 mM, the intensity of the far-UV CD signal shows the expected increase as the protein becomes stabilised. However, this increase reaches a plateau at $[Ca^{2+}] > 50$ mM at a level which suggests that approximately 15 % of the protein remains unfolded. The same pattern of behaviour is also observed with Ca^{2+}-titrations performed using Tyr-138 fluorescence at the same GuHCl concentration (Fig. 3.11B). Thus, under these conditions, the stabilising effect of calcium saturates before CaM becomes totally refolded, indicating that low-affinity binding of calcium to the unfolded state may occur.

Some support for this conclusion is provided by studies on synthetic peptide analogues corresponding to the binding loops of the calcium-binding sites of CaM and troponin C (Reid et al., 1981; Kanellis et al., 1983; Buchta et al., 1986; Borin et al., 1989). These studies have shown that these unstructured peptides can bind calcium with low affinity and that the binding process does not induce any significant change in the conformation of the peptide, which remains largely unstructured. The experimentally measured values for these binding constants for calcium vary widely but are generally in the range 20-700 M^{-1}. Inspection of Eq. (2.16) (Section 2.3.7, Chapter 2) shows that saturation would be predicted when $K_1'K_2'[Ca^{2+}]^2 >> 1$; the observed plateau at $[Ca^{2+}] > 50$ mM would then correspond to K_1' and K_2' values of the order of 50 M^{-1}.

Although it can be concluded that calcium probably binds to the unfolded state of CaM and its isolated fragments with low affinity, this cannot account fully for the poor agreement between the observed and the estimated interaction free energies for these proteins. This is because significant differences between $\Delta\Delta G_b$(obs) and $\Delta\Delta G_b$(calc) are observed at low $[Ca^{2+}]$ (< 1 mM), where $K_1'K_2'[Ca^{2+}]^2$ cannot be greater than one. Therefore a different explanation is required. The second possibility listed above, namely possible direct effects of denaturants on the binding of calcium to the native state, is investigated in Chapter 4.

3.3.4 Thermal denaturation

The thermal unfolding of apo-Tr1C and apo-Tr2C has been monitored by far-UV CD. Typical curves are shown in Figure 3.12A. The thermal denaturation profiles for the two isolated domains conform to simple two-state transitions. The measured T_m

and ΔH_m values are 50.3 °C and 45.6 kcal/mol for apo-Tr1C and 49.4 °C and 36.5 kcal/mol for apo-Tr2C (Table 3.6). The ΔG_{20} values (Table 3.6), calculated using ΔC_p values of 0.727 kcal/(K·mol) for apo-Tr1C and 0.804 kcal/(K·mol) for apo-Tr2C (Sorensen and Shea, 1998), show that apo-Tr1C is more stable than apo-Tr2C, in agreement with the chemical denaturation data (Tables 3.1 and 3.2).

The thermal denaturation curve for intact apo-CaM measured by far-UV CD is shown in Figure 3.12B. The T_m and ΔH_m obtained from the analysis are 45.7 °C and 29.1 kcal/mol for transition CaM-1 (C-domain) and 59.5 °C and 46.1 kcal/mol for transition CaM-2 (N-domain). As in the case of chemical unfolding, the curve for intact CaM cannot be reproduced by the sum of the curves of the tryptic fragments. The calculated ΔG_{20} values (Table 3.6) indicate that the C-domain in apo-CaM is less stable than the isolated apo-Tr2C by approximately 0.5 kcal/mol, while the N-domain in apo-CaM is more stable than apo-Tr1C by approximately 0.8 kcal/mol. The thermal unfolding of the C-domain in intact apo-CaM has also been monitored using Tyr-138 fluorescence and absorption. Typical curves are shown in Figure 3.13. The corresponding analyses (Table 3.6), confirm that apo-Tr2C is more stable than the C-domain in intact apo-CaM. Table 3.6 also reports the percentages of unfolded molecules at 20 and 37 °C calculated from the ΔG values. It is important to note that the C-domain in intact apo-CaM is significantly (~ 24%) unfolded at 37 °C and ~ 7% unfolded at 20 °C. In contrast, the more stable N-domain is only 0.2% and 1.5% unfolded at 20 and 37 °C, respectively.

Thermal unfolding of holo-CaM (in 1 mM calcium) is shown in Figure 3.12B. It is clear that the T_m for both domains is increased to very high values (> 80 °C) in the presence of calcium, in accord with the effects of calcium in the chemical denaturation experiments described here, and in agreement with previously published data on thermal unfolding (Brzeska et al., 1983; Tsalkova and Privalov, 1985; Martin and Bayley, 1986). Any detailed analysis of the effects of calcium on thermal unfolding requires knowledge of the dependence of calcium-affinity upon temperature and has not been explored further in this work.

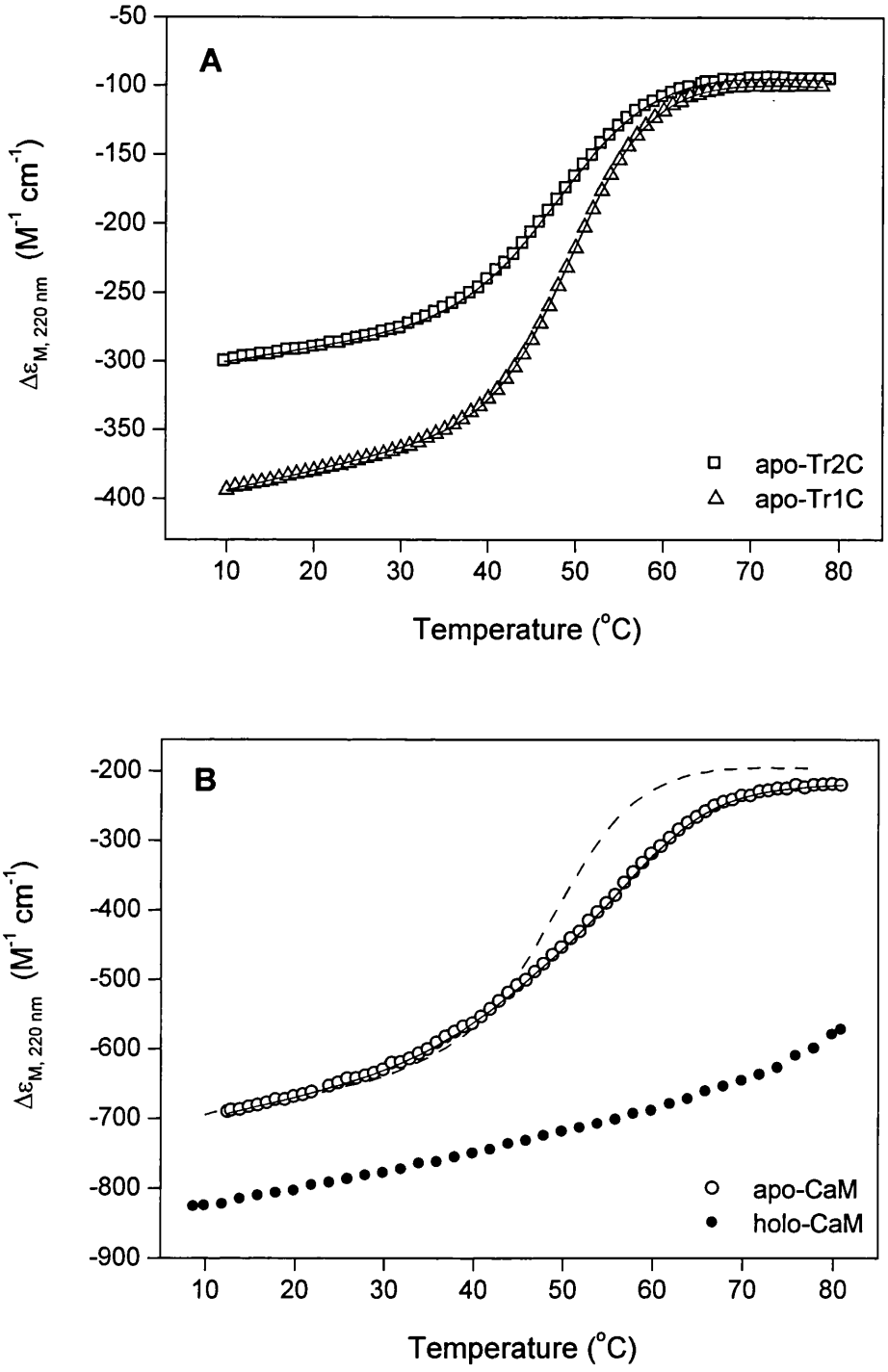

Figure 3.12 **(A)** Thermal denaturation of apo-Tr1C (△) and apo-Tr2C (□). **(B)** Thermal denaturation of CaM at 0 (○) and 1 (●) mM Ca^{2+}. The solid lines are the computed best fits. The dotted line represents the sum of the curves for apo-Tr1C and apo-Tr2C. Unfolding was monitored in 25 mM Tris, 100 mM KCl, pH 8, using far-UV CD.

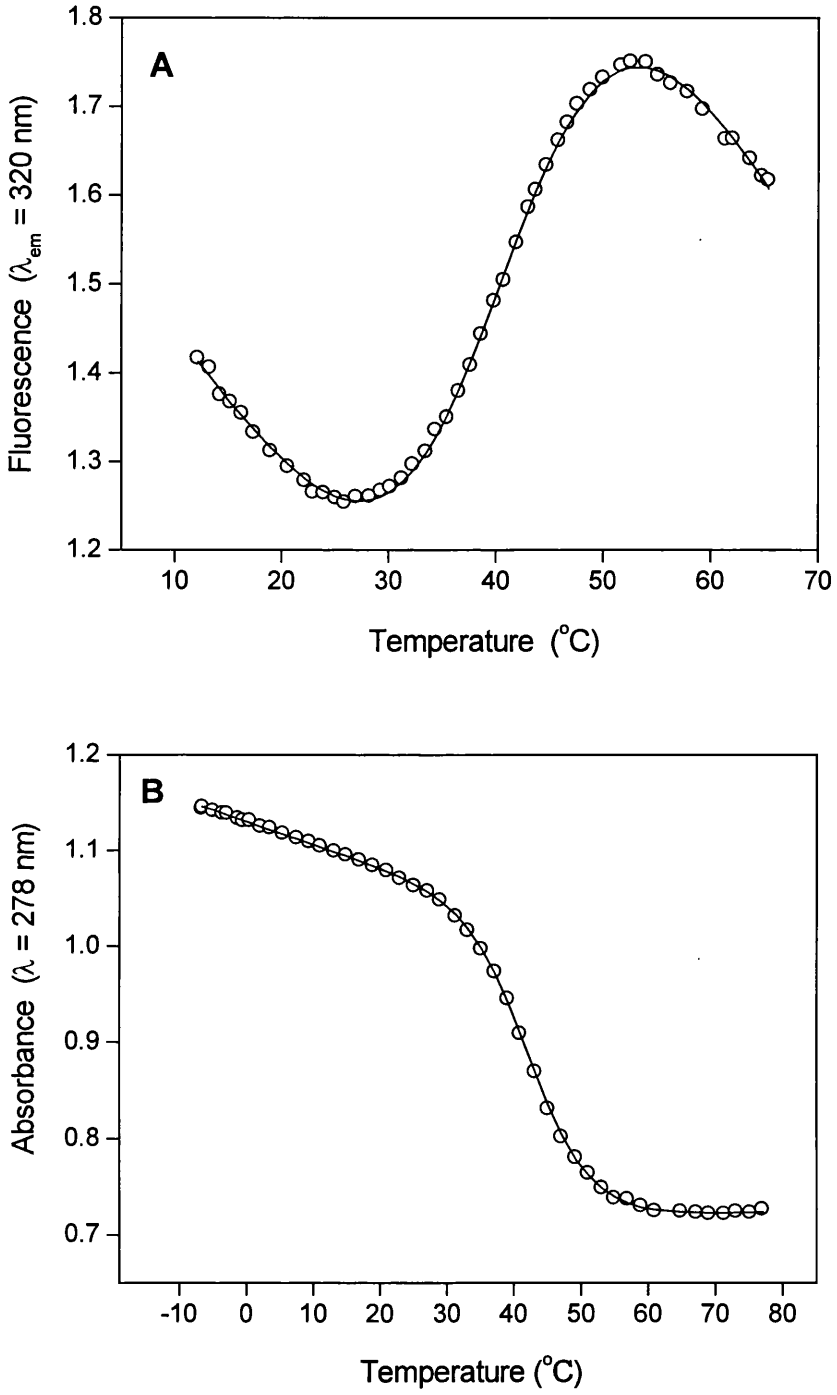

Figure 3.13 **(A)** Thermal denaturation of apo-CaM (C-domain) monitored in 10 mM Hepes, 100 mM KCl, pH 8, using Tyr-138 fluorescence. **(B)** Thermal denaturation of apo-CaM (C-domain) monitored in 25 mM Tris, 100 mM KCl, 20% methanol, pH 8, using Tyr-138 absorption.

Table 3.6 Thermal unfolding of apo-Tr1C, apo-Tr2C, and apo-CaM

Transition	Method [a]	T_m (°C)	ΔH_m (kcal/mol)	ΔG_{20} [b] (kcal/mol)	% unfolded (20 °C)	ΔG_{37} [b] (kcal/mol)	% unfolded (37 °C)
apo-Tr1C	CD	50.3	45.6	3.21	0.4	1.67	6.2
apo-Tr2C	CD	49.4	36.5	2.22	2.2	1.21	12.3
apo-CaM-1[c]	CD	45.7	29.1	1.43	7.1	0.69	24.6
apo-CaM-2[c]	CD	59.5	46.1	3.69	0.2	2.55	1.6
apo-CaM-C[c]	Fluo	42.8	31.5	1.59	6.1	0.54	29.4
apo-CaM-C	Abs	43.2	35.7	1.92	3.6	0.65	25.8

[a] CD, Flu, and Abs identify unfolding monitored using far-UV CD, Tyr-138 fluorescence, and Tyr-138 absorption.

[b] Values of ΔG_T were calculated using ΔC_p values of 0.727 kcal/(K·mol) for apo-Tr1C (and CaM-2) and 0.804 kcal/(K·mol) for apo-Tr2C (and CaM-1) (Sorensen and Shea, 1998).

[c] CaM-1 and CaM-2 indicate the first and second transitions resolved for intact CaM, assigned to the C-domain and N-domain respectively. CaM-C represents the unfolding transition of the C-domain in intact CaM, monitored using Tyr-138 fluorescence or absorption.

3.3.5 Chemical denaturation of the apo-CaM-FFF_u complex

As mentioned above, one of the surprising observations in the thermal unfolding experiments is that the C-domain of apo-CaM is more than 20% unfolded under near physiological conditions (37 °C, 100 mM KCl, pH 7.5). However, apo-CaM *in vivo* could be stabilised by interaction with magnesium (see Chapter 6) or by interaction with target sequences, many of which have affinities in the μM range (unpublished observations from this laboratory). In order to investigate the latter possibility, the unfolding of apo-CaM was studied in the presence of the 18 residue target peptide FFF_u, which forms a low affinity 1:1 complex with apo-CaM. The affinity is strongly dependent upon ionic strength (K_d ~ 60 μM in the presence of 100 mM KCl, ~ 1 μM in the absence of KCl), and is much lower than for holo-CaM (K_d ~ 0.6 nM, Martin, S. R., unpublished observations). Since the peptide does not contain any fluorescent residues (Trp or Tyr), the fluorescence signal in the unfolding experiment comes entirely from Tyr-138 in the C-domain of CaM; the curves therefore monitor the unfolding of this domain. Urea unfolding profiles were measured for apo-CaM (12 μM) in the absence and the presence of FFF_u (at 40 and 100 μM FFF_u), in a buffer with low KCl concentration (< 5 mM). The results of the LEM analyses are listed in Table 3.7 and the fractions of unfolded protein calculated using these parameters are shown in Figure 3.14A.

As in the case of calcium binding, the binding of this target sequence to CaM increases the stability of the protein. The ligand interaction free energies, $\Delta\Delta G_b$, have been estimated as $\Delta G°_{20}$(+ FFF_u) - $\Delta G°_{20}$(no FFF_u) and are ~ 1.3 and 2 kcal/mol for 40 and 100 μM total FFF_u, respectively. Measuring the stability of the C-domain in apo-CaM at low KCl concentration is particularly difficult because at 20°C and at low ionic strength this domain is significantly unfolded (see Chapter 4) and thus the unfolding curve is not complete (Fig. 3.14A). Nevertheless the $\Delta G°_{20}$ value for apo-CaM under these conditions can be estimated with acceptable accuracy. The measured $\Delta\Delta G_b$ values permit the evaluation of the association constant for apo-CaM and FFF_u. The association constant K_a at each peptide concentration has been calculated using the equation:

$$\Delta\Delta G_b = RT \ln (1 + K_a[FFF_u])$$

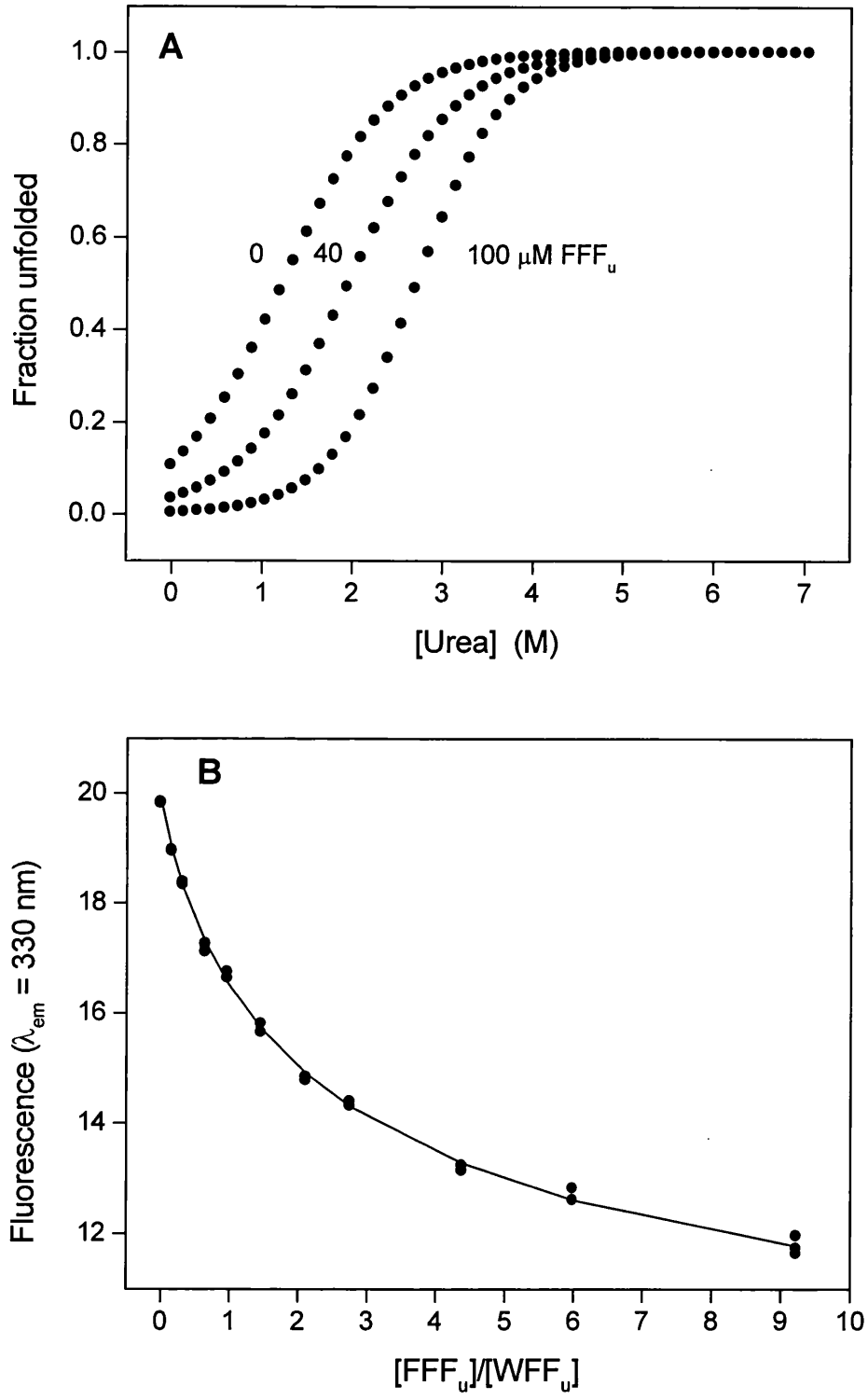

Figure 3.14 **(A)** Fraction of unfolded protein for the C-domain of apo-CaM in the presence of 0, 40, and 100 μM FFF_u (at low [KCl]). The curves were calculated using the data of Table 3.7. **(B)** Competition assay: titration of the apo-CaM-WFF_u complex with FFF_u, monitored by Trp fluorescence in 25 mM Tris, 3 mM KCl, pH 8, at 20 °C.

Table 3.7 Urea-unfolding of the apo-CaM C-domain in the presence of the target peptide FFF_u, monitored by Tyr-138 fluorescence

$[FFF_u]^a$ (μM)	$[U]_{1/2}$ (M)	$\Delta G°_{20}{}^b$ (kcal/mol)	$\Delta\Delta G_b{}^c$ (kcal/mol)	$K_d{}^d$ (μM)
0	0.6	0.5		
40	1.97	1.81	1.3	3.4
100	2.71	2.49	2.0	2.9

[a] Total peptide concentration. The free peptide concentration was $[FFF_{TOT}]$ - [CaM] = $[FFF_{TOT}]$ – 12 μM.

[b] $\Delta G°_{20}$ values were calculated as $-[U]_{1/2} \cdot m_{av}$, with m_{av} = -0.92 kcal/mol·M (see Section 2.3.6.1, Chapter 2).

[c] $\Delta\Delta G_b$ values were calculated as $\Delta G°_{20}$(+ FFF_u) - $\Delta G°_{20}$(no FFF_u).

[d] K_d values were calculated using the equation $\Delta\Delta G_b = RT \ln (1 + K_a[FFF_u])$ (see Section 2.3.7, Chapter 2), with $K_d = 1/K_a$.

where $[FFF_u]$ is the free peptide concentration (see Section 2.3.7, Chapter 2). The dissociation constants ($K_d = 1/K_a$) obtained from the two experiments at 40 and 100 μM total FFF_u are approximately 3 μM and are in very good agreement (Table 3.7).

The affinity of apo-CaM for FFF_u has also been determined using a competition assay in which FFF_u was used to displace the peptide WFF_u from its complex with apo-CaM (see Section 2.3.5, Chapter 2). The K_d for the interaction of WFF_u with apo-CaM in the absence of KCl is ~ 270 nM (Martin, S. R., unpublished observations). The analysis of the data (Fig. 3.14B) gave a K_d for the interaction of FFF_u with apo-CaM of approximately 1 μM, in agreement with the results of the denaturation experiments.

3.3.6 Kinetics of unfolding and refolding of Tr2C and intact calmodulin

In the previous sections, the conformational stability of CaM and its isolated domains was investigated using steady-state (equilibrium) methods. Many of the experimental protocols used rely on the assumption that the kinetics of folding and unfolding are fast. In order to confirm this assumption, kinetic studies have been performed using the stopped-flow technique, monitoring the Tyr-138 fluorescence signal in Tr2C and in the C-domain of intact CaM.

The kinetic experiments were based on the fact that at urea concentrations in the range 3.4 to 5.5 M, Tr2C and the C-domain of intact CaM are unfolded in the absence of calcium but are folded in the presence of $[Ca^{2+}] \geq 0.3$ mM (see Sections 3.3.2 and 3.3.3). Therefore the kinetics of **refolding** of Tr2C and the C-domain of CaM were studied by adding calcium to a solution of unfolded apo-Tr2C or apo-CaM in urea. Similarly, the kinetics of **unfolding** were studied by adding excess EDTA to a solution of folded holo-Tr2C or holo-CaM in urea. These processes have been studied as a function of calcium concentration at different urea concentrations (in 100 mM KCl).

The kinetics of **unfolding** of the C-domain in intact CaM were studied by stopped-flow mixing a solution of 20 mM EDTA (in 3.4 M urea) with a solution of 12 μM CaM plus 5 mM calcium (in 3.4 M urea). A single exponential process was observed, even though two processes (namely calcium dissociation and protein unfolding) are occurring. The observed rate (7.3 s^{-1}) is closely similar to the rate constant of 8.0 s^{-1} obtained for the dissociation of calcium in the absence of denaturant (Martin et al., 1992; and see Section 4.3.3, Chapter 4). The unfolding reaction under these conditions may be formally represented as:

$$N{\cdot}Ca_2 \xrightarrow{k_{12}} N \underset{k_{32}}{\overset{k_{23}}{\rightleftharpoons}} U \qquad (\text{with } k_{23} >> k_{32})$$

where N and U represent the native and unfolded forms of the protein, respectively. The simplest interpretation of the results is that the rate-limiting step is the rate of dissociation of calcium from the native state of CaM (k_{12}) and that the rate constant for the unfolding step (k_{23}) must therefore be greater than or equal to 7.3 s^{-1}.

Refolding experiments with Tr2C were performed at urea concentrations of 3.4, 4.5, and 5.5 M with calcium concentrations varied in the range 0.15 – 1.5 mM (after 1:1

mixing). A single exponential process was observed under all conditions, even though two processes (namely calcium binding and protein refolding) are occurring. An example of typical stopped-flow data is shown in Figure 3.15A and the observed rates (k_{obs}) for Tr2C are plotted in Figure 3.15B as a function of calcium and urea concentration. The observed rates appear to vary linearly with $[Ca^{2+}]$ for any particular urea concentration. At any single $[Ca^{2+}]$ the observed rates decrease as the urea concentration increases.

Two limiting kinetic models may be considered. In the first (more likely) scheme the calcium binds only to the folded protein; in the second, calcium is able to bind to the denatured state and then the protein refolds.

$$U \underset{k_{21}}{\overset{k_{12}}{\longleftrightarrow}} N + 2Ca \underset{k_{32}}{\overset{k_{23}}{\longleftrightarrow}} Ca_2{\cdot}N \qquad \text{(Scheme I)}$$

$$U + 2Ca \underset{k_{21}}{\overset{k_{12}}{\longleftrightarrow}} Ca_2{\cdot}U \underset{k_{32}}{\overset{k_{23}}{\longleftrightarrow}} Ca_2{\cdot}N \qquad \text{(Scheme II)}$$

Note that only a single domain is being considered and that the binding of calcium has been reduced to a single step. Each of these two-step schemes must be associated with two observed rates, which should be resolvable when they are sufficiently well separated. However, only a single process may be observed if the other is too fast (or occurs with small amplitude), or if one of the steps has no associated spectroscopic change. Expressions for the observed rates (fast and slow) are given in Table 3.8. These are derived with the assumption that one of the steps is much faster than the other and for pseudo first-order conditions ($[Ca^{2+}] >> [Tr2C]$). These are therefore limiting cases only. In each case only the slow process would be observed. The fast step would not be observable either because there is probably no spectroscopic change associated with the step (scheme II, step 1-2 fast) or because the amplitude would be too small to be observable (the other three cases). Scheme I with step 2-3 fast can be eliminated as a possibility because it predicts that the observed rate would decrease with increasing $[Ca^{2+}]$. Scheme II (step 1-2 fast) predicts a linear dependence on $[Ca^{2+}]$ reaching a plateau ($k_{23} + k_{32}$) at high $[Ca^{2+}]$. The two remaining possibilities (scheme I, step 1-2 fast and scheme II, step 2-3 fast) predict a simple linear dependence on $[Ca^{2+}]$.

Table 3.8 Fast and slow observed rates expressed in terms of the intrinsic rate constants

Scheme	Fast step	$k_{obs(Fast)}$	$k_{obs(Slow)}$
I	1-2	$k_{12} + k_{21}$	$\frac{k_{23}\,K[Ca]_T}{1+K} + k_{32}$ where $K = \frac{k_{12}}{k_{21}}$
I	2-3	$k_{23}[Ca]_T + k_{32}$	$\frac{k_{21}}{1+K[Ca]_T} + k_{12}$ where $K = \frac{k_{23}}{k_{32}}$
II	1-2	$k_{12}[Ca]_T + k_{21}$	$\frac{k_{23}K[Ca]_T}{1+K[Ca]_T} + k_{32}$ where $K = \frac{k_{12}}{k_{21}}$
II	2-3	$k_{23} + k_{32}$	$k_{12}[Ca]_T + \frac{k_{21}}{K+1}$ where $K = \frac{k_{23}}{k_{32}}$

Scheme II with step 1-2 fast can probably be eliminated from consideration because the intercept of the linear plot of k_{obs} versus $[Ca^{2+}]$ (equal to k_{32}) should presumably increase with increasing [urea] and this is clearly not the case. Scheme II with step 2-3 fast can be eliminated for the same reason. In this case the intercept should be equal to $k_{21}/(K+1)$. K (= k_{23}/k_{32}) must clearly decrease significantly with increasing [urea] but remain greater than 1 at all concentrations (since the protein refolds). Since k_{21} presumably remains constant (or increases) with increasing [urea], the intercept of the plot of k_{obs} versus $[Ca^{2+}]$ should again increase with increasing [urea].

This leaves scheme I with step 1-2 fast as the most plausible model. There are, however, some significant problems with this interpretation. First, the intercept should be k_{32}, the rate of Ca^{2+} dissociation. This has been measured at ~ 8 s^{-1} in both the presence and absence of 3.4 M urea (see above). The observed intercepts appear to be greater than 8 s^{-1} and to vary somewhat with [urea]. The errors in the determination of the intercepts are, however, large. A value for K (= k_{12}/k_{21}) can be calculated from the

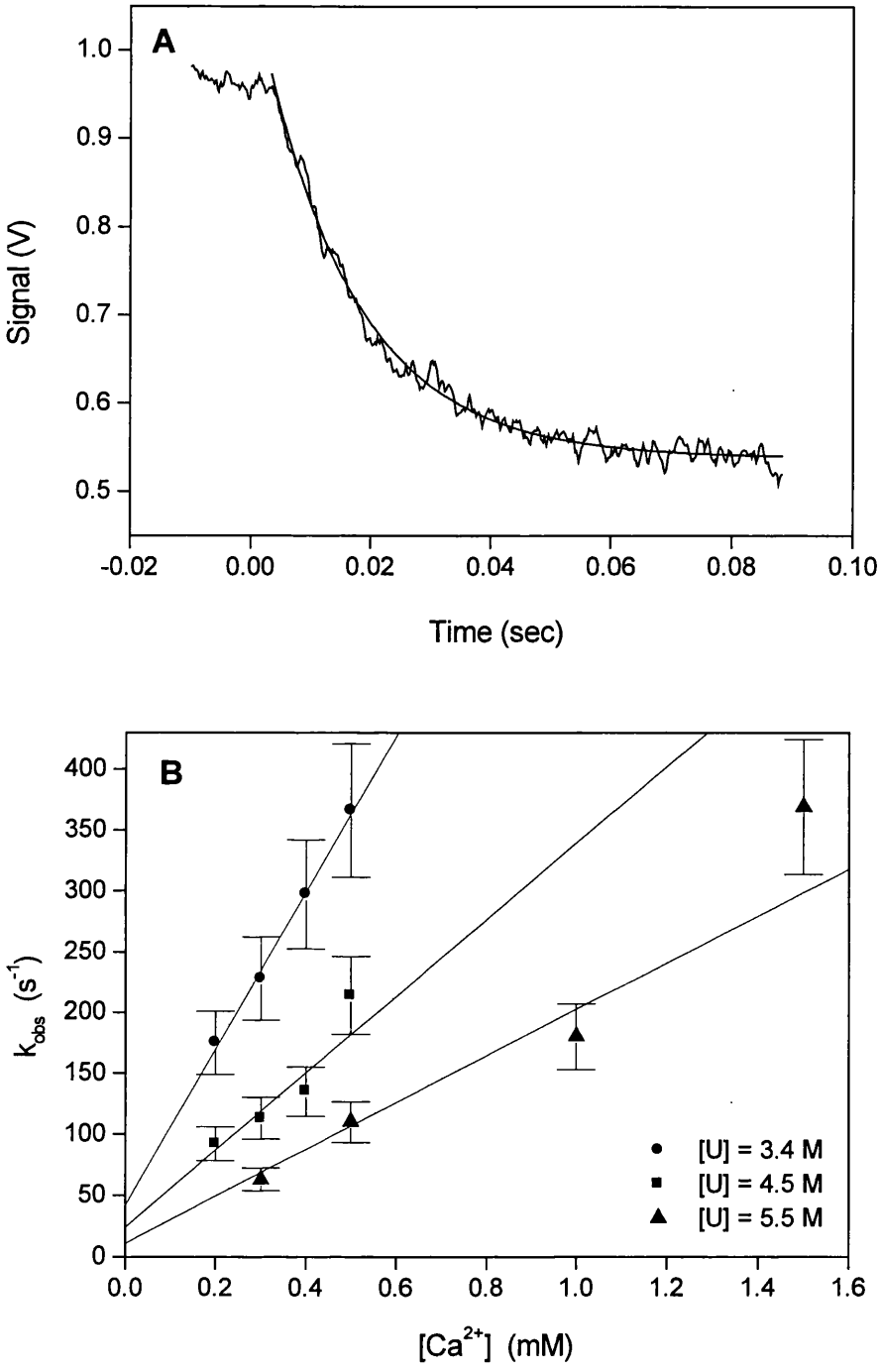

Figure 3.15 **(A)** Stopped-flow data showing the kinetics of refolding and calcium binding of Tr2C in the presence of 5.5 M urea. The calcium concentration after 1:1 mixing was 0.3 mM. The solid line is the computed best fit. **(B)** Observed rates for the reactions of refolding and calcium binding of Tr2C in the presence of 3.4 (●), 4.5 (■), and 5.5 (▲) M urea, as a function of calcium concentration (after 1:1 mixing). The error bars represent a 15% uncertainty on each value. All the stopped flow curves were measured in 25 mM Tris, 100 mM KCl, pH 8, at 20 °C.

urea-unfolding data for apo-Tr2C ($\Delta G° = 2$, $m = -0.92$, see Table 3.1) to be 0.14, 0.03, and 0.005 at 3.4, 4.5, and 5.5 M urea, respectively. Since K is less than 1 the slope of the plot of k_{obs} versus $[Ca^{2+}]$ should be approximately equal to $k_{23}K$ and there should be a 28-fold difference (0.14/0.005) between the slopes at 3.4 and 5.5 M urea. Although values of k_{23} estimated from the plots are in a reasonable range (of the order of 10^7 $M^{-1}s^{-1}$) the variation in the slope is much smaller than predicted. One possible explanation is that the condition that step 1-2 is very much faster than step 2-3 does not hold over the whole range of $[Ca^{2+}]$ investigated. The rate of the fast step ($k_{12} + k_{21}$) must be determined largely by the unfolding rate constant, k_{21} (since k_{12}/k_{21} is less than 1 under all conditions – see above). Since k_{21} must increase with increasing [urea] (Manyusa and Whitford, 1999), the rate of the fast step will be lowest at 3.4 M urea and this is where the condition step 1-2 very much faster than step 2-3 is most likely to break down. Computer simulations show that the consequence of this would be that k_{obs} at high $[Ca^{2+}]$ would be less than the value predicted by the equation in Table 3.8, resulting in a decreased slope and an increased intercept. Thus, it may be concluded that the mechanism of refolding involves calcium binding to the native state and this binding perturbs the unfolding equilibrium in favour of the native form.

In the case of intact CaM, the kinetics of refolding of the C-domain have been studied in 2.5, 3.4, 3.85, 4.5 and 5.5 M urea and at calcium concentrations in the range 0.15-2.5 mM. The interpretation of the data obtained from these experiments is complex. At all urea and calcium concentrations, there was one process with an observed rate in the range 20-45 s^{-1}. Under many conditions a second faster component was also detected with observed rate in the range 100-360 s^{-1}. It was not possible to determine accurately the dependence of this faster process on urea or calcium concentration. Interestingly, the kinetics of refolding of intact CaM are significantly different from those of Tr2C, suggesting that domain interactions may also be important in kinetic processes. However, it can be concluded that for both Tr2C and the C-domain in intact CaM the kinetics of refolding are fast and the process is completed within 3 to 50 ms.

3.4 Discussion

3.4.1 Chemical and thermal denaturation of calmodulin and its domains

The results of the chemical and thermal denaturation experiments on CaM and its proteolytic fragments have shown that the apo-forms of these proteins have relatively low stability ($\Delta G°_{20}$ ~ 2-3 kcal/mol), which is a common feature with small (non cross-linked) globular proteins. The C-domain of apo-CaM is particularly unstable, being approximately 24% unfolded under near physiological conditions (37 °C, 100 mM KCl, pH 8.0), while the more stable N-domain is less than 2% unfolded. Thus, in spite of the close sequence homology (48 % sequence identity, 69 % similarity) and structural similarity of the N- and C-domains, their stabilities in the absence of Ca^{2+} differ by approximately 2 kcal/mol. The $\Delta G°_{20}$ values obtained for apo-CaM and its domains using thermal denaturation are consistent with those determined by chemical unfolding; however, they agree somewhat better with the values determined using urea as a denaturant, than with the ones determined using GuHCl (Tables 3.1 and 3.2).

The results obtained from these studies are in good agreement with some of the previous investigations on the stability of CaM and its domains. The higher stability of the N-domain (and Tr1C) relative to the C-domain (and Tr2C) in the absence of calcium has been observed in several studies performed by optical spectroscopic methods, microcalorimetry and NMR (Brzeska et al., 1983; Tsalkova and Privalov, 1985; Martin and Bayley, 1986; Kuboniwa et al., 1995; Protasevich et al., 1997). In particular, the thermal denaturation parameters obtained in this work (Table 3.6) are in very good agreement with those reported recently by Sorensen and Shea (1998), who have monitored the thermal unfolding of intact CaM and its isolated fragments by far-UV CD.

Previous studies on CaM's stability have also shown that apo-CaM is significantly more sensitive to proteolytic attack than Ca^{2+}-CaM (Walsh et al., 1977; Kawasaki et al., 1986; Mackall and Klee, 1991). The low stability of apo-CaM and in particular of the C-domain could therefore enhance its susceptibility to proteolytic cleavage *in vivo*, at resting calcium concentrations. However, apo-CaM has been reported to interact (more strongly than Ca^{2+}-CaM) with certain target proteins, notably neuromodulin (Alexander et al., 1987) and neurogranin (Baudier et al., 1991). Such

interactions, and possibly those with Mg^{2+}, could provide some protection against this intrinsic instability of the apo-form. The interactions of CaM with Mg^{2+} are investigated in Chapter 6, whilst the feasibility of the mechanism in which apo-CaM is stabilised by target sequence interactions has been demonstrated by the experiments with FFF_u.

The stabilising effects of calcium on CaM and its fragments have been known for many years (Brzeska et al., 1983; Martin and Bayley, 1986) and are predicted theoretically (see Chapter 2). The results presented here clearly show that these proteins are indeed greatly stabilised in the presence of calcium and, in addition, that the binding of calcium induces a reversal of the relative stability of the domains. Thus, the C-domain, which is less stable than the N-domain in the apo-state, becomes more stable than the N-domain in the presence of calcium, owing to its higher calcium affinity. Unfortunately, the agreement between the observed ligand interaction free energies ($\Delta\Delta G_b$(obs)) and the calculated ones ($\Delta\Delta G_b$(calc)) is rather poor, especially in the case of GuHCl, but also in the case of denaturation of Tr2C with urea. In contrast, the agreement between calculated and observed $\Delta\Delta G_b$ values is good in the case of the experiments with the FFF_u peptide. One of the possible mechanisms which could explain this observation, namely the binding of calcium to the denatured state, has been investigated. However, the experimental results have shown that such binding is not significant at calcium concentrations below 50 mM and therefore cannot fully account for the differences in the observed and predicted $\Delta\Delta G_b$ values. Another possible explanation is that the presence of the denaturant could have an effect on the affinity of the fully-folded protein for calcium. This possibility will be explored in Chapter 4.

The kinetics of unfolding and refolding of Tr2C and of the C-domain in intact CaM have been investigated as a function of calcium and denaturant concentration. The stopped flow experiments have shown that the rate of unfolding of holo-CaM is limited by the dissociation rate for Ca^{2+} ($\sim 7\ s^{-1}$). Refolding experiments with Tr2C suggest that the observed rate for refolding/unfolding (equal to the sum of the rate constants for refolding (k_F) and unfolding (k_U)) is much greater than the rate of Ca^{2+} binding to the folded protein (for $[Ca^{2+}]$ in the range 0.15-1.5 mM). If the rate constant for Ca^{2+}-binding is taken to be $\sim 10^7\ M^{-1}\ s^{-1}$, this implies that the rate constant for unfolding must be $> 10^4\ s^{-1}$. Taking the equilibrium unfolding constant K_U ($= k_U/k_F$) to be ~ 10 in

3.4 M urea (calculated using the values in Table 3.1) gives a refolding rate of > 1000 s^{-1} under these conditions.

Since the rate of refolding is expected to be inversely proportional to the urea concentration (Manyusa and Whitford, 1999), it may be concluded that k_F in the absence of urea will be >> 1000 s^{-1}. Because the equilibrium unfolding constant in the absence of urea is ~ 0.05 (see Section 3.3.2) the rate of unfolding in zero urea must be >> 50 s^{-1}. Although the refolding kinetics of Tr2C are simpler than those of intact CaM, these calculations are consistent with the results of preliminary T-jump experiments with the C-domain of apo-CaM, which have shown that in aqueous buffer the rates of unfolding and refolding at 20°C are ~ 200 and ~ 5000 s^{-1}, respectively (Rabl, C. -R., Martin, S. R., and Bayley, P. M., unpublished results).

A comparison of the results obtained with urea and GuHCl shows that these two denaturants give different $\Delta G°_{20}$ values for both CaM and its isolated fragments. In particular, in the case of the apo-proteins, the stability is consistently higher when measured using GuHCl than when measured using urea (see Tables 3.1 and 3.2). In contrast, in the case of the holo-proteins, the stabilising effect of calcium binding is much smaller when estimated with GuHCl-unfolding than with urea-unfolding (see Table 3.3). The possible reasons for these differences will be investigated in Chapter 4.

3.4.2 Inter-domain interactions

The analysis of the unfolding profiles from chemical and thermal denaturation experiments reported here has shown that the thermodynamic stabilities of the isolated domains are different from those of the corresponding domains in intact CaM. In the absence of calcium, the C-domain of intact apo-CaM is less stable than apo-Tr2C, whilst the N-domain of intact apo-CaM is more stable than apo-Tr1C. At calcium concentrations ≥ 0.3 mM, the order in which the domains unfold is reversed, with the C-domain now more stable than the N-domain. Under these conditions, the N-domain of intact holo-CaM is less stable than holo-Tr1C, whilst the C-domain of intact holo-CaM is more stable than holo-Tr2C. Thus, whichever domain unfolds first in intact CaM appears to be destabilised compared to the corresponding isolated fragment, whilst the second appears to be stabilised compared to the isolated fragment. This has been observed both in the presence and in the absence of calcium and similar effects

are obtained in either thermal or chemical denaturation. It may also be noted that the total free energy of unfolding (ΔG) for the intact protein, both in the presence and in the absence of calcium, is close to the sum of the free energies of unfolding of the isolated domains. This indicates that the extent to which the ΔG for the transition CaM-1 is decreased relative to the isolated domain, corresponds to the extent to which the ΔG for the transition CaM-2 is increased.

The explanation for the experimental observation that the stabilities of the domains in the intact protein differ from those of the isolated fragments requires the postulate that interactions between the two domains of a given CaM molecule occur during the process of unfolding. In particular, the results suggest that there may be equilibrium unfolding intermediates in which there are interactions between one domain in the folded state and the other in the unfolded state. Differences between intact CaM and the isolated domain Tr2C have also been observed in the kinetics of refolding (see Section 3.3.6), suggesting that the presence of such intermediates may also have important kinetic consequences.

In the case of holo-CaM, the interdomain interactions are thought to occur between the folded holo-C-domain and the unfolded N-domain (which is most likely to be calcium-free, but could be calcium-saturated at very high calcium concentrations). Under these conditions, these interactions could be hydrophobic in nature and could involve the large hydrophobic surface of the holo-C-domain and the hydrophobic residues which are solvent-exposed in the unfolded N-domain. However, as noted above, these effects on domain stability are also observed in the absence of calcium. In this case, the inter-domain interactions must occur between the unfolded apo-C-domain and the folded apo-N-domain, in which the exposed surface is known to be negatively charged and less hydrophobic than that of the holo-domains. The mode of interaction between the two domains may therefore be less specific and involve different mechanisms.

Although several published equilibrium and kinetic studies have supported the conclusion that the two domains of CaM behave as autonomous units (Martin et al., 1985; Martin and Bayley, 1986; Linse et al., 1991a; Martin et al., 1996), inter-domain interactions have been postulated in optical spectroscopy and scanning microcalorimetry studies of wild-type CaM (Pedigo and Shea, 1995; Shea et al., 1996; Sorensen and Shea, 1998) and of mutants of CaM and SynCaM (Martin et al., 1992;

Maune et al., 1992a; Protasevich et al., 1997). These works have reported evidence that in the fully folded state of CaM the conformational and calcium-binding properties of one domain can be affected by the presence of the other domain. Similar conclusions have also been obtained in the case of yeast CaM, which is the most divergent form of CaM among all eukaryotic species, but still shares a high percentage of sequence identity with the highly conserved calmodulins (60% with vertebrate CaM) (Nakashima et al., 1999; Lee and Klevit, 2000).

Thus, different experimental approaches have indicated that there are specific interactions between the two domains in the native state of CaM. The data presented here do not provide direct evidence for specific inter-domain interactions in the fully folded state of CaM, and the model proposed to interpret the results of this work is based on interactions occurring in a partially unfolded state of CaM. However, the presence of interactions between the domains in the native form cannot be excluded *a priori* and provides further evidence that the two domains can indeed come into contact.

CHAPTER 4

EFFECTS OF IONIC STRENGTH AND pH ON STABILITY AND Ca^{2+}-BINDING

4.1 Introduction

Most of the studies on the conformational stability of CaM, Tr1C and Tr2C described in Chapter 3 were performed in the presence of 100 mM KCl, in order to reproduce physiological ionic strength conditions. The results demonstrated that the stabilities of the apo-forms of these proteins, especially the C-domain of intact CaM, are very low. Changes in solution conditions (such as pH, ionic strength, and buffer composition) might be expected to have significant effects on the stabilities of proteins that have low overall thermodynamic stability. Changes in pH and ionic strength might be particularly important in the case of CaM, which carries a large overall negative charge at neutral pH (see Section 1.1.1, Chapter 1). The work in this chapter therefore characterises the dependence of the stabilities of CaM and its isolated domains on ionic strength, pH, and other factors.

4.2 Materials and methods

The experimental approaches employed in the studies described in this chapter (optical spectroscopy, urea denaturation, and stopped-flow kinetics) are fully described in Chapter 2. Far-UV CD has been employed to monitor the unfolding of the intact protein and of the isolated domains; Tyr-138 fluorescence and absorption have been used to monitor selectively the unfolding of the C-domain in intact CaM and of Tr2C.

Some of the important mathematical relationships are now summarised here for convenience. The theory and data analysis procedures for two-state unfolding transitions are discussed in Sections 2.3.6.1 in Chapter 2. According to the Linear Extrapolation model (LEM), the free energy of unfolding (ΔG) for a simple two-state transition is given by:

$$\Delta G = \Delta G° + m\,[D]$$

where $\Delta G°$ is the free energy for unfolding in the absence of denaturant and m is a constant that describes the dependence of ΔG on denaturant concentration ([D]).

In the case of thermal denaturation, the free energy of unfolding, ΔG, is given by the Gibbs-Helmholtz equation as:

$$\Delta G = \Delta H_m\,(1\text{-}T/T_m) + \Delta C_p\,(T - T_m - T \ln (T/T_m))$$

where T_m is the transition midpoint temperature (°K), ΔH_m is the van't Hoff enthalpy at the midpoint temperature, ΔC_p is the heat capacity change, and T is the temperature (°K). Biphasic unfolding transitions have been analysed by treating the system as two separate two-state transitions (see Section 2.3.6.2).

In the case of calcium binding to a CaM domain the full expression for the ligand interaction free energy is:

$$\Delta\Delta G_b = -RT \ln\left(\frac{1 + K'_1[Ca] + K'_1 K'_2 [Ca]^2}{1 + K_1[Ca] + K_1 K_2 [Ca]^2}\right)$$

where [Ca] is the free calcium concentration and the K_i and K'_i are the stoichiometric calcium association constants for binding to the native and unfolded states of that domain, respectively. Simpler forms of this equation apply under particular conditions (see Section 2.3.7, Chapter 2).

4.3 Results

4.3.1 Effects of ionic strength on the stability of the apo-proteins

The effect of ionic strength on the stabilities of the apo-proteins has been studied by measuring their free energies of unfolding ($\Delta G°_{20}$) at different KCl concentrations. Figure 4.1 shows the far-UV CD data for urea-induced unfolding of apo-Tr1C and apo-Tr2C in the presence of ~5, 30 and 100 mM KCl. Figure 4.2A shows the corresponding far-UV CD unfolding curves for apo-CaM in the presence of ~5, 100, and 200 mM KCl. The parameters obtained from the LEM analyses are listed in Table 4.1. The results show that the stabilities of apo-CaM and the isolated fragments are significantly increased by increases in the ionic strength of the medium. For all the proteins studied an increase in [KCl] from ~5 to 100 mM gives an increase in the measured $\Delta G°_{20}$ values of between 0.8 and 1 kcal/mol. This stabilising effect of ionic strength is particularly significant in the case of the C-domain of intact apo-CaM, since its very low stability at [KCl] ~ 5 mM ($\Delta G°_{20}$ ~ 0.5 kcal/mol) means that the protein is significantly unfolded (~ 30% at 20 °C) under these solvent conditions. Increasing [KCl] to 200 mM reduces the percentage of unfolded molecules to ~ 3.7%. A similar, but smaller, effect is observed for apo-Tr2C, which is ~ 11% unfolded at 20°C in the presence of ~ 5 mM KCl.

In order to characterise the effects of higher concentrations of KCl on the secondary structure of apo-CaM far-UV intensities were monitored as a function of [KCl] in the range 0-700 mM (Figure 4.2B). The data show that the intensity of the far-UV signal increases continuously over this range of [KCl] as the protein is refolded. More stable proteins, such as apo-Tr1C, show much smaller effects – data not shown. However, the far-UV CD signal of apo-CaM at [KCl] = 700 mM is clearly more intense than would be expected if the effect derived only from complete refolding of the protein. This suggests that there may be some non-specific effect of high concentrations of KCl on this particular signal. Consistent with this idea, control titrations performed with holo-CaM (in the presence of 1 mM calcium) showed that the far-UV CD signal of the holo-protein increases by ~ 3% over the [KCl] range 0-600 mM (see Fig. 4.3). Applying a similar (approximate) correction to the data of Fig. 4.2B suggests that complete refolding of apo-CaM probably occurs at [KCl] ~ 250 mM, consistent with the effects of KCl on the free energy of unfolding reported in Table 4.1.

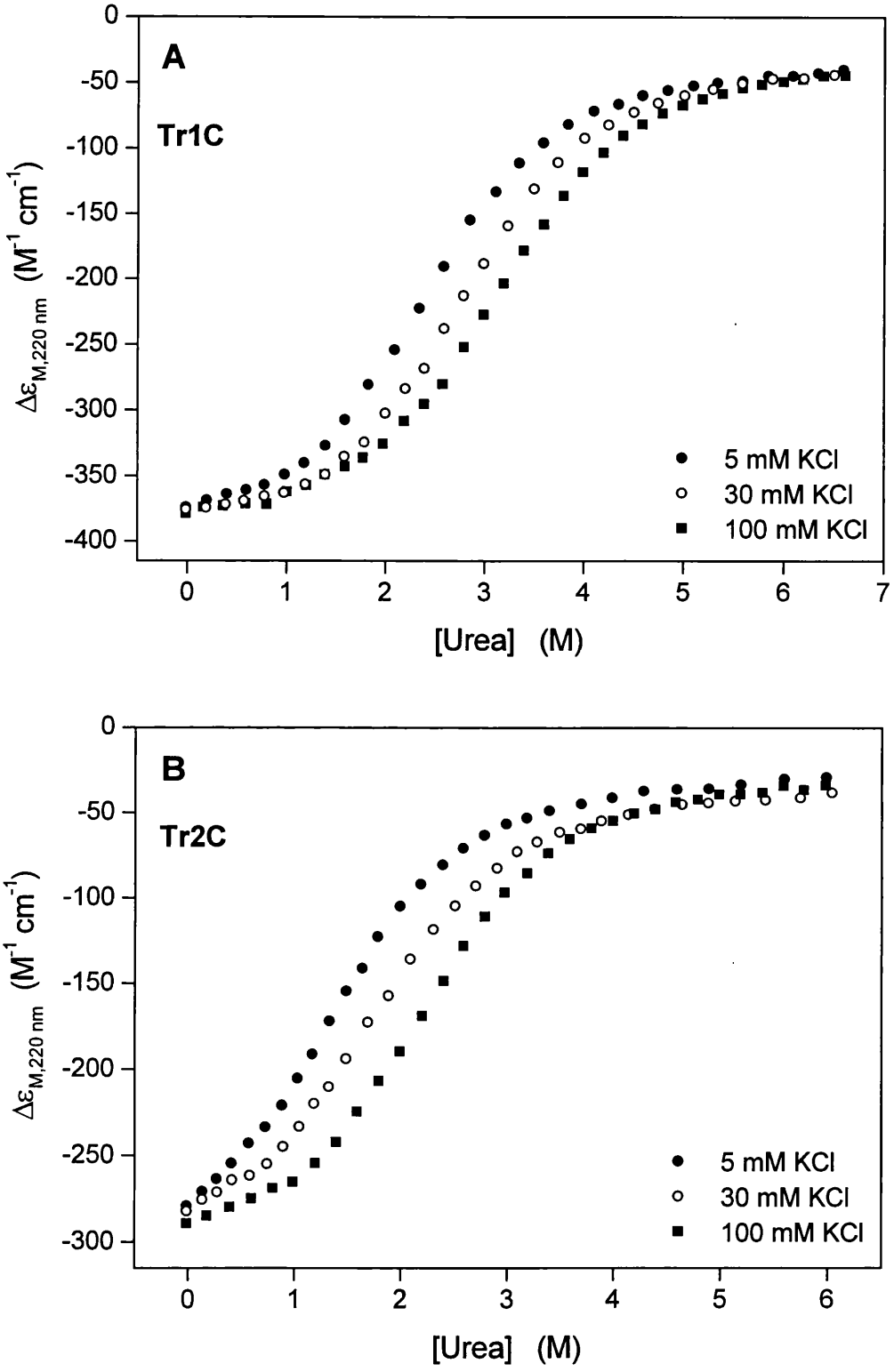

Figure 4.1 Urea-induced denaturation of apo-Tr1C **(A)** and apo-Tr2C **(B)** at ~5 (●), 30 (○), and 100 (■) mM KCl. Unfolding was monitored at 20 °C in 25 mM Tris, pH 8, using far-UV CD.

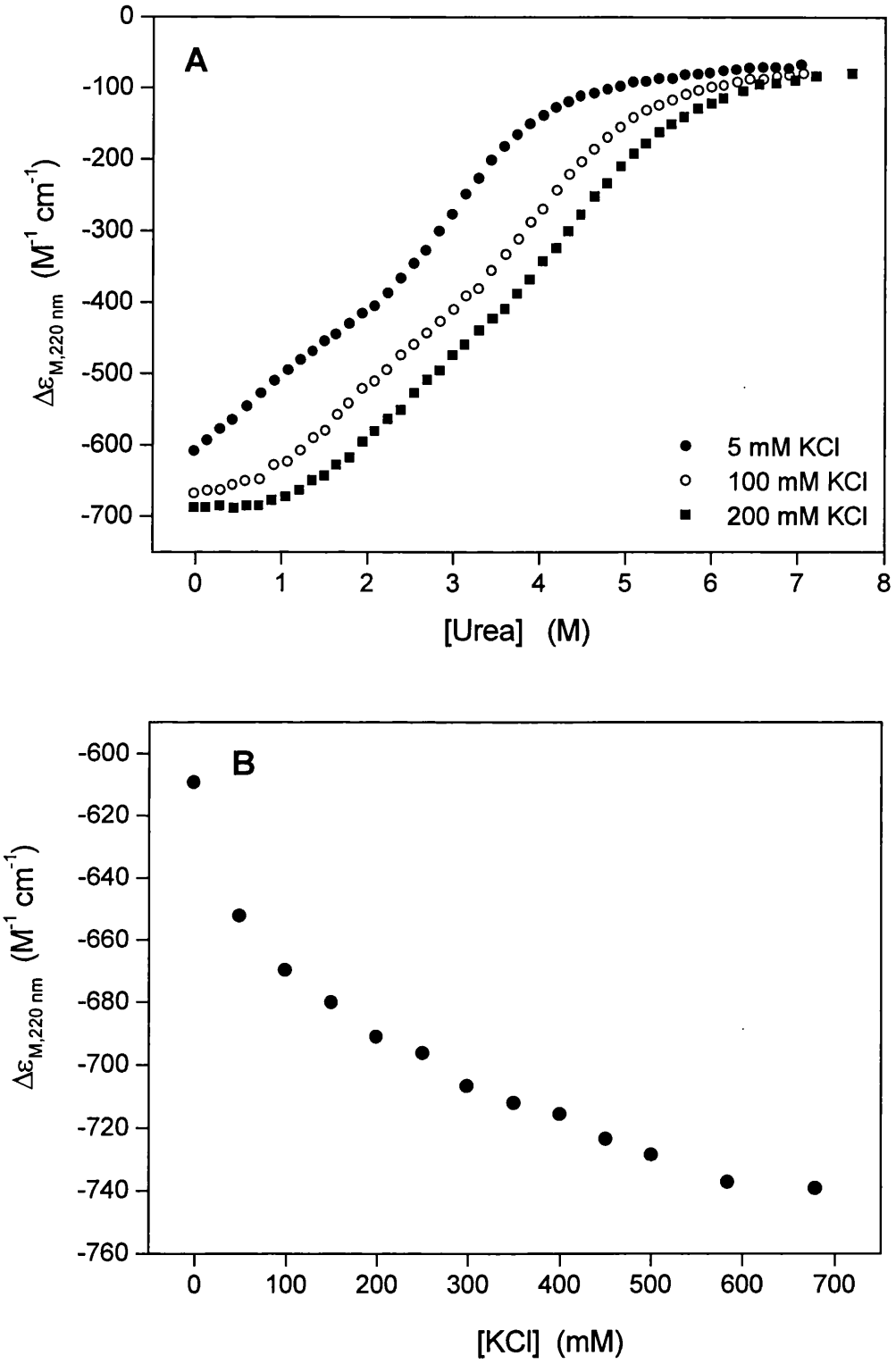

Figure 4.2 **(A)** Urea-induced denaturation of apo-CaM at ~5 (●), 100 (○), and 200 (■) mM KCl. Unfolding was monitored at 20 °C in 25 mM Tris, pH 8, using far-UV CD. **(B)** KCl titration of apo-CaM monitored at 20 °C in 25 mM Tris, pH 8, using far-UV CD.

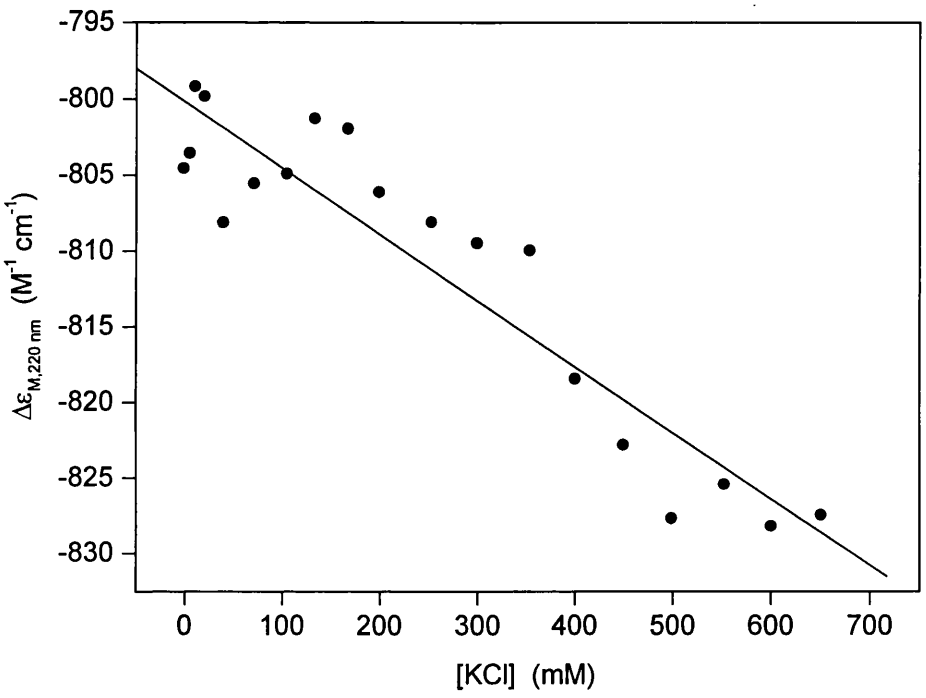

Figure 4.3 KCl titration of holo-CaM in 1 mM Ca^{2+} monitored at 20 °C in 25 mM Tris, pH 8, using far-UV CD.

Table 4.1 Effects of KCl on urea-unfolding of apo-Tr1C, apo-Tr2C, and apo-CaM, monitored using far-UV CD

Transition	[KCl] (mM)	$[U]_{1/2}$ (M)	$\Delta G°_{20}$ [a] (kcal/mol)	% unfolded (20°C)
Tr1C	< 5	2.34	2.15	2.4
	30	2.77	2.55	1.2
	100	3.09	2.84	0.8
Tr2C	< 5	1.31	1.21	11
	30	1.69	1.55	6.5
	100	2.17	2.00	3.1
CaM-1 [b]	< 5	~ 0.6	~ 0.5	~ 30
CaM-2 [b]	< 5	2.99	2.75	0.9
CaM-1	100	1.65	1.52	6.8
CaM-2	100	4.05	3.73	0.2
CaM-1	200	2.07	1.90	3.7
CaM-2	200	4.32	3.97	0.1

[a] $\Delta G°_{20}$ values were calculated as $-[U]_{1/2} \cdot m_{av}$, with m_{av} = -0.92 kcal/mol·M (see Section 2.3.6.1, Chapter 2).

[b] CaM-1 and CaM-2 indicate the first and second transitions resolved for intact CaM, assigned to the C- and N-domains respectively.

The magnitude of the stabilising effect of ionic strength has also been investigated by experiments in which apo-CaM was titrated with KCl in the presence of 2 or 5 M urea. The far-UV CD data are shown in Figure 4.4. The protein, partially unfolded at these denaturant concentrations, is refolded as the KCl concentration is increased. In particular, the urea-unfolding curves obtained with apo-CaM at different KCl concentrations (Figure 4.2A) show that in the absence of KCl and at 2 M urea the N-domain is substantially folded, whilst the C-domain is approximately 90% unfolded. Thus, the increase in the far-UV CD signal observed in the KCl titration at 2 M urea corresponds to the refolding of the apo-C-domain, which at 500 mM KCl is only approximately 7% unfolded. The $\Delta G°_{20}$ values calculated from the percentages of unfolded protein present indicate that increasing [KCl] from zero to 500 mM induces an increase in the free energy of unfolding of the apo-C-domain of approximately 2.8 kcal/mol.

The dependence of the stability of apo-CaM on [KCl] has also been studied with thermal unfolding experiments performed by monitoring the Tyr-138 fluorescence signal from the C-domain. Typical curves measured in zero and 100 mM KCl are shown in Figure 4.5A and the results of the analyses are reported in Table 4.2. Given the difficulties associated with determining small ΔG^{o}_{20} values, there is reasonable agreement between the values obtained here and those obtained for the CaM-1 transition (C-domain) using urea-unfolding monitored by far-UV CD (Table 4.1).

One of the conclusions of the chemical unfolding experiments described in Chapter 3 was that the denaturants urea and GuHCl give significantly different $\Delta G°_{20}$ values for CaM and its isolated fragments. In particular, the measured stabilities of the apo-proteins are consistently higher when measured using GuHCl than when measured using urea. This observation suggests that the apo-proteins may be stabilised by low concentrations of GuHCl because this denaturant (unlike urea) is positively charged and therefore causes changes in the ionic strength of the solution. In order to confirm this stabilising effect, Tyr-138 fluorescence measurements of thermal unfolding of the C-domain of apo-CaM have been performed in 0.1 and 0.2 M GuHCl. The results (Table 4.2) show that these small non-denaturing concentrations of GuHCl do indeed have a significant stabilising effect, which is similar to that of KCl. The stabilising effect of 0.2 M GuHCl is, however, less than that of 0.2 M KCl because of the other effect of the denaturant in reducing the free energy of unfolding.

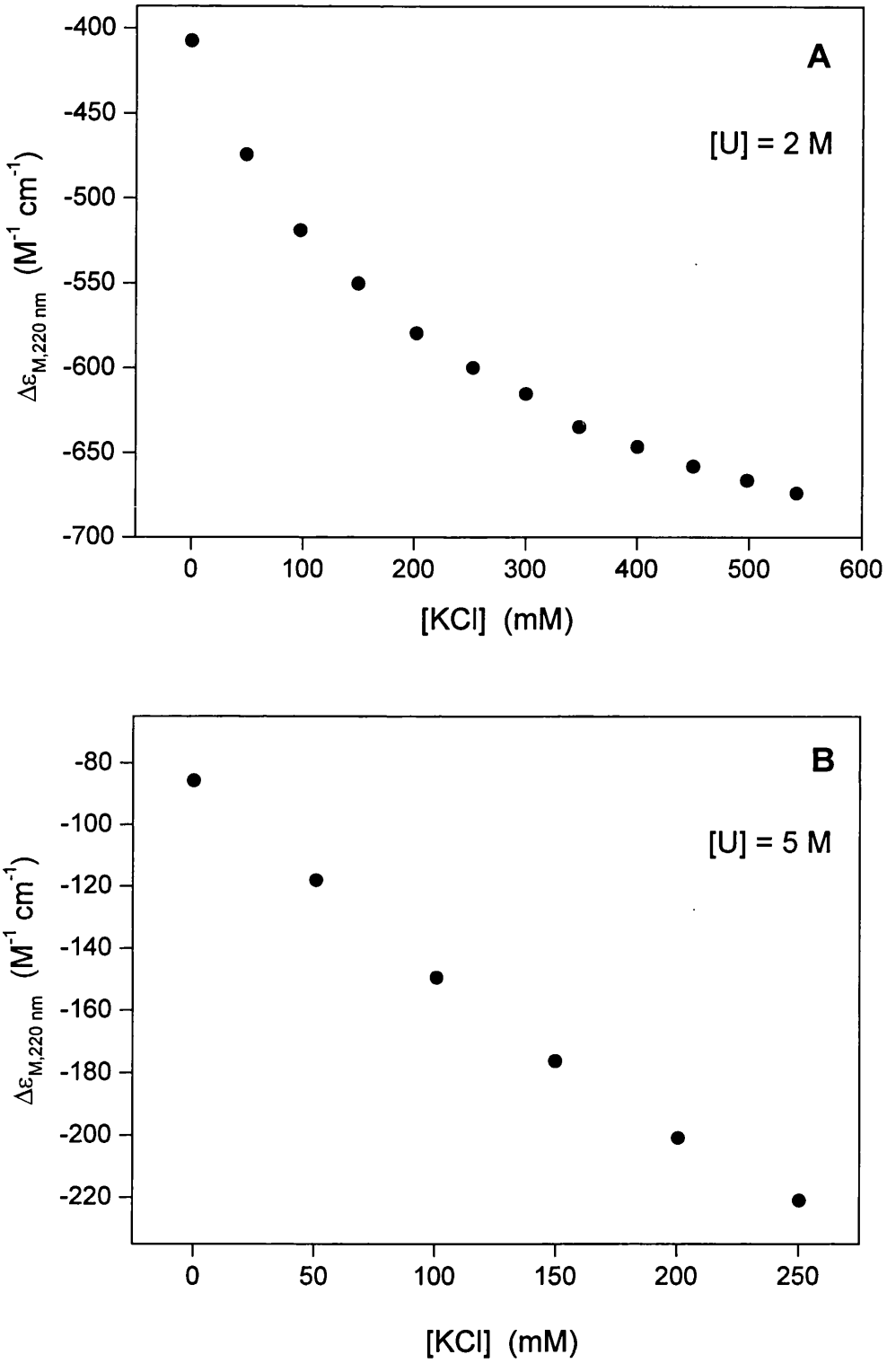

Figure 4.4 KCl titrations of apo-CaM in 2 M **(A)** and 5 M **(B)** urea monitored at 20 °C in 25 mM Tris, pH 8, using far-UV CD.

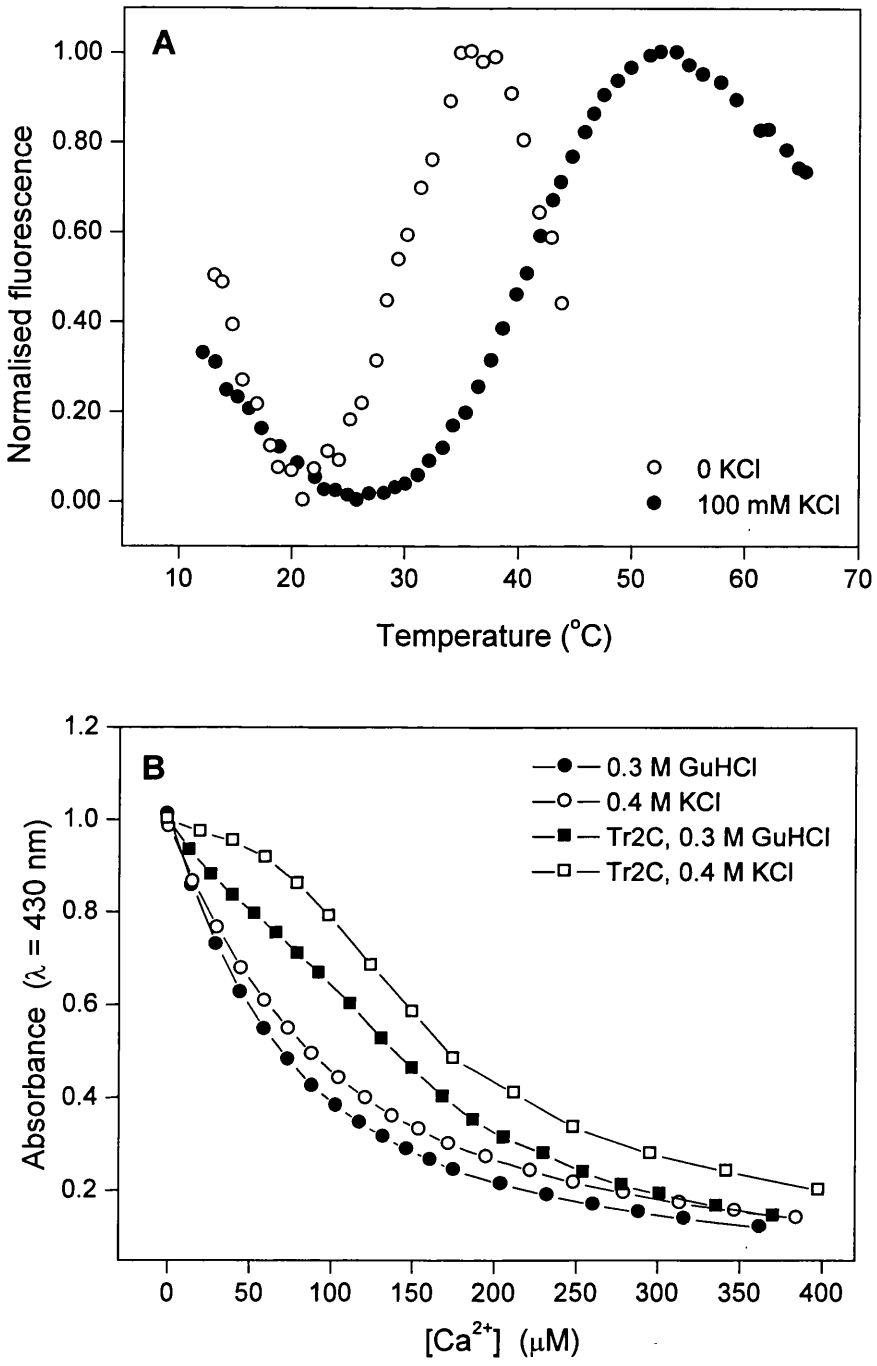

Figure 4.5 **(A)** Thermal denaturation of apo-CaM (C-domain) in 0 (○) and 100 (●) mM KCl. Unfolding was monitored in 10 mM Hepes, pH 7.5, using Tyr-138 fluorescence. The data have been arbitrarily normalised in order to facilitate comparison. **(B)** Ca^{2+} titrations of 5-nitro BAPTA in the absence (circles) and in the presence (squares) of Tr2C, in 0.3 M GuHCl plus 0.1 M KCl (closed symbols), and 0.4 M KCl (open symbols). The measurements were performed at 20 °C, in 25 mM Tris, pH 8, using absorption spectroscopy.

Table 4.2 Effects of KCl on thermal unfolding of the apo-CaM C-domain, monitored using Tyr-138 fluorescence

Salt	T_m (°C)	ΔH_m (kcal/mol)	ΔG_{20}[a] (kcal/mol)	% unfolded (20°C)
None	31.3	25.3	0.81	20
0.1 M KCl	42.8	31.5	1.59	6.1
0.2 M KCl	47.3	33.5	1.89	3.7
0.1 M GuHCl	42.7	32.9	1.69	5.2
0.2 M GuHCl	44.9	32.3	1.75	4.8

[a] Values of ΔG_{20} were calculated using ΔC_p = 0.804 kcal/(K·mol) (Sorensen and Shea, 1998).

4.3.2 Effects of GuHCl on Ca^{2+}-binding

Another problem observed in Chapter 3 (see Section 3.3.3.3) is that the measured stabilising effects of calcium are generally much smaller than the predicted values. The difference between the experimentally observed ligand interaction free energies ($\Delta\Delta G_b$(obs)) and the theoretically calculated ones ($\Delta\Delta G_b$(calc)) (see Table 3.3) is particularly high in the case of GuHCl-induced unfolding. As discussed in Chapter 3, the fact that calcium probably binds to the denatured state and thereby decreases the ligand interaction free energy cannot fully explain this observation. The second possible explanation mentioned in Chapter 3 was that the presence of the denaturant could have a direct effect on the affinity of the native state of the protein for calcium.

In order to explore this possibility, stoichiometric association constants for Ca^{2+} binding to the CaM fragments were measured in the presence of GuHCl at

concentrations which induced only very limited unfolding of the apo-proteins. Initial experiments performed with 5,5'-dibromo BAPTA ($K_{Ca} = 5.7 \cdot 10^5\ M^{-1}$ in 100 mM KCl) in the presence of 0.3 M GuHCl showed that the stoichiometric association constants of the fragments were indeed reduced; to the point where they could no longer be measured using this particular indicator. Therefore the low affinity indicator, 5-nitro BAPTA, was used in further experiments and its calcium-binding constants were measured in the standard buffer (0.1 M KCl) and in this buffer plus 0.3 M GuHCl or plus an additional 0.3 M KCl, as a control. At 0.1 M KCl, the measured calcium-binding constant for 5-nitro BAPTA is $3.3 \cdot 10^4\ M^{-1}$ (Table 4.3) and at the higher ionic strength, with either KCl or GuHCl, it is reduced by approximately a factor of two ($K_{Ca} = 1.5 \cdot 10^4\ M^{-1}$ for 0.4 M KCl and $1.8 \cdot 10^4\ M^{-1}$ for 0.1 M KCl plus 0.3 M GuHCl). The stoichiometric association constants measured for Tr1C and Tr2C using this indicator are given in Table 4.3 and typical titration curves obtained using Tr2C are shown in Fig. 4.5B. The results indicate that the calcium binding to the fragments is significantly weakened by both salts, but to different extents. In the presence of 0.4 M KCl the products of the stoichiometric association constants (K_1K_2) for both fragments are reduced by approximately one order of magnitude.

Table 4.3 Calcium binding constants for 5-nitro BAPTA and the tryptic fragments of CaM

Conditions	K_{Ca} (M^{-1}) for 5-nitroBAPTA	K_1K_2 (M^{-2}) for Tr1C	K_1K_2 (M^{-2}) for Tr2C
0.1M KCl[a]	$3.3 \cdot 10^4$	$1.45 \cdot 10^{10}$	$2.40 \cdot 10^{11}$
0.4 M KCl	$1.5 \cdot 10^4$	$1.35 \cdot 10^9$	$2.65 \cdot 10^{10}$
0.1 M KCl + 0.3 M GuHCl	$1.8 \cdot 10^4$	$1.55 \cdot 10^8$	$2.80 \cdot 10^9$
0.1 M KCl + 0.3 M Urea	$3.1 \cdot 10^4$	n.d.	$1.85 \cdot 10^{11}$

[a] The constants determined for Tr1C and Tr2C in 0.1M KCl agree well with those determined using 5,5'-dibromo BAPTA (Bayley et al., 1996).

The effects of increasing ionic strength on the Ca^{2+}-binding constants can be predicted using a semi-empirical form of the Debye-Hückel limiting law, as described by Harrison and Bers (1987). According to this model, the variation in a binding constant K induced by changing the ionic strength from I to I' can be calculated using the following equation:

$$\log_{10} K(I') = \log_{10} K(I) + 2xy\,(\log_{10} f(I) - \log_{10} f(I'))$$

where f is an adjustment factor, and x and y represent the valencies of the cation and anion of the binding species, respectively. The adjustment factor f was calculated as:

$$\log_{10} f(I) = A\left(\frac{\sqrt{I}}{1+\sqrt{I}} - 0.25 \cdot I\right)$$

where A was determined using:

$$A = 1.8246\frac{10^6}{(\varepsilon T)^{3/2}}$$

where T (°K) is the absolute temperature and ε is the dielectric constant of water at that temperature (ε(293 K) = 80.1).

Using this method, it is possible to predict the reduction in the average binding constant ($K_{av} = (K_1K_2)^{1/2}$) for an isolated CaM domain that is expected for an increase of ionic strength from 0.1 to 0.4 M. The predicted reduction in K_{av} is by a factor of 2.8 for a net charge on the calcium binding loop of –3 and by a factor of 3.9 for a net charge on the calcium binding loop of –4. These values are in reasonable agreement with the experimentally observed factors of ~ 3.3 obtained for the reduction in $K_{av(N)}$ (the average net charge on calcium-binding loops I and II in the N-domain is –3) and ~ 3.0 obtained for the reduction in $K_{av(C)}$ (the average net charge on calcium-binding binding loops III and IV in the C-domain is –3.5).

As observed above, the presence of GuHCl also reduces the affinity of Tr1C and Tr2C for Ca^{2+}, but, in this case, unlike the situation for Ca^{2+} binding to 5-nitro BAPTA itself, the effect of GuHCl is very much greater than that of KCl. In fact, in the presence of 0.3 M GuHCl, the products K_1K_2 for both fragments are reduced by approximately two orders of magnitude. Thus, the results show that GuHCl does have effects on the binding of Ca^{2+} to Tr1C and Tr2C, which cannot be accounted for by the

increased ionic strength alone. Therefore there must be some direct competition between GuHCl and calcium binding. As a control, the calcium-binding constants for 5-nitro BAPTA and Tr2C have also been measured in the presence of 0.3 M urea. At this urea concentration the affinity of the indicator for calcium is not significantly reduced and the constants of Tr2C are barely affected (Table 4.3).

4.3.3 Kinetics of Ca^{2+} dissociation

The changes in calcium affinity observed for Tr1C and Tr2C in the presence of KCl and GuHCl can, in principle, arise from changes in either the association or the dissociation rate constants. The kinetics of Ca^{2+} dissociation from the C-domain of intact CaM were therefore measured using Tyr-138 fluorescence (at 20°C) in the presence of different concentrations of KCl, GuHCl and urea. The dissociation of the two Ca^{2+} ions from the C-domain occurs as a single exponential process, with observed rates 7.4, 8.0 and 10.2 s^{-1} in zero, 100 mM and 300 mM KCl respectively. The rates measured in the presence of 0.1 M and 0.2 M GuHCl were 11.8 and 12.9 s^{-1}, and the rates obtained in the presence of 0.3 M and 3.4 M urea were 8.4 and 7.3 s^{-1} (Table 4.4). These results indicate that the calcium dissociation rates for the C-domain of CaM do not depend significantly on ionic strength, even though there are major changes in calcium affinity over the range of ionic strength studied (Linse et al., 1991a, and present work). The dissociation rates are slightly increased in the presence of denaturants, but not nearly enough to account for the reduced calcium affinity. Thus, the changes in the calcium-binding constants observed under these different solvent conditions must be principally due to changes in the calcium association rates, resulting from both medium (ionic strength) and competition effects.

4.3.4 Effects of pH

Another important parameter which could, in principle, have a major effect on the stability of CaM is pH. The effects of pH on the structural properties of CaM have been investigated by performing pH titrations monitored by both far-UV CD and Tyr-138 fluorescence. The far-UV CD titrations with apo-CaM and CaM in the presence of 1 mM Ca^{2+} (at 5.5 °C) are shown in Figure 4.6A. The far-UV CD intensities vary

Table 4.4 Kinetics of Ca^{2+}-dissociation from the C-domain of CaM

Conditions	k_{obs} (sec^{-1}) [a]
no KCl	7.4
0.1 M KCl	8.0
0.3 M KCl	10.2
0.1 M GuHCl	11.8
0.2 M GuHCl	12.9
0.3 M Urea	8.4
3.4 M Urea	7.3

[a] The uncertainties are ± 0.5 sec^{-1} for each value.

significantly in the pH region 7.5 - 5.7, but in opposite directions; the signal of apo-CaM increases upon lowering the pH, whilst that of CaM in the presence of 1 mM Ca^{2+} diminishes (cf., Bayley and Martin, 1992). The net result is that the difference between the signals observed at neutral pH (attributed to the Ca^{2+}-induced conformational change) is substantially smaller at pH 5.5 and below. The reduction in the signal from CaM in the presence of 1 mM Ca^{2+} is not due to loss of calcium, which only becomes significant (at this [Ca^{2+}]) below pH ~ 4.5 (Milos et al., 1986). The secondary structures of apo- and holo-CaM therefore appear to be much more similar at slightly acidic pH's (pH 4.5 to 5.5) than they are at neutral pH.

The pH titrations monitored using Tyr-138 fluorescence have been performed with apo-CaM and CaM in the presence of 1 mM Ca^{2+} in standard buffer (25 mM Tris, 100 mM KCl) at 20 °C. In the presence of KCl, the protein precipitates when the pH is lowered to approximately 4.0 (i.e., close to the isoelectric point). The same experiments have therefore been performed in the absence of KCl, in 25 mM Tris. Under these solvent conditions, CaM again precipitates as the pH approaches 4, but then becomes soluble again when the pH is lowered still further. The titration curves measured in the

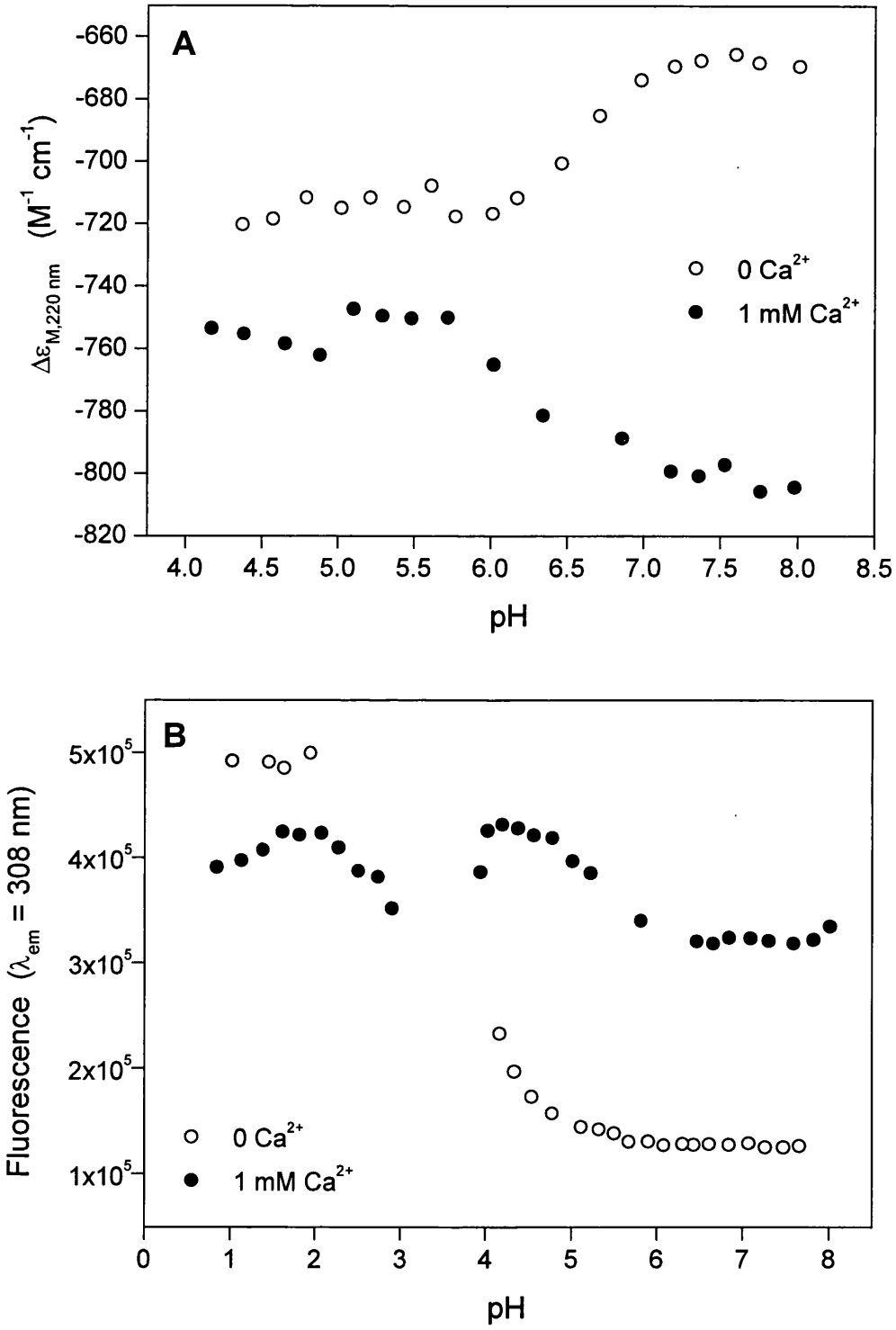

Figure 4.6 **(A)** pH titrations of apo-CaM (○) and CaM in 1 mM Ca^{2+} (●) monitored at 5.5 °C in 25 mM Tris, 100 mM KCl, pH 8, using far-UV CD. **(B)** pH titrations of apo-CaM (○) and CaM in 1 mM Ca^{2+} (●) monitored at 20 °C in 25 mM Tris, pH 8, using Tyr-138 fluorescence.

absence of KCl are shown in Figure 4.6B. The results obtained in the pH range 8 to 4 are the same as those measured in the presence of 100 mM KCl. No significant signal changes are measured for either apo-CaM or CaM in 1 mM Ca^{2+} in the pH range 7.7 - 5.5, where changes in the far-UV CD signal are observed. There are, however, significant changes below pH 5.5, where the intensities of both signals increase. At pH 2 and below, the apo-CaM signal becomes similar to that of the signal of CaM in the presence of 1 mM Ca^{2+}. This observation is not surprising, since at pH 2 protons will bind to the carboxylate groups in the Ca^{2+} binding loops of CaM, and Ca^{2+} will no longer be bound (Török et al., 1992). Thus, at very acidic pH's, the environment of Tyr-138 in the C-domain of apo-CaM is significantly different from that in the pH range 8 to 5. The results obtained using CD and fluorescence spectroscopy are therefore very different. The changes in secondary structure measured by far-UV CD occur in a pH range (7.5 - 5.7) where there is little change in the Tyr-138 fluorescence signal.

In order to investigate whether the observed changes in secondary structure affect the conformational stability of CaM, urea-unfolding experiments have been performed with apo-CaM and holo-CaM (in 0.3 mM Ca^{2+}) at pH 6.5, in 25 mM MES and 100 mM KCl. The far-UV CD unfolding profiles are shown in Figure 4.7A. The results of the LEM analyses for apo-CaM are $[U]_{1/2}$ = 1.78 M and $\Delta G°_{20}$ = 1.64 kcal/mol for transition CaM-1, corresponding to the C-domain, and $[U]_{1/2}$ = 4.06 M and $\Delta G°_{20}$ = 3.74 kcal/mol for transition CaM-2, corresponding to the N-domain. For holo-CaM the results are $[U]_{1/2}$ = 5.16 M and $\Delta G°_{20}$ = 4.75 kcal/mol for transition CaM-1, corresponding to the N-domain, and $[U]_{1/2}$ = 7.21 M and $\Delta G°_{20}$ = 6.63 kcal/mol for transition CaM-2, corresponding to the C-domain. These data are very similar to those measured for apo-CaM and holo-CaM (in 0.3 mM Ca^{2+}) at pH 8.0 (Tables 3.1 and 3.4). Therefore the results indicate that, although changes are observed in the secondary structure of both apo- and holo-CaM between pH 8.0 and 6.5, the stability of the protein remains essentially unchanged.

These conclusions have been confirmed by thermal denaturation experiments performed with apo-CaM at pH 6.5 under the same buffer conditions. The unfolding curve is shown in Figure 4.7B and the parameters obtained from the analysis are ΔH_m = 30.3 kcal/mol and T_m = 44.2 °C for transition CaM-1, corresponding to the C-domain, and ΔH_m = 44.8 kcal/mol and T_m = 57.5 °C for transition CaM-2, corresponding to the

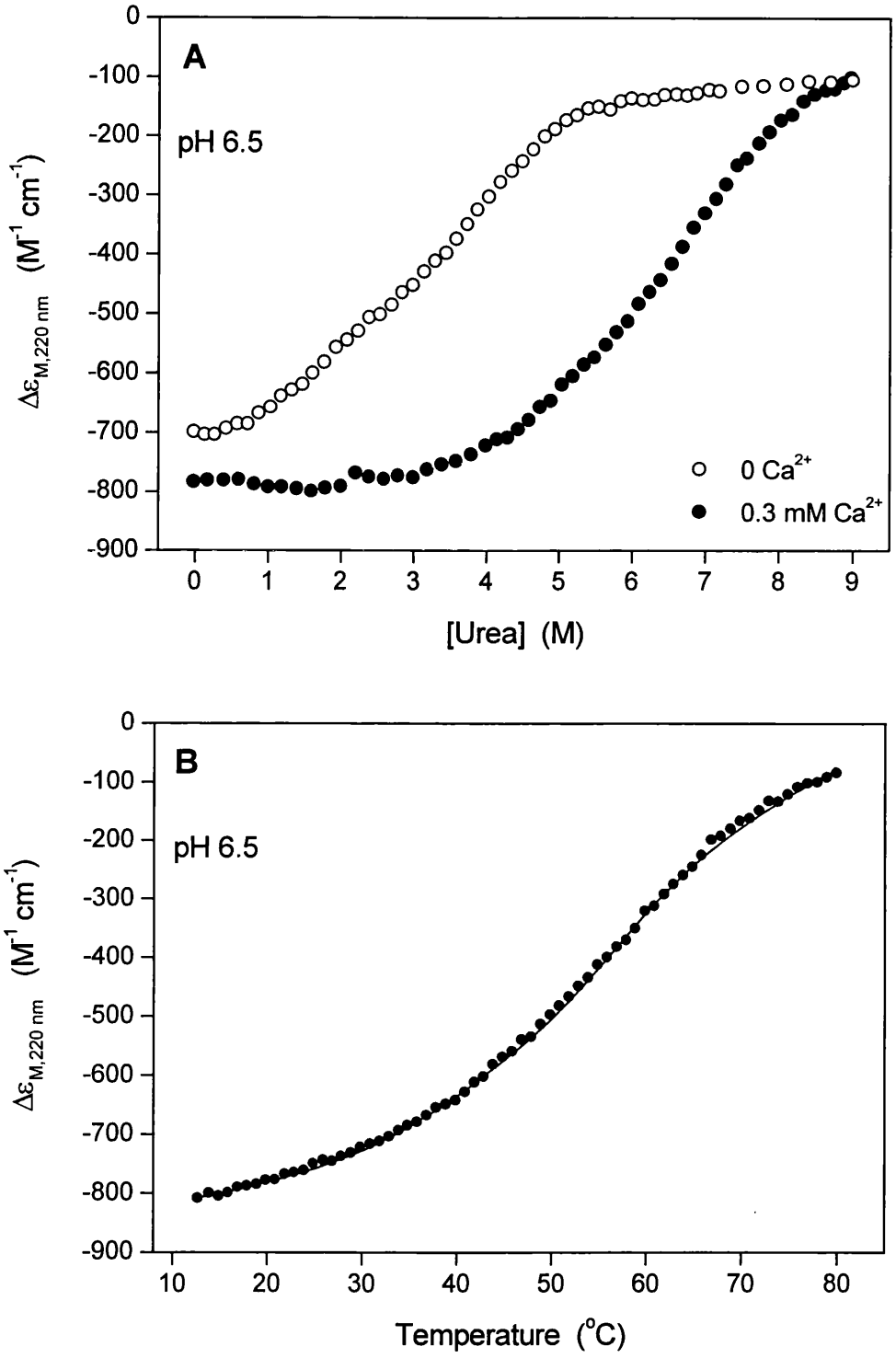

Figure 4.7 **(A)** Urea-induced denaturation of CaM at 0 (○) and 0.3 (●) mM Ca^{2+}. Unfolding was monitored at 20 °C in 25 mM MES, 100 mM KCl, pH 6.5, using far-UV CD. **(B)** Thermal denaturation of apo-CaM in 25 mM MES, 100 mM KCl, pH 6.5, monitored using far-UV CD. The solid line is the computed best fit.

N-domain. These data gave ΔG_{20} values of 1.55 and 3.47 kcal/mol for transitions CaM-1 and CaM-2, respectively. These values are very similar, though not identical, to the ΔG_{20} values of 1.43 and 3.69 kcal/mol obtained for transitions CaM-1 and CaM-2 at pH 8.0. The agreement between the thermal denaturation and urea-unfolding data at pH 6.5 is also good.

4.4 Discussion

4.4.1 Effects of ionic strength and differences between urea and GuHCl

The results of the thermal and urea-unfolding experiments performed at different KCl concentrations have shown that the stabilities of apo-CaM and its isolated apo-domains are strongly dependent upon ionic strength conditions, with stability increasing with increasing ionic strength. This stabilising effect is particularly evident in the case of the C-domain in apo-CaM, which is approximately 30% unfolded at [KCl] < 5 mM and only 3.7% unfolded at 200 mM KCl. The sensitivity of the intensity of the far-UV CD spectrum of apo-CaM to solution conditions was previously noted by Martin and Bayley (1986). Evidence for a stabilising effect of increasing ionic strength has also been reported for a related calcium-binding protein, chicken troponin C (Fredricksen and Swenson, 1996).

Individual secondary structural elements in a protein may be stabilised by favourable interactions between oppositely charged residues or destabilised by unfavourable interactions between groups with the same charge. At neutral pH, CaM carries a large overall negative charge, so that the low thermodynamic stability of this protein is probably associated with unfavourable interactions between negatively charged groups. The stabilising effect of KCl would then be due to screening of these charges by K^+ ions. Another possible explanation of the observed effect of KCl would be that K^+ ions may stabilise apo-CaM by directly binding to the Ca^{2+} binding sites, thus substituting for Ca^{2+}. However, NMR studies have shown that K^+ ions interact weakly and non-specifically with CaM and no direct competition between K^+ and Ca^{2+} for the EF-hands sites is observed (Linse et al., 1991a).

The strong dependence of the stability of CaM on ionic strength indicates that electrostatic interactions play an important role in determining the stability of this

protein. Similar conclusions were obtained from a study of the thermostability of apo-SynCaM mutants in which clusters of acidic amino acids have been replaced by basic amino acids (Protasevich et al., 1997). The contribution of electrostatic interactions to protein stability have also been investigated in the case of the calcium binding protein calbindin D_{9k}, which contains two EF-hand motifs, and can thus be compared to a single CaM domain (Forsén et al., 1989; Akke and Forsén, 1990). The stability of a series of calbindin D_{9k} mutants, in which negatively charged residues in a calcium binding loop have been mutated to side-chain amide analogs (Glu to Gln and Asp to Asn) has been studied by urea denaturation. Interestingly, the results have shown that the neutralisation of the negative charges induces an increase in the stability of calbindin. Thus, it was demonstrated that clusters of negatively charged residues on the protein surface, a characteristic of proteins containing EF-hand motifs, can indeed interact unfavourably and lower the stability of the native form of the protein.

Thermal denaturation experiments have shown that a stabilising effect similar to that of KCl is also observed in the case of GuHCl. Because of the ionic nature of this denaturant, apo-CaM and its isolated fragments are stabilised by low, non-denaturing concentrations of GuHCl and, as a result, the $\Delta G°_{20}$ values measured for the apo-proteins using GuHCl are higher than those measured using urea. Similar behaviour, with a maximal stabilising effect at 0.3 M GuHCl, has been reported by Fredricksen and Swenson (1996) in experiments with residues 1-85 of chicken troponin C. The possible consequences of the ionic nature of GuHCl in the determination of protein stability have been discussed by Monera et al. (1994). Therefore it can be concluded that in the case of highly charged proteins, where electrostatic interactions may contribute significantly to the stability of the protein, any estimate of the stability obtained from GuHCl-induced unfolding may be unreliable.

Moreover, the results of the calcium binding experiments performed using the chelator 5-nitro BAPTA have shown that GuHCl, even at relatively low concentrations (0.3 M), can greatly reduce the affinity of Tr1C and Tr2C for calcium, whilst urea at the same concentration has very little effect. The calcium binding constants of CaM and its tryptic fragments are known to be reduced by factors of more than 40-fold on increasing the ionic strength from 0 to 0.1M with KCl (Linse et al., 1991a). A further reduction in affinity on increasing the ionic strength from 0.1 to 0.4 M is therefore not unexpected and indeed the magnitude of the effects observed with KCl are well

predicted by the Debye-Hückel limiting law (see Section 4.3.2). The much greater effects observed with GuHCl cannot, therefore, be accounted for by changes in ionic strength alone and direct competion with Ca^{2+} binding is suggested (see below). Interestingly, the reduction in calcium affinity observed in the presence of additional salt (with either KCl or GuHCl) is only associated with a very small increase in the calcium dissociation rate constant. The association rate constant must, therefore, be significantly reduced, especially in the presence of GuHCl. This observation is consistent with the view that negative charges on the protein surface are important in determining the association rate constant for calcium binding to proteins containing EF-hands (Martin et al., 1990).

It is generally thought that the guanidinium ion (GuH^+) binds to a large number of very low affinity sites ($K \sim 0.6\ M^{-1}$) in both the native and denatured states of proteins (Makhatadze and Privalov, 1992); the denaturing effect derives from the fact that there are significantly more of these sites available in the unfolded form. The reduced calcium affinity could, at least in principle, derive from the existence of several low affinity sites in the immediate vicinity of the calcium-binding loop of the folded protein. Alternatively, it has been suggested (Pace et al., 1990) that in particular proteins there may be one or more sites for GuH^+ binding that are more specific and where the ion is bound with greater affinity ($K \sim 10\text{-}20\ M^{-1}$). Binding of a single ion with an affinity of this magnitude in or close to a calcium binding loop might also account for the observed effects.

These observations explain why the stabilising effect of calcium appears to be much smaller when the stabilities of the holo-proteins are estimated using GuHCl-unfolding. However, imperfect agreement between the observed and calculated ligand interaction free energies has also been observed in the case of urea-unfolding of holo-Tr2C in 0.3 mM calcium (Chapter 3, Table 3.3). The possibility that high concentrations of urea also compete with calcium binding in some way cannot, therefore, be excluded. Nevertheless, the results obtained with urea-unfolding of the apo-proteins are in good agreement with those obtained using thermal denaturation and it can be concluded that the unfolding parameters determined using urea are likely to be more appropriate than those measured using GuHCl for thermodynamic analysis.

4.4.2 Effects of pH

The studies on ionic strength described above have shown that unfavourable electrostatic interactions between negatively charged groups probably contribute significantly to the low thermodynamic stability of CaM. It might therefore be expected that variations in pH would also affect the stability of the protein. The pH titrations performed using far-UV CD have shown that decreasing the pH from 7.5 to 5.7 increases the apparent α-helical content of apo-CaM, but decreases that of holo-CaM. Lowering the pH to 2.0 does not cause any further change in the signal from apo-CaM, showing that there is no acid-induced unfolding at this pH (Török et al., 1992). The consequence of this behaviour is that the calcium-induced increase in α-helical content is much smaller at pH 5.7. The shapes of the curves suggest that the changes observed in the signals could be associated with small conformational transitions, possibly due to protonation of His 107, the only residue in CaM with a pK_a in this pH range. However, it must be noted that the overall change in intensity represents a relatively small percentage (approximately 8%) of the total signal for both the apo- and holo-forms. Nevertheless, this result may account, at least in part, for the observation that the NMR structures of apo- and holo-CaM (generally determined at pH's in the range 6 – 6.5) (Ikura et al., 1991; Kuboniwa et al., 1995; Zhang et al., 1995a) appear to be much more similar than the differences in far-UV CD observed at neutral pH (Martin and Bayley, 1986, and references therein) would suggest.

The pH titrations monitored by fluorescence show that there is no change in the Tyr-138 signal in the pH range where the far-UV CD signal changes (7.5 - 5.5). Since the large increase in the fluorescence signal occurs in a pH range (5.5 - 4.3) where there is no change in the far-UV CD signal, it is presumably related to local changes in the environment of Tyr-138. The fluorescence spectrum of apo-CaM at neutral pH (see Fig. 3.1B, Chapter 3) is significantly different from that of tyrosine model compounds, having unusually low overall intensity and a significant long wavelength component. One possible explanation is that the fluorescence of Tyr-138 in apo-CaM may be quenched by carboxylate groups located close to the fluorophore (Lehrer and Leavis, 1974). The protonation of such carboxylates would be expected to occur in this pH range. This would remove the carboxylate quenching effect and therefore account for the observed increase in the tyrosyl fluorescence at pH < 5.5.

The conclusion from these preliminary studies on pH effects is that the stabilities of apo- and holo-CaM at pH 6.5 are essentially the same as those at pH 8.0. The observation that the unfolding parameters observed in the presence of 0.3 mM Ca^{2+} are similar at the two pH's shows that the ligand interaction free energy is the same. This observation is a useful confirmation of the suggestion that any change in the calcium affinity of CaM in this pH range is probably small (cf., Linse et al., 1991a).

The studies described here and in Chapter 3 have characterised the dependence of the stability of CaM on environmental conditions, such as temperature, ionic composition, metal ion binding, and pH. The results show that apo-CaM is a protein with very low intrinsic stability. The stability of such proteins is readily perturbed by changes in environmental conditions, and, by extension, mutation. The effects of specific mutations on the stability of CaM are investigated in the next chapter.

CHAPTER 5

STABILITY AND Ca^{2+}-BINDING PROPERTIES OF THE β-SHEET MUTANTS OF CALMODULIN

5.1 Introduction

In Chapters 3 and 4 of this work the conformational stability of CaM was studied using thermally- and chemically-induced unfolding of the intact protein and its isolated fragments, under different solvent conditions. Site-specific mutagenesis is another method that has been widely used in order to investigate the general features of protein stability and to assess the contribution of individual residues to protein structure and stability. The effects of a single mutation on the stability of a protein vary widely, depending on the importance of the substituted residue in maintaining the native conformation and on the chemical nature of the newly introduced residue. Previous studies have shown that the thermodynamic stability of CaM can be significantly perturbed by single point mutations, which can affect to different extents the structure and stability of the protein, its Ca^{2+} binding properties, and the strength of interaction with target molecules (see Section 1.3, Chapter 1).

In the EF-hand calcium-binding motif, the calcium is bound to the 12-residue loop sequence and co-ordinates to conserved residues at positions 1, 3, 5, 7, 9 and 12 of

Table 5.1 Amino acid sequences for the four Ca^{2+} binding loop regions of *Drosophila melanogaster* calmodulin

Loop	Sequence											
	1	**2**	**3**	**4**	**5**	**6**	**7**	**8**	**9**	**10**	**11**	**12**
I	D_{20}	K	D	G	D	G	T	I_{27}	T	T	K	E_{31}
II	D_{56}	A	D	G	N	G	T	I_{63}	D	F	P	E_{67}
III	D_{93}	K	D	G	N	G	F	I_{100}	S	A	A	E_{104}
IV	D_{129}	I	D	G	D	G	Q	V_{136}	N	Y	E	E_{140}

the loop (Falke et al., 1994). The amino acid sequences for the four loop regions of *Drosophila* CaM are shown in Table 5.1. Two non-coordinating residues are also highly conserved; the Gly at position 6 and the large hydrophobic residue at position 8. The latter, almost invariably Ile or Val in eukaryotic calmodulins (Falke et al., 1994), is part of the short antiparallel β-sheet that links the two EF-hands within a domain back to back. It has been suggested that this small β-sheet may have an important role in the cooperativity of calcium binding (Linse et al., 1991a). In addition, the two position-8 residues within each domain, which are within van der Waals contact, form part of the hydrophobic core of the domain and are presumably important in stabilising the native conformation of CaM.

In this work the properties of six mutants of calmodulin have been examined; in each of these mutants, the residue at position 8 (either Ile or Val; see Table 5.1) in one of the calcium binding loops has been mutated to either Gly, Pro, or Ala. The positions of these residues are shown in Figure 5.1. Two of these mutants, known generally as β-sheet mutants, have a mutation in the N-domain (CaM(I27G) and CaM(I63G)) and four have a mutation in the C-domain (CaM(I100G), CaM(V136G), CaM(V136P), and CaM(V136A)). Previous studies have characterised some of the structural and calcium-binding properties of these mutant proteins using absorption, Tyr-138 fluorescence, and

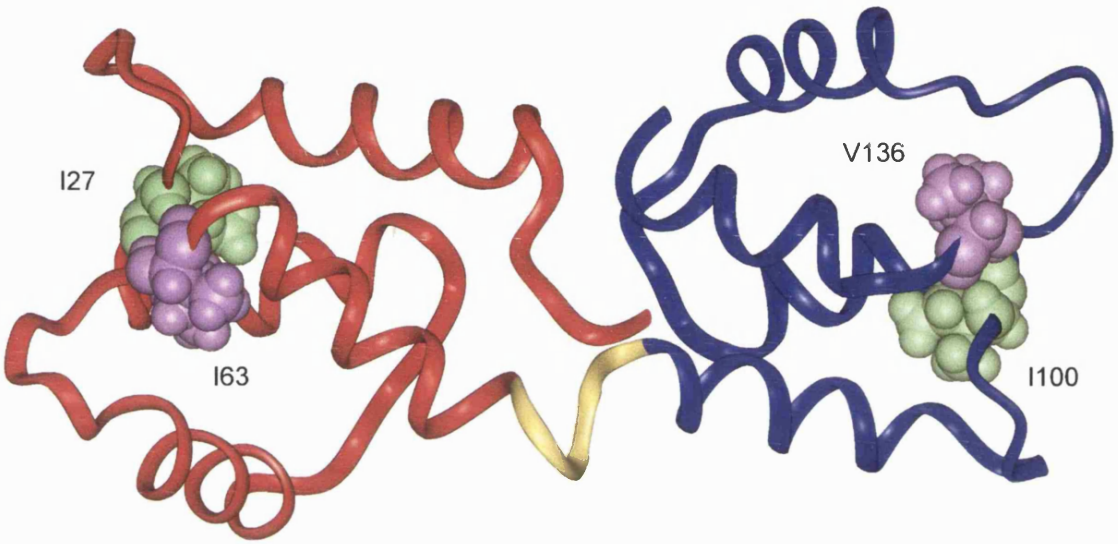

Figure 5.1 Solution structure of calcium-free calmodulin. The N-domain is shown in red, the C-domain in blue, and the flexible central linker which connects the two domains is shown in yellow. The hydrophobic residues at position 8 in each calcium binding loop are shown in green and violet. The figure was prepared using the coordinates deposited by Kuboniwa et al. (1995) (PDB entry code 1CFC).

near- and far-UV CD spectroscopy (Browne et al., 1997; Martin, S. R., Frise, M. C., and Bayley. P. M., unpublished results). The results showed that the mutation caused significant unfolding of the mutated apo-domain (at 20 °C), in all cases. However, the extent of unfolding (always > 50%) was different for the different mutations. The addition of 1 mM Ca^{2+} stabilised the proteins and largely restored the native-like secondary structure for all the mutants, except V136G and V136P. For these two mutants, the native conformation was only restored by the further binding of a high-affinity target peptide, such as WFF_p from skeletal muscle myosin light chain kinase (see Section 2.1.7). Far-UV CD intensities at 220 nm (a measure of α-helical content) for WT CaM and the six mutants are listed in Table 5.2. Thermal unfolding studies showed that the melting temperature of the mutated domain was decreased by at least 40°C in both the apo- and holo-forms of all the mutants. The surprising aspect of this work was that the dramatic destabilisation caused by the mutation of the highly

Table 5.2 Effects of mutations on secondary structure: far-UV CD intensities at 220 nm ($-\Delta\varepsilon_{M,\,220nm}$)

Protein	Apo-CaM	Holo-CaM (1 mM Ca)	Holo-CaM + WFF_p[a]
WT CaM	670	805	947
I27G[b]	528	791	938
I63G[b]	515	781	952
I100G[b]	461	785	945
V136G[b]	465	533	933
V136P	490	534	950
V136A	629	787	951

[a] The sequence of the peptide WFF_p is: Ac-KKRWKKNFIAVSAANRFK-NH_2.

[b] Data from Browne et al. (1997).

conserved residue at position 8 did not appear to be accompanied by major changes in the affinities of the proteins for calcium and for target peptide sequences. The stoichiometric Ca^{2+} binding constants measured for WT CaM and the mutants are shown in Table 5.3.

In this work, this series of β-sheet mutants has been further examined in order to quantitate the stabilities in more detail. In addition, the apo-forms of these proteins represent a particularly interesting system in the context of this work because their conformation, with the mutated domain largely unfolded and the non-mutated one folded, reproduces the intermediate state present during unfolding of WT CaM (see Chapter 3). They therefore provide a test system for verifying the model of interdomain interactions used to interpret the results obtained with WT CaM.

Table 5.3 Macroscopic Ca^{2+}-binding constants for WT CaM and the six β-sheet mutants

Protein	$\log(K_1K_2)$	$\log(K_3K_4)$
WT CaM[a]	11.65	9.67
I27G[b]	12.29	8.70
I63G[b]	12.10	8.23
I100G[b]	11.03	9.70
V136G[b]	11.40	9.46
V136P[c]	11.18	9.21
V136A[c]	11.10	9.51

[a] From Bayley et al. (1996).

[b] From Browne et al. (1997).

[c] Martin, S. R., Frise, M. C., and Bayley. P. M., unpublished results.

5.2 Materials and methods

The experimental approaches employed in the studies described in this chapter (optical spectroscopy, urea denaturation, and stopped-flow kinetics) are fully described in Chapter 2. Some of the important mathematical relationships are summarised here for convenience.

The theory and data analysis procedures for two-state unfolding transitions are discussed in Sections 2.3.6.1 in Chapter 2. According to the Linear Extrapolation model (LEM), the free energy of unfolding (ΔG) for a simple two-state transition is given by:

$$\Delta G = \Delta G^{\circ} + m\,[D]$$

where ΔG° is the free energy for unfolding in the absence of denaturant and m is a constant that describes the dependence of ΔG on denaturant concentration ([D]).

In the case of calcium binding to a CaM domain the full expression for the ligand interaction free energy is:

$$\Delta\Delta G_b = -RT\ln\left(\frac{1+K'_1[Ca]+K'_1K'_2[Ca]^2}{1+K_1[Ca]+K_1K_2[Ca]^2}\right)$$

where [Ca] is the free calcium concentration and the K_i and K'_i are the stoichiometric calcium association constants for binding to the native and unfolded states of that domain, respectively. Simpler forms of this equation apply under particular conditions (see Section 2.3.7, Chapter 2).

5.3 Results

5.3.1 Urea-unfolding of the apo-proteins

The stabilities of the six β-sheet mutants in the absence of Ca^{2+} have been assessed using urea-induced unfolding monitored with far-UV CD. Figure 5.2A shows the curves obtained for the two N-domain mutants, I27G and I63G; Figure 5.2B shows the curves obtained for the four C-domain mutants, I100G, V136G, V136P, and V136A. The form of these unfolding profiles confirms previous observations (Browne

et al., 1997) that the mutated domain is substantially unfolded in the absence of Ca^{2+} for all the proteins studied. Assuming that the non-mutated domain is normally folded, a comparison of the intensities measured in the absence of urea with the known values for apo-Tr1C and apo-Tr2C indicates the following approximate values for the degree of unfolding of the mutated domain at 20°C: 50-60% (V136A), 70-75% (I27G and I63G), 90-95% (I100G, V136G, and V136P). This analysis suggests that the ΔG°_{20} values for the mutated domains must be in the range 0 kcal/mol (V136A) to –1.7 kcal/mol (I100G, V136G, and V136P). This instability of the mutated domain means that it is only possible to obtain free energies of unfolding for the normally folded, non-mutated domain in the absence of Ca^{2+}. The curves obtained for the two N-domain mutants are almost superimposable (Fig. 5.2A), as are the curves for the four C-domain mutants (Fig. 5.2B). Thus, any effect of the mutation on the stability of the non-mutated domain does not appear to depend on which of the two residues is mutated. This is confirmed by the results of the numerical analyses given in Table 5.4.

The *m* values obtained from the LEM analyses of the unfolding curves of the non-mutated domains vary in the range -0.86 to -1.08 kcal/(mol·M) and the average value (-0.96 kcal/(mol.M)) is very similar to the values obtained for the two domains of WT apo-CaM (see Table 3.1, Chapter 3). This observation suggests that any direct effect of the mutation on the non-mutated domain is only limited and that this domain retains the same structural characteristics as the corresponding WT domain. Therefore the average *m* value used in the analyses of the WT proteins has also been employed to calculate the ΔG°_{20} values reported in Table 5.4 as $-m_{av}\cdot[U]_{1/2}$ (where m_{av} = -0.92 kcal/(mol·M), see Section 2.3.6.1, Chapter 2). This permits a direct comparison of the ΔG°_{20} values obtained for the non-mutated apo-domains in the β-sheet mutants with the value for the corresponding apo-domain in WT CaM.

Such a comparison shows that in the case of the C-domain mutants, the stability of the non-mutated apo-N-domain ($\Delta G^{\circ}_{20} \sim 3.8$ kcal/mol) is very similar to that of the WT apo-N-domain and is therefore higher than that of apo-Tr1C ($\Delta G^{\circ}_{20} \sim 3.7$ and 2.8 kcal/mol, respectively (Table 3.1, Chapter 3)). Thus, the apo-N-domain is stabilised compared to apo-Tr1C when the C-domain unfolds first (as in WT CaM) and when the C-domain is already unfolded as a direct consequence of the mutation. In contrast, in the case of the N-domain mutants, the stability of the non-mutated apo-C-domain ($\Delta G^{\circ}_{20} \sim 2.2$-2.3 kcal/mol) is significantly higher than that of the WT apo-C-domain

and is slightly higher than that of apo-Tr2C ($\Delta G°_{20}$ ~ 1.5 and 2.0 kcal/mol, respectively (Table 3.1, Chapter 3)). Therefore the apo-C-domain is destabilised compared to apo-Tr2C when it unfolds first (as in WT CaM), but is stabilised when the N-domain is already unfolded as a direct result of the mutation. The relative stabilities of these proteins are compared in Figure 5.3, where the fractions of unfolded molecules are plotted as a function of the urea concentration. These results confirm the observations made with WT apo- and holo-CaM in Chapter 3, namely that whichever domain unfolds first in the intact protein appears to be destabilised compared to the corresponding isolated fragment whilst the other domain (unfolding second) appears to be stabilised compared to the isolated fragment.

Table 5.4 Urea-unfolding of the non-mutated apo-domain in the β-sheet mutants, monitored by far-UV CD

Protein	Domain [a]	*m* (kcal/(mol·M))	$[U]_{1/2}$ (M)	$\Delta G°_{20}$ [b] (kcal/mol)
I27G	C	-0.89	2.47	2.27
I63G	C	-0.86	2.44	2.24
I100G	N	-0.95	4.15	3.82
V136G	N	-0.95	4.15	3.82
V136P	N	-1.02	4.13	3.80
V136A	N	-1.08	4.13	3.80

[a] C and N indicate whether the data refer to the C- or the N-domain of CaM.

[b] $\Delta G°_{20}$ values were calculated as $-[U]_{1/2} \cdot m_{av}$, with m_{av} = -0.92 kcal/mol·M (see Section 2.3.6.1, Chapter 2).

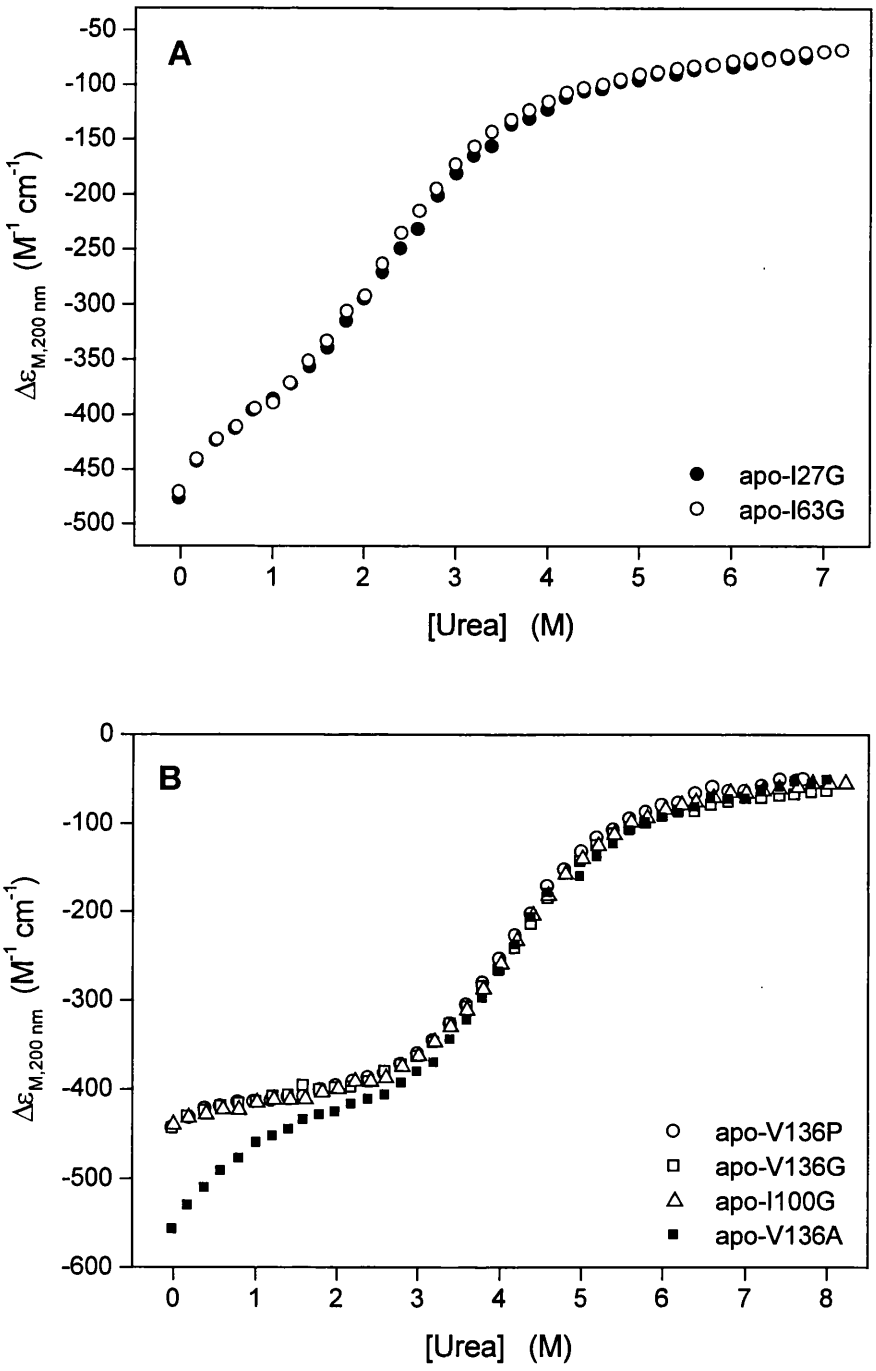

Figure 5.2 **(A)** Urea-induced denaturation of the N-domain CaM mutants I27G (●) and I63G (○) in the absence of Ca^{2+}. **(B)** Urea-induced denaturation of the C-domain CaM mutants V136P (○), V136G (□), I100G (△), and V136A (■) in the absence of Ca^{2+}. Unfolding was monitored at 20 °C in 25 mM Tris, 100 mM KCl, pH 8, using far-UV CD.

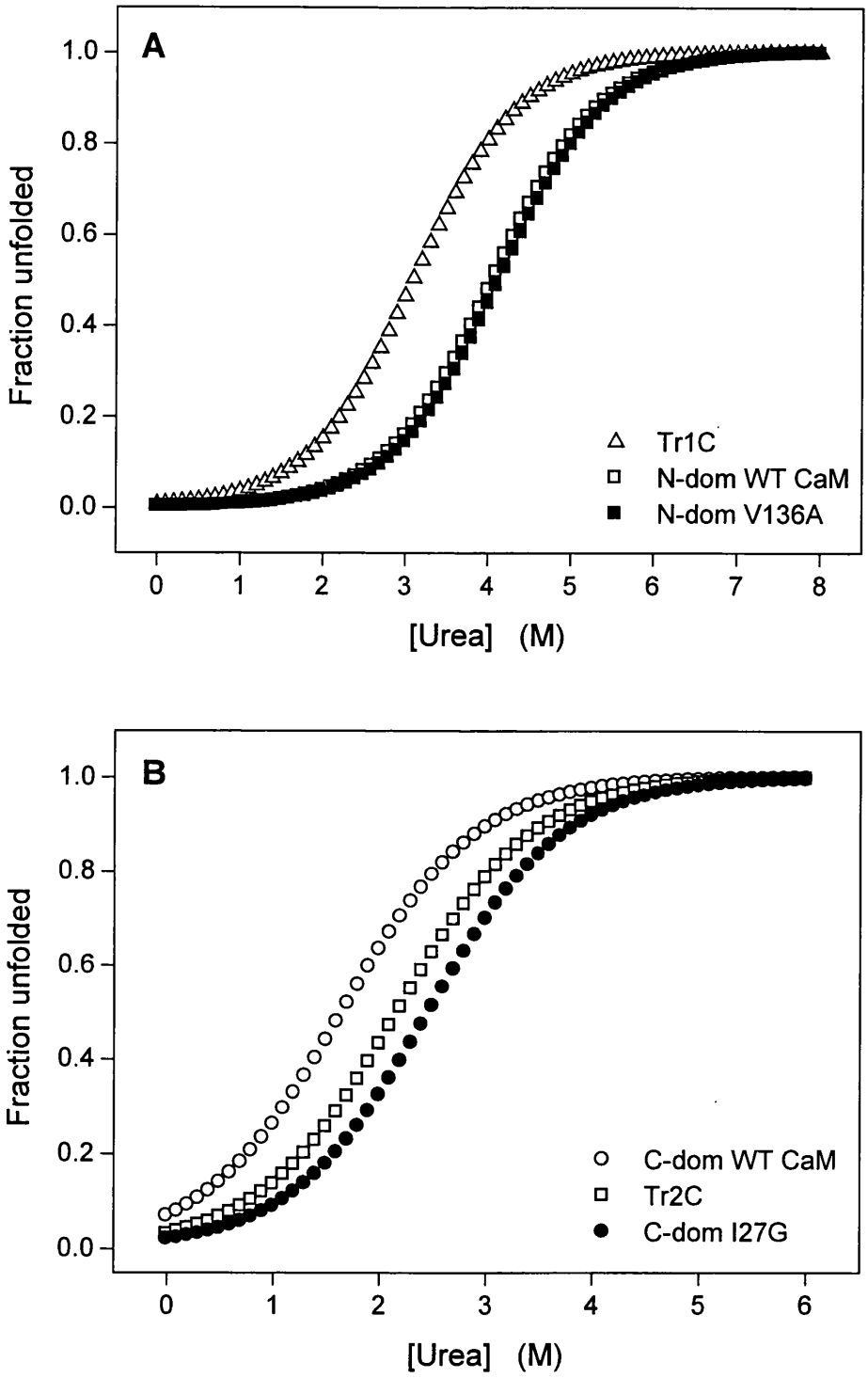

Figure 5.3 **(A)** Fractions of unfolded protein for apo-Tr1C (△), the apo-N-domain of WT CaM (□), and the apo-N-domain of V136A (■). **(B)** Fractions of unfolded protein for apo-Tr2C (□), the apo-C-domain of WT CaM (○), and the apo-C-domain of I27G (●). The curves were calculated using the data of Table 3.1 (Chapter 3) and Table 5.4.

5.3.2 Urea-unfolding of the holo-proteins

Previous results from this laboratory (Browne et al., 1997; Frise, M. C., Martin, S. R., Browne, J. P., and Bayley, P. M., unpublished results) have shown that the mutated domain in all the β-sheet mutants is substantially unfolded in the absence of Ca^{2+} but can be largely refolded in the presence of 1 mM Ca^{2+}, except in the cases of V136G and V136P (see Section 5.1). Therefore, the stabilities of the mutated domains in the mutants I27G, I63G, I100G, and V136A, have been measured at different Ca^{2+} concentrations using urea-induced unfolding experiments. Methods to assess the stabilities of V136G and V136P are described later.

Figure 5.4A shows the urea-unfolding profiles of I100G in 1 and 3 mM Ca^{2+}, monitored by far-UV CD. The curves correspond to unfolding of the mutated C-domain, which is, as expected, stabilised and therefore refolded in the presence of Ca^{2+}. The non-mutated N-domain is, of course, more stable and only begins to unfold at much higher urea concentrations (> 6 M; see Section 3.3.3.2, Chapter 3). The results of the LEM analyses are listed in Table 5.5. The $\Delta G°_{20}$ values obtained for the C-domain in the presence of 1 and 3 mM Ca^{2+} are 2.36 and 3.28 kcal/mol, respectively. Using these data, it is possible to estimate the stability of the unfolded apo-C-domain ($\Delta G°_{20}$(apo)) by subtracting the calculated ligand interaction free energy, $\Delta\Delta G_b$, from the measured $\Delta G°_{20}$(holo) values at a particular Ca^{2+} concentration. The ligand interaction free energies were calculated with Equation (2.17) (Section 2.3.7, Chapter 2) using the stoichiometric binding constants measured in previous studies ($\log(K_1)$ = 5.06, $\log(K_1K_2)$ = 11.03, Table 5.3 (Browne et al., 1997)); i.e., with the assumption (valid for WT CaM) that the constants K_1 and K_2 reflect Ca^{2+} binding to the C-domain (see Section 2.3.1.1, Chapter 2). The data at 1 and 3 mM Ca^{2+} gave values of $\Delta G°_{20}$(apo) for the unfolded apo-domain of –4.4 and –4.7 kcal/mol, respectively. Values of this magnitude would imply that the mutated C-domain was totally (> 99%) unfolded at 20 °C. However, inspection of the urea-unfolding profile for apo-I100G in Figure 5.2B and the results of far-UV thermal unfolding studies (Browne et al., 1997) show that the mutated C-domain is, in fact, between 5 and 10% folded at 20°C (corresponding to $\Delta G°_{20}$(apo) values in the range -1.75 to -1.3 kcal/mol). Therefore the estimate of –4.4 to –4.7 kcal/mol for the free energy of unfolding of the mutated apo-C-domain based on the measured values of K_1 and K_2 appears to be far too negative. If, as

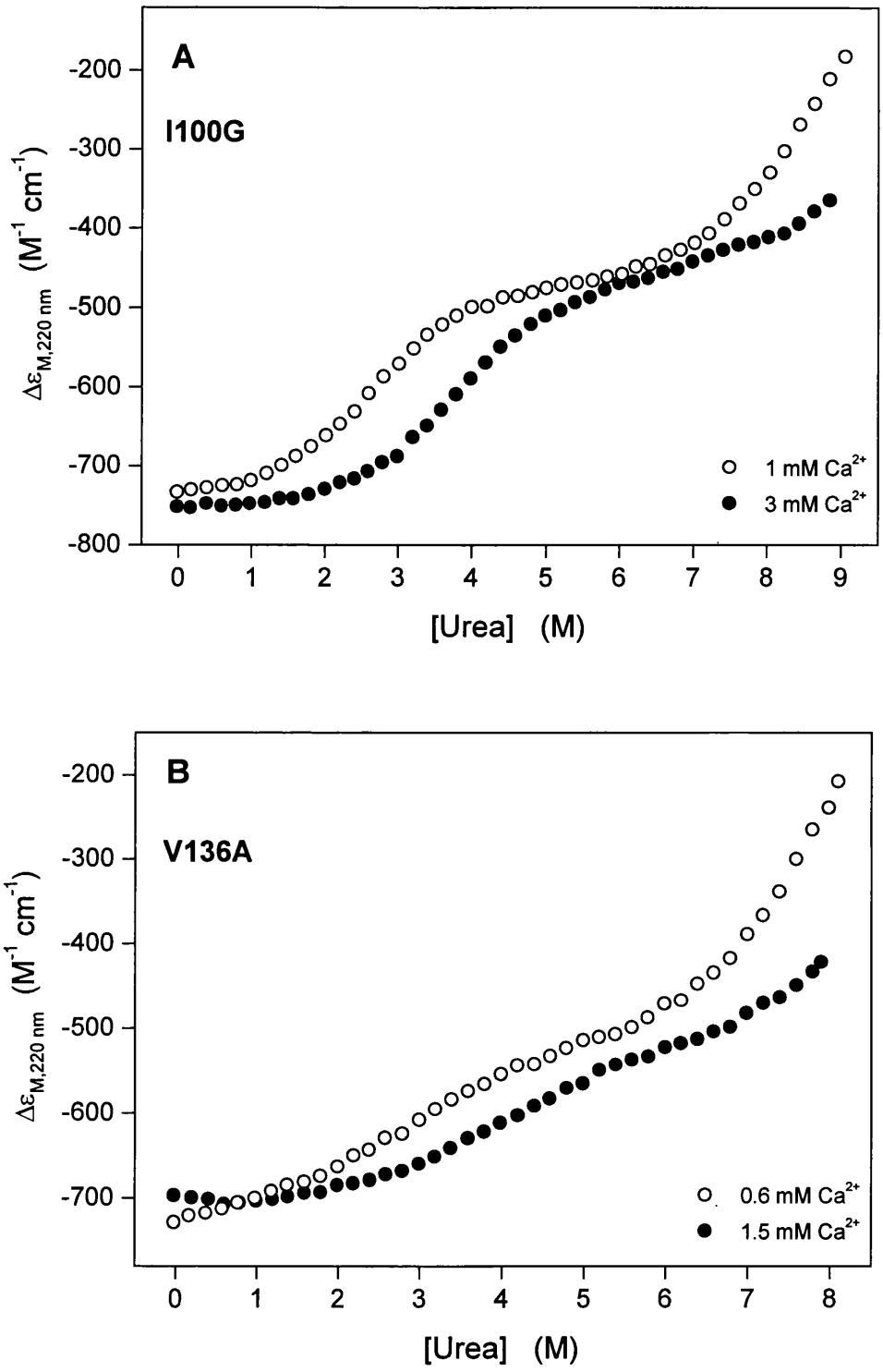

Figure 5.4 **(A)** Urea-induced denaturation of I100G at [Ca^{2+}] = 1 (○) and 3 (●) mM Ca^{2+}. **(B)** Urea-induced denaturation of V136A at [Ca^{2+}] = 0.6 (○) and 1.5 (●) mM Ca^{2+}. Unfolding was monitored at 20 °C in 25 mM Tris, 100 mM KCl, pH 8, using far-UV CD.

seems likely, the estimates of $\Delta G°_{20}$(apo) based on the observed degree of unfolding at 20°C (90-95%) are correct, then the observed ligand interaction free energy ($\Delta G°_{20}$(holo) - estimated $\Delta G°_{20}$(apo)) at 1 mM Ca^{2+} is ~ 4 kcal/mol, significantly less than that observed with WT CaM (> 6 kcal/mol; see Section 3.3.3.2, Chapter 3).

Somewhat similar conclusions can be drawn in the case of holo-V136A. The urea-unfolding profiles for this protein in 0.6 and 1.5 mM Ca^{2+} are shown in Figure 5.4B (unfolding of the non-mutated N-domain is again only observed at high [urea]) and the results of the LEM analyses are listed in Table 5.5. It may be noted that the transitions appear to be somewhat broader and of slightly lower overall amplitude than those observed with I100G. This may be related to the fact that the pre-transition baselines appear to be steeper for this particular protein. The $\Delta G°_{20}$ values obtained for the holo-C-domain in the presence of 0.6 and 1.5 mM Ca^{2+} are 2.66 and 3.42 kcal/mol, respectively. Using the previously measured stoichiometric Ca^{2+} binding constants ($\log(K_1)$ = 4.24, $\log(K_1K_2)$ = 11.18; Frise, M. C., Martin, S. R., Browne, J. P., and Bayley, P. M.; unpublished results), $\Delta G°_{20}$(apo) values for the mutated C-domain were calculated to be –3.7 and –4.0 kcal/mol. Again, these values imply that the apo-C-domain is more than 99% unfolded at 20 °C, but the far-UV CD unfolding curve in Figure 5.4B shows that the C-domain is, in fact, more than 40% folded in the absence of urea (corresponding to a $\Delta G°_{20}$(apo) value of ~ –0.1 kcal/mol). Here again then, the estimated free energy of unfolding of the mutated apo-C-domain based on the measured values of K_1 and K_2 appears to be far too negative. If the $\Delta G°_{20}$(apo) value of -0.1 kcal/mol is, in fact, correct then the observed ligand interaction free energy ($\Delta G°_{20}$(holo) – estimated $\Delta G°_{20}$(apo)) at 0.6 mM Ca^{2+} is ~ 2.8 kcal/mol, again significantly less than that observed with WT CaM (~ 5.9 kcal/mol; see Section 3.3.3.2, Chapter 3).

Figure 5.5 shows the urea-unfolding profiles of I27G and I63G monitored by far-UV CD in the presence of different Ca^{2+} concentrations. In the case of these proteins it is the non-mutated C-domain that unfolds normally at high urea concentrations. In the urea-unfolding profile of I63G in 0.3 mM Ca^{2+} the portion corresponding to the C-domain is almost complete and could be analysed. The parameters obtained from the LEM analysis ($[U]_{1/2}$ = 7.17 M, $\Delta G°_{20}$ = 6.60 kcal/mol) are in good agreement with the far-UV CD data for WT C-domain at the same Ca^{2+}

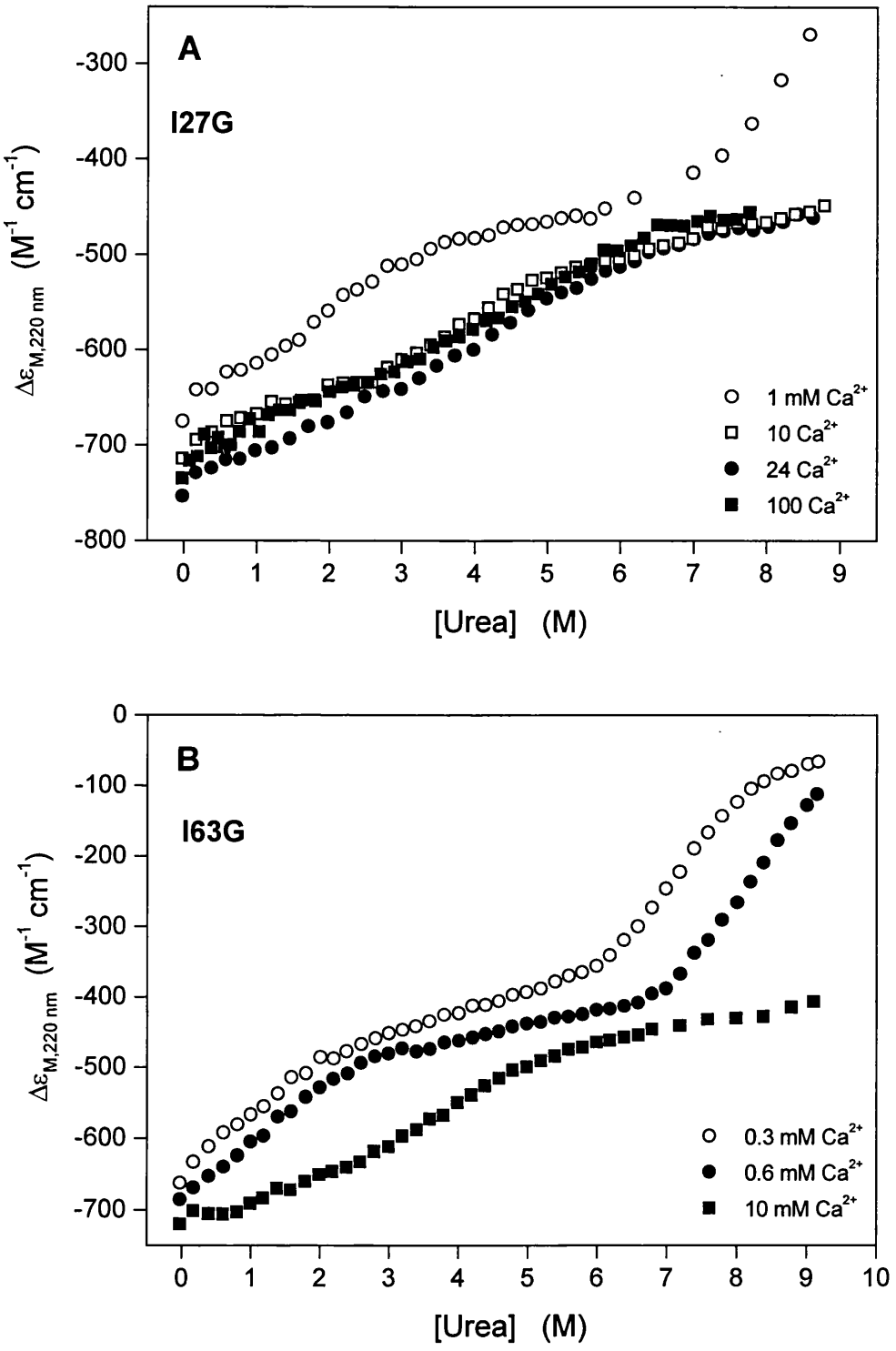

Figure 5.5 **(A)** Urea-induced denaturation of I27G at [Ca^{2+}] = 1 (○), 10 (□), 24 (●), and 100 (■) mM Ca^{2+}. **(B)** Urea-induced denaturation of I63G at [Ca^{2+}] = 0.3 (○), 0.6 (●), and 10 (■) mM Ca^{2+}. Unfolding was monitored at 20 °C in 25 mM Tris, 100 mM KCl, pH 8, using far-UV CD.

concentration ($\Delta G°_{20}$ = 6.81 kcal/mol), thus confirming that the mutation does not have specific effects on the structure and stability of the non-mutated domain.

For I27G and I63G, the interpretation of the portion of the curve corresponding to unfolding of the mutated N-domain is much more complex. In the case of I27G, this portion of the curve is very broad at all [Ca^{2+}] and cannot be analysed as a simple two-state transition. This again could be attributed to the presence of a unusually steep pre-transition baseline but it is notable that some of the curves (particularly that for 1 mM Ca^{2+}) also show evidence for biphasic behaviour with a particularly rapid decrease in CD intensity at low [Urea]. What is clear from these data is that the stabilising effect of calcium appears to saturate at 10 mM Ca^{2+}, since the curves at 10, 24, and 100 mM Ca^{2+} are more-or-less superimposable.

Table 5.5 Urea-unfolding of the β-sheet mutants in the presence of Ca^{2+}, monitored by far-UV CD

Protein	Domain [a]	[Ca^{2+}] (mM)	*m* (kcal/(mol·M))	$[U]_{1/2}$ (M)	$\Delta G°_{20}$ [b] (kcal/mol)
I100G	C	1	-0.94	2.57	2.36
	C	3	-0.92	3.57	3.28
V136A	C	0.6	-0.95	2.89	2.66
	C	1.5	-0.72	3.72	3.42
I63G	C	0.3	-1.25	7.17	6.60
	N	10	-0.83	4.17	3.84

[a] C and N indicate whether the data refer to the C- or the N-domain of CaM.

[b] $\Delta G°_{20}$ values were calculated as $-[U]_{1/2} \cdot m_{av}$, with m_{av} = -0.92 kcal/mol·M (see Section 2.3.6.1, Chapter 2).

In the case of I63G (Figure 5.5B), only the curve at 10 mM Ca^{2+} analyses as a simple two-state transition (the results of the LEM analyses are in Table 5.5); the other two curves and particularly that at 0.3 mM Ca^{2+} appear to have some slight biphasic character as with I27G. As observed in the previous section, the degree of unfolding of the mutated apo-domain of I63G is ~ 70-75% at 20°C. This corresponds to an estimated $\Delta G°_{20}$(apo) value of ~ –0.5 to –0.6 kcal/mol. The observed ligand interaction free energy ($\Delta G°_{20}$(holo) – estimated $\Delta G°_{20}$(apo)) at 10 mM Ca^{2+} (4.4 kcal/mol) is probably significantly less than that for WT CaM. The latter value cannot be measured but may be estimated from the value measured in 0.6 mM Ca^{2+} (2.2 kcal/mol) to be approximately 5.5 kcal/mol. As for the C-domain mutants, when the appropriate stoichiometric constants (i.e. those corresponding to the N-domain, K_3K_4 from Table 5.3) are used to calculate a value for $\Delta\Delta G_b$, then the predicted $\Delta G°_{20}$(apo) (= ($\Delta G°_{20}$(holo) – $\Delta\Delta G°_b$) = –1.84 kcal/mol) is significantly more negative than the value derived from experimental observations (~ –0.5 to –0.6 kcal/mol).

The situation of the mutants V136G and V136P is different from that of the other four β-sheet mutants because far-UV CD experiments have shown that the addition of 1 mM Ca^{2+} cannot restore the native conformation of the mutated C-domain, which is fully unfolded in the apo-state (Browne et al., 1997, and unpublished results from this laboratory). In order to see whether the native structure of the mutated domain can be restored at Ca^{2+} concentrations greater than 1 mM, Ca^{2+} titrations have been performed with V136G and V136P using far-UV CD and absorption spectroscopy. The far-UV CD curve obtained with V136G (Figure 5.6) shows that Ca^{2+} concentrations greater than 1 mM do induce a further increase in the secondary structure content of the protein and the signal change saturates at approximately 70 mM Ca^{2+}. However, the total change induced by calcium in the range 1-70 mM is only 34 % of the change required to restore the native conformation of WT holo-CaM; thus, even very high concentrations of calcium cannot fully refold the mutated C-domain.

Figure 5.7 shows the results obtained with the Ca^{2+} titration of V136G monitored by absorption spectroscopy. The spectra measured for the mutant protein in 1 to 80 mM Ca^{2+} are compared with the spectrum of WT holo-CaM in 1 mM Ca^{2+} (Fig. 5.7A). Figure 5.7B shows the absorption signal at 288 nm as a function of Ca^{2+} concentration. The data show that, as observed using far-UV CD, the addition of calcium does not induce the complete refolding of the mutated C-domain. In this case

the calcium-induced change in the signal corresponds to only 21% of the total change required to restore the signal of WT holo-CaM. The difference between the far-UV CD and the absorption results may depend on the fact that the absorption titration monitors local changes in the environment of Tyr-138, in Ca^{2+} binding loop IV, whilst far-UV CD monitors changes occurring in the whole C-domain.

The results obtained with V136P are similar to those obtained with V136G. The Ca^{2+} titration curve monitored using far-UV CD (shown in Figure 5.8A) indicates that the addition of calcium does not induce the complete refolding of the mutated C-domain. The increase in intensity is only 22% of the total change that would be required to restore the far-UV CD intensity of WT holo-CaM. In order to investigate the possibility that calcium at high concentrations has specific effects on the secondary structure of CaM, a Ca^{2+} titration has been performed with WT holo-CaM, monitored by far-UV CD. The data (Figure 5.8B) show that the change in the signal in the range 0.6 to 200 mM Ca^{2+} is approximately 1%. Therefore high concentrations of Ca^{2+} do not have specific effects on the secondary structure of WT CaM and the changes observed in the case of the β-sheet mutants can be attributed to the refolding of the proteins.

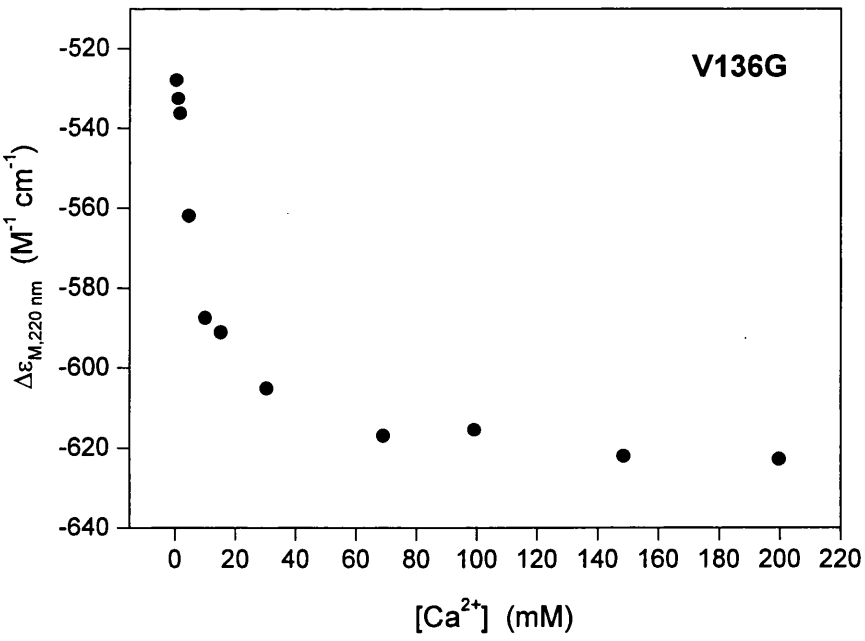

Figure 5.6 Ca^{2+} titration (1-200 mM) of V136G monitored at 20 °C in 25 mM Tris, 100 mM KCl, pH 8, using far-UV CD.

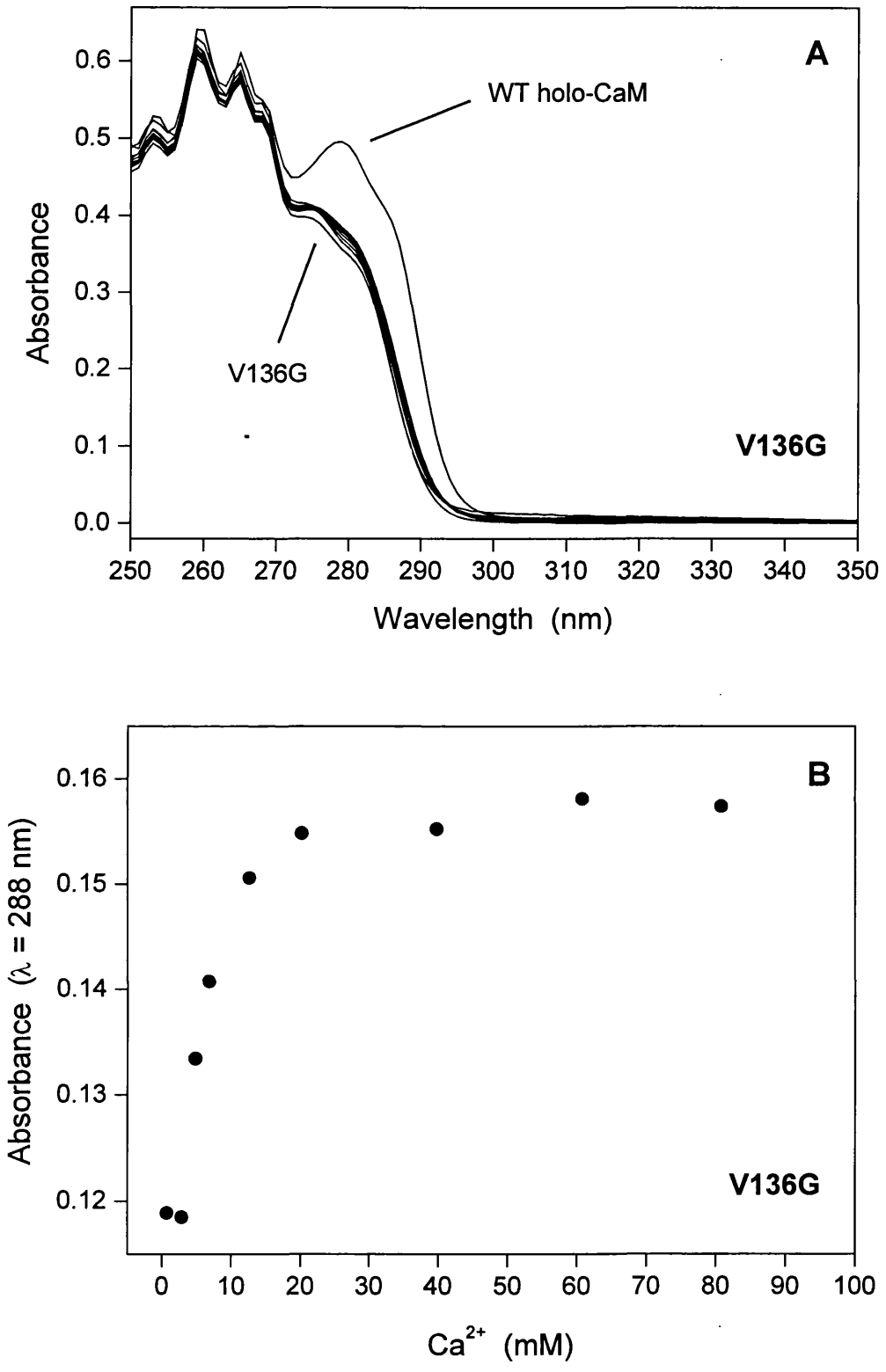

Figure 5.7 Ca^{2+} titration (1-80 mM) of V136G monitored at 20 °C in 25 mM Tris, 100 mM KCl, pH 8, using absorption spectroscopy. **(A)** Spectra. The spectrum of WT CaM in 1 mM Ca^{2+} is reported for comparison. **(B)** Signal at 288 nm.

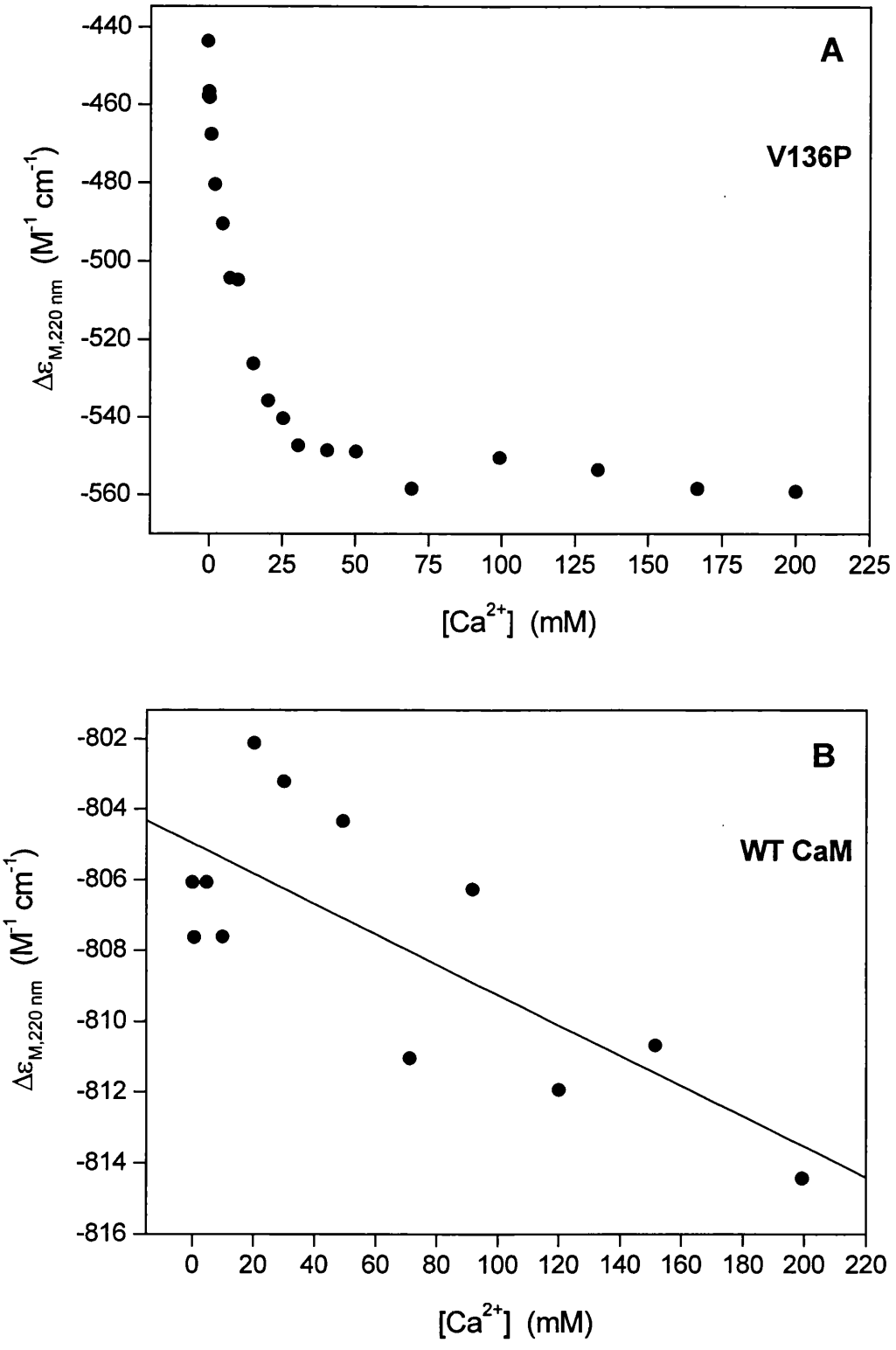

Figure 5.8 **(A)** Ca^{2+} titration (0-200 mM) of apo-V136P. **(B)** Ca^{2+} titration (0.6-200 mM) of WT holo-CaM. The data were collected at 20 °C in 25 mM Tris, 100 mM KCl, pH 8, using far-UV CD.

5.3.3 Calcium binding properties

The analysis in the previous section showed that, if the product of the first two stoichiometric Ca^{2+} association constants (K_1K_2) (Table 5.3) is used as the estimate of C-domain Ca^{2+} affinity, then the $\Delta G°_{20}$ values calculated for the mutated apo-C-domains of I100G and V136A are much lower than the available experimental data indicate. This suggests the possibility that this product is not, in fact, a good measure of C-domain Ca^{2+} affinity for these mutants. In order to investigate this question, Ca^{2+} binding to the mutated domains has been studied using other approaches.

Ca^{2+} binding to the C-domain of WT CaM and to the β-sheet mutants has been monitored directly using Tyr-138 fluorescence measurements. The titration curves for WT CaM and three of the mutants are shown in Figure 5.9A. For WT CaM, the change in the Tyr-138 signal is approximately 70% complete at a $[Ca^{2+}]/[CaM]$ ratio of 2. This result is consistent with the known Ca^{2+} binding properties of the wild-type protein, which predict that the C-domain would be ~ 70-75% occupied under these conditions (see Section 2.3.1.2, Chapter 2). The binding of Ca^{2+} to the C-domain of one of the N-domain mutants (I63G) has been studied in the same way. The curve for this protein (Figure 5.9A) clearly shows that the C-domain is more than 90% occupied at $[Ca^{2+}]/[CaM] = 2$. The degree of occupancy of the C-domain at this point obviously depends on both the absolute calcium affinities ($K_{av(C)}$ and $K_{av(N)}$) and on their ratio ($K_{av(C)}/K_{av(N)}$). The experimental result shows that the ratio ($K_{av(C)}/K_{av(N)}$) must be greater for I63G than for WT CaM. This could derive from a reduction in the affinity of the mutated domain ($K_{av(N)}$) but would also be consistent with there being an increase in the affinity ($K_{av(C)}$) of the non-mutated C-domain.

For the two C-domain mutants studied here (I100G and V136G), the situation is very different (Fig. 5.9A). There is very little change in the Tyr-138 signal after the addition of the first two equivalents of calcium (i.e., at $[Ca^{2+}]/[CaM] = 2$) and the change is only completed at high Ca^{2+} concentrations. The former observation shows that calcium binds first to the N-domain for these two mutants; the latter observation shows that the Ca^{2+} affinity of the mutated C-domain ($K_{av(C)}$) is greatly reduced compared to the WT C-domain. In the case of I100G the first two calcium ions appear to bind almost exclusively to the N-domain. This suggests that the affinity of the N-domain ($K_{av(N)}$) may have been increased by the mutation in the C-domain since calculations based on the known stoichiometric calcium association constants (see

Section 2.3.1.2, Chapter 2) show that the N-domain of WT CaM would only be some 60% occupied under these conditions, even in the complete absence of C-domain calcium binding.

Thus, the effects of the mutation of the residue at position 8 on the Ca^{2+} affinity of the mutated domain are much greater than was originally suggested (Browne et al., 1997). The effect is particularly pronounced in the case of V136G, as also indicated by the observation that the native conformation of this protein cannot be restored in the presence of 1 mM Ca^{2+}. Therefore, in the case of the C-domain mutants, the product of the first two stoichiometric Ca^{2+} binding constants (K_1K_2) cannot reflect the binding of Ca^{2+} to the C-domain, as it does in the case of WT CaM. There is also reasonably convincing evidence that the mutations may actually increase the affinity of the non-mutated domain for Ca^{2+}.

In order to investigate further the Ca^{2+} binding properties of the β-sheet mutants, the kinetics of Ca^{2+} dissociation from the C-domain have been measured at 20 °C by monitoring the Tyr-138 fluorescence signal with the stopped flow technique. The curve obtained with I27G is shown in Figure 5.9B as an example. The dissociation of the two Ca^{2+} ions from the C-domain occurs as a single exponential process, with observed rate 8.0 s^{-1} for WT CaM. In the case of the C-domain mutants I100G and V136G the observed rates were 160 and 100 s^{-1}, respectively, whilst for the N-domain mutants I27G and I63G the measured rates were 3.0 and 3.1 s^{-1} respectively. Thus, the rate of Ca^{2+} dissociation from the C-domain is increased by the mutations in the C-domain and decreased by the mutations in the N-domain. These results are consistent with the observation that the Ca^{2+}-affinity of the C-domain is strongly reduced by the C-domain mutations, but it is enhanced by the N-domain mutations.

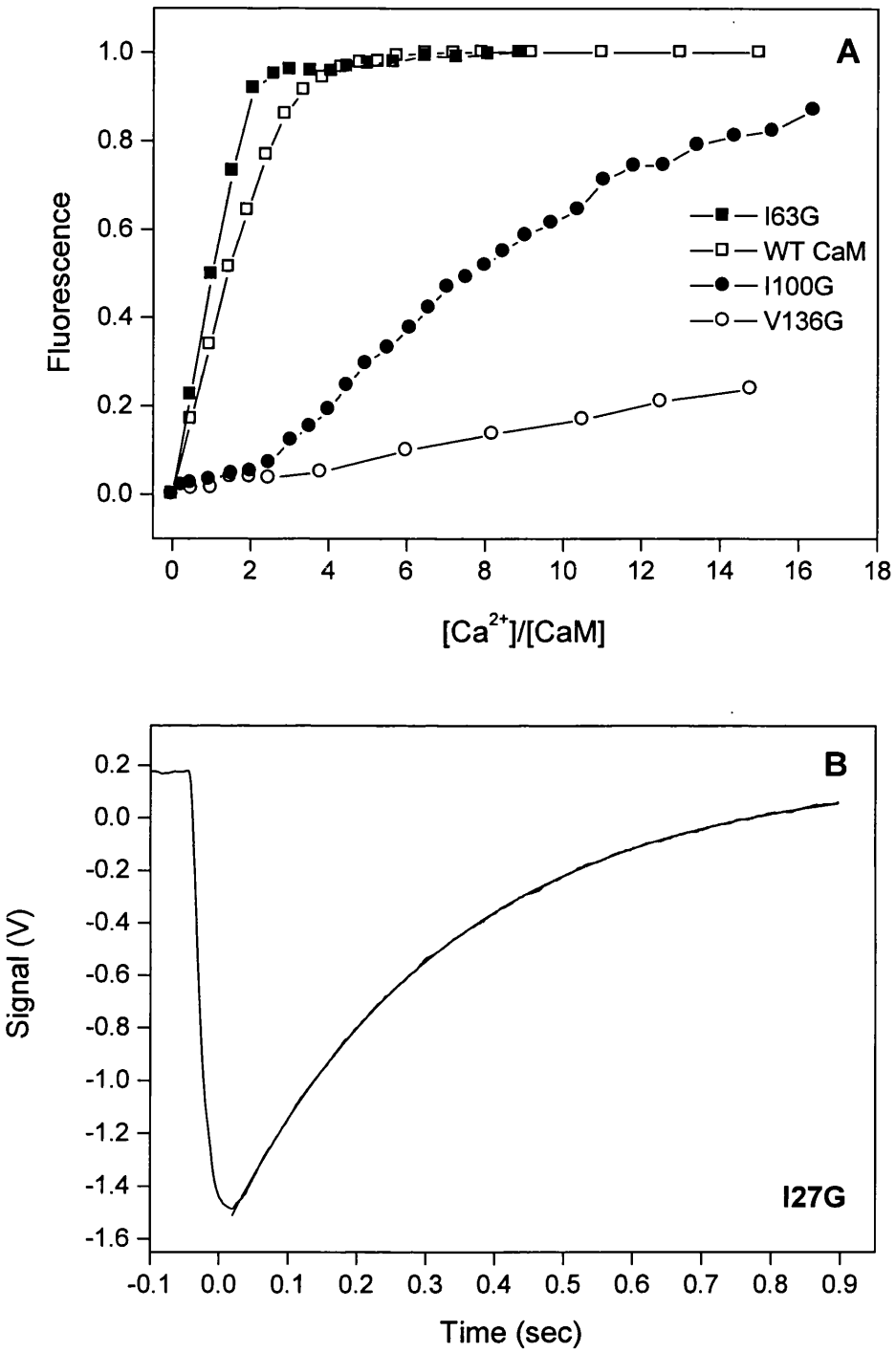

Figure 5.9 **(A)** Ca^{2+} titrations of WT CaM (–□–), I63G (–■–), I100G (–●–), and V136G (–○–), monitored at 20 °C in 25 mM Tris, 100 mM KCl, pH 8, using Tyr-138 fluorescence. **(B)** Kinetics of calcium dissociation from the C-domain of I27G. The stopped flow trace was monitored in 25 mM Tris, 100 mM KCl, pH 8, using Tyr-138 fluorescence. The solid line is the computed best fit.

5.4 Discussion

5.4.1 Urea-unfolding of the apo-proteins

The studies on the stability of the β-sheet mutants have shown that the highly conserved hydrophobic residues at position 8 in each calcium binding loop play an essential role in stabilising calmodulin's domains (Browne et al., 1997, and this work). In the absence of calcium, the structural effects of replacing either Ile or Val with Gly and Pro are dramatic and cause a substantial unfolding of the domain carrying the mutation. These results can be rationalised in terms of the different properties of the residues involved. The large effects on the stability caused by the mutation of Ile or Val to Gly are most likely to be due to the small size of the glycine side chain (a single hydrogen atom), which creates a cavity in the interior of the mutated domain, to its relatively low hydrophobicity (Creighton, 1992), and to the greater conformational flexibility conferred on the polypeptide backbone by this residue. The properties of Pro are more similar to those of Ile and Val in terms of size and hydrophobicity, but the rigid constraints that the cyclic ring imposes on the backbone are probably the cause of the disruption of the mutated domain. In contrast, the extent of the destabilisation induced by the substitution of Val with Ala is smaller and induces only a partial unfolding of the mutated domain. The side chain of alanine is smaller and less hydrophobic than that of Val, but this mutation is more conservative than the ones described above. In addition, it can be noted that the series of homologous replacements of the residue at position 8 in each binding loop with Gly causes similar effects on calcium binding sites I, II and III, but not on site IV. In fact, in the case of V136G the addition of calcium does not induce the complete refolding of the protein. This problem will be further discussed below.

Although the mutations have very different effects on the stabilities of the mutated domains, the urea-unfolding experiments on the apo-proteins have shown that the mutations in loops I and II affect the stability of the non-mutated C-domain in exactly the same way. Thus, the stabilities of the C-domains in I27G and I63G are almost identical. Similarly, the mutations in loops III and IV have the same effect on the stability of the non-mutated N-domain and the stabilities of the N-domains in I100G, V136G, V136P, and V136A are therefore the same.

The *m* values obtained in the LEM analyses of the non-mutated domains of the apo-proteins are very similar to the ones obtained for the domains of WT CaM and its isolated fragments. This permits a straightforward comparison of the stabilities of the WT and the mutant proteins. The data show that the stability of the non-mutated N-domain in the C-domain mutants is approximately the same as the WT apo-N-domain and is higher than that of apo-Tr1C. In contrast, the stability of the non-mutated C-domain in the N-domain mutants is higher than that of the WT apo-C-domain and of apo-Tr2C. These observations are consistent with the data obtained with WT CaM and its fragments and show that the first domain to unfold is always destabilised compared to the corresponding isolated fragment and the second domain to unfold is always stabilised compared to the corresponding isolated fragment. The important fact is that these results therefore confirm the idea that there are interdomain interactions between one folded domain and the other unfolded domain, which affect the stability of both domains in intact CaM.

5.4.2 Urea-unfolding of the holo-proteins

As shown for the WT protein, the addition of calcium to the mutant apo-proteins has a stabilising effect which induces at least partial refolding of the mutated domain. In the simpler cases, I100G and V136A, the presence of calcium seems to induce the complete refolding of the mutated C-domains and it has been possible to estimate stabilities at different Ca^{2+} concentrations. The $\Delta G°_{20}$ values obtained at any particular calcium concentration are higher for V136A than for I100G, consistent with the observation that the mutated apo-domain is only 40% unfolded in the case of V136A but approximately 90% unfolded for I100G. The important result from the work with these mutants is that the ligand interaction free energy (calculated as measured $\Delta G°_{20}$(holo) minus estimated $\Delta G°_{20}$(apo)) is very significantly less than that observed with WT CaM (see Section 5.3.2). This suggests that the mutation significantly weakens calcium binding.

In the case of the N-domain mutants, the interpretation of the results of the urea-unfolding experiments with the holo-proteins is more complex. First, the shape of the curves for unfolding of the mutated N-domain in I27G is clearly not the same as that obtained for the non-mutated domains or for the domains of WT CaM. In particular, the

unfolding profiles indicate a decreased cooperativity of the unfolding transition and the first points of the curves seem to suggest that the unfolding curve corresponding to the N-domain could be biphasic. Second, for both I27G and I63G the amplitudes of the transitions are somewhat smaller than those of the WT domains. A possible interpretation is that the refolding of the N-domain does not occur as a single cooperative two-state process, but that the parts of the domain containing calcium binding sites I and II behave independently. In this case the data would indicate that the part of the domain with the site carrying the mutation cannot be completely refolded by calcium and the unfolding curves measured by far-UV CD would correspond only to the refolding of the non-mutated portion of the domain.

The situation with the C-domain mutants V136G and V136P is somewhat similar to that with the N-domain mutants; the addition of calcium is clearly not able to induce the complete refolding of the mutated domain. The increase in helicity caused by high calcium concentrations is only approximately 50% of the change required to restore the native conformation. A possible interpretation of these data is that the effects of the mutation are so severe that the portion of the domain containing site IV cannot be completely refolded by the binding of calcium. In this case the change in the far-UV CD signal would correspond to the refolding of the portion of the domain containing site III. This would appear to be the most probable explanation for these particular mutants.

5.4.3 Calcium binding properties

Many of the results obtained with the urea-unfolding experiments appeared to be in conflict with the suggestion that the mutations had only a small effect on the calcium affinity of the mutated domain (Browne et al., 1997). This suggestion derived from the observation, confirmed in more recent studies in this laboratory, that the mutations have very small effects on the measured stoichiometric calcium association constants (see Table 5.3). The effects of the mutations on calcium affinity have therefore been re-assessed using two more direct methods.

1) Calcium binding to the C-domain mutants has been assessed using Tyr-138 fluorescence titrations (section 5.3.3). The results showed very clearly that the mutations reduced the calcium affinity of the mutated domain ($K_{av(C)}$) in I100G, and

to a greater extent in V136G. Perhaps more interestingly, there was a strong suggestion in the experiments with I100G that the mutation in the C-domain had also increased the affinity of the non-mutated N-domain ($K_{av(N)}$). The experimental results with an N-domain mutant I63G showed that the ratio ($K_{av(C)}/K_{av(N)}$) is greater for this mutant than for WT CaM. This could derive from a reduction in the affinity of the mutated domain ($K_{av(N)}$) but would also be consistent with there being an increase in the affinity ($K_{av(C)}$) of the non-mutated C-domain.

2) The calcium affinity of the C-domain has also been assessed more indirectly using stopped-flow kinetic studies of calcium dissociation. The experiments (section 5.3.3) showed that mutations in the C-domain (I100G and V136G) increased the rate of calcium dissociation from the mutated domain by a factor of up to 20. More interestingly, studies with I27G and I63G showed that these N-domain mutations reduced the rate of calcium dissociation from the non-mutated C-domain by a factor of approximately three. Recent studies in this laboratory using the chromophoric chelator Quin2 have shown that mutations in the C-domain increase the rate of calcium dissociation from the C-domain and reduce the rate of calcium dissociation from the non-mutated N-domain (Martin, S. R., unpublished results).

These experiments demonstrate that the mutation of the residue at position 8 in each binding loop causes a significant reduction of the Ca^{2+} affinity of the mutated domain, but increases the affinity of the non-mutated domain. Two questions must then be answered. How can the mutations have such a small effect on the stoichiometric association constants and by what mechanism is the affinity of the non-mutated domain increased?

The pattern of stoichiometric association constants observed for WT CaM can be obtained with many combinations of site constants and interaction factors (see Section 2.3.1.1, Chapter 2). Based on the known calcium binding properties of WT CaM a reasonable set of constants is $k_I = k_{II} = 7 \cdot 10^3\ M^{-1}$ (with $\alpha_{I,II} = 100$) and $k_{III} = k_{IV} = 7 \cdot 10^4\ M^{-1}$ (with $\alpha_{III,IV} = 65$). These constants give $\log(K_1K_2) = 11.5$ and $\log(K_3K_4) = 9.68$, close to the values measured for WT CaM (see Table 5.3). The pattern of stoichiometric constants obtained for the mutants can be obtained by reducing the affinity of the appropriate site in the mutated domain and increasing the affinities of the sites in the non-mutated domain. Thus:

- $k_I = 700\ M^{-1}$, $k_{II} = 7 \cdot 10^3\ M^{-1}$ (with $\alpha_{I,II} = 100$) and $k_{III} = k_{IV} = 1.5 \cdot 10^5\ M^{-1}$ (with $\alpha_{III,IV} = 65$) gives $\log(K_1K_2) = 12.2$ and $\log(K_3K_4) = 8.7$, close to the values measured for I27G (see Table 5.3);
- $k_I = k_{II} = 3.5 \cdot 10^4\ M^{-1}$ (with $\alpha_{I,II} = 100$) and $k_{III} = 10^3\ M^{-1}$, $k_{IV} = 7 \cdot 10^4\ M^{-1}$ (with $\alpha_{III,IV} = 65$) gives $\log(K_1K_2) = 11.1$ and $\log(K_3K_4) = 9.63$, close to the values measured for I100G (see Table 5.3).

Although this is, of course, only a mathematical exercise it does show that major changes in the affinities of individual sites can leave the overall pattern of stoichiometric association constants relatively unchanged. However, it must be noted that this is only possible when the decrease in the affinity of the mutated site is accompanied by a significant increase in the affinities of the sites in the non-mutated domain.

Although the effect of the mutation on the affinity of the mutated site is not unexpected, the effect on sites in the other domain is more surprising. One possible explanation is that the binding of calcium to the non-mutated domain promotes the interaction with the other unfolded domain. If this is the case, then this interaction would also be expected to increase the affinity of the non-mutated domain for calcium, in much the same way as the interaction with a target sequence increases calcium affinity.

In conclusion, the mutations studied here affect the protein in the following ways:

- They reduce the calcium affinity of the mutated domain, but increase the calcium affinity of the non-mutated domain.
- They reduce the stability of the mutated domain in the absence of calcium by between 1.5 and 4.3 kcal/mol compared with the corresponding wild type domain.
- Because they reduce the calcium affinity, they also reduce the stabilising effect of calcium.

Evidence for mutations in one domain of CaM affecting the structural and calcium binding properties of the non-mutated domain was previously reported in the study of another series of mutant calmodulins. The BQ and BK series of mutants consist of proteins in which the Glu at position 12 in each calcium binding loop is replaced respectively by Gln or Lys (Beckingham, 1991). Spectroscopic studies of these proteins showed that mutations in the N-domain result in a reduction of the

calcium affinity of the C-domain, whereas mutations in the C-domain seem to increase the calcium affinity of the N-domain by reducing the rate of calcium dissociation (Martin et al., 1992; Maune et al., 1992a). Thus, as for the β-sheet mutants, interactions between the N- and C-domains were postulated also for the BQ and BK series of mutant calmodulins.

CHAPTER 6

INTERACTIONS OF MAGNESIUM WITH CALMODULIN

6.1 Introduction

The intracellular Mg^{2+} concentration is of the order of 1-2 mM (Ebel and Gunther, 1980) whilst that of Ca^{2+} is ~ 0.1 μM under resting conditions and increases to 1-10 μM upon stimulation (Berridge et al., 1998). Calcium-binding proteins must therefore be able to discriminate against Mg^{2+} by responding to an increase in Ca^{2+} concentration in the presence of a 100 to 10,000-fold excess of Mg^{2+}. Several studies have concluded that Mg^{2+} binds to CaM and competes directly with Ca^{2+} binding (Haiech et al., 1981; Tsai et al., 1987; Ouyang and Vogel, 1998; Malmendal et al., 1999b). Although the reported binding constants show considerable variation, possibly due to different experimental conditions, they are mostly in the range 10^2 to 10^4 M^{-1} and there is good evidence that Mg^{2+}, unlike Ca^{2+}, binds preferentially to the N-terminal domain of CaM (Tsai et al., 1987; Malmendal et al., 1999b). The possible effects of Mg^{2+} on the recognition and activation of targets by Ca^{2+}-CaM have also been investigated in some studies (Ohki et al., 1993; Ohki et al., 1997; Ozawa et al., 1999). Although it has been suggested that the presence of Mg^{2+} does inhibit the formation of active Ca^{2+}-CaM-target complexes, this question has not yet been fully

addressed. It is clearly very important that the effects of Mg^{2+} on Ca^{2+}/CaM signalling processes should be understood in detail.

An important conclusion of the studies on the stability of CaM described in Chapter 3 is that the C-domain of apo-CaM has very low thermodynamic stability and under near physiological conditions (37 °C, 100 mM KCl, pH 7.5) is more than 20% unfolded (see Section 3.3.4). However, it was also shown that the interactions with Ca^{2+} and with target sequences can stabilise the protein and significantly reduce the percentage of unfolding. Thus, the binding of Mg^{2+} could also be an important stabilising factor for CaM *in vivo*, especially at resting Ca^{2+} concentrations.

The aims of the work in this Chapter, therefore, are to characterise the interactions of Mg^{2+} with CaM and in particular to measure:

- the conformational effects of Mg^{2+} binding to CaM
- the Mg^{2+} affinity of the N- and C-domains of CaM
- the effects of Mg^{2+} on the stability of CaM
- the degree of competition between Ca^{2+} and Mg^{2+}
- the effects of Mg^{2+} on the binding of CaM to typical target sequences.

6.2 Materials and methods

The experimental approaches employed in the studies described in this chapter (optical spectroscopy, fluorescence and absorbance titrations, and urea denaturation) are fully described in Chapter 2. Some of the important mathematical relationships are summarised here for convenience.

The stoichiometric association constants for Mg^{2+} binding (K^*_1 and K^*_2) derived from urea-unfolding data (reported in Table 6.2) were calculated using the equation:

$$\Delta\Delta G_b = -RT\ln\left(\frac{1}{1+K^*_1[Mg]+K^*_1K^*_2[Mg]^2}\right) \qquad (6.1)$$

with the following assumptions:

1) that the binding of Mg^{2+} to the unfolded state is not significant at the magnesium concentrations employed (see Section 2.3.7, Chapter 2);

2) that the two intrinsic association constants for the binding of Mg^{2+} to a single domain of CaM are the same (i.e. the sites are identical) and there is no cooperativity between binding sites within one domain (cf., Malmendal et al., 1998).

Thus $k^*_I = k^*_{II} = k^*$ and $\alpha_{I,II} = \alpha_{II,I} = 1$

Then $K^*_1 = k^*_I + k^*_{II} = 2k^*$ $K^*_2 = k^*_I k^*_{II} \alpha_{I,II} / K^*_1 = k^*/2$

and $K^*_2 = K^*_1/4$

The definitions of the intrinsic and stoichiometric association constants and the relationship between them are given in Section 2.3.1.1, (Chapter 2).

The theory describing the competition between Ca^{2+} and Mg^{2+} for the same sites in a CaM domain is given in Section 2.3.1.3 (Chapter 2). The apparent (measured) average Ca^{2+} affinities of the N- and C-domains of intact CaM in the presence of Mg^{2+} are calculated as:

$$K^{Ca}_{av(C),app} = \sqrt{K_{1,app} K_{2,app}} \qquad K^{Ca}_{av(N),app} = \sqrt{K_{3,app} K_{4,app}} \tag{6.2}$$

where $K_{i,app}$ is the apparent stoichiometric association constant for the binding of the i^{th} Ca^{2+} ion in the presence of Mg^{2+}. These apparent average binding constants for Ca^{2+} are related to the true average binding constants for Ca^{2+} and Mg^{2+} by the following approximate expression:

$$K^{Ca}_{av(D),app} \approx \frac{K^{Ca}_{av(D)}}{1 + K^{Mg}_{av(D)}[Mg]} \tag{6.3}$$

where $K^{Ca}_{av(D)}$ and $K^{Mg}_{av(D)}$ are the average binding constants for the binding of Ca^{2+} and Mg^{2+}, respectively, to a calmodulin domain D.

6.3 Results

6.3.1 Conformational effects of Mg^{2+}

Figures 6.1 and 6.2 show the absorption, Tyr-138 fluorescence, near-UV CD, and far-UV CD spectra of CaM under various conditions. The optical properties of apo-CaM and Ca^{2+}-CaM in both the folded and unfolded states have been described previously (see Section 3.3.1, Chapter 3). The spectra of Mg^{2+}-CaM were recorded in 10 or 20 mM $MgCl_2$ in the absence of KCl and are labelled Mg. The absorption, far- and near-UV CD spectra of Mg^{2+}-CaM are closely similar to those of apo-CaM in 0.2 M KCl (labelled apo). This observation shows that Mg^{2+}, like KCl, refolds the protein, which under these low-salt conditions is partially unfolded (see Table 4.1, Chapter 4). However, the spectra show that, unlike Ca^{2+}, which causes an increase in the secondary structure content and significant changes in the tertiary structure of the protein, Mg^{2+} does not induce changes in either the secondary or the tertiary structure of CaM. The intensity of the Tyr-138 fluorescence spectrum of Mg^{2+}-CaM is intermediate between that of the unfolded protein (U) and Ca^{2+}-CaM (Ca). Thus, in this case the intensity of the Mg^{2+}-CaM spectrum is not similar to that of apo-CaM (apo); however, since the CD results show that the secondary and tertiary structures of CaM remain unchanged upon addition of Mg^{2+}, the changes observed in the Tyr-138 emission must derive principally from local structural rearrangements induced by occupancy of site IV.

Figures 6.1 and 6.2 also show the spectra recorded with apo-CaM in 25 mM Tris without added KCl. Experiments on the effects of ionic strength on the stability of CaM have shown that the C-domain of apo-CaM is substantially unfolded under these solvent conditions (these results are described in Chapter 4). Consistent with this, the absorption, Tyr-138 fluorescence and near-UV CD spectra (labelled T) have intensities that are intermediate between those of folded (in 0.2 M KCl, labelled apo) and unfolded (U) apo-CaM and they show that 30-40% of the apo-C-domain is unfolded in the absence of KCl. In the case of far-UV CD, the spectrum recorded in the absence of KCl is much closer to that of fully folded apo-CaM because the N-domain, which accounts for ~ 55% of the total CD signal (Drabikowski et al., 1982; Martin and Bayley, 1986), is not significantly unfolded under these solvent conditions (see Table 4.1, Chapter 4).

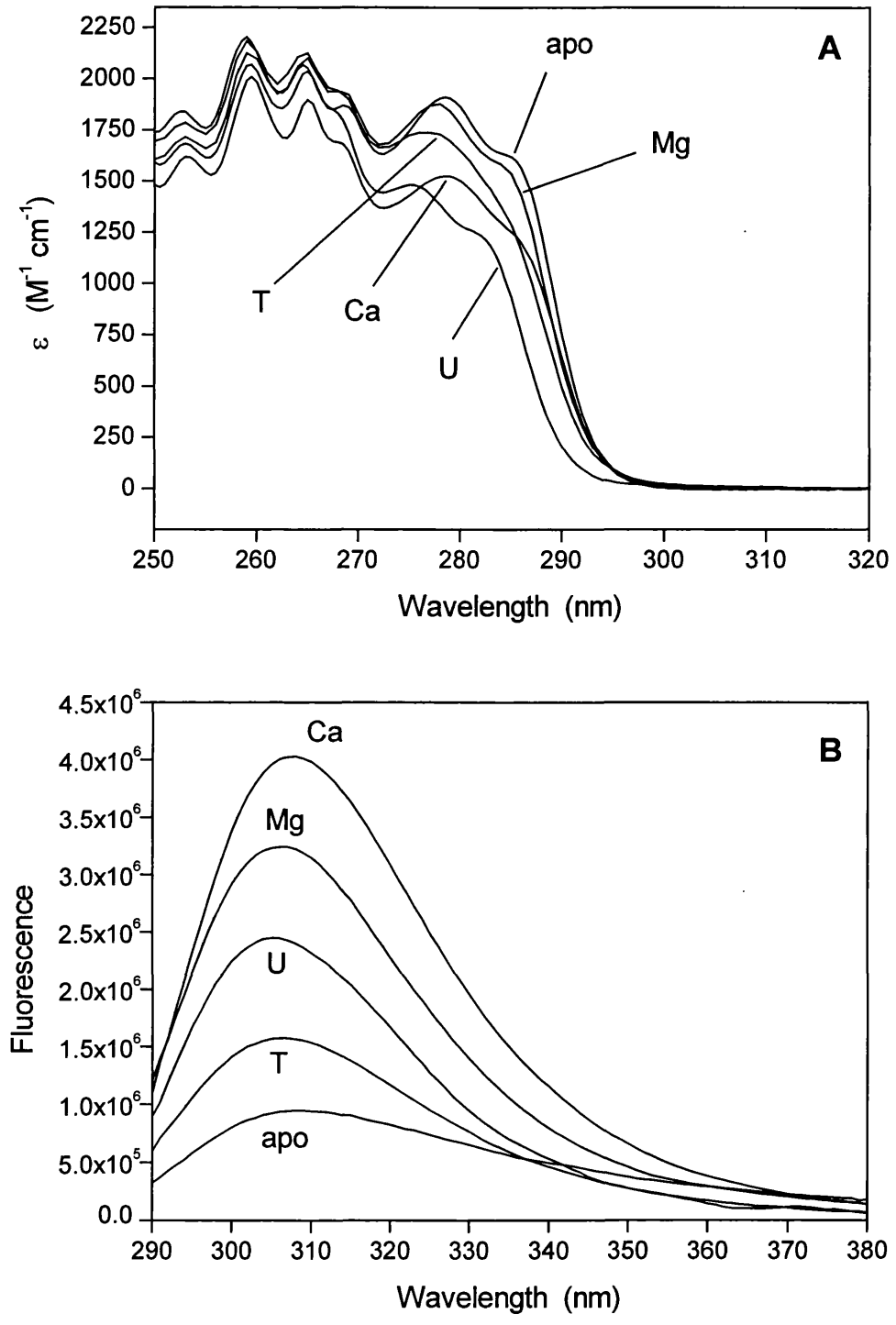

Figure 6.1 Absorption **(A)** and Tyr-138 fluorescence **(B)** spectra of CaM recorded at 20 °C under different solvent conditions. (apo), apo-CaM in 25 mM Tris, 0.2 M KCl; (T), apo-CaM in 25 mM Tris; (Mg), Mg^{2+}-CaM in 25 mM Tris, 20 mM $MgCl_2$; (Ca), Ca^{2+}-CaM in 25 mM Tris, 0.1 M KCl, 1 mM $CaCl_2$; (U) unfolded CaM in 25 mM Tris, 0.1 M KCl, 6 M GuHCl.

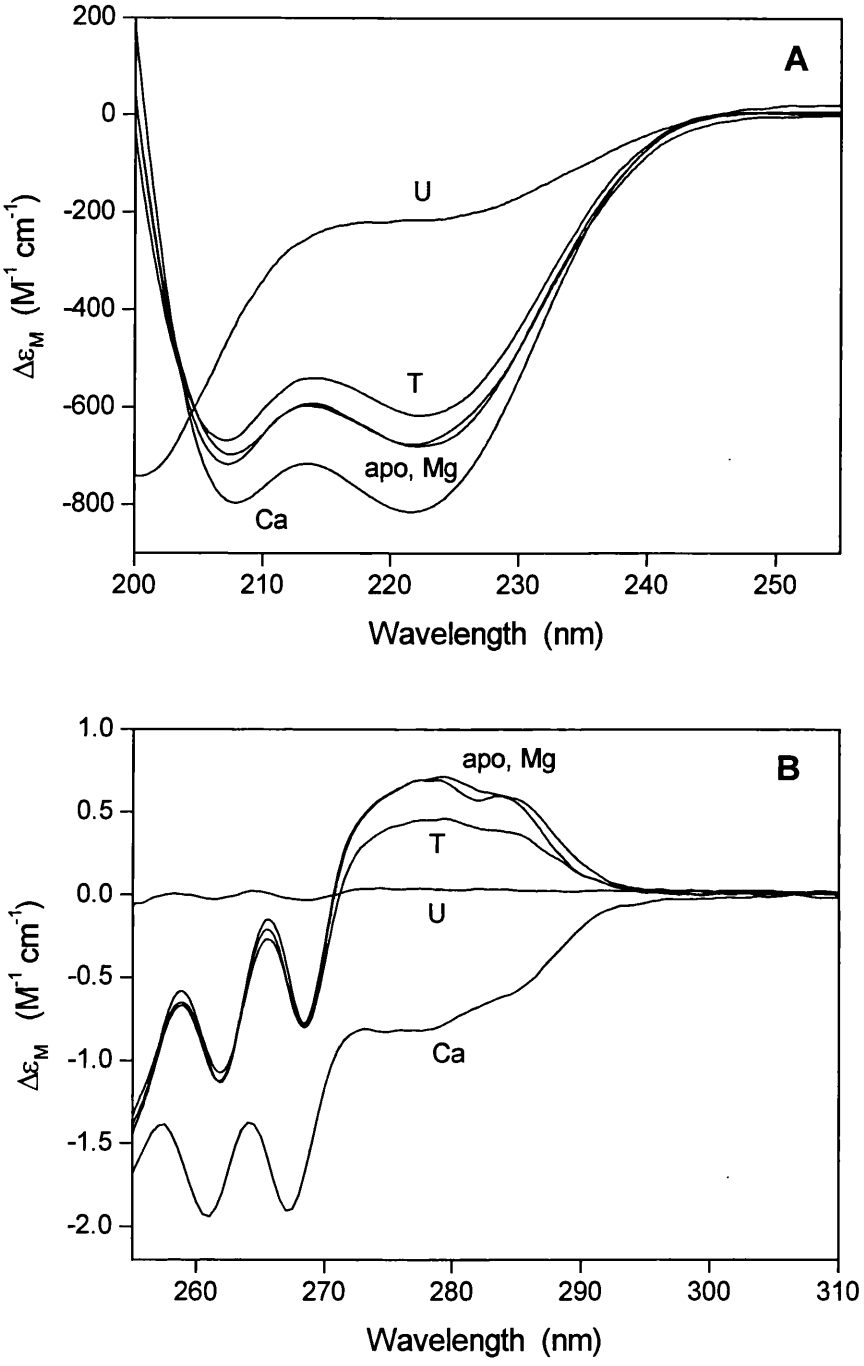

Figure 6.2 Far- **(A)** and near- **(B)** UV CD spectra of CaM under different solvent conditions. (apo), apo-CaM in 25 mM Tris, 0.2 M KCl, at 20 °C; (T), apo-CaM in 25 mM Tris, at 20 °C; (Mg), Mg^{2+}-CaM in 25 mM Tris, 20 mM $MgCl_2$, at 20 °C; (Ca), Ca^{2+}-CaM in 25 mM Tris, 0.1 M KCl, 1 mM $CaCl_2$, at 20 °C. The spectrum for unfolded CaM (U) was recorded in 25 mM Hepes at 75 °C in the case of far-UV CD and in 25 mM Tris, 0.1 M KCl, 6 M GuHCl, at 20 °C in the case of near-UV CD.

6.3.2 Direct determination of Mg^{2+} affinities

The binding of Mg^{2+} to CaM has been studied using the change in Tyr-138 fluorescence described in the previous section (see Fig. 6.1B). These experiments therefore selectively monitor Mg^{2+} binding to the C-terminal domain of CaM. Figure 6.3 shows Mg^{2+} titrations of apo-CaM (at ~ 7 μM) performed in the absence of KCl and in the presence of 100 mM KCl. The total intensity change is significantly larger in the presence of KCl because the salt refolds the C-domain of apo-CaM and this causes the decrease in the Tyr-138 fluorescence emission at the starting point of the titration (see Fig. 6.1B). The free Mg^{2+} concentrations at the midpoints of the fluorescence changes are approximately 1.7 mM (no KCl) and 5.7 mM (100 mM KCl). These values

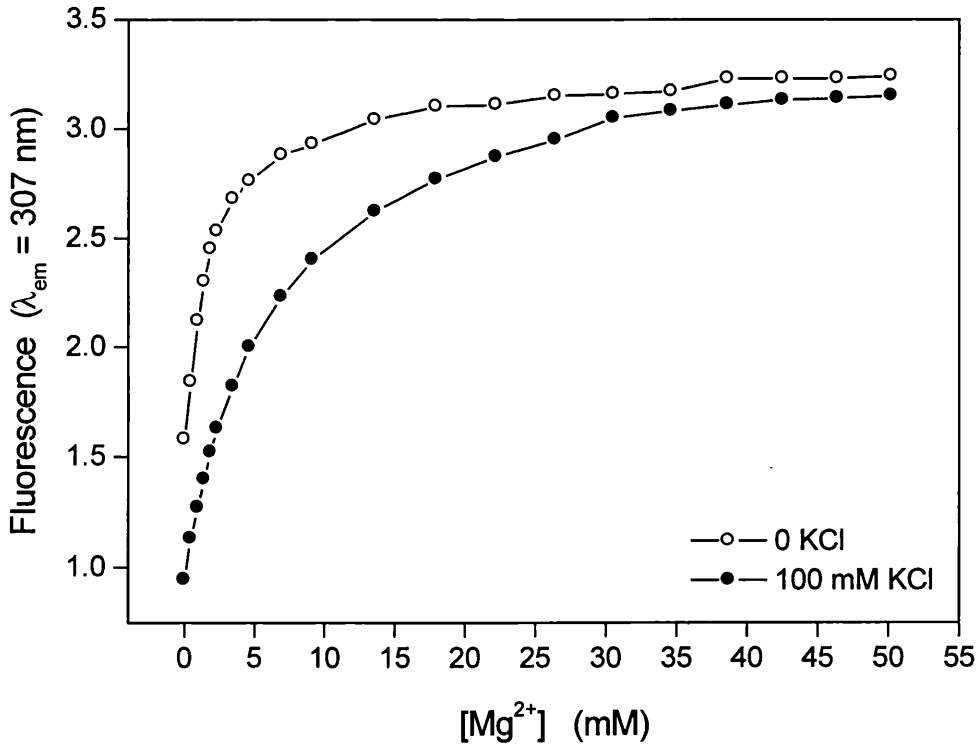

Figure 6.3 Mg^{2+} titrations of apo-CaM performed at 20 °C in 25 mM Tris, pH 8, in the absence of KCl (–○–) and in the presence of 100 mM KCl (–●–). The curves were monitored using Tyr-138 fluorescence.

correspond to an average Mg^{2+} affinity for the C-domain ($K^{Mg}_{av(C)}$) of 580 M^{-1} (no KCl) and 175 M^{-1} (100 mM KCl). The corresponding values for calcium (i.e. $K^{Ca}_{av(C)}$) are $2 \cdot 10^7$ M^{-1} (no KCl) and $6 \cdot 10^5$ M^{-1} (100 mM KCl) (Linse et al., 1991a). The binding of Mg^{2+} to the N-terminal domain of CaM may be studied in a similar way by using Mg^{2+}-induced changes in the tryptophan fluorescence of the T26W mutant of SynCaM (Martin, S. R., unpublished observations).

The results of these direct determinations (summarised in Table 6.1) confirm that the affinities of individual CaM domains for Mg^{2+} are in the range 200-3000 M^{-1} (depending on the ionic strength) and that Mg^{2+} does indeed bind preferentially to the N-terminal domain of CaM. The effect of increasing ionic strength on metal ion affinity appears to be significantly smaller in the case of Mg^{2+}, but this is difficult to quantify in more detail because of the ionic strength contribution from the Mg^{2+} itself.

Table 6.1 Average stoichiometric association constants for the binding of Ca^{2+} and Mg^{2+} to the C- and N-domains of CaM, determined by direct titration

[KCl] (mM)	$K^{Mg}_{av(C)}$ (M^{-1})	$K^{Ca}_{av(C)}$ (M^{-1})	$K^{Mg}_{av(N)}$ (M^{-1})	$K^{Ca}_{av(N)}$ (M^{-1})
0	580	$2 \cdot 10^7$ [a]	2700 [b]	$3.5 \cdot 10^6$ [a]
25	330 [b]	$2.5 \cdot 10^6$ [a]	1250 [b]	$3.5 \cdot 10^5$ [a]
100	175	$6 \cdot 10^5$ [a]	570 [b]	$6 \cdot 10^4$ [a]

[a] Linse et al., 1991a.

[b] Martin, S. R., unpublished results.

6.3.3 Urea-induced denaturation of Mg^{2+}-CaM

In order to investigate the effects of Mg^{2+} binding on the stability of CaM, urea-induced denaturation of CaM and its isolated domains in the presence of Mg^{2+} has been monitored using far-UV CD under different ionic strength conditions. This method, as the studies described in Chapter 3 have shown, can also give an estimate of the Mg^{2+} affinities of the isolated fragments and of both domains in intact CaM.

Figure 6.4A shows the unfolding profiles measured for Tr1C and Tr2C in the presence of 10 mM Mg^{2+} but in the absence of KCl (the total ionic strength of this solution is I = 30 mM); the curves obtained for the apo-forms of the fragments in 30 mM KCl (i.e. under the same ionic strength conditions), are included for comparison. It is evident that the Mg^{2+}-loaded proteins are, as expected, substantially more stable than the apo-proteins. Table 6.2 shows the results of the LEM analyses for these experiments. The $\Delta G°_{20}$ values obtained for Tr1C and Tr2C in 10 mM Mg^{2+} (no KCl) are 5.08 and 3.05 kcal/mol, respectively. Thus, in the presence of magnesium, Tr1C is considerably more stable than Tr2C. This means that Mg^{2+} binding, unlike Ca^{2+} binding, does not reverse the order of domain stability observed with the apo-proteins.

Inspection of Figure 6.4A shows that the shift in the transition midpoint induced by Mg^{2+} is greater for Tr1C than for Tr2C. This observation is confirmed by the values of the ligand interaction free energies, $\Delta\Delta G_b$, calculated as $\Delta G°_{20}$(plus Mg^{2+}) - $\Delta G°_{20}$(apo), using $\Delta G°_{20}$(apo) values taken from Table 4.1 in Chapter 4. These $\Delta\Delta G_b$ values are 2.53 kcal/mol for Tr1C and 1.5 kcal/mol for Tr2C, indicating that the stabilisation induced by Mg^{2+} binding under these solvent conditions is greater for Tr1C than for Tr2C by more than 1 kcal/mol. This is again the opposite of the situation observed with the Ca^{2+}-saturated proteins and gives further confirmation for the conclusion that Tr1C binds Mg^{2+} with higher affinity than does Tr2C. The stoichiometric association constants K^*_1 and K^*_2, reported in Table 6.2, were calculated from the ligand interaction free energies using Eq. 6.1 (see Section 6.2). The average Mg^{2+} affinities of Tr1C and Tr2C (calculated using $K^{Mg}_{av} = (K^*_1K^*_2)^{1/2}$) are 778 and 263 M^{-1}, respectively, at a total ionic strength of I = 30 mM, in reasonable agreement with the values determined for the corresponding domains in intact CaM by direct titration at I = 25 mM (see section 6.3.2).

Figure 6.4B shows the urea-unfolding profiles obtained for CaM and its isolated domains in the presence of 10 mM Mg^{2+} and 70 mM KCl (the total ionic strength of

this solution is I = 100 mM). The results of the LEM analyses are summarised in Table 6.2. The calculated ligand interaction free energies show that the stabilising effect of Mg^{2+} is significantly smaller under these higher ionic strength conditions (the $\Delta\Delta G_b$ values are ~0.5 kcal/mol lower for both Tr1C and Tr2C). This is, of course, the expected result because the affinities for Mg^{2+} are lower at higher ionic strength (see Section 6.3.2). The average Mg^{2+} affinities of Tr1C and Tr2C (calculated using $K^{Mg}_{av} = (K^*_1 K^*_2)^{1/2}$) are 467 and 122 M^{-1}, respectively, in excellent agreement with the values determined for the corresponding domains in intact CaM by direct titration at I = 100 mM (see section 6.3.2).

The unfolding profile for intact Mg^{2+}-CaM in Figure 6.4B clearly shows two resolvable transitions, denoted as CaM-1 and CaM-2 in Table 6.2. The $\Delta G°_{20}$ values are 2.66 kcal/mol for the transition CaM-1 and 5.58 kcal/mol for the transition CaM-2. Since Mg^{2+}-Tr1C is more stable than Mg^{2+}-Tr2C, and because it is reasonable to assume that the relative stability of the isolated domains is maintained in the intact protein, the transition CaM-1 has been assigned to the C-domain and the transition CaM-2 has been assigned to the N-domain of CaM. The average Mg^{2+} affinities for the domains in intact CaM (K^{Mg}_{av}) were calculated to be 166 M^{-1} for the transition CaM-1 (C-domain) and 390 M^{-1} for the transition CaM-2 (N-domain) (Table 6.2). These values are in good agreement with values of 175 M^{-1} and 580 M^{-1} measured using Tyr-138 (C-domain, WT-CaM) and Trp-26 (N-domain, SynCaM(T26W)), confirming the assignment of the CaM-1 and CaM-2 transitions.

The curves in Figure 4.6B also show that, as observed for apo-CaM and for Ca^{2+}-CaM, the sum of the unfolding curves for the isolated fragments differs from the unfolding curve for intact CaM. The C-domain in intact Mg^{2+}-CaM (which unfolds first) is destabilised by ~ 0.3 kcal/mol compared with Tr2C whilst the N-domain (which unfolds second) is stabilised by ~ 0.7 kcal/mol compared with Tr1C.

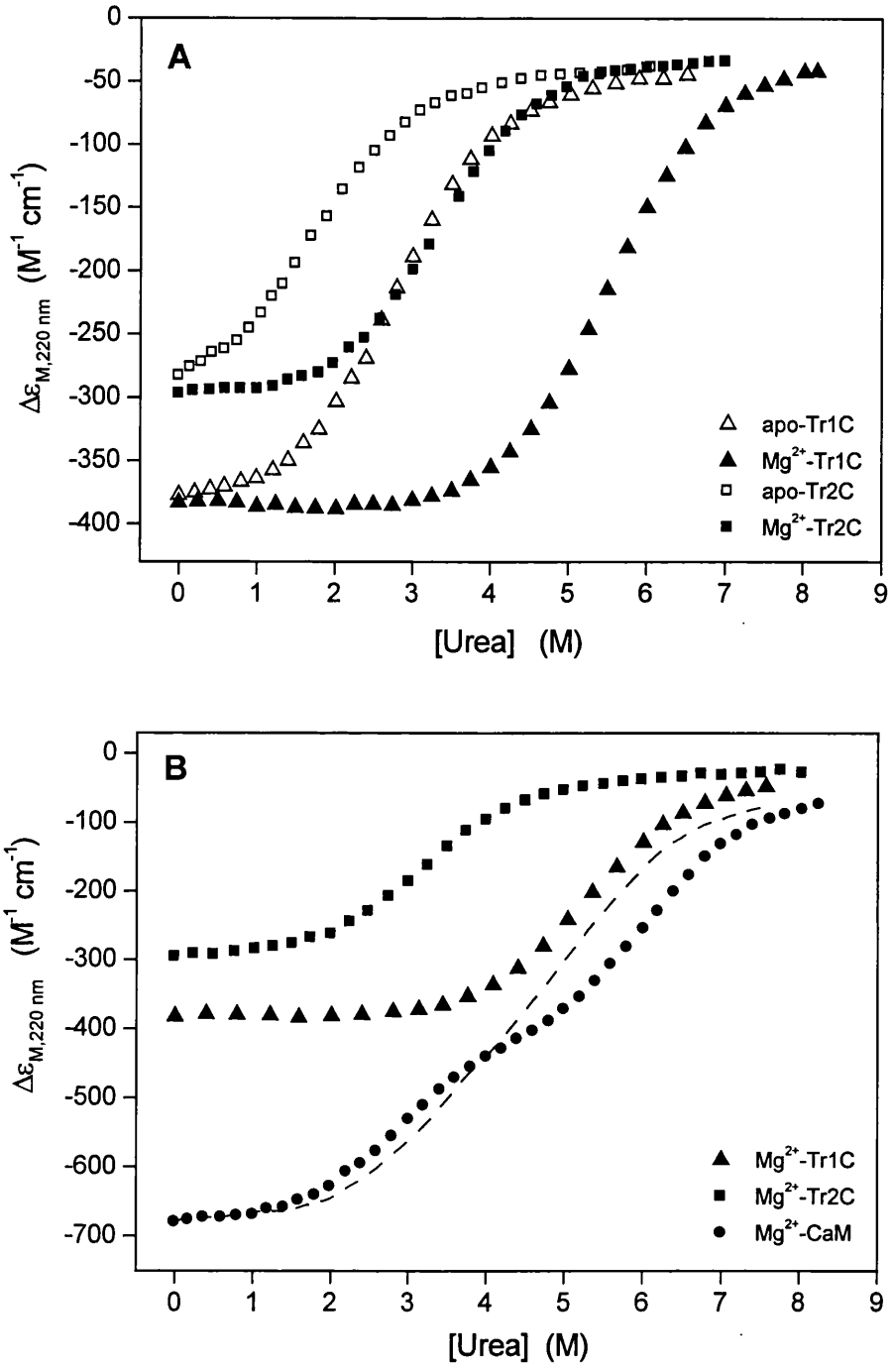

Figure 6.4 **(A)** Urea-induced denaturation of Tr1C and Tr2C at 0 (△, □) and 10 mM $MgCl_2$ (▲, ■), monitored at 20 °C using far-UV CD. The buffers used were 25 mM Tris, 30 mM KCl, pH 8 for the apo-proteins, and 25 mM Tris, pH 8 in the presence of Mg^{2+}. **(B)** Urea-induced denaturation of Tr1C (▲), Tr2C (■), and CaM (●) at 10 mM $MgCl_2$. The curves were measured at 20 °C in 25 mM Tris, 70 mM KCl, pH 8, using far-UV CD. The dotted line represents the sum of the curves for Tr1C and Tr2C.

Table 6.2 Effect of 10 mM $MgCl_2$ on urea-unfolding of Tr1C, Tr2C, and CaM

Transition	I [a] (mM)	$\Delta G°_{20}$ [b] (kcal/mol)	$[U]_{1/2}$ (M)	$\Delta\Delta G_b$ [c] (kcal/mol)	K^*_1 [d] (M^{-1})	K^*_2 [d] (M^{-1})	K^{Mg}_{av} [e] (M^{-1})
Tr1C	30	5.08	5.52	2.53	1556	389	778
	100	4.86	5.28	2.02	933	233	467
Tr2C	30	3.05	3.32	1.50	525	131	263
	100	2.93	3.18	0.93	244	61	122
CaM-1 [f]	100	2.66	2.89	1.14	332	83	166
CaM-2 [f]	100	5.58	6.06	1.85	779	195	390

[a] Mg^{2+} concentrations were included in the calculation of the ionic strength (I).

[b] $\Delta G°_{20}$ values were calculated as $-[U]_{1/2} \cdot m_{av}$, where m_{av} = -0.92 kcal/mol·M (see Section 2.3.6.1 in Chapter 2).

[c] $\Delta\Delta G_b$ values were calculated as $\Delta G°_{20}$(plus Mg^{2+}) - $\Delta G°_{20}$(apo) using $\Delta G°_{20}$(apo) values from Table 3.1 (Chapter 3) and Table 4.1 (Chapter 4).

[d] K^*_1 and K^*_2 are the estimated stoichiometric association constants for Mg^{2+}, calculated by assuming that $\Delta\Delta G_b = -RT \ln\{1/(1 + K^*_1[Mg^{2+}] + K^*_1K^*_2[Mg^{2+}]^2)\}$ and that $K^*_2 = K^*_1/4$, i.e. that there is no cooperativity between binding sites (see Section 6.2).

[e] K^{Mg}_{av} values were calculated as $K^{Mg}_{av} = (K^*_1K^*_2)^{1/2}$.

[f] CaM-1 and CaM-2 identify the first and second transitions resolved for intact CaM, assigned to the C- and N-domains respectively.

6.3.4 Competition between Ca^{2+} and Mg^{2+}

The effect of Mg^{2+} on Ca^{2+} binding has been assessed by measuring the stoichiometric calcium association constants in the presence of different Mg^{2+} concentrations. Titrations with the chromophoric chelator 5,5'-dibromo-BAPTA were performed in the presence of 0, 1, 2, 5 and 10 mM $MgCl_2$, with the ionic strength maintained at a constant value (0.1 M) by appropriate variation in the total KCl concentration. The presence of Mg^{2+} does not interfere with this assay since the association constant of the chelator with Mg^{2+} is < 5 M^{-1} under these solution conditions (Martin, S. R., unpublished results; cf., Pethig et al., 1989).

The titrations are shown in Figure 6.5 and the results of the analyses are presented in Table 6.3. The products of the apparent stoichiometric association constants for Ca^{2+} binding in the presence of Mg^{2+}, $K_{1,app}K_{2,app}$ and $K_{3,app}K_{4,app}$, reflect binding to the C- and N-terminal domains of CaM, respectively (see Section 2.3.1.1, Chapter 2). The constants $K^{Ca}_{av(N),app}$ and $K^{Ca}_{av(C),app}$ are the corresponding apparent average Ca^{2+} affinities for the N- and C-terminal domains, respectively, as defined by Eq. 6.2 (Section 6.2). For both domains, the measured Ca^{2+} affinity decreases significantly as the Mg^{2+} concentration is increased. The product $K_{1,app}K_{2,app}$ (reflecting C-domain affinity) is reduced by approximately one order of magnitude as $[Mg^{2+}]$ is increased from 0 to 10 mM. The effect of Mg^{2+} is significantly greater for $K_{3,app}K_{4,app}$ (reflecting N-domain affinity) which is reduced by approximately one order of magnitude on increasing $[Mg^{2+}]$ from 0 to 5 mM, and is not measurable with this particular chelator at $[Mg^{2+}] > 5$ mM.

Finally, the experimentally measured values of $K^{Ca}_{av(C),app}$ and $K^{Ca}_{av(N),app}$ were used to estimate the average association constants for Mg^{2+} ($K^{Mg}_{av(C)}$ and $K^{Mg}_{av(N)}$) using Eq. 6.3 (Section 6.2). These values are, of course, very sensitive to errors in the product of the stoichiometric association constants (typically 0.1-0.15 in log units). Nevertheless, the calculated values are in satisfactory agreement with values of 175 M^{-1} and 580 M^{-1} measured for the C- and N-domains using direct fluorescence titrations (see Section 6.3.2).

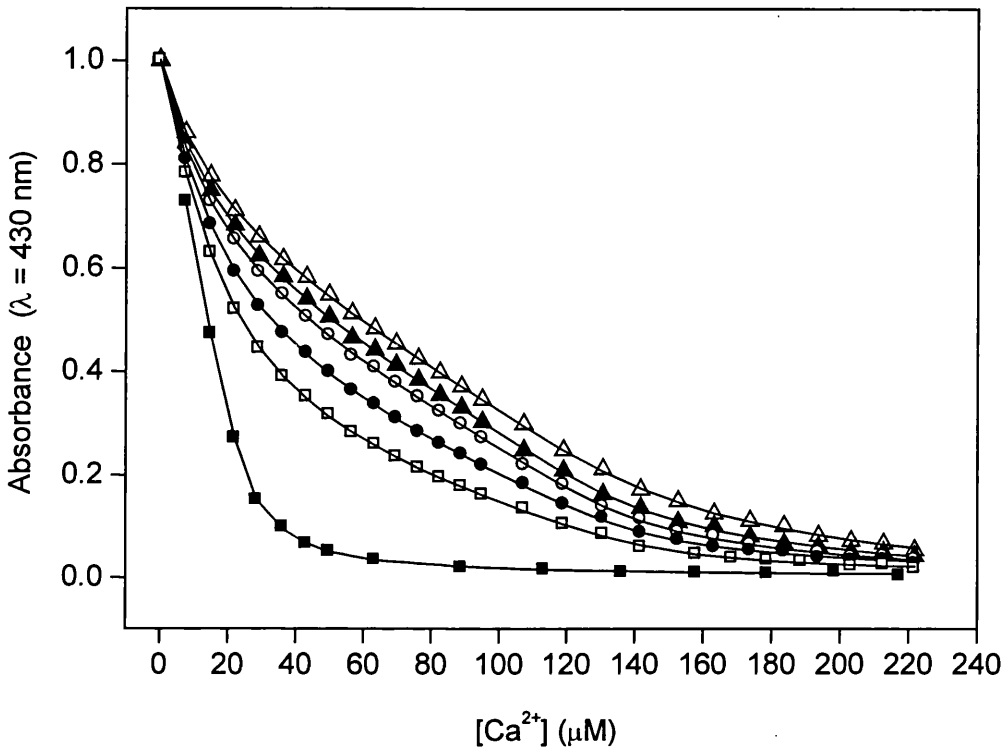

Figure 6.5 Ca^{2+} titrations performed with the chromophoric chelator 5,5'-dibromo-BAPTA alone (–■–), and in the presence of CaM at 0 (–△–), 1 (–▲–), 2 (–○–), 5 (–●–) and 10 (–□–) mM $MgCl_2$. The curves were measured at 20 °C in 25 mM Tris, pH 8, using absorption spectroscopy. The ionic strength in each experiment was maintained at 0.1 M by appropriate variation in the total KCl concentration.

Table 6.3 Apparent stoichiometric binding constants for Ca^{2+} in the presence of Mg^{2+}

$[Mg^{2+}]$ (mM)	$K_{1,app}K_{2,app}$ [a] (M^{-2})	$K^{Ca}_{av(C),app}$ [b] (M^{-1})	Calculated $K^{Mg}_{av(C)}$ [c] (M^{-1})	$K_{3,app}K_{4,app}$ [a] (M^{-2})	$K^{Ca}_{av(N),app}$ [b] (M^{-1})	Calculated $K^{Mg}_{av(N)}$ [c] (M^{-1})
0	$3.55 \cdot 10^{11}$	$5.96 \cdot 10^{5}$	--	$4.07 \cdot 10^{9}$	$6.38 \cdot 10^{4}$	--
1	$2.75 \cdot 10^{11}$	$5.25 \cdot 10^{5}$	133	$2.29 \cdot 10^{9}$	$4.79 \cdot 10^{4}$	332
2	$1.91 \cdot 10^{11}$	$4.37 \cdot 10^{5}$	181	$7.76 \cdot 10^{8}$	$2.79 \cdot 10^{4}$	643
5	$6.61 \cdot 10^{10}$	$2.57 \cdot 10^{5}$	263	$4.57 \cdot 10^{8}$	$2.14 \cdot 10^{4}$	396
10	$3.80 \cdot 10^{10}$	$2.26 \cdot 10^{5}$	163	--	--	--

[a] $K_{i,app}$ is the apparent stoichiometric association constant for the binding of the i^{th} Ca^{2+} ion in the presence of Mg^{2+} and is defined in Section 2.3.1.3 in Chapter 2.

[b] $K^{Ca}_{av(C),app}$ and $K^{Ca}_{av(N),app}$ represent the average apparent Ca^{2+} affinities of the N- and C-domains in the presence of Mg^{2+} and they were calculated as: $K^{Ca}_{av(C),app} = (K_{1,app}K_{2,app})^{1/2}$ and $K^{Ca}_{av(N),app} = (K_{3,app}K_{4,app})^{1/2}$

[c] $K^{Mg}_{av(C)}$ and $K^{Mg}_{av(N)}$ were calculated from the values of $K^{Ca}_{av(C),app}$ and $K^{Ca}_{av(N),app}$ in the absence and in the presence of Mg^{2+} using Eq. 6.3 (see Section 6.2).

6.3.5 Effect of Mg^{2+} on the interaction of calmodulin with NM2

In order to investigate the effects of Mg^{2+} on the interaction of CaM with target sequences, the affinity of CaM for the peptide NM2 has been determined using direct fluorometric titrations in the presence and in the absence of Ca^{2+} and Mg^{2+}. NM2 corresponds to part of the CaM-binding domain of neuromodulin (with an I4W substitution) and binds with high affinity to Ca^{2+}-CaM (K_d ~ 30 nM in 100 mM KCl and K_d ~ 11 nM in the absence of KCl) (Martin, S.R. and Bayley, P.M., manuscript in preparation). Recent work from this laboratory has shown that NM2 also interacts with apo-CaM; the interaction is much weaker than that with Ca^{2+}-CaM and is strongly dependent on ionic strength.

The experimental approach presented here (see Section 2.3.4, Chapter 2) is based on the fact that the tryptophan fluorescence emission spectrum of the peptide changes depending on the nature of the species with which it interacts. The spectrum of uncomplexed NM2 has an emission maximum at 356 nm (typical of free tryptophan). The apo-CaM-NM2 complex has an emission maximum at 340 nm and the intensity is enhanced by a factor of ~ 1.2. The Mg^{2+}-CaM-NM2 and Ca^{2+}-CaM-NM2 complexes emit at 335 nm (enhancement ~ 1.3-fold) and 324 nm (enhancement ~ 2-fold), respectively. These different spectral characteristics permit the determination of the dissociation constants (K_d's) for the interaction of the peptide with CaM under different solvent conditions. Since the binding of NM2 to apo-CaM is stronger at low ionic strength, in the experiments performed in the absence of Ca^{2+} the KCl concentration was < 1 mM. When the affinity was measured in the presence of Ca^{2+} (with [Ca^{2+}] varied from 10 to 100 μM), 100 mM KCl was added to the solvent and the NM2 affinity was measured in the absence and in the presence of 5 mM Mg^{2+}. The NM2 concentration was 1.2 μM in all experiments and the CaM concentration was varied in the range 0-6 μM. A typical titration of NM2 with CaM in 100 μM Ca^{2+} and 100 mM KCl is shown in Figure 6.6. The spectra shown in this figure were not corrected for small contributions from CaM (fluorescence signal of Tyr-138). The results of these experiments (Table 6.4) may be summarised as follows:

- The K_d for the interaction of NM2 with apo-CaM at low ionic strength is ~ 53 nM (Table 6.4). In the presence of 5 mM Mg^{2+} ([KCl] < 1 mM), the measured K_d is increased to ~ 780 nM. This 15-fold reduction in affinity is only partly attributable to the ionic strength contribution from the added magnesium (I = 15 mM), because the K_d for the interaction of NM2 with apo-CaM is increased only 5-fold (260 nM) and 10-fold (490 nM) by 15 and 30 mM KCl, respectively (Martin, S. R., unpublished observations).
- The affinities of CaM for NM2 measured in the presence of 100 and 26 μM Ca^{2+} are the same within experimental error (K_d ~ 34 and ~ 31 nM, respectively, at [KCl] = 100 mM); this value is in very good agreement with that of ~ 30 nM previously obtained in the presence of 1 mM Ca^{2+} (Martin, S.R. and Bayley, P.M., manuscript in preparation). In the presence of lower concentrations of Ca^{2+} (10 μM), the apparent affinity of CaM for NM2 is decreased by a factor of ~ 2 (K_d ~ 70 nM).

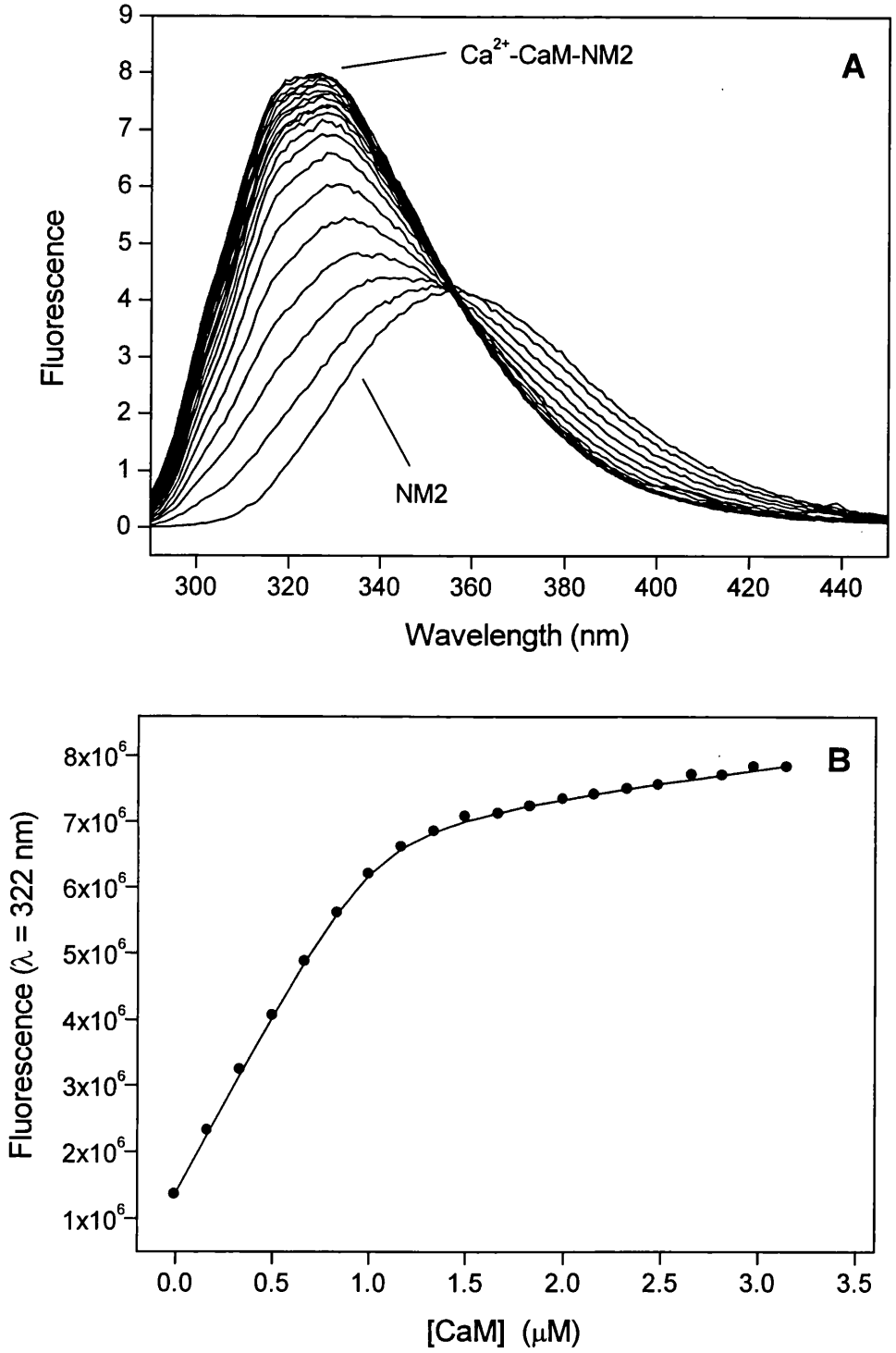

Figure 6.6 CaM titration of NM2 in the presence of 100 μM Ca^{2+}, monitored in 25 mM Tris, 100 mM KCl, pH 8, using Trp fluorescence. **(A)** Spectra. **(B)** Fluorescence intensity at 322 nm. The solid line is the computed best fit.

Thus, decreasing the total Ca^{2+} concentration from 1 mM to 10 μM reduces the affinity of CaM for NM2 by only a factor of ~ 2.

- The affinities of CaM for NM2 measured in the presence of 5 mM Mg^{2+} plus 100, 26, and 10 μM Ca^{2+} (at [KCl] = 100 mM) are 72, 75, and 158 nM, respectively. Thus, the presence of Mg^{2+} has the effect of reducing the apparent affinity of CaM for NM2 by a factor of ~ 2 at all calcium concentrations studied.

The implications of these observations will be discussed in the next section.

Table 6.4 Observed dissociation constants for the binding of NM2 to CaM in the absence and in the presence of 5 mM Mg^{2+}

		no Mg^{2+}	+ 5 mM Mg^{2+}
[KCl] (mM)	$[Ca^{2+}_{TOT}]$ (μM)	K_d (nM)	K_d (nM)
< 1	0	53 (23)	780 (470)
100	100	34 (7)	72 (20)
100	26	31 (9)	75 (14)
100	10	70 (7)	158 (18)

6.4 Discussion

6.4.1 Binding of Mg^{2+} to calmodulin: effects on conformation and stability

In this work, the affinity of the C-domain of intact CaM for Mg^{2+} has been measured directly using the changes in the C-domain Tyr-138 fluorescence signal. The values obtained for the average Mg^{2+} affinity $K^{Mg}_{av(C)}$ were 580 M^{-1} (no KCl) and 175 M^{-1} (100 mM KCl). The corresponding values for the N-domain ($K^{Mg}_{av(N)}$) are 2700 M^{-1} (no KCl) and 570 M^{-1} (100 mM KCl) – see Table 6.1. The Mg^{2+} affinity of CaM has also been estimated using the ligand interaction free energy values ($\Delta\Delta G_b$) obtained from the experiments on urea-unfolding of CaM in the presence of 10 mM $MgCl_2$ (Table 6.2). The average affinities estimated for the C- and N-domain in the presence of 70 mM KCl (I =100 mM) were: $K^{Mg}_{av(C)}$ = 166 M^{-1} and $K^{Mg}_{av(N)}$ = 390 M^{-1}. These values are in good agreement with those determined by direct titration. The average affinities obtained from the urea-unfolding experiments on the isolated domains (K^{Mg}_{av} = 778 M^{-1} (no KCl) and 467 M^{-1} (70 mM KCl, I = 100 mM) for Tr1C; K^{Mg}_{av} = 263 M^{-1} (no KCl) and 122 M^{-1} (70 mM KCl, I =100 mM) for Tr2C (Table 6.2)) also agree with the values determined for the corresponding domains in intact CaM by direct titrations and are in fair agreement with values reported by Tsai et al. (1987) and Malmendal et al. (1998) from NMR experiments.

The absorption, near-UV and far-UV CD spectra of CaM in the presence of Mg^{2+} reported here show that the binding of Mg^{2+} does not affect the secondary or tertiary structure of CaM. These results are consistent with several NMR studies in which it was concluded that the effects of Mg^{2+} on the structure of CaM are limited to the immediate vicinity of the metal-ion-binding site (Seamon, 1980; Ohki et al., 1997; Malmendal et al., 1999b). Thus, Mg^{2+} is thought not to induce the hydrophobic surface exposure which is characteristic of Ca^{2+} binding and which allows CaM to interact with target sequences (Crivici and Ikura, 1995). This hypothesis is supported by the observation that the hydrophobic probe TNS binds to Ca^{2+}-CaM (generating an intense fluorescence signal) but not to apo-CaM or to CaM in the presence of 10 mM $MgCl_2$ (Follenius and Gerard, 1984). Similarly, work in this laboratory has shown that the addition of Ca^{2+} to two dansyl maleimide labelled cysteine mutants of CaM (S38C and N111C) causes a large blue shift in the fluorescence signal of the probe, presumably

because the probe interacts with newly exposed hydrophobic surfaces on the protein. This effect is not observed upon Mg^{2+} binding.

The studies on the stability of CaM and its isolated domains have shown that both domains of CaM are, as expected, stabilised in the presence of Mg^{2+}. The increase in stability induced by the presence of 10 mM Mg^{2+} is ~ 1 kcal/mol for the C-domain and ~ 2 kcal/mol for the N-domain (in the absence of KCl), consistent with the N-domain binding Mg^{2+} with higher affinity than the C-domain. As for other forms of CaM (see Chapter 3), the unfolding curve for intact Mg^{2+}-CaM cannot be represented by the sum of the unfolding curves for Mg^{2+}-Tr1C and Mg^{2+}-Tr2C.

In conclusion, Mg^{2+} binds some three to five-fold more strongly to the N-domain than to the C-domain, whereas Ca^{2+} binds some eight-fold more strongly to the C-domain than to the N-domain. Thus, the ratio K^{Ca}_{av}/K^{Mg}_{av} is ~ 3000 for the C-domain, but only ~ 100 for the N-domain. The optical spectra of CaM in the presence of Mg^{2+} show that the effects of Mg^{2+}-binding are limited to the metal binding loop; there are no global conformational effects and no Mg^{2+}-induced hydrophobic exposure. At resting Ca^{2+} concentrations (~ 0.1 μM), intracellular concentrations of Mg^{2+} (1-5 mM) could stabilise the intrinsically unstable C-domain of CaM by up to ~ 0.7 kcal/mol.

6.4.2 Effects of Mg^{2+} on the binding of Ca^{2+} and of target sequences

The Ca^{2+} titrations performed with the chelator 5,5'-dibromo-BAPTA in the presence of Mg^{2+} have shown that the apparent Ca^{2+} affinity decreases as the Mg^{2+} concentration is increased. The average Ca^{2+} affinity in the presence of 5 mM Mg^{2+} is decreased by a factor of ~ 2.3 for the C-domain and by a factor of ~ 3 for the N-domain (Table 6.3). The average Mg^{2+} affinities, $K^{Mg}_{av(C)}$ and $K^{Mg}_{av(N)}$, calculated from these apparent Ca^{2+} affinities are in good agreement with the values obtained from the direct fluorescence titrations (Table 6.1) and from the urea-unfolding experiments (Table 6.2). Finally, the K^{Mg}_{av} values calculated from apparent Ca^{2+} affinities measured by direct fluorescence titrations of WT CaM and CaM(T26W) performed in the presence of 5 and 10 mM Mg^{2+} (Table 6.5) are also in good agreement with the values measured by direct methods. These observations suggest that the effects of Mg^{2+} are associated with direct competition with Ca^{2+} binding, as deduced from several NMR studies (Seamon,

1980; Tsai et al., 1987; Ohki et al., 1997; Ouyang and Vogel, 1998), rather than being the result of Mg^{2+} acting as an allosteric regulator (Milos et al., 1986; Gilli et al., 1998).

Table 6.5 Apparent stoichiometric binding constants for Ca^{2+} in the presence of Mg^{2+}

	Tyr-138		Trp-26	
$[Mg^{2+}]$ (mM)	$K^{Ca}_{av(C),app}$ [a] (M^{-1})	Calculated $K^{Mg}_{av(C)}$ [b] (M^{-1})	$K^{Ca}_{av(N),app}$ [a] (M^{-1})	Calculated $K^{Mg}_{av(N)}$ [b] (M^{-1})
0	$5.55 \cdot 10^5$	--	$4.67 \cdot 10^4$	--
5	$3.12 \cdot 10^5$	167	$9.90 \cdot 10^3$	745
10	$2.22 \cdot 10^5$	150	$5.52 \cdot 10^3$	748

The values in the Table are from experiments performed using the Tyr-138 fluorescence signal in WT CaM and the Trp-26 fluorescence signal in CaM(T26W) (Martin, S.R. et al., manuscript in preparation).

[a] $K^{Ca}_{av(C),app}$ and $K^{Ca}_{av(N),app}$ represent the average apparent Ca^{2+} affinities of the N- and C-domains in the presence of Mg^{2+}

[b] $K^{Mg}_{av(C)}$ and $K^{Mg}_{av(N)}$ were calculated from the values of $K^{Ca}_{av(C),app}$ and $K^{Ca}_{av(N),app}$ in the absence and in the presence of Mg^{2+} using Eq. 6.3 (Section 6.2).

6.4.2.1 Dependence of NM2 affinity on Ca^{2+} concentration

The CaM titrations performed in the absence of Mg^{2+} have shown that the affinity of CaM for NM2 decreases only slightly at low [Ca^{2+}] (see Table 6.4). The explanation for this observation is given in this section. The interaction of CaM with four Ca^{2+} ions and a target peptide P can be represented schematically as follows:

$$\begin{array}{ccc} CaM + 4Ca & \xleftrightarrow{K_1K_2K_3K_4} & Ca_4\text{-}CaM \\ + & & + \\ P & & P \\ K_p \updownarrow & & \updownarrow K_{p,4} \\ CaM\text{-}P + 4Ca & \xleftrightarrow{K_{1,p}K_{2,p}K_{3,p}K_{4,p}} & Ca_4\text{-}CaM\text{-}P \end{array}$$

where K_1, K_2, K_3, and K_4 are the stoichiometric association constants for Ca^{2+} binding in the absence of the peptide, $K_{1,p}$, $K_{2,p}$, $K_{3,p}$, and $K_{4,p}$ are the stoichiometric association constants for Ca^{2+} binding to CaM with a peptide bound, K_p is the association constant for the binding of the peptide to apo-CaM, and $K_{p,4}$ is the association constant for the binding of the peptide to Ca_4-CaM. The stoichiometric association constants for Ca^{2+} binding in the presence of the peptide can also be expressed as:

$$K_{i,p} = f_i K_i \qquad \text{(where i = 1-4)}$$

where f_i is the factor which defines the effect of the peptide on the stoichiometric association constant for the i^{th} calcium (note that for a Ca^{2+} independent interaction, $f_1 = f_2 = f_3 = f_4 = 1$, and $K_{p,4} = K_p$). The apparent affinity of the peptide in the presence of different free [Ca^{2+}] is given by:

$$K_{p,4,app} = K_p \frac{1 + f_1K_1[Ca] + f_1f_2K_1K_2[Ca]^2 + f_1f_2f_3K_1K_2K_3[Ca]^3}{1 + K_1[Ca] + K_1K_2[Ca]^2 + K_1K_2K_3[Ca]^3 + K_1K_2K_3K_4[Ca]^4} + \tag{6.4}$$

$$+K_p \frac{f_1f_2f_3f_4K_1K_2K_3K_4[Ca]^4}{1 + K_1[Ca] + K_1K_2[Ca]^2 + K_1K_2K_3[Ca]^3 + K_1K_2K_3K_4[Ca]^4}$$

When [Ca] $\rightarrow \infty$ then $K_{p,4,app} = f_1f_2f_3f_4K_p = K_{p,4}$, but at low [$Ca^{2+}$] the apparent affinity will be less than $K_{p,4}$. Values of the stoichiometric Ca^{2+} binding constants measured in the presence of NM2 (in 100 mM KCl) suggest that the appropriate enhancement factors for this particular target are approximately:

$$f_1 \sim 10 \qquad f_2 \sim 10 \qquad f_3 \sim 3 \qquad f_4 \sim 3$$

(unpublished results from this laboratory). These factors indicate that the effect of the NM2 peptide on Ca^{2+} affinity is higher for the C-domain (f_1 and f_2) than for the N-domain (f_3 and f_4). Also, since $f_1f_2f_3f_4 \sim 1000$, the association constant for binding of NM2 to Ca_4-CaM is predicted to be:

$$K_{p,4} = f_1f_2f_3f_4\,K_p \sim 1000\,K_p$$

The K_d measured in this work for the binding of NM2 to CaM in the presence of 100 μM Ca^{2+} (in 100 mM KCl) is ~ 30 nM (Table 6.4). This value can be compared with that of ~ 39 μM obtained in this laboratory for the binding of NM2 to apo-CaM (in 100 mM KCl) (Martin, S.R. and Bayley, P.M., manuscript in preparation). These affinities differ by a factor ~ 1000, in very good agreement with the above prediction.

Thus, Equation (6.4) can be used to calculate the apparent affinity of CaM for NM2 as a function of the free Ca^{2+} concentration. The results of these calculations are presented in Table 6.6. The K_d values (= $1/K_{p,4,app}$) show little variation as [Ca^{2+}] is decreased from 100 μM to 40 μM. At lower [Ca^{2+}] (10-20 μM), the peptide affinity is reduced by a factor ~ 2-3 and substantial reductions are observed only at [Ca^{2+}] ~ 2-5 μM. These results are in good qualitative agreement with the measured NM2 affinity (Table 6.4), which is reduced by a factor of ~ 2 when the total Ca^{2+} concentration is lowered from 100 μM to 10 μM (corresponding to ~ 5 μM free Ca^{2+}).

A calculation of the concentrations of the species populated at 10 μM total Ca^{2+} shows that CaM (1.5-2 μM) is mostly present as Ca_2-CaM and Ca_4-CaM, with the C-domain mostly Ca^{2+}-saturated and the N-domain Ca^{2+}-free in ~ 50% of the molecules. The fact that at this Ca^{2+} concentration the affinity for NM2 is only 2-fold lower than at higher [Ca^{2+}] suggests that the affinity of CaM for NM2 is not much affected by the absence of Ca^{2+} from the N-domain and therefore that the interaction between CaM and the peptide occurs mainly with the C-domain of CaM. The situation with a peptide that interacted primarily with the N-domain of CaM would clearly be very different.

Table 6.6 Calculated dissociation constants for the binding of NM2 to CaM in the absence and in the presence of 5 mM Mg^{2+}

	no Mg^{2+}	+ 5 mM Mg^{2}
$[Ca^{2+}_{free}]$ (μM)	$K_{d,app}$ [a] (nM)	$K_{d,app}$ [b] (nM)
100	46	52
80	47	55
60	48	62
40	53	80
20	71	147
10	125	286
5	247	536
2	581	1618

[a] These K_d values were calculated using Eq. (6.4) and the following values: $K_1 = 2 \cdot 10^5\ M^{-1}$, $K_2 = 2 \cdot 10^6\ M^{-1}$, $K_3 = 2 \cdot 10^4\ M^{-1}$, $K_4 = 2 \cdot 10^5\ M^{-1}$ (Bayley et al., 1996), $f_1 = f_2 = 10$, $f_3 = f_4 = 3$, $K_p = 2.56 \cdot 10^4\ M^{-1}$ (Martin, S.R. and Bayley, P.M., manuscript in preparation).

[b] These K_d values were calculated using Eq. (6.5) and the following values: $K^*_1 = 1110\ M^{-1}$, K^*_2 393= M^{-1}, $K^*_3 = 164\ M^{-1}$, $K^*_4 = 58\ M^{-1}$, $K^*_{1(1)} = 0.75\ K^*_1$, $K^*_{2(1)} = 0.66\ K^*_2$, $K^*_{3(1)} = 0.5\ K^*_3$, $K^*_{1(2)} = 0.5\ K^*_1$, $K^*_{1(3)} = 0.25\ K^*_1$, $K^*_{2(2)} = 0.33\ K^*_2$; the other constants are defined as above.

6.4.2.2 NM2 affinity in the presence of Ca^{2+} and Mg^{2+}

The results of the titrations of NM2 with CaM in the presence of 5 mM Mg^{2+} have shown that, in the absence of Ca^{2+} (at low ionic strength), Mg^{2+} has the effect of decreasing the affinity for NM2 by a factor of ~ 15. As noted above, this is only partly attributable to the effect of Mg^{2+} in increasing the ionic strength. Since Mg^{2+} does not induce the hydrophobic exposure caused by Ca^{2+} binding, the interaction with NM2 is probably primarily electrostatic in nature, and the additional effect of Mg^{2+} may therefore be related to neutralisation of charged groups important in this interaction.

In the presence of 100 mM KCl, Mg^{2+} induces a reduction in the affinity for NM2 at all Ca^{2+} concentrations studied (see Table 6.4). These observations are in agreement with those of Ohki et al. (1993 and 1997), who showed that Mg^{2+} inhibits the formation of the complex of CaM with target molecules at low Ca^{2+} concentration, suggesting that Mg^{2+} could, therefore, have important physiological effects. However, it should be noted that the effect of Mg^{2+} on NM2 affinity under near physiological conditions (100 mM KCl) is relatively small, since the affinity of CaM for the peptide is reduced by only a factor of ~ 2 even at low, physiologically relevant, Ca^{2+} concentrations. Why does the presence of Mg^{2+} have such a small effect?

The effect of Mg^{2+} may be predicted using the following theoretical approach. The apparent association constant for the binding of a peptide to CaM in the presence of Ca^{2+} and Mg^{2+} is:

$$K_{p,app} = \frac{[CaM - P]}{[CaM][P]}$$

where CaM-P and CaM represent the sums of all calmodulin species with and without the peptide bound, respectively. This apparent association constant can be expressed as:

$$K_{p,app} = K_p \frac{a}{b} \qquad (6.5)$$

where K_p is the association constant for the interaction with apo-CaM and

$$\begin{aligned} a = {} & 1 + f_1K_1[Ca] + f_1f_2K_1K_2[Ca]^2 + f_1f_2f_3K_1K_2K_3[Ca]^3 + f_1f_2f_3f_4K_1K_2K_3K_4[Ca]^4 + \\ & + K^*_1[Mg] + K^*_1K^*_2[Mg]^2 + K^*_1K^*_2K^*_3[Mg]^3 + K^*_1K^*_2K^*_3K^*_4[Mg]^4 + \\ & + f_1K_1K^*_{1(1)}[Ca][Mg] + f_1K_1K^*_{1(1)}K^*_{2(1)}[Ca][Mg]^2 + \end{aligned}$$

$$+ f_1K_1K^*_{1(1)}K^*_{2(1)}K^*_{3(1)}\,[Ca][Mg]^3 + f_1f_2K_1K_2K^*_{1(2)}\,[Ca]^2[Mg] +$$
$$+ f_1f_2K_1K_2K^*_{1(2)}K^*_{2(2)}\,[Ca]^2[Mg]^2 + f_1f_2\,f_3K_1K_2K_3K^*_{1(3)}\,[Ca]^3[Mg]$$

$$\begin{aligned} b = {} & 1 + K_1\,[Ca] + K_1K_2\,[Ca]^2 + K_1K_2K_3\,[Ca]^3 + K_1K_2K_3K_4\,[Ca]^4 + K^*_1\,[Mg] + \\ & + K^*_1K^*_2\,[Mg]^2 + K^*_1K^*_2K^*_3\,[Mg]^3 + K^*_1K^*_2K^*_3K^*_4\,[Mg]^4 + \\ & + K_1K^*_{1(1)}\,[Ca][Mg] + K_1K^*_{1(1)}K^*_{2(1)}\,[Ca][Mg]^2 + \\ & + K_1K^*_{1(1)}K^*_{2(1)}K^*_{3(1)}\,[Ca][Mg]^3 + K_1K_2K^*_{1(2)}\,[Ca]^2[Mg] + \\ & + K_1K_2K^*_{1(2)}K^*_{2(2)}\,[Ca]^2[Mg]^2 + K_1K_2K_3K^*_{1(3)}\,[Ca]^3[Mg] \end{aligned}$$

K_1, K_2, K_3, and K_4 are the stoichiometric association constants for the binding of Ca^{2+} to CaM; f_1, f_2, f_3, and f_4 are the factors which define the effect of the presence of the peptide on the Ca^{2+} affinity; K^*_1, K^*_2, K^*_3, and K^*_4 are the stoichiometric association constants for the binding of Mg^{2+} to CaM; and $K^*_{x(y)}$ is the stoichiometric association constant for the binding of the x^{th} Mg^{2+} ion to CaM with y Ca^{2+} ions bound. For simplicity, the affinity of CaM for Mg^{2+} is assumed not to depend on whether or not the peptide is bound.

Equation (6.5) has been used to calculate the apparent affinity of CaM for NM2 in the presence of 5 mM Mg^{2+} and at different free Ca^{2+} concentrations. The stoichiometric association constants for Mg^{2+} binding have been estimated in the following way. The K^{Mg}_{av} values for the N- and C-domains obtained from urea-denaturation or Tyr-138 fluorescence experiments (see Sections 6.3.2 and 6.3.3) are ~ 390 M^{-1} (N-domain) and ~ 165 M^{-1} (C-domain). If there is no Mg^{2+}-Mg^{2+} cooperativity (Malmendal et al., 1998) and assuming, for simplicity, that the two sites in a domain have the same affinity for Mg^{2+}, then

$$K^{Mg}_{av(N)} = (k^*_Ik^*_{II})^{1/2} \quad \text{and} \quad k^*_I = k^*_{II} = 390\ M^{-1}$$
$$K^{Mg}_{av(C)} = (k^*_{III}k^*_{IV})^{1/2} \quad \text{and} \quad k^*_{III} = k^*_{IV} = 165\ M^{-1}$$

The stoichiometric association constants K^*_1, K^*_2, K^*_3, and K^*_4 can then be calculated using the equations which define the relationship between the stoichiometric and the intrinsic association constants (see Section 2.3.1.1). The following values have been obtained:

$$K^*_1 = 1110\ M^{-1} \qquad K^*_3 = 164\ M^{-1}$$
$$K^*_2 = 393\ M^{-1} \qquad K^*_4 = 58\ M^{-1}$$

The stoichiometric constants for binding of Mg^{2+} to CaM species containing one to three calcium ions have been estimated using the appropriate statistical factors as:

$$K^*_{1(1)} = 0.75\ K^*_1 \qquad K^*_{1(2)} = 0.5\ K^*_1$$
$$K^*_{2(1)} = 0.66\ K^*_2 \qquad K^*_{1(3)} = 0.25\ K^*_1$$
$$K^*_{3(1)} = 0.5\ K^*_3 \qquad K^*_{2(2)} = 0.33\ K^*_2$$

The K_d values ($1/K_{p,app}$) calculated using Eq. (6.5) are reported in Table 6.6 and show that, at free Ca^{2+} concentrations in the range 100-60 μM, the affinity for the peptide is not much affected by the presence of 5 mM Mg^{2+}. For free Ca^{2+} concentrations in the range 40-5 μM, the affinity is reduced by a factor of ~ 2 and only at $[Ca^{2+}]$ lower than 1 μM is it reduced significantly. These calculations reproduce closely the situation observed experimentally with the binding of CaM to NM2. The effects of Mg^{2+} on this particular target peptide are small because it interacts predominantly with the C-domain of CaM. Once again, the situation would be expected to be very different for a target sequence which interacted predominantly with the N-domain of CaM.

CHAPTER 7

GENERAL CONCLUSIONS

In this work, the thermodynamic stability of CaM and its isolated domains has been investigated using the optical spectroscopic techniques absorption, fluorescence, and far- and near-UV CD (Chapters 3 and 4). The effects of binding of ligands such as calcium, magnesium, and target protein sequences on the stability of CaM have been studied and rationalised (Chapters 3 and 6). The problems of the relative stability of the N- and C-domains and of the effects of single mutations on the folding and Ca^{2+} binding properties of CaM have also been addressed (Chapter 5). The results are discussed in detail in the Discussion sections of each Chapter. The general features and conclusions are summarised here.

7.1 Thermodynamic stability of the apo-proteins

The unfolding of CaM and its tryptic fragments has been investigated under a variety of different solvent conditions. Thermal and chemical denaturation experiments have permitted a quantitative analysis of the thermodynamic stability of these proteins. The results have shown that, in the absence of calcium, the stability of CaM and its

isolated domains is very low ($\Delta G°_{20}$ ~ 2-3 kcal/mol) and depends strongly on environmental factors, such as temperature and ionic strength (see Chapters 3 and 4).

As concluded in several previous studies (by thermal denaturation), the results have also indicated that the N- and C-domains of CaM have different stabilities, in spite of their high sequence homology and structural similarity. The $\Delta G°_{20}$ values obtained from thermal and chemical unfolding experiments have shown that in intact apo-CaM the N-domain is approximately 2 kcal/mol more stable than the C-domain. This difference becomes particularly important under near physiological conditions (37 °C, 100 mM KCl, pH 8.0), where the C-domain of apo-CaM is approximately 24% unfolded, while the N-domain is less than 2% unfolded. This observation was very surprising and suggested the possibility that the C-domain of apo-CaM might be stabilised *in vivo*, at resting calcium concentrations (~ 0.1 μM), by interactions with other ligands or target proteins. Such interactions would reduce the susceptibility to proteolytic cleavage. In this work, urea unfolding experiments performed in the presence of magnesium or of a target peptide have shown that the interaction with these ligands could possibly provide a means of stabilisation for both domains of apo-CaM (see below). It has been suggested that the low stability and high flexibility of the C-domain of apo-CaM may be important in providing a structural basis for the higher affinity of this domain for Ca^{2+} and for target sequences (Zhang and Yuan, 1998).

Thermal and urea denaturation experiments have shown that the stability of apo-CaM and its domains is further reduced under low ionic strength conditions. Both domains are significantly unfolded at low KCl concentration and an increase in ionic strength can refold the proteins. The stabilising effect of KCl can, under certain denaturing conditions, induce as much as 80% refolding of the C-domain of apo-CaM. This enhancement in protein stability by increasing ionic strength is probably due to screening of the negative charges present on the surface of apo-CaM. Repulsive interactions between acidic residues (CaM has a large overall negative charge at neutral pH) may in fact be the cause of the low stability of CaM in the absence of calcium. In order to test this hypothesis, it would be interesting to characterise the stability of apo-CaM at lower pH values. Unfortunately, CaM cannot be studied in the pH range in which the acidic residues are usually protonated (the intrinsic pK_a values for Asp and Glu are 3.9 and 4.3), owing to aggregation problems. The results of chemical and thermal denaturation experiments performed in this work with apo- and holo-CaM at

pH 8.0 and 6.5 show that the stabilities of these proteins are essentially the same in this limited pH range (see Chapter 4).

As noted above, the thermodynamic stability of apo-CaM has been investigated using both thermal and chemical unfolding, employing the denaturants urea and GuHCl. The results obtained using these methods are consistent within experimental error. The chemical unfolding data have been analysed using the Linear Extrapolation Method (LEM, see Chapter 2), and the choice of this model is supported by the good agreement between thermal and chemical unfolding data. However, the thermal unfolding results for apo-CaM and its domains agree slightly better with the data obtained using urea, than with those obtained using GuHCl.

Differences in the parameters obtained with urea and GuHCl have been observed both in the absence and in the presence of calcium and are particularly marked in the latter case. Investigations into the properties of these two denaturants have shown that the behaviour of GuHCl is much more complex than that of urea. Firstly, due to the charged nature of GuHCl, low (non-denaturing) concentrations of this denaturant actually increase the stability of apo-CaM and its domains, exerting an effect similar to that observed with KCl. As a consequence, the stability of the apo-proteins measured using GuHCl is higher than that measured using urea. Secondly, GuHCl dramatically reduces the calcium affinity of CaM and its fragments. Experiments performed with GuHCl and KCl have indicated that this effect is only partly attributable to increased ionic strength and that there must be some direct competition between GuHCl and calcium binding. Low concentrations of urea have been shown to have a negligible effect on the calcium affinity of CaM. Therefore, the use of urea as a denaturant is more appropriate in the study of the stability of CaM and of other proteins that bind metal ions or that are sensitive to changes in the ionic strength of the solution.

7.2 Ligand binding

According to the ligand binding theory (Schellman, 1975), the binding of a ligand which interacts more strongly with the native state than with the denatured state of a protein stabilises the folded structure of the protein. In this work, this effect has

been measured for CaM in the presence of calcium, magnesium, and of the target peptide FFF_u from the CaM binding sequence of skeletal muscle myosin light chain kinase (see Chapters 3 and 6). In all of these cases, in agreement with the theory, the extent of stabilisation induced by binding of the ligand depends on the following parameters: a) the ligand affinities of the native and denatured states of CaM, and b) the free ligand concentration (see Chapter 2). This is true regardless of the saturation state of the protein; that is, the apparent stability of the protein is increased by the presence of the ligand whether the protein is fully saturated or not, and the effect is also present at ligand concentrations above those required for complete saturation. The ligand concentration at which the stabilising effect saturates is determined by the affinities of the native and denatured states for the ligand. This concept is very important in the study of the stability of proteins interacting with ligands, because very rarely is the free ligand concentration taken into account. Generally, the protein under study is simply referred to as "holo", without considering that its stability must vary dramatically with changes in the free ligand concentration.

7.2.1 Calcium

The thermodynamic stability of CaM and its isolated domains has been investigated as a function of calcium concentration. As expected, in the presence of calcium, these proteins are considerably more stable than in the apo state. In agreement with several previous reports, thermal unfolding studies have shown that the effect of calcium on the thermal stability of CaM is such that the melting temperatures of both domains are increased from 46-60 °C (apo-forms) to greater than 80 °C even at relatively low calcium concentrations. The stabilities of the holo-proteins have therefore been assessed using urea and GuHCl denaturation methods.

As observed for the apo-proteins, the N- and C-terminal domains of holo-CaM have different stabilities. However, in the presence of calcium ($\geq$ 0.3 mM) the order of unfolding of the domains is reversed, so that the C-domain is more stable than the N-domain. The greater effect of calcium on the C-domain is due to the significantly higher affinity of this domain for calcium (see Chapter 1). At the calcium concentrations used in this study, the observed increase in the apparent stability of CaM

domains induced by calcium (i.e. the ligand interaction free energy) varies from 1-3 kcal/mol (0.3-1 mM calcium) to ~ 8 kcal/mol (100 mM calcium).

A comparison between the values of ligand interaction free energy determined experimentally and those calculated theoretically, assuming that calcium binding to the denatured state of CaM is negligible, has shown that the stabilising effect of calcium is much lower than predicted. Calcium titrations in the presence of denaturants have demonstrated that the reasons for this observation are that a) calcium binding to the denatured state of CaM becomes significant (K' ~ 50 M^{-1}) at high calcium concentrations, thus reducing the extent of stabilisation of the native state; and b) the calcium affinity of native CaM is strongly affected by the presence of denaturants (GuHCl in particular, see above). Thus, especially when measured using GuHCl, the values of free energy of unfolding obtained for CaM and its fragments in the presence of calcium are underestimates of the actual stabilities of these proteins.

The reactions of refolding and unfolding of CaM have also been studied kinetically as a function of calcium and denaturant concentration (see Chapter 3). The results indicate that the rate constants of unfolding and refolding in, for example, 3.4 M urea, are > 10^4 s^{-1} and > 1000 s^{-1}, respectively.

7.2.2 Magnesium

The interaction of CaM with magnesium has been investigated using optical spectroscopic techniques (see Chapter 6). In agreement with previous NMR studies, the results have shown that the binding of magnesium does not induce the conformational change and the exposure of hydrophobic surfaces observed upon calcium binding and that the effects of magnesium are localised in the metal binding loops. Thus, the secondary and tertiary structures of Mg^{2+}-CaM, assessed by far- and near-UV CD, and absorption spectroscopy, appear to be very similar to those of apo-CaM.

The affinity of CaM and its isolated domains for magnesium has been measured by direct fluorometric titration and using the ligand interaction free energy values obtained from urea unfolding experiments. The results are in good agreement and indicate that the average Mg^{2+} affinity of the N-domain is three to five-fold higher than that of the C-domain (~ 570 and 175 M^{-1}, respectively, in 100 mM KCl). This is the opposite of the situation with calcium, since the Ca^{2+} affinity of the C-domain is ~ 6

fold higher than that of the N-domain. The results also indicate that magnesium binds to the same sites as calcium and competes directly with calcium binding, thus reducing the calcium affinity of both domains. The effect is greater for the N-domain, since its calcium affinity is lower and the magnesium affinity is higher than that of the C-domain. Thus, magnesium increases the intrinsic differences in the calcium binding properties of the two domains.

The studies on the conformational stability of CaM in the presence of 10 mM Mg^{2+} have shown that the interaction with Mg^{2+} does stabilise the protein, as expected from the theory of ligand binding. Because of the relative Mg^{2+}-affinities of the N- and C-domains, the stabilising effect is larger for the N-domain than for the C-domain and thus the order of unfolding of the domains remains the same as that in apo-CaM, with the N-domain more stable than the C-domain. A schematic representation of the urea-induced unfolding of the N- and C-terminal domains of intact CaM under different solvent conditions (apo, Ca^{2+}-loaded, and Mg^{2+}-loaded) is shown in Figure 7.1. In the absence of calcium, at 20 °C, 5 mM Mg^{2+} increases the stability of the N- and C-domains by ~ 1.3 and 0.7 kcal/mol, respectively. Thus, magnesium could indeed stabilise apo-CaM and in particular the intrinsically unstable C-domain *in vivo*.

7.2.3 Target sequences

Urea unfolding experiments performed with the peptide FFF_u from the CaM binding region of sk-MLCK have shown that the interaction of CaM with a target sequence stabilises the protein, as observed for the other ligands studied in this work. The ligand interaction free energy measured for the C-domain of apo-CaM in the presence of 28 μM free peptide, at low ionic strength, is approximately 1.3 kcal/mol. Consistent with the theory, the extent of stabilisation induced by interaction with the peptide depends on the free peptide concentration and on the affinity of CaM for the peptide.

The affinity of CaM for target sequences is generally strongly dependent on ionic strength and on the ionic composition of the solvent. In the case of Ca^{2+}-dependent target interactions, the increase in target affinity induced by the presence of calcium is dramatic and can be of more than six orders of magnitude (e.g. the affinity for the peptide WFF is increased by a factor of ~ 10^7 in the presence of calcium). A

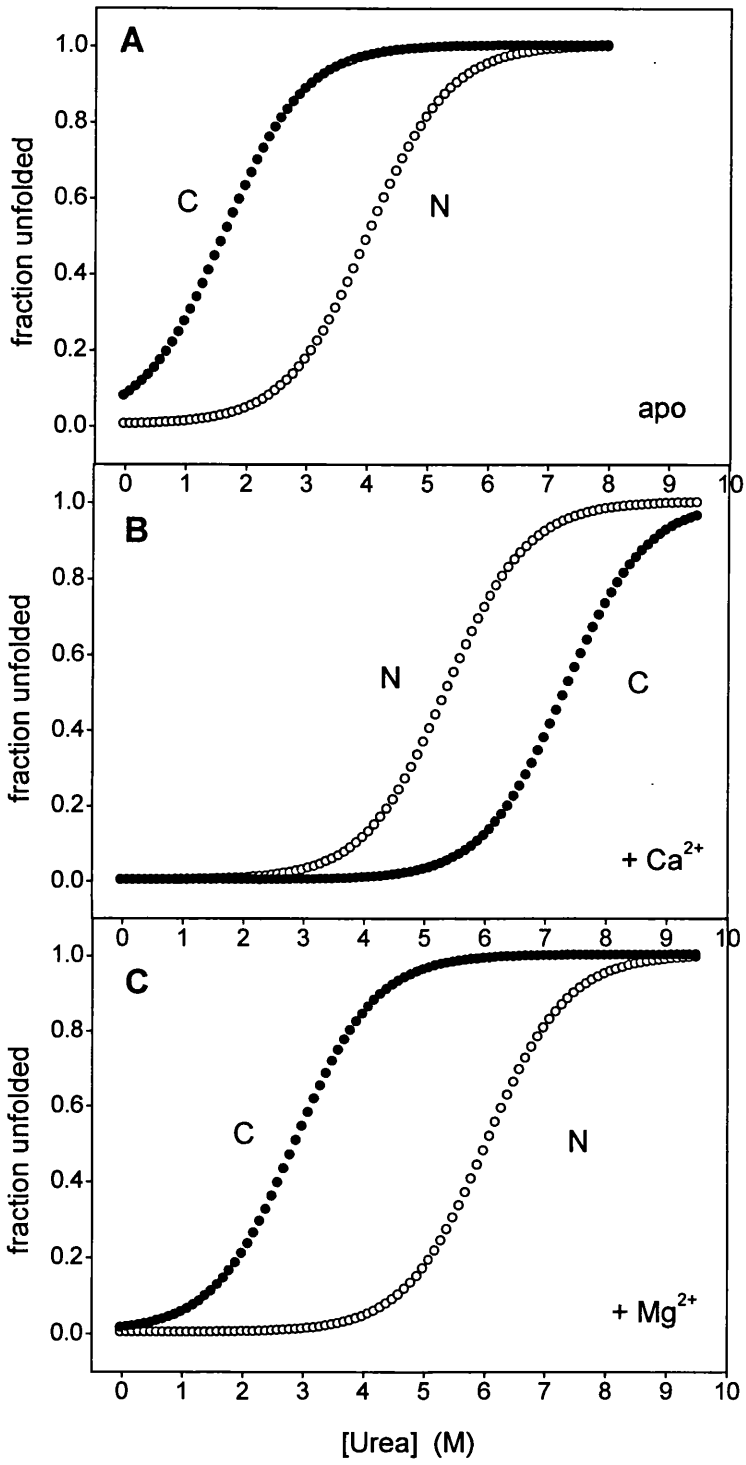

Figure 7.1 Fractions of unfolded protein for the N- (○) and C- (●) terminal domains of intact CaM as a function of urea concentration, under the following conditions: (**A**) apo-protein, (**B**) 0.3 mM Ca^{2+}, (**C**) 10 mM Mg^{2+}. The curves were calculated using the data of Tables 3.1 and 3.4 in Chapter 3, and 6.2 in Chapter 6.

different situation is observed for targets which show similar affinity for apo- and Ca^{2+}-CaM, such as neuromodulin.

In this work, the interaction of CaM with the peptide NM2, derived from the CaM binding region of neuromodulin, has been investigated under different solvent conditions (see Chapter 6). In the presence of saturating calcium concentrations, the affinity of CaM for NM2 is approximately 30 nM (at physiological ionic strength) and, as expected, it decreases as $[Ca^{2+}]$ is decreased. However, the results have shown that significant reductions in the NM2 affinity are only observed when $[Ca^{2+}]$ is lowered to 1-2 μM, close to intracellular $[Ca^{2+}]$ under conditions of stimulation. This observation is consistent with the interaction CaM-NM2 occurring mainly through the C-domain of CaM, which has higher Ca^{2+}-affinity than the N-domain. The situation would be different in the case of a target sequence interacting preferentially with the N-domain. It is thus important to note that the apparent target affinity of CaM measured *in vitro* depends strongly on calcium concentration just as the apparent calcium affinity depends on peptide and CaM concentrations. The affinity of CaM for the target *in vivo* is probably significantly lower than that measured under "normal" *in vitro* conditions.

In the presence of physiological concentrations of magnesium, the affinity of CaM for NM2 is slightly reduced. The results suggest that the reason for this observation is the direct competition of Mg^{2+} with Ca^{2+}-binding, rather than a specific effect of Mg^{2+} on the interaction with the target. This competition is more effective for the N-domain than for the C-domain, owing to the differential calcium and magnesium affinities of the two domains. As a consequence, magnesium enhances the difference in affinity of the N- and C-domains for NM2, by reducing the peptide affinity of the N-domain more than that of the C-domain. The small effect of magnesium on the affinity of Ca^{2+}-CaM for NM2 is therefore consistent with NM2 interacting mainly with the C-domain. Thus, the extent of the reduction in affinity of Ca^{2+}-CaM for a target sequence caused by magnesium reflects the mode of binding to the target. A strong reduction in affinity implies that the N-domain of CaM is involved in the interaction with the target, while a small effect of magnesium indicates that the interaction occurs predominantly through the C-domain.

These observations suggest a possible mechanism of interaction of CaM with targets which bind preferentially to the C-domain of CaM. As was previously proposed (Bayley et al., 1996), under resting calcium concentrations, a crucial role in target

binding and activation could be played by the species Ca_2-CaM, in which only the C-domain is Ca^{2+}-loaded and possibly bound to the enzyme. Under these conditions, the N-domain would be calcium-free and not bound to the target. The results of this work support this model and show that magnesium could have a significant role in modulating the relative affinities of the two domains for a target sequence.

7.3 Interdomain interactions

A surprising result obtained from the denaturation studies of CaM and its tryptic fragments is that the stabilities of the isolated domains are different from those of the corresponding domains in intact CaM. This has been observed for all CaM species studied, i.e. apo-CaM, Ca^{2+}-CaM, and Mg^{2+}-CaM (see Chapters 3 and 6). In the case of apo-CaM, for example, the C-domain is less stable than Tr2C, whilst the N-domain is more stable than Tr1C. The same pattern has been found in the presence of magnesium. In the case of Ca^{2+}-loaded proteins, the order of unfolding of the domains is reversed and now it is the N-domain which is less stable than Tr1C, whilst the C-domain is more stable than Tr2C. Thus, interestingly, whichever domain unfolds first in intact CaM is destabilised compared to the corresponding isolated fragment, whilst the domain which unfolds second is stabilised compared to the isolated fragment. The same effects have been obtained using both thermal and chemical denaturation. These results therefore show that this is a general phenomenon which is not specifically related to the ionic composition of the solvent, nor to the conformation of CaM (which changes significantly in the absence and the presence of calcium), or to the technique employed to monitor the unfolding reaction.

A consequence of these observations is that the difference in stability between the N- and C-domains of CaM is smaller for the isolated domains than for the domains in intact CaM. The free energies of unfolding for apo-Tr1C and apo-Tr2C, for example, differ by ~ 1 kcal/mol, whereas the stabilities of the domains in intact apo-CaM differ by ~ 2 kcal/mol. Thus, the intrinsic stabilities of the two domains are similar, as might be expected given their structural homology, but the difference between their folding properties is enhanced in the intact protein.

These results strongly suggest that interactions exist between the N- and C-domains of CaM during unfolding. In particular, in order to explain the specific patterns obtained for the stabilities of the individual domains, it is necessary to postulate the existence of an intermediate state during unfolding, in which one domain in the unfolded state interacts with the other domain in the folded state. Such interaction would in fact increase the stability of one domain and, at the same time, decrease that of the other domain. This interaction could be hydrophobic in nature and occur between the solvent-exposed hydrophobic surfaces on the folded domain and the hydrophobic residues which become exposed upon unfolding. However, the fact that the same effect is also observed with apo- and Mg^{2+}-CaM, in which the exposure of hydrophobic surfaces is known to be small, suggests that the mechanism of interaction could be more complex.

The hypothesis of inter-domain interactions has also been confirmed by the studies on the stability and calcium binding properties of the β-sheet mutants of CaM (see Chapter 5). These mutants effectively mimic the situation occurring during the unfolding of WT CaM, in that, in the absence of calcium, the domain carrying the mutation is more than 50% unfolded in all cases, while the non-mutated domain retains the native-like fold. A first observation, then, is that the replacement of the hydrophobic residue at position 8 in the calcium-binding loops by either Gly, Pro, or Ala dramatically reduces the stability of the domain containing the mutation, causing its partial or complete unfolding. This indicates that the role of this residue in each EF-hand of CaM is crucial for the interior packing and the stability of the domain. The binding of calcium increases the stability of both domains and, in most cases, restores at least part of the native-like structure of the mutated domain. In addition, the results have shown that the presence of the unfolded domain affects the stability and the calcium affinity of the non-mutated domain. In particular, the non-mutated domain, either N- or C-terminal, appears to be more stable than the corresponding fragment of WT CaM and to bind calcium with higher affinity than that of the corresponding domain of WT CaM. These observations support the model of inter-domain interactions occurring in the partially unfolded state of CaM, between one folded and one unfolded domain.

In conclusion, these studies have indicated that CaM is a protein of low intrinsic stability, and thus is liable to major perturbation of its unfolding properties by environmental factors, such as ionic strength and temperature, by the ionic composition of the solvent, and by mutation. In particular, the differential affinities of the two domains of CaM for the ligands calcium and magnesium have been shown to play an essential role in modulating CaM's interactions with target sequences. Moreover, although the domains are largely independent, significant inter-domain interactions have been detected during the process of unfolding, which affect the stability of both domains.

These physical properties of CaM relate to the general questions of the thermodynamic coupling of ligand binding and stability and of the stability of a sub-domain relative to that of the whole protein in multi-domain proteins. Intensive investigation of the unfolding reactions of small globular proteins has shown that the unfolding process with these proteins closely approximates to a two state transition, which is usually highly cooperative. In general, this mechanism cannot be applied to the study of the stability of multimeric proteins, which presents several problems. In this respect, CaM represents an interesting system, because although the high independence of the two domains permits the assessment of their stability as autonomous folding units, the use of the model of two two-state unfolding transitions permits the detection of interdomain interactions in the intact protein. The results of this work illustrate general features which could be relevant to the study of folding and stability of other proteins.

BIBLIOGRAPHY

Akke, M., and Forsén, S. (1990). Protein stability and electrostatic interactions between solvent exposed charged side chains. *Proteins: Struct. Funct. Genet. 8*, 23-29.

Alexander, A., Cimler, B. M., Meier, K. E., and Storm, D. R. (1987). Regulation of calmodulin binding to P-57, a neurospecific calmodulin binding protein. *J. Biol. Chem. 262*, 6108-6113.

Andersson, M., Malmendal, A., Linse, S., Ivarsson, I., Forsén, S., and Svensson, L. A. (1997). Structural basis for the negative allostery between Ca^{2+}- and Mg^{2+}-binding in the intracellular Ca^{2+}-receptor calbindin D_{9k}. *Protein Sci. 6*, 1139-1147.

Anfinsen, C. B. (1973). Principles that govern the folding of protein chains. *Science 181*, 223-230.

Aune, K. C., and Tanford, C. (1969). Thermodynamics of the denaturation of lysozyme by guanidine hydrochloride. II. Dependence on denaturant concentration at 25 °C. *Biochemistry 8*, 4586-4590.

Babu, Y. S., Bugg, C. E., and Cook, W. J. (1988). Structure of calmodulin refined at 2.2 Angstrom resolution. *J. Mol. Biol. 204*, 191-204.

Babu, Y. S., Sack, J. S., Greenhough, T. J., Bugg, C. E., Means, A. R., and Cook, W. J. (1985). Three-dimensional structure of calmodulin. *Nature 315*, 37-40.

Barbato, G., Ikura, M., Kay, L. E., Pastor, R. W., and Bax, A. (1992). Backbone dynamics of calmodulin studied by ^{15}N relaxation using inverse detected two-dimensional NMR spectroscopy: the central helix is flexible. *Biochemistry 31*, 5269-5278.

Barth, A., Martin, S. R., and Bayley, P. M. (1998). Specificity and symmetry in the interaction of calmodulin domains with the skeletal muscle myosin light chain kinase target sequence. *J. Biol. Chem. 273*, 2174-2183.

Baudier, J., Deloulme, J. C., Dorsselaer, A. V., Black, D., and Matthes, H. W. (1991). Purification and characterization of a brain-specific protein kinase C substrate, neurogranin (p17). Identification of a consensus amino acid sequence between neurogranin and neuromodulin (GAP43) that corresponds to the protein kinase

C phosphorylation site and the calmodulin-binding domain. *J. Biol. Chem. 266*, 229-237.

Bayley, P. M., Findlay, W. A., and Martin, S. R. (1996). Target recognition by calmodulin: dissecting the kinetics and affinity of interaction using short peptide sequences. *Protein Sci. 5*, 1215-1228.

Bayley, P. M., and Martin, S. R. (1992). The α-helical content of calmodulin is increased by solution conditions favouring protein crystallisation. *Biochem. Biophys. Acta 1160*, 16-21.

Beckingham, K. (1991). Use of site-directed mutations in the individual calcium-binding sites of calmodulin to examine calcium-induced conformational changes. *J. Biol. Chem. 266*, 6027-6030.

Berridge, M. J., Bootman, M. D., and Lipp, P. (1998). Calcium - a life and death signal. *Nature 395*, 645-649.

Borin, G., Ruzza, P., Rossi, M., Calderan, A., Marchiori, F., and Peggion, E. (1989). Conformation and ion-binding properties of peptides related to calcium binding domain III of bovine brain calmodulin. *Biopolymers 28*, 353-369.

Browne, J. P., Strom, M., Martin, S. R., and Bayley, P. M. (1997). The role of β-sheet interactions in domain stability, folding and target recognition reactions of calmodulin. *Biochemistry 36*, 9550-9561.

Brzeska, H., Venyaminov, S. V., Grabarek, Z., and Drabikowski, W. (1983). Comparative studies on thermostability of calmodulin, skeletal muscle troponin C and their tryptic fragments. *FEBS Lett. 153*, 169-173.

Buchta, R., Bondi, E., and Fridkin, M. (1986). Peptides related to the calcium binding domains II and III of calmodulin. *Int. J. Peptide Protein Res. 28*, 289-297.

Callender, R. H., Dyer, R. B., Gilmanshin, R., and Woodruff, W. H. (1998). Fast events in protein folding: the time evolution of primary processes. *Annu. Rev. Phys. Chem. 49*, 173-202.

Chapman, E. R., Au, D., Alexander, K. A., Nicolson, T. A., and Storm, D. R. (1991). Characterization of the calmodulin binding domain of neuromodulin. *J. Biol. Chem. 266*, 207-213.

Chattopadhyaya, R., Meador, W. E., Means, A. R., and Quiocho, F. A. (1992). Calmodulin structure refined at 1.7 Angstrom resolution. *J. Mol. Biol. 228*, 1177-1192.

Clarke, A. R., and Waltho, J. P. (1997). Protein folding pathways and intermediates. *Curr. Opin. Biotech. 8*, 400-410.

Cox, J. A., Comte, M., Malnoe, A., Burger, D., and Stein, E. A. (1984). Mode of action of the regulatory protein calmodulin. *Met. Ions Biol. Syst. 17*, 215-273.

Coyne, M. D., Cornelius, P., Venditti, N., Toscano, D. G., Gross, M. K., and Toscano Jr, W. A. (1985). Purification and properties of calmodulin from adrenal cortex. *Arch. Biochem. Biophys. 236*, 629-637.

Creighton, T. E. (1992). *Protein folding*, W.H. Freeman and Company, New York.

Creighton, T. E. (1993). *Proteins: structures and molecular properties*, W.H. Freeman and Company, New York.

Crivici, A., and Ikura, M. (1995). Molecular and structural basis of target recognition by calmodulin. *Annu. Rev. Biophys. Biomol. Struct. 24*, 85-116.

Dasgupta, M., Honeycutt, T., and Blumenthal, D. K. (1989). The γ-subunit of skeletal muscle phosphorylase kinase contains two noncontiguous domains that act in concert to bind calmodulin. *J. Biol. Chem. 264*, 17156-17163.

Davis, T. N. (1992). What's new with calcium? Meeting review. *Cell 71*, 557-564.

Declercq, J.-P., Tinant, B., Parello, J., and Rambaud, J. (1991). Ionic interactions with parvalbumin. Crystal structure determination of pike 4.10 parvalbumin in four different ionic environments. *J. Mol. Biol. 220*, 1017-1039.

Dill, K. A., and Chan, H. S. (1997). From Levinthal to pathways to funnels. *Nature Struct. Biol. 4*, 10-19.

Dotsch, V., Wider, G., Siegal, G., and Wüthrich, K. (1995). Interaction of urea with an unfolded protein, the DNA-binding domain of the 434-repressor. *FEBS Lett. 366*, 6-10.

Drabikowski, W., Brzeska, H., and Venyaminov, S. Y. (1982). Tryptic fragments of calmodulin. *J. Biol. Chem. 257*, 11584-11590.

Dunbar, J., Yennawar, H. P., Banerjee, S., Luo, J., and Farber, G. K. (1997). The effect of denaturants on protein structure. *Protein Sci. 6*, 1727-1733.

Eaton, W. A., Munoz, V., Thompson, P. A., Chan, C.-K., and Hofrichter, J. (1997). Submillisecond kinetics of protein folding. *Curr. Opin. Struct. Biol. 7*, 10-14.

Ebel, H., and Gunther, T. (1980). Magnesium metabolism: a review. *J. Clin. Chem. Clin. Biochem. 18*, 257-270.

Evenäs, J., Thulin, E., Malmendal, A., Forsén, S., and Carlstrom, G. (1997). NMR studies of the E140Q mutant of the carboxy-terminal domain of calmodulin reveal global conformational exchange in the Ca^{2+}-saturated state. *Biochemistry 36*, 3448-3457.

Falke, J. J., Drake, S. K., Hazard, A. L., and Perseen, O. B. (1994). Molecular tuning of ion binding to calcium signaling proteins. *Quart. Rev. Biophys. 27*, 219-290.

Fersht, A. R. (1997). Nucleation mechanisms in protein folding. *Current Opinion in Structural Biology 7*, 3-9.

Findlay, W. A., Gradwell, M. J., and Bayley, P. M. (1995a). Role of the N-terminal region of the skeletal muscle myosin light chain kinase target sequence in its interaction with calmodulin. *Protein Sci. 4*, 2375-2382.

Findlay, W. A., Martin, S. R., Beckingham, K., and Bayley, P. M. (1995b). Recovery of native structure by calcium binding site mutants of calmodulin upon binding of sk-MLCK target peptides. *Biochemistry 34*, 2087-2094.

Finn, B. E., Evenäs, J., Drakenberg, T., Waltho, J. P., Thulin, E., and Forsén, S. (1995). Calcium-induced structural changes and domain autonomy in calmodulin. *Nature Struct. Biol. 2*, 777-783.

Follenius, A., and Gerard, D. (1984). Fluorescence investigations of calmodulin hydrophobic sites. *Biochem. Biophys. Res. Commun. 119*, 1154-1160.

Forsén, S., Akke, M., Brodin, P., Bayley, P. M., Drakenberg, T., Grundstrom, T., Johansson, C., Linse, S., Martin, S. R., and Thulin, E. (1989). Neutralization of surface charges markedly affects the properties of bovine calbindin D_{9k}. *Adv. Exp. Med. Biol. 255*, 185-194.

Fredricksen, R. S., and Swenson, C. A. (1996). Relationship between stability and function for isolated domains of troponin C. *Biochemistry 35*, 14012-14026.

Gao, Z. H., Krebs, J., VanBerkum, M. F. A., Tang, W.-J., Maune, J. F., Means, A. R., Stull, J. T., and Beckingham, K. (1993). Activation of four enzymes by two series of calmodulin mutants with point mutations in individual Ca^{2+} binding sites. *J. Biol. Chem. 268*, 20096-20104.

Gill, S. C., and von Hippel, P. H. (1989). Calculation of protein extinction coefficients from amino acid sequence data. *Anal. Biochem. 182*, 319-326.

Gilli, R., Lafitte, D., Lopez, C., Kilhoffer, M.-C., Makarov, A., Briand, C., and Haiech, J. (1998). Thermodynamic analysis of calcium and magnesium binding to calmodulin. *Biochemistry 37*, 5450-5456.

Greenfield, N. J. (1996). Methods to estimate the conformation of proteins and polypeptides from circular dichroism data. *Anal. Biochem. 235*, 1-10.

Hagen, S. J., Hofrichter, J., Szabo, A., and Eaton, W. A. (1996). Diffusion-limited contact formation in unfolded cytochrome c: Estimating the maximum rate of protein folding. *Proc. Natl. Acad. Sci. USA 93*, 11615-11617.

Haiech, J., Klee, C. B., and Demaille, J. G. (1981). Effects of cations on affinity of calmodulin for calcium: ordered binding of calcium ions allows the specific activation of calmodulin-stimulated enzymes. *Biochemistry 20*, 3890-3897.

Haiech, J., Kilhoffer, M. C., Lukas, T. J., Craig, T. A., Roberts, D. M., and Watterson, D. M. (1991). Restoration of the calcium binding activity of mutant calmodulins toward normal by the presence of a calmodulin binding structure. *J. Biol. Chem. 266*, 3427-3431.

Harrison, S. M., and Bers, D. M. (1987). The effect of temperature and ionic strength on the apparent Ca-affinity of EGTA and the analogous Ca-chelators BAPTA and dibromo-BAPTA. *Biochim. Biophys. Acta 925*, 133-143.

Hartl, F. U. (1996). Molecular chaperones in cellular protein folding. *Nature 381*, 571-580.

Honig, B. (1999). Protein folding: from the Levinthal paradox to structure prediction. *J. Mol. Biol. 293*, 283-293.

Houdusse, A., and Cohen, C. (1995). Target sequence recognition by the calmodulin superfamily: implications from light chain binding to the regulatory domain of scallop myosin. *Proc. Natl. Acad. Sci. USA 92*, 10644-10647.

Ikura, M., Clore, G. M., Gronenborg, A. M., Zhu, G., Klee, C. B., and Bax, A. (1992). Solution structure of a calmodulin-target peptide complex by multidimensional NMR. *Science 256*, 632-638.

Ikura, M., Kay, L. E., and Bax, A. (1990). A novel approach for sequential assignment of ^{1}H, ^{13}C and ^{15}N spectra of larger proteins: heteronuclear triple-resonance three-dimensional NMR spectroscopy. Application to calmodulin. *Biochemistry 29*, 4659-4667.

Ikura, M., Spera, S., Barbato, G., Kay, L. E., Krinks, M., and Bax, A. (1991). Secondary structure and side-chain ^{1}H and ^{13}C resonance assignments of

calmodulin in solution by heteronuclear multidimensional NMR spectroscopy. *Biochemistry 30*, 9216-9228.

Kanellis, P., Yang, J., Cheung, H. C., and Lenkinski, R. E. (1983). Synthetic peptide analogs of skeletal troponin C: fluorescence studies of analogs of the low-affinity calcium binding site II. *Arch. Biochem. Biophys. 220*, 530-540.

Kawasaki, H., Kurosu, Y., Kasai, H., Isobe, T., and Okuyama, T. (1986). Limited digestion of calmodulin with trypsin in the presence or absence of various metal ions. *J. Biochem. (Tokyo) 99*, 1409-1416.

Klee, C. B. (1988). Interaction of calmodulin with Ca^{2+} and target proteins. *Calmodulin* (Cohen, P., and Klee, C. B., Eds.) pp 35-56, Elsevier, Amsterdam.

Klevit, R. E., Blumenthal, D. K., Wemmer, D. E., and Krebs, E. G. (1985). Interaction of calmodulin and a calmodulin-binding peptide from myosin light chain kinase: major spectral changes in both occur as the result of complex formation. *Biochemistry 24*, 8152-8157.

Kretsinger, R. H., and Nockolds, C. E. (1973). Carp muscle calcium-binding protein. *J. Biol. Chem. 248*, 3313-3326.

Kretsinger, R. H., Rudnick, S. E., and Weisman, L. J. (1986). Crystal structure of calmodulin. *J. Inorg. Biochem. 28*, 289-302.

Krueger, J. K., Gallagher, S. C., Wang, C. A., and Trewhella, J. (2000). Calmodulin remains extended upon binding to smooth muscle caldesmon: a combined small-angle scattering and Fourier transform infrared spectroscopy study. *Biochemistry 39*, 3979-3987.

Kuboniwa, H., Tjandra, N., Grzesiek, S., Ren, H., Klee, C. B., and Bax, A. (1995). Solution structure of calcium-free calmodulin. *Nature Struct. Biol. 2*, 768-776.

Lee, S. Y., and Klevit, R. E. (2000). The whole is not the simple sum of its parts in calmodulin from *S. Cerevisiae*. *Biochemistry 39*, 4225-4230.

Lehrer, S. S., and Leavis, P. C. (1974). Fluorescence and conformational changes caused by proton binding to troponin C. *Biochem. Biophys. Res. Comm. 58*, 159-165.

Levinthal, C. (1968). Are there pathways for protein folding? *J. Chim. Phys. 65*, 44-45.

Linse, S., Helmersson, A., and Forsén, S. (1991a). Calcium binding to calmodulin and its globular domains. *J. Biol. Chem. 266*, 8050-8054.

Linse, S., Johansson, C., Brodin, P., Grundstrom, T., Drakenberg, T., and Forsén, S. (1991b). Electrostatic contributions to the binding of Ca^{2+} in Calbindin D_{9k}. *Biochemistry 30*, 154-162.

Mackall, J., and Klee, C. B. (1991). Calcium-induced sensitization of the central helix of calmodulin to proteolysis. *Biochemistry 30*, 7242-7247.

Makhatadze, G. I., and Privalov, P. L. (1992). Protein interactions with urea and guanidinium chloride. A calorimetric study. *J. Mol. Biol. 226*, 491-505.

Malmendal, A., Evenäs, J., Thulin, E., Gippert, G. P., Drakenberg, T., and Forsén, S. (1998). When size is important. *J. Biol. Chem. 273*, 28994-29001.

Malmendal, A., Evenäs, J., Forsén, S., and Akke, M. (1999a). Structural dynamics in the C-terminal domain of calmodulin at low calcium levels. *J. Mol. Biol. 293*, 883-899.

Malmendal, A., Linse, S., Evenäs, J., Forsén, S., and Drakenberg, T. (1999b). Battle for the EF-hands: magnesium-calcium interference in calmodulin. *Biochemistry 38*, 11844-11850.

Manyusa, S., and Whitford, D. (1999). Defining folding and unfolding reactions of apocytochrome *b5* using equilibrium and kinetic fluorescence measurements. *Biochemistry 38*, 9533-9540.

Martin, R. B., and Richardson, F. S. (1979). Lanthanides as probes for calcium in biological systems. *Quart. Rev. Biophys. 12*, 181-209.

Martin, S. R., and Bayley, P. M. (1986). The effects of Ca^{2+} and Cd^{2+} on the secondary and tertiary structure of bovine testis calmodulin. *Biochem. J. 238*, 485-490.

Martin, S. R., Bayley, P. M., Brown, S. E., Porumb, T., Zhang, M., and Ikura, M. (1996). Spectroscopic characterization of a high-affinity calmodulin-target peptide hybrid molecule. *Biochemistry 35*, 3508-3517.

Martin, S. R., Linse, S., Bayley, P. M., and Forsén, S. (1986). Kinetics of cadmium and terbium dissociation from calmodulin and its triptic fragments. *Eur. J. Biochem. 161*, 595-601.

Martin, S. R., Linse, S., Johansson, C., Bayley, P. M., and Forsén, S. (1990). Protein surface charges and Ca^{2+} binding to individual sites in calbindin D_{9k}: stopped-flow studies. *Biochemistry 29*, 4188-4193.

Martin, S. R., Maune, J. F., Beckingham, K., and Bayley, P. M. (1992). Stopped-flow studies of calcium dissociation from calcium-binding-site mutants of *Drosophila melanogaster* calmodulin. *Eur. J. Biochem. 205*, 1107-1114.

Martin, S. R., Teleman, A. A., Bayley, P. M., Drakenberg, T., and Forsén, S. (1985). Kinetics of calcium dissociation from calmodulin and its triptic fragments. A stopped-flow fluorescence study using Quin 2 reveals a two-domain structure. *Eur. J. Biochem. 151*, 543-5506.

Matthews, C. R. (1993). Pathways of protein folding. *Annu. Rev. Biochem. 62*, 653-683.

Maune, J. F., Beckingham, K., Martin, S. R., and Bayley, P. M. (1992a). Circular dichroism studies on calcium binding to two series of Ca^{2+} binding site mutants of *Drosophila melanogaster* calmodulin. *Biochemistry 31*, 7779-7786.

Maune, J. F., Klee, C. B., and Beckingham, K. (1992b). Ca^{2+} binding and conformational change in two series of point mutations to the individual Ca^{2+}-binding sites of calmodulin. *J. Biol. Chem. 267*, 5286-5295.

McCammon, J. A. (1996). A speed limit for protein folding. *Proc. Natl. Acad. Sci. USA 93*, 11426-11427.

Meador, W. E., Means, A. R., and Quiocho, F. A. (1992). Target enzyme recognition by Calmodulin: 2.4 Å structure of a calmodulin-peptide complex. *Science 257*, 1251-1255.

Meador, W. E., Means, A. R., and Quiocho, F. A. (1993). Modulation of calmodulin plasticity in molecular recognition on the basis of X-rays structures. *Science 262*, 1718-1721.

Milos, M., Schaer, J.-J., Comte, M., and Cox, J. A. (1986). Calcium-proton and calcium-magnesium anatagonism in calmodulin: microcalorimetric and potentiometric analyses. *Biochemistry 25*, 6279-6287.

Moncrieffe, M. C., Venyaminov, S. Y., Miller, T. E., Guzman, G., Potter, J. D., and Prendergast, F. G. (1999). Optical spectroscopic characterization of single tryptophan mutants of chicken skeletal troponin C: evidence for interdomain interaction. *Biochemistry 38*, 11973-11983.

Monera, O. D., Kay, C. M., and Hodges, R. S. (1994). Protein denaturation with guanidine hydrochloride or urea provides a different estimate of stability depending on the contributions of electrostatics interactions. *Protein Sci. 3*, 1984-1991.

Mori, M., Konno, T., Ozawa, T., Murata, M., Imoto, K., and Nagayama, K. (2000). Novel interaction of the voltage-dependent sodium channel (VDSC) with

calmodulin: does VDSC acquire calmodulin-mediated Ca^{2+}-sensitivity? *Biochemistry 39*, 1316-1323.

Mukherjea, P., and Beckingham, K. (1993). Calcium binding site mutants of calmodulin adopt abnormal conformations in complexes with model target peptides. *Biochem. Mol. Biol. International 29*, 555-563.

Mukherjea, P., Maune, J. F., and Beckingham, K. (1996). Interlobe communication in multiple calcium-binding site mutants of *Drosophila* calmodulin. *Protein Sci. 5*, 468-477.

Myers, J. K., Pace, C. N., and Scholtz, J. M. (1995). Denaturant *m* values and heat capacity changes: relation to changes in accessible surface areas of protein unfolding. *Protein Sci. 4*, 2138-2148.

Nakashima, K., Ishida, H., Ohki, S., Hikichi, K., and Yazawa, M. (1999). Calcium binding induces interaction between the N- and C-terminal domains of yeast calmodulin and mudulates its overall conformation. *Biochemistry 38*, 98-104.

Newton, D. L., Oldewurtel, M. D., Krinks, M. H., Shiloach, J., and Klee, C. B. (1984). Agonist and antagonist properties of calmodulin fragments. *J. Biol. Chem. 259*, 4419-4426.

Ohgushi, M., and Wada, A. (1983). "Molten globule state": a compact form of globular proteins with mobile side chains. *FEBS Lett. 164*, 21-24.

Ohki, S., Ikura, M., and Zhang, M. (1997). Identification of Mg^{2+}-binding sites and the role of Mg^{2+} on target recognition by calmodulin. *Biochemistry 36*, 4309-4316.

Ohki, S., Iwamoto, U., Aimoto, S., Yazawa, M., and Hikichi, K. (1993). Mg^{2+} inhibits formation of $4Ca^{2+}$-calmodulin-enzyme complex at lower Ca^{2+} concentration. *J. Biol. Chem. 268*, 12388-12392.

Olwin, B. B., and Storm, D. R. (1985). Calcium binding to complexes of calmodulin and calmodulin binding proteins. *Biochemistry 24*, 8081-8086.

O'Neil, K. T., and DeGrado, W. F. (1990). How calmodulin binds its targets: sequence independent recognition of amphiphilic alpha-helices. *Trends Biochem. Sci. 15*, 59-64.

Osawa, M., Tokumitsu, H., Swindells, M. B., Kurihara, H., Orita, M., Shibanuma, T., Furuya, T., and Ikura, M. (1999). A novel target recognition revealed by calmodulin in complex with Ca^{2+}-calmodulin-dependent kinase kinase. *Nature Struct. Biol. 6*, 819-824.

Ouyang, H., and Vogel, H. J. (1998). Metal ion binding to calmodulin: NMR and fluorescence studies. *BioMetals 11*, 213-222.

Ozawa, T., Sasaki, K., and Umezawa, Y. (1999). Metal ion selectivity for formation of the calmodulin-metal-target peptide ternary complex studied by surface plasmon resonance spectroscopy. *Biochim. Biophys. Acta 1434*, 211-220.

Pace, C. N. (1986). Determination and analysis of urea and guanidine hydrochloride denaturation curves. *Meth. Enzymol. 131*, 266-280.

Pace, C. N. (1990). Conformational stability of globular proteins. *TIBS 15*, 14-17.

Pace, C. N., Laurents, D. V., and Thomson, J. A. (1990). pH dependence of the urea and guanidine hydrochloride denaturation of ribonuclease A and ribonuclease T1. *Biochemistry 29*, 2564-2572.

Pande, V. S., Grosberg, A. Y., Tanaka, T., and Rokhsar, D. S. (1998). Pathways for protein folding: is a new view needed? *Curr. Opin. Struct. Biol. 8*, 68-79.

Pedigo, S., and Shea, M. A. (1995). Quantitative endoproteinase GluC footprinting of cooperative Ca^{2+} binding to calmodulin: proteolytic susceptibility of E31 and E87 indicates interdomain interactions. *Biochemistry. 34*, 1179-1196.

Peersen, O. B., Madsen, T. S., and Falke, J. J. (1997). Intermolecular tuning of calmodulin by target peptides and proteins: differential effects on Ca^{2+} binding equlibria and kinetics. *Protein Sci. 6*, 1-14.

Persechini, A., Mc Millan, K., and Leakey, P. (1994). Activation of myosin light chain kinase and nitric oxide synthase activities by calmodulin fragments. *J. Biol. Chem. 269*, 16148-16154.

Pethig, R., Kuhn, M., Payne, R., Adler, E., Chen, T.-H., and Jaffe, L. F. (1989). On the dissociation constants of BAPTA-type calcium buffers. *Cell Calcium 10*, 491-498.

Plaxco, K. W., and Dobson, C. M. (1996). Time-resolved biophysical methods in the study of protein folding. *Curr. Opin. Struct. Biol. 6*, 630-636.

Porumb, T. (1994). Determination of calcium binding constants by flow-dialysis. *Anal. Biochem. 220*, 227-234.

Privalov, P. L., and Khechinashvilli, N. N. (1974). A thermodynamic approach to the problem of stabilisation of globular protein structure: a calorimetric study. *J.Mol. Biol. 86*, 665-684.

Protasevich, I., Ranjbar, B., Lobachov, V., Makarov, A., Gilli, R., Briand, C., Lafitte, D., and Haiech, J. (1997). Conformation and thermal denaturation of apocalmodulin: role of electrostatic mutations. *Biochemistry 36*, 2017-2024.

Reid, R. E., Gariepy, J., Saund, A. K., and Hodges, R. S. (1981). Calcium-induced protein folding. Structure-affinity relationships in synthetic analogs of the helix-loop-helix calcium binding unit. *J. Biol. Chem. 256*, 2742-2751.

Rhoads, A. R., and Friedberg, F. (1997). Sequence motifs for calmodulin recognition. *FASEB J. 11*, 331-340.

Schellman, J. A. (1975). Macromolecular binding. *Biopolymers 14*, 999-1018.

Schellman, J. A. (1987). The thermodynamic stability of proteins. *Ann. Rev. Biophys. Biophys. Chem. 16*, 115-137.

Schellman, J. A. (1994). The thermodynamics of solvent exchange. *Biopolymers 34*, 1015-1026.

Schellman, J. A., and Gassner, N. C. (1995). The enthalpy of transfer of unfolded proteins into solutions of urea and guanidinium chloride. *Biophys. Chem. 59*, 259-275.

Seamon, K. B. (1980). Calcium- and magnesium-dependent conformational states of calmodulin as determined by nuclear magnetic resonance. *Biochemistry 19*, 207-215.

Seckler, R., and Jaenicke, R. (1992). Protein folding and protein refolding. *FASEB J. 6*, 2545-2552.

Shakhnovich, E. I. (1997). Theoretical studies of protein-folding thermodynamics and kinetics. *Curr. Opin. Struct. Biol. 7*, 29-40.

Shea, M. A., Verhoeven, A. S., and Pedigo, S. (1996). Calcium-induced interactions of calmodulin domains revealed by quantitative thrombin footprinting of Arg37 and Arg106. *Biochemistry. 35*, 2943-2957.

Shortle, D. (1996). The denatured state (the other half of the folding equation) and its role in protein stability. *FASEB J. 10*, 27-34.

Shortle, D., and Meeker, A. K. (1986). Mutant forms of staphylococcal nuclease with altered patterns of guanidine hydrochloride and urea denaturation. *Proteins: Struct. Funct. Genet. 1*, 81-89.

Siivari, K., Zhang, M., Palmer, A. G., III, and Vogel, H. J. (1995). NMR studies of the methionine methyl groups in calmodulin. *FEBS Lett. 366*, 104-108.

Sorensen, B. R., and Shea, M. A. (1998). Interactions between domains of apo calmodulin alter calcium binding and stability. *Biochemistry 37*, 4244-4253.

Starovasnik, M. A., Su, D. R., Beckingham, K., and Klevit, R. E. (1992). A series of point mutations reveal interactions between the calcium-binding sites of calmodulin. *Protein Sci. 1*, 245-253.

Strickland, E. H. (1974). Aromatic contributions to the circular dichroism spectra of proteins. *CRC Crit. Rev. Biochem. 2*, 113.

Strynadka, N. C. J., and James, M. N. G. (1988). Two trifluoperazine-binding sites on calmodulin predicted from comparative molecular modeling with troponin-C. *Proteins Struct. Func. Genet. 3*, 1-17.

Suko, J., Wyskovsky, W., Pidlich, J., Hauptner, R., Plank, B., and Hellmann, G. (1986). Calcium release from calmodulin and its C-terminal or N-terminal halves in the presence of the calmodulin antagonists phenoxybenzamine and melittin measured by stopped-flow fluorescence with Quin 2 and intrinsic tyrosine. Inhibition of calmodulin-dependent protein kinase of cardiac sarcoplasmic reticulum. *Eur. J. Biochem. 159*, 425-434.

Swindells, M. B., and Ikura, M. (1996). Pre-formation of the semi-open conformation by the apo-calmodulin C-terminal domain and implications for binding IQ-motifs. *Nature Struct. Biol. 3*, 501-504.

Tan, R.-Y., Mabuchi, Y., and Grabarek, Z. (1996). Blocking the Ca^{2+}-induced conformational transitions in calmodulin with disulfide bonds. *J. Biol. Chem. 271*, 7479-7483.

Tanford, C. (1970). Protein denaturation. Part C. Theoretical models for the mechanism of denaturation. *Adv. Protein Chem. 24*, 1-95.

Thulin, E., Andersson, A., Drakenberg, T., Forsén, S., and Vogel, H. J. (1984). Metal ion and drug binding to proteolytic fragments of calmodulin: proteolytic, cadmium-113, and proton nuclear magnetic resonance studies. *Biochemistry 23*, 1862-1870.

Török, K., Lane, A. N., Martin, S. R., Janot, J.-M., and Bayley, P. M. (1992). Effects of calcium binding on the internal dynamic properties of bovine brain calmodulin, studied by NMR and optical spectroscopy. *Biochemistry 31*, 3452-3462.

Trewhella, J., Blumethal, D. K., Rokop, S. E., and Seeger, P. A. (1990). Small-angle scattering studies show distinct conformations of calmodulin in its complexes

with two peptides based on the regulatory domain of the catalytic subunit of phosphorylase kinase. *Biochemistry 29*, 9316-9324.

Tsai, M.-D., Drakenberg, T., Thulin, E., and Forsén, S. (1987). Is the binding of magnesium(II) to calmodulin significant? An investigation by magnesium-25 nuclear magnetic resonance. *Biochemistry 26*, 3635-3643.

Tsalkova, T. N., and Privalov, P. L. (1985). Thermodynamic study of domain organization in troponin C and calmodulin. *J. Mol. Biol. 181*, 533-544.

Urbauer, J. L., Ehrhardt, M. R., Bieber, R. J., Flynn, P. F., and Wand, A. J. (1995). Structural analysis of a novel interaction by calmodulin: high-affinity binding of a peptide in the absence of calcium. *Biochemistry 34*, 8099-8109.

Venyaminov, S. Y., Baikalov, I. A., Shen, Z. M., Wu, C.-S. C., and Yang, J. T. (1993). Circular dichroic analysis of denatured proteins: inclusion of denatured proteins in the reference set. *Anal. Biochem. 214*, 17-24.

Walsh, M., Stevens, F. C., Kuznicki, J., and Drabikowski, W. (1977). Characterisation of tryptic fragments obtained from bovine brain protein modulator of cyclic nucleotide phophodiesterase. *J. Biol. Chem. 252*, 7440-7443.

Wandosell, F., Serrano, L., and Avila, J. (1986). A calcium binding protein from *Drosophila melanogaster* which activates cAMP phosphodiesterase: comparison of this protein with porcine brain calmodulin. *Arch. Biochem. Biophys. 247*, 147-154.

Wrabl, J., and Shortle, D. (1999). A model of the changes in denatured state structure underlying m value effects in staphylococcal nuclease. *Nature Struct. Biol. 9*, 876-883.

Wu, X., and Reid, R. E. (1997). Conservative D133E mutation of calmodulin site IV drastically alters calcium binding and phosphodiesterase regulation. *Biochemistry 36*, 3608-3616.

Yang, J. T., Wu, C.-S. C., and Martinez, H. M. (1986). Calculation of protein conformation from circular dichroism. *Meth. Enzymol. 130*, 208-269.

Yazawa, M., Ikura, M., Hikichi, K., Ying, L., and Yagi, K. (1987). Communication between two globular domains of calmodulin in the presence of mastoparan or caldesmon fragment. *J. Biol. Chem. 262*, 10951-10954.

Yazawa, M., Vorherr, T., James, P., Carafoli, E., and Yagi, K. (1992). Binding of calcium by calmodulin: influence of the calmodulin binding domain of the plasma membrane calcium pump. *Biochemistry 31*, 3171-3176.

Yon, J. M. (1997). Protein folding: concepts and perspectives. *Cell. Mol. Life Sci. 53*, 557-567.

Yuan, T., Weljie, A. M., and Vogel, H. J. (1998). Tryptophan fluorescence quenching by methionine and selenomethionine residues of calmodulin: orientation of peptide and protein binding. *Biochemistry 37*, 3187-3195.

Zhang, M., Tanaka, T., and Ikura, M. (1995a). Calcium-induced conformational transition revealed by the solution structure of apo calmodulin. *Nature Struct. Biol. 2*, 758-767.

Zhang, M., and Yuan, T. (1998). Molecular mechanisms of calmodulin's functional versatility. *Biochem. Cell Biol. 76*, 313-323.

Zhang, M., Yuan, T., Aramini, J. M., and Vogel, H. J. (1995b). Interaction of calmodulin with its binding domain of rat cerebellar nitric oxide synthase. *J. Biol. Chem. 270*, 20901-20907.

Zou, Q., Habermann-Rottinghaus, S. H., and Murphy, K. P. (1998). Urea effects on protein stability: hydrogen bonding and the hydrophobic effect. *Proteins: Struct. Funct. Genet. 31*, 107-115.

APPENDIX 1

CALMODULIN STRUCTURES AND CALCIUM COORDINATION IN AN EF-HAND

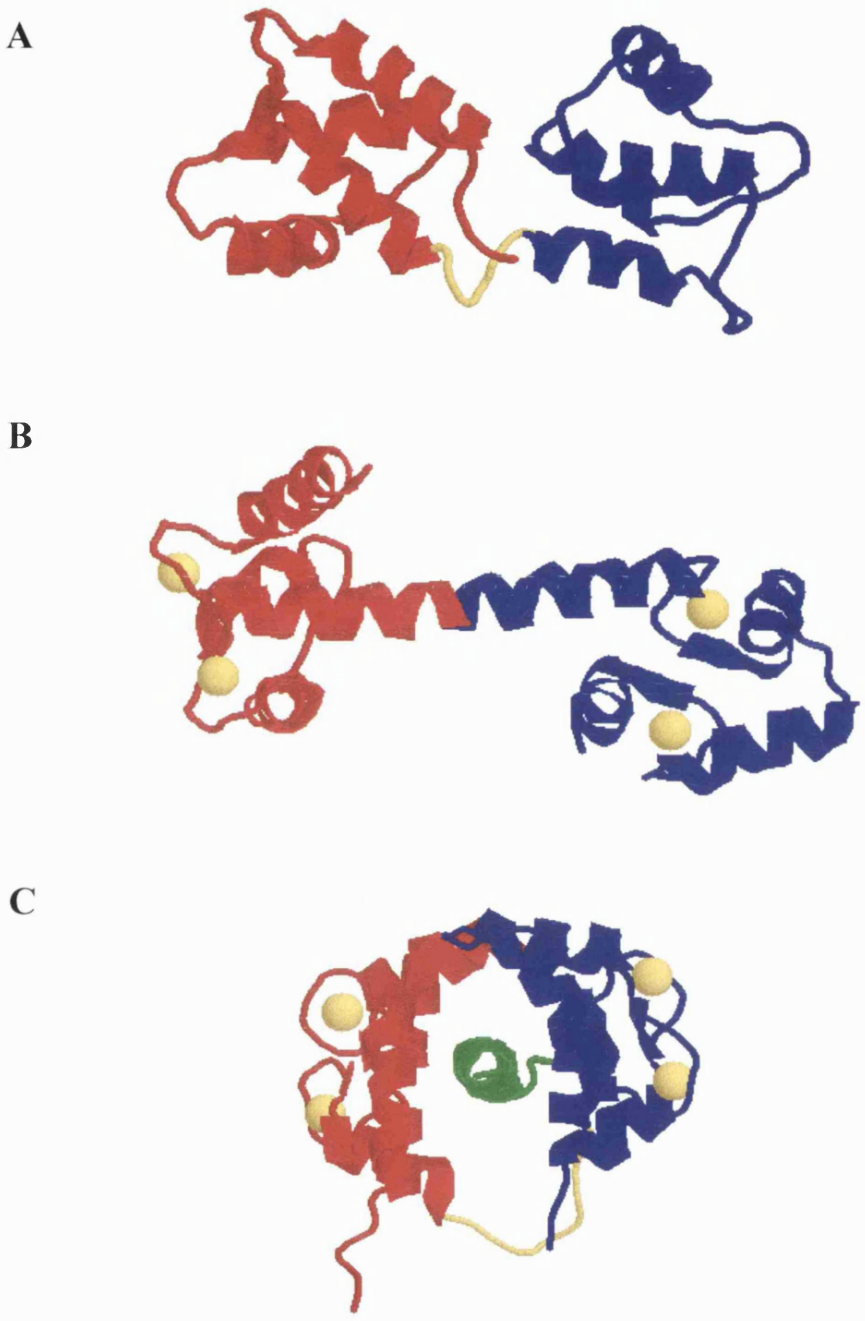

Figure A.1 **(A)** Solution structure of calcium-free CaM (PDB entry code: 1CFC; Kuboniwa et al., 1995). **(B)** Crystal structure of calcium-saturated CaM (PDB entry code: 1CLL; Chattopadhyaya et al., 1992). **(C)** Solution structure of calcium-saturated CaM complexed with a target peptide from the calmodulin binding region of rabbit skeletal myosin light chain kinase (PDB entry code: 2BBM; Ikura et al., 1992). The N-domain is shown in red, the C-domain in blue, the flexible central linker which connects the two domains is shown in yellow, and the peptide in green. The figure was prepared using the program Rasmol.

A

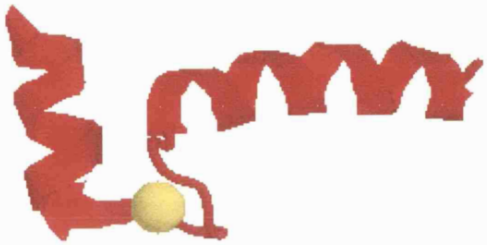

B

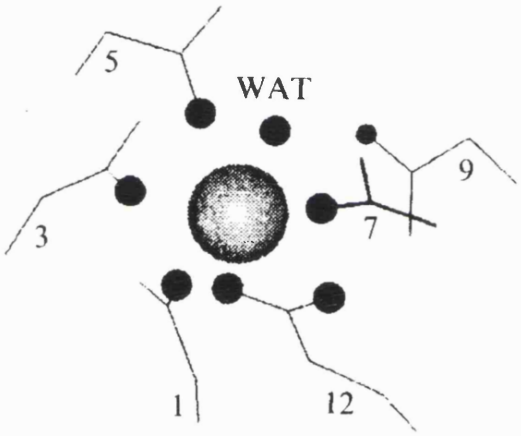

Figure A.2 **(A)** Structure of a helix-loop-helix EF-hand. (The N-terminal EF-hand of CaM, taken from the crystal structure of calcium-saturated CaM. PDB entry code: 1CLL; Chattopadhyaya et al., 1992). The figure was prepared using the program Rasmol. **(B)** Calcium coordination geometry in a representative EF-hand site. The seven coordinating oxygen atoms are represented as small spheres. The numbers indicate the positions of the approximately octahedral coordinating residues in the calcium binding loop. WAT indicates the oxygen of a water molecule. The ligand coordination is: 1 X, 3 Y, 5 Z, 7 –Y, 9 (WAT) –X, 12 –Z. The figure was taken from Falke et al. (1994).

APPENDIX 2

PUBLICATIONS

Masino, L., Martin, S.R., and Bayley, P.M. (2000). Ligand binding and thermodynamic stability of a multi-domain protein, calmodulin. *Protein Sci. 9*, 1519-1529.

Martin, S. R., Masino, L., and Bayley, P. M. (2000). Enhancement by Mg^{2+} of domain specifity in Ca^{2+}-dependent interactions of calmodulin with target sequences. *Protein Sci.* (In press).

Abbruzzetti, S., Crema, E., Masino, L., Vecli, A., Viappiani, C., Small, J. R., Libertini, L. J., and Small, E. W. (2000). Fast events in protein folding: structural volume changes accompanying the early events in the N→I transition of apomyoglobin induced by ultrafast pH jump. *Biophys. J. 78*, 405-415.

Abbruzzetti, S., Masino, L., Viappiani, C., Libertini, L. J., Small, J. R., and Small, E. W. (1996). Rapid, photoinduced proton transfer: dependence on acceptor size, shape and concentration. *Biophys J. 70*, A178.

Masino, L., Martin, S. R., and Bayley, P. M. (1999). Calcium-mediated folding equilibria of calmodulin and its separate domains. *Biophys. J. 76*, A109.

Masino, L., Martin, S. R., Browne, J. P., Frise, M. C., and Bayley, P. M. (2000). The effect of point mutations in EF-hands on the conformation, stability, and calcium affinity of calmodulin. *Biophys J. 78*, 423A.